Reactivity of Rh(III) acyl complexes and their roles in catalytic mechanisms

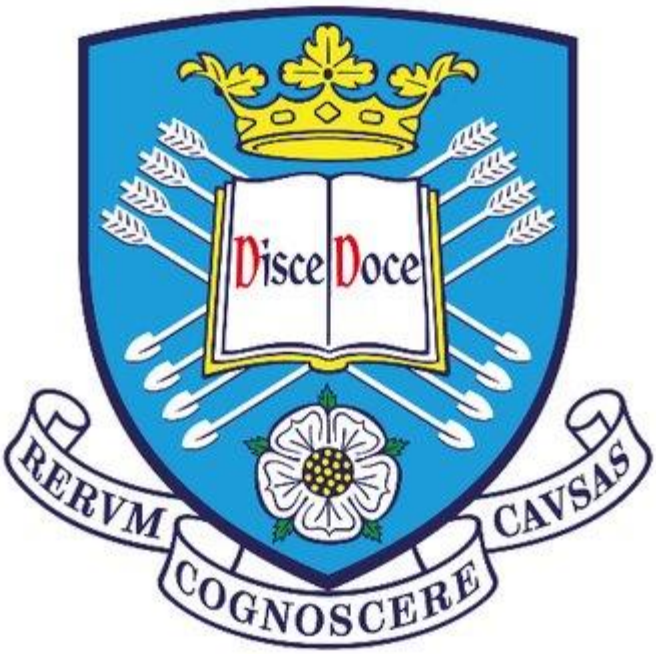

David Griffin

Supervisor: Dr. A. Haynes

A thesis submitted for the degree of Doctor of Philosophy

Department of Chemistry

University of Sheffield

August 2018

Summary

Chapter 1

This chapter introduces catalysis and fundamental aspects of organometallic chemistry, including ligand effects in catalysis. The mechanism of methanol carbonylation is discussed including a recent proposal for an alternate mechanism of product formation. The intermediate proposed for this alternative product formation mechanism is also a proposed intermediate for decarbonylative dehydration.

Chapter 2

Chapter two provides full experimental details for all procedures described in this thesis.

Chapter 3

Chapter three investigates the reactions of a range of Rh(III) acetyl diphosphine species with carboxylates. Most complexes reacted readily with acetate or benzoate to give a rhodium acetyl carboxylate complex, observed *in situ* and subsequently eliminated an anhydride. In the presence of carbon monoxide, a known Rh(I) species was formed upon reductive elimination. The coordination of carboxylate to rhodium was determined to be bidentate by ATR IR spectroscopy and DFT. The reaction of these complexes with silver trifluoroacetate produced a mixture of mono- and di-trifluoroacetate complexes. Reductive elimination of anhydride from rhodium trifluoroacetate acetyl complexes was slow.

Chapter 4

Chapter four extends the investigation of the reactions of Rh(III) acetyl complexes with carboxylates, utilising unsymmetrical heterodifunctional ligands. Reactions of these Rh(III) acetyl complexes with acetate and benzoate proceeded via substitution of an iodide ligand and subsequent reductive elimination of an anhydride. Anhydride elimination from these complexes was much slower than for complexes in Chapter three as such several rhodium acetyl carboxylate complexes were isolated and crystal structures obtained by X-ray crystallography. The reaction of these rhodium acetyl complexes with silver trifluoroacetate proceeded by abstraction of an iodide ligand by silver and coordination of trifluoroacetate,

these complexes did not eliminate an anhydride as such several species were isolated and characterised.

Chapter 5

Chapter five investigates the reactivity of Rh(III) acetyl diphosphine complexes with nitrogen containing nucleophiles. N-methyl aniline did not react with these complexes. Diethylamine reacted rapidly with Rh(III) acetyl diphosphine complexes to form N,N-diethyl acetamide. The formation of N,N-diethyl acetamide was tracked kinetically via IR spectroscopy. Activation parameters for these reactions were determined, the entropy of activation was large and negative indicating an associative mechanism.

Chapter 6

Chapter six gives an introduction to decarbonylative dehydration as a method of accessing linear alpha olefins from long chain fatty acids. A range of Rh(I) complexes were tested as catalysts for decarbonylative dehydration, which were generally high yielding but gave poor selectivity for terminal alkenes. Deuterium was found in the alkene product when using deuterated acetic anhydride, this was quantified to determine percentage incorporation. Following on from a previous observation of acetylation of an iminophosphine ligand when used for decarbonylative dehydration the mechanism of acetylation was probed.

Chapter 7

Chapter seven consists of suggestions for future work and conclusions.

Chapter 8

Chapter eight gives supplementary spectroscopic and additional details.

Acknowledgements

I would like to thank my supervisor Dr Tony Haynes for his constant support and guidance throughout my PhD. I am grateful for the opportunity I had to work in his research group.

I would also like to thank the teaching staff that have helped me grow as a GTA throughout my time in Sheffield Dr Ed Warminski, Dr Jenny Burnham, the Lab Teaching Committee and Alison in teaching labs. Special thanks go out to Dr Julie Hyde for giving me the opportunity to teach at Nanjing Tech University and Dr Jamie Wright for their help in Nanjing and for job applications.

Thanks to all the staff at Sheffield for their help throughout my PhD. For X-ray crystallography I would like to thank Harry Adams, Dr Craig Robertson and Dr Tom Roseveare. I would like to extend my gratitude to Sue 'Bradders' Bradshaw, Dr Sandra van Meurs and Craig (again) for their help with NMR spectroscopy. Also a big thanks to all the guys down at stores and Dan the glassblower. Special thanks also go out to Dr Anthony Meijer and Dr Theo Keane for their assistance with DFT calculations.

Many thanks go out to the past members of the Haynes group Christopher Parks, Stephen Repper (Lab dad) and Dean Cocker for all of their invaluable help at the start of my PhD and the great times in the office and at tea. And of course, many thanks for the present members of the Haynes group and the other two members of the Burritrio Liam Woodhead and Sam Ivko for helping keep me sane during writing and the crosswords.

Special thanks go out to all the people from tea over the years for the great chat, all the folks at Tuesday chemistry football and my housemates especially Jon, Jerry, Peter and Ash.

And lastly I would to thank my family for their constant love and support and Lucy who has helped immeasurably throughout my PhD.

Abbreviations

General

Ac	acetyl
acac	acetylacetonate
Ar	aryl
atm	atmosphere
Bu	butyl
^{t}Bu	tertiary-butyl
Bz	benzoyl
COD	1,5-cycloocatadiene
Cy	cyclohexyl
DFT	density functional theory
DMPU	1,3-Dimethyl-3,4,5,6-tetrahydro-2(1H)pyrimidone
Et	ethyl
L	ligand
LAO	linear alpha olefin
M	metal
Me	methyl
min	minutes
nbd	norbornadiene
Ph	phenyl
^{i}Pr	iso-propyl
R	alkyl or aryl group
TFA	trifluoroacetate
THF	tetrahydrofuran
o-Tol	ortho-tolyl
o-Anis	ortho-anisyl
Piv	pivaloyl (^{t}BuCO)

Infrared Spectroscopy

IR	infra-red

cm^{-1}	wavenumbers
A	absorbance
ν	stretching frequency
ν(CO)	carbonyl stretching frequency

NMR spectroscopy

NMR	nuclear magnetic resonance
δ	chemical shift
ppm	parts per million
s	singlet
d	doublet
dd	doublet of doublets
t	triplet
dt	doublet of triplets
ddt	doublet of doublet of triplets
br	broad
sept	septet
m	multiplet
arom	aromatic multiplet
J	coupling constant (Hz)

Ligands

dppm	bis(diphenylphosphino)methane
dppe	1,2-bis(diphenylphosphino)ethane
dppp	1,3- bis(diphenylphosphino)propane
dppb	1,4- bis(diphenylphosphino)butane
xantphos	4,5-bis bis(diphenylphosphino)-9,9-dimethylxanthene
DPEphos	oxydi-2,1-phenylene-bis(diphenylphosphine)
dppmS	bis(diphenylphosphino)methane monosulfide
dppmSe	bis(diphenylphosphino)methane monoselenide
dipimp	2-[(2,6-diisopropylphenylimino)methylpryidine
dipiep	2-[(2,6-diisopropylphenylimino)ethylpyridine

PN-R iminophosphine ligands

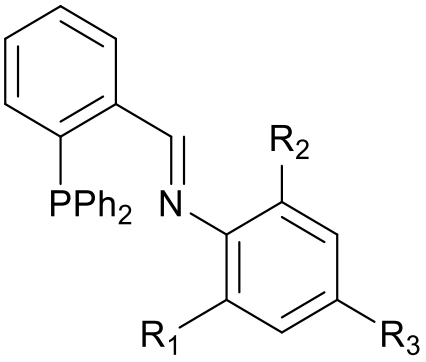

R_1	R_2	R_3	Abbreviation
^{i}Pr	^{i}Pr	H	PN-^{i}Pr$_2$Ph
Me	Me	H	PN-Me$_2$Ph
Me	Me	Me	PN-Mes
OMe	H	H	PN-*o*Anis

Pyridyl-imine ligands

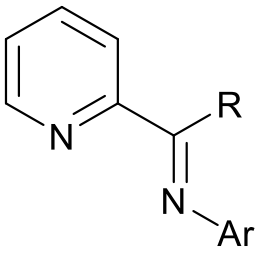

R	Ar	Abbreviation
H	2,6-^{i}Pr$_2$C$_6$H$_3$	dipimp
Me	2,6-^{i}Pr$_2$C$_6$H$_3$	dipiep

Chapter 1

General Introduction

1.0 Catalysis

A catalyst is a chemical compound which can increase the rate of a chemical reaction, without being consumed by the reaction. The overall Gibbs free energy of the reaction ΔG^{θ} is unaffected by the catalyst, but the catalyst provides an alternative reaction pathway which has a lower energy of activation ($\Delta G^{\ddagger}$), Figure 1.1.

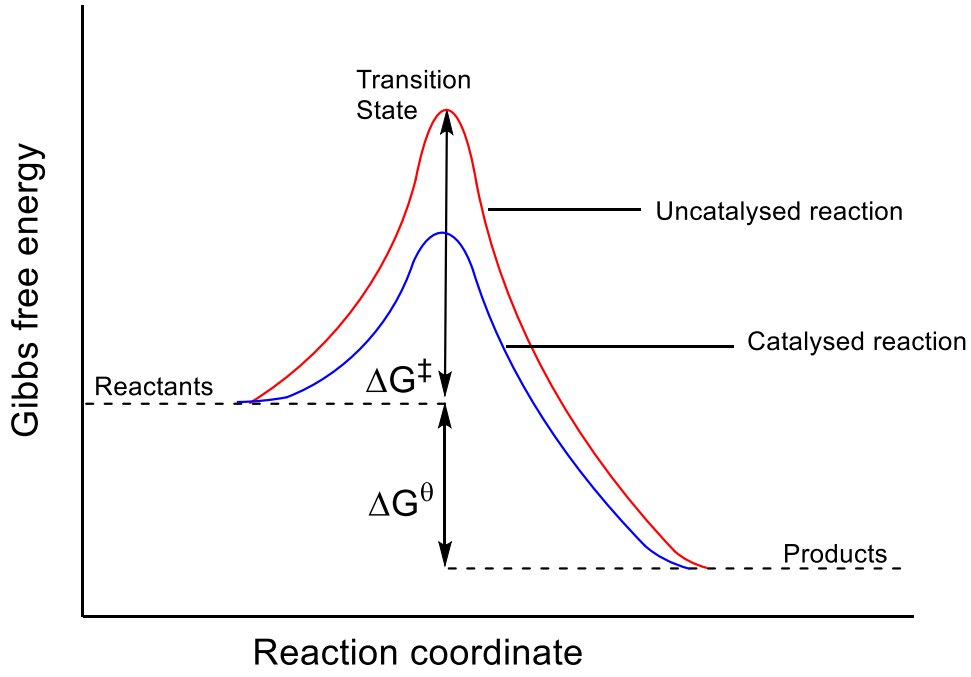

Figure 1.1: Gibbs free energy profile for a catalysed (blue) and uncatalyzed (red) reaction.

The term catalyst can be applied to a wide variety of reactions; for example most biochemical reactions are catalysed by enzymes. Catalysts can be categorised based upon what phase the catalyst and substrate are in. Homogeneous catalysis occurs when the catalyst and substrate are in the same phase. Heterogeneous catalysis occurs when the catalyst and substrate are in different phases.

1.0.1 Heterogeneous catalysis

Typically, a heterogeneous catalyst is a solid and the reagents are liquid or gaseous, which makes product separation easy. Heterogeneous catalysts are usually robust and can easily be reactivated. Due to these advantages heterogeneous systems are used for a large variety of industrial processes.

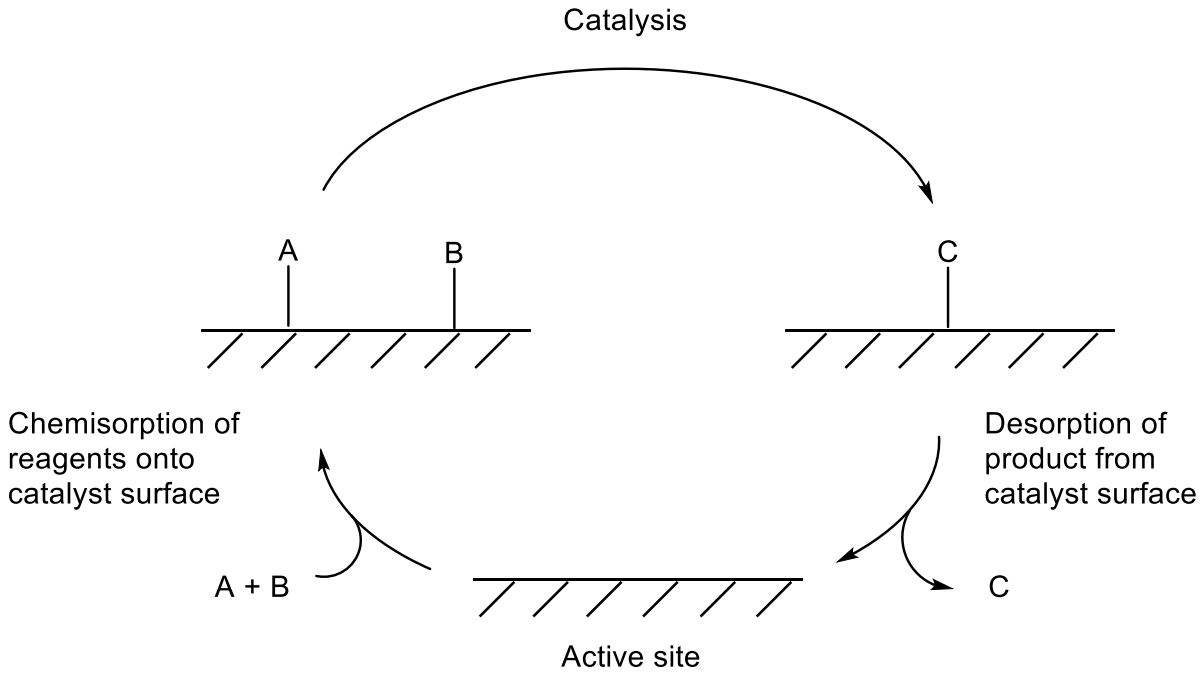

Scheme 1.1: General schematic of the heterogeneously catalysed reaction A + B → C.

A generic mechanism for a heterogeneous catalytic reaction is shown in Scheme 1.1. Reagents A and B are chemisorbed onto the catalyst surface. These species then react together to give product C, which is still chemisorbed. This product can then undergo desorption to liberate C and regenerate the active site.

The disadvantages of heterogeneous catalysis are the often-harsh reaction conditions required, poor product selectivity and lack of reproducibility. It is often difficult to obtain mechanistic information about reactions at the active site, due to difficulty of characterising

surface-bound species. The efficiency of these processes can also be limited by mass transport issues and catalyst poisoning.

Examples of industrial processes that use heterogeneous catalysts are oxidation, hydrogenation (Haber-process,[1] Fischer Tropsch synthesis[2]), Zeigler-Natta polymerisation,[3] catalytic cracking of crude oil[4] and hydrodesulfurization.[5] as summarised in Table 1.1.

Table 1.1: Examples of industrially used heterogeneous catalysis

Process	Reaction	Catalyst
Haber	$N_2 + 3H_2 \rightarrow 2NH_3$	Fe, Ru, Os
Fischer-Tropsch	$CO + H_2 \rightarrow CH_4$, alkanes, alcohols	Fe, Co, Ni
Zeigler-Natta polymerisation	$nC_3H_6 \rightarrow (C_3H_6)_n$	$TiCl_3/Al_2O_3$
Cracking of crude oil	Long chain alkanes →smaller alkanes, cycloalkanes, alkenes	Zeolite
Hydrodesulfurization	$H_2 + R_2S \rightarrow H_2S + R_2$	Mo-Co on alumina

1.0.2 Homogeneous catalysis

Homogeneous catalysis occurs when a catalyst is in the same phase as the reactants, typically a soluble transition metal complex. This allows every metal centre to be an active site, in contrast to a surface in heterogeneous catalysis. However, the presence of the catalyst in solution leads to some disadvantages, namely the difficulty of product separation and lower relative stability of catalytic species. This can increase the cost of reusing the catalyst. Due to these issues, fewer industrial processes use homogeneous catalysis with transition metals. However, there are several advantages to using a homogeneous catalyst such as greater selectivity and often higher yields. Also, much milder conditions can be used relative to heterogeneous processes.

The mechanisms for homogeneous processes are much easier to study *in situ* using spectroscopic techniques. Mechanisms can be clarified through reaction kinetics studies and identification of organometallic intermediates. This information can be used to tune catalyst properties, such as by altering ligands. This contrasts with heterogeneous catalysis where active sites are less well defined, with product distributions used to analyse potential mechanisms.

Due to these advantages, homogeneous catalysis is employed in a wide range of industrial processes. Examples include methanol carbonylation (Monsanto and Cativa process)[6,7], methyl acetate carbonylation (Eastman process),[8] ethene methoxycarbonylation/CO copolymerisaion,[9,10] alkene hydroformylation (Oxo process),[11–13] alkene oxidation (Wacker process)[14] and hydrogenation.[15,16] summarised in Table 1.2.

Table 1.2: Examples of industrially used homogeneous catalysis

Process	Reaction	Catalyst
Methanol Carbonylation	$CH_3OH + CO \rightarrow CH_3COOH$	Rh/Ir
Methoxycarbonylation	$C_2H_4 + CO + CH_3OH \rightarrow C_2H_5COOMe$	Pd/PR_3
Alkene Hydroformylation	$RCH{=}CH_2 + CO + H_2 \rightarrow RCH_2CH_2CHO$	Co/PR_3 or Rh/PPh_3
Alkene oxidation	$C_2H_4 + {}^1/_2O_2 \rightarrow CH_3CHO$	$PdCl_2/CuCl_2$
Hydrogenation	$RCH{=}CH_2 + H_2 \rightarrow RCH_2CH_3$	Rh/PPh_3 or Ru/PR_3

Many of these processes use carbon monoxide to introduce a carbonyl functionality, with the CO usually being generated as a mixture with H_2 (syn-gas) by steam reforming or partial oxidation of fossil fuel feedstocks (e.g. methane or coal).

1.1 Transition metals in homogeneous catalysis

1.1.1 Ligand co-ordination and activation

This thesis will deal with metal complexes of carbon monoxide and phosphines, so it is important to understand how these ligands coordinate to metals.

1.1.2 CO binding

Carbon monoxide has a lone pair on C in a σ-type orbital. This is able to donate electron density to the metal, shown in Figure 1.2 (a). However, CO is a weak base and thus forms weak donor bonds, such as with the Lewis acid, BH_3. A second interaction, between the vacant π* orbitals of CO and occupied metal d-orbitals, is known as back-bonding, as shown in Figure 1.2 (b). This back-bonding strengthens the M-C bond but weakens the C-O bond. The combination of σ-donation and π-back-donation is known as synergic bonding.

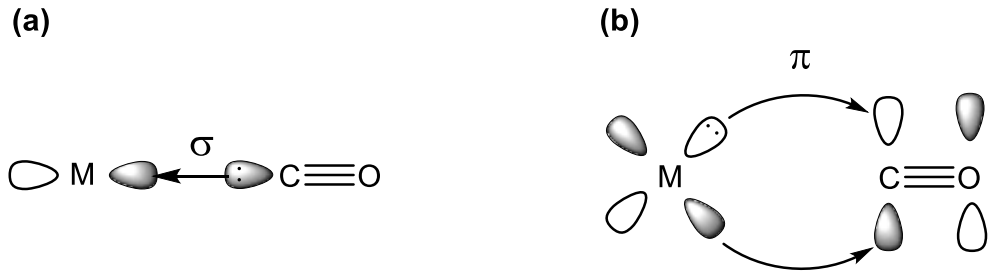

Figure 1.2: Interaction between metal and carbon monoxide orbitals in a metal-carbonyl complex

The effect of this back-donation into the CO π*-orbitals can be observed spectroscopically. Free CO has a ν(CO) at 2143 cm^{-1} whereas metal carbonyl complexes typically absorb in the region 2125-1850 cm^{-1}. The CO carbon is activated and as such is more electrophilic, making it more susceptible to attack by nucleophiles. This allows for migratory insertion reactions to occur.

1.1.3 Phosphines

Phosphine ligands have a lone pair which make them strong σ-donors, and good Lewis bases. They can also accept electron density from the metal into their P-C σ*antibonding orbitals. The energy of the σ*orbitals can be lowered through the use of electron withdrawing substituents such as fluorine. By changing the substituents on the phosphine, the steric and electronic properties can be manipulated.[17,18] The steric properties are usually quantified by the Tolman cone angle, measured 2.28 Å away from the phosphorus centre, as shown in Figure 1.3. The electronic properties are quantified by the Tolman electronic parameter, which is the frequency of the A_1 ν(CO) vibration mode of $[Ni(CO)_3L]$.

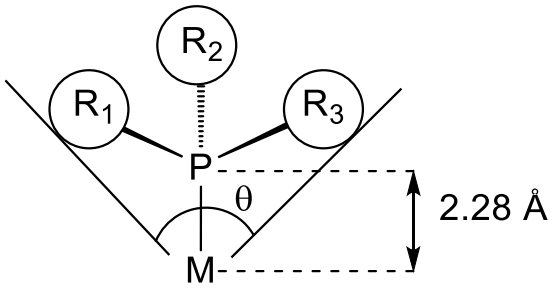

Figure 1.3: Tolman cone angle

This thesis is mostly concerned with diphosphine ligands. The use of diphosphine ligands in catalytic processes has been widely studied.[19–21] Diphosphine ligands bind more strongly than monodentate phosphines due to the chelate effect. Having two points of contact with a metal centre gives more restricted conformations. Many diphosphines are only able to coordinate *cis*, where two monophosphines would coordinate *trans* due to the trans effect.

Effects of the P-M-P bond angle, also known as the bite angle, have been widely studied, Figure 1.4. These arise from two factors. The first is the steric bite angle effect, which is concerned with steric interactions (ligand-ligand or ligand substrate) generated by changing the bite angle and keeping phosphorus constituents the same. The second effect is the

electronic bite angle effect which is associated with electronic changes in the metal centre when changing the bite angle.

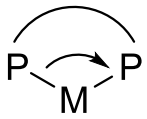

Figure 1.4: Diphosphine bite angle

1.2 Methanol carbonylation

1.2.1 Monsanto process

Acetic acid is a widely used commodity chemical with 12.9 million tonnes being produced in 2014.[22] It is used in the manufacture of vinyl acetate, acetic anhydride and cellulose acetate amongst other products. Its many derivatives are used across a broad range of sectors such as chemicals, printing/dyeing, rubber, electronics, pesticides and food processing.

A large portion of this acetic acid is made via methanol carbonylation. There are two widely used homogeneous methanol carbonylation reactions, the Monsanto and Cativa processes which use Rh and Ir catalysts respectively. These processes have been the subject of numerous reviews.[6,23,24] This section will summarise the key points in the Monsanto cycle.

Scheme 1.2 shows the catalytic cycle for the Monsanto process. There are two cycles, an organic (inner) and an organometallic (outer) cycle. The inner organic cycle is somewhat simplified as in the presence of acetic acid, methanol undergoes esterification to give methyl acetate, which is then activated by the HI promoter to form methyl iodide.

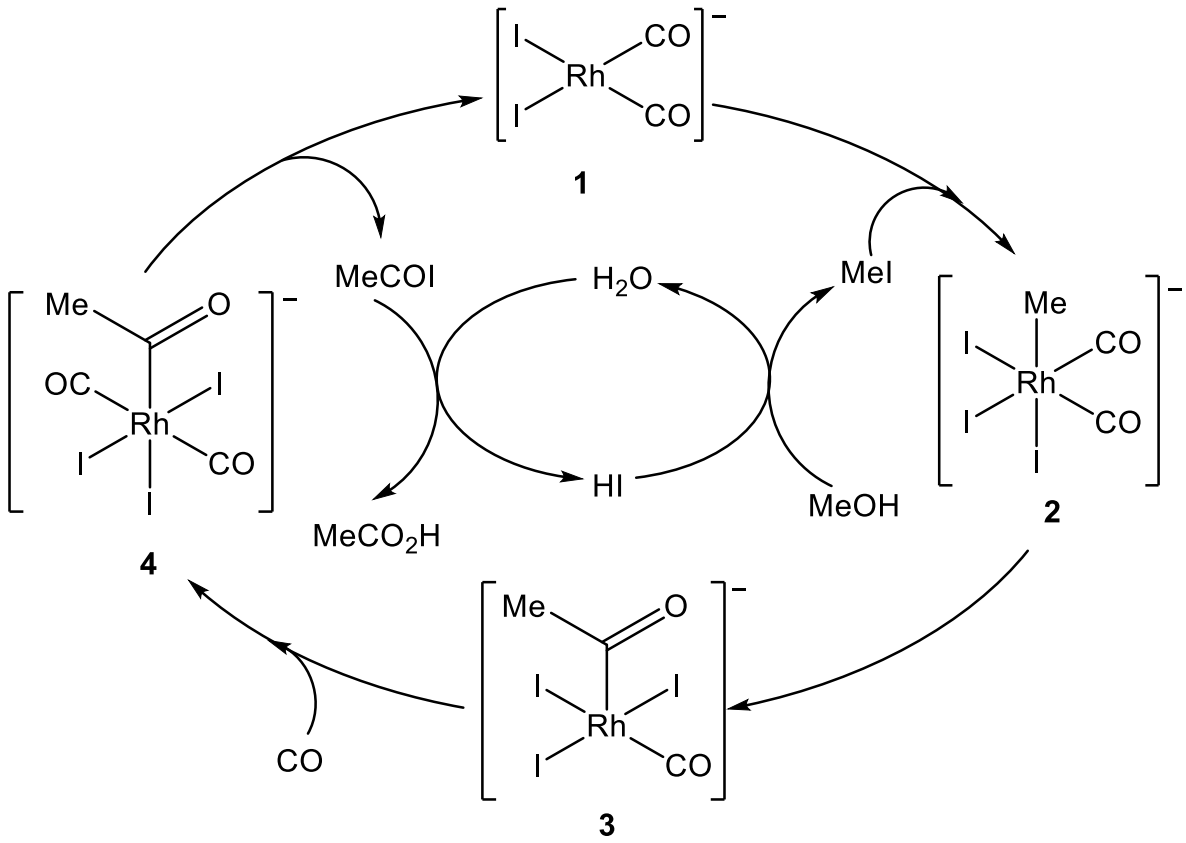

Scheme 1.2: Mechanism for methanol carbonylation in the Monsanto process

The active catalytic species in the outer organometallic cycle, is cis-$[Rh(CO)_2I_2]^-$ (**1**). This species undergoes oxidative addition of iodomethane to form $[Rh(Me)(CO)_2I_3]^-$ (**2**). This oxidative addition is the rate determining step under normal catalytic conditions, with the reaction being first order with respect to both MeI and **1**. The methyl complex $[Rh(Me)(CO)_2I_3]^-$ (**2**) is short lived and rapidly undergoes migratory insertion to form $[Rh(COMe)(CO)I_3]^-$ (**3**) followed by coordination of CO to give $[Rh(COMe)(CO)_2I_3]^-$ (**4**). Product formation is typically depicted as occurring by reductive elimination of acetyl iodide, which is hydrolysed to give acetic acid, and reformation of **1**. Jones proposed that reductive elimination is rate limiting below 8 wt. % water.[7] Kalck et al proposed an alternative route to product formation, which will be discussed further below. [25]

The water-gas shift reaction is a known side reaction which converts CO and H_2O and into CO_2 and H_2, shown in Scheme 1.3. Under certain conditions there can be a build-up of $[Rh(CO)_2I_4]^-$, a catalytically inactive species. This species can react with water and CO to complete the water-gas shift reaction and regenerate $[Rh(CO)_2I_2]^-$.

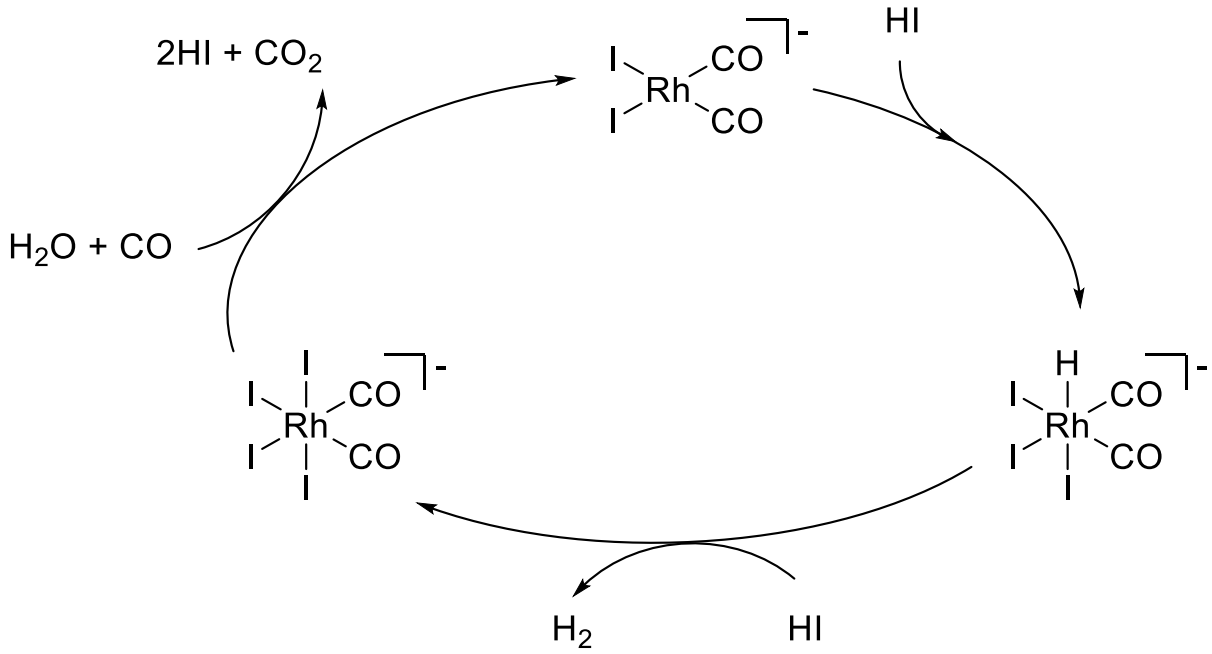

Scheme 1.3: Rhodium catalysed water-gas shift reaction.

Oxidative addition is the most studied step in the methanol carbonylation cycle. The activation parameters of oxidative addition were found to be comparable to those for the overall carbonylation process. [26,27] The large negative entropy of activation is indicative of S_N2 attack by the Rh(I) complex on MeI, with subsequent coordination of I^- to complete oxidative addition. Some studies have focused on the use of promoters to enhance the rate of oxidative addition. Hoechst-Celanese use an LiI promoter,[28] Sunley et al reported on the use of a ruthenium promoted system,[29] whereas Yuan et al have reported on the use of transition metal salts,[30] oxometallic acids[31] and phosphates[32]as promoters.

An analogous iridium based catalytic cycle for methanol carbonylation known as the Cativa process is also operated commercially in the production of acetic acid. More iridium is

required to achieve comparable activity to the rhodium-based system. However less than 8 wt.% of water is required compared to around 14-15 wt.% used for the Monsanto cycle.[23] The iridium-catalysed cycle is similar to the Monsanto cycle, but whereas the rhodium-based cycle consists solely of anionic species the iridium-catalysed cycle consists of anionic and neutral species.[33] The rate determining step in the Cativa cycle is methyl migration, in contrast to oxidative addition in the Monsanto cycle.

1.2.2 Eastman process

The Eastman Chemical Co. and BP Chemicals operate anhydrous processes for methyl acetate carbonylation, using LiI and quaternary ammonium iodide promoters respectively. The catalytic cycle for methyl acetate carbonylation is shown in Scheme 1.4.[34,35] The key organometallic species are the same as those observed for the Monsanto cycle, but there are several key differences. This cycle is operated under anhydrous conditions, so the water-gas shift side reaction does not occur. Lithium iodide is used as a promoter and forms LiOAc *in situ* both these species are proposed to act as promoters by generating catalyst species which are more active towards oxidative addition of methyl iodide.[36] Product formation is proposed to occur via reductive elimination of acetyl iodide, which reacts with acetate to give acetic anhydride.

The process operates under similar conditions with temperatures exceeding 175 ^{o}C and pressures in excess of 50 bar. Due to the anhydrous nature of this cycle some issues arise. The lack of cation to regenerate $[Rh(CO)_2I_2]^-$, the lack of reducing agent to prevent oxidation of $[Rh(CO)_2I_2]^-$ to $[Rh(CO)_2I_4]^-$ and slow regeneration of MeI. The addition of small amounts of H_2 helps prevent build-up of $[Rh(CO)_2I_4]^-$ providing a cation to help regenerate $[Rh(CO)_2I_2]^-$. The addition of LiI assisted with regeneration of methyl iodide by reaction with methyl acetate to form LiOAc and MeI. This acetate forms in situ rapidly reacts to form acetic anhydride.[37] The process is operated with large excess of LiI, which gives reaction rates that are first order in

MeI and Rh. It has been proposed that this excess of iodide generates $[Rh(CO)_2I_3]^{2-}$ which enhances the rate of oxidative addition of MeI.[38]

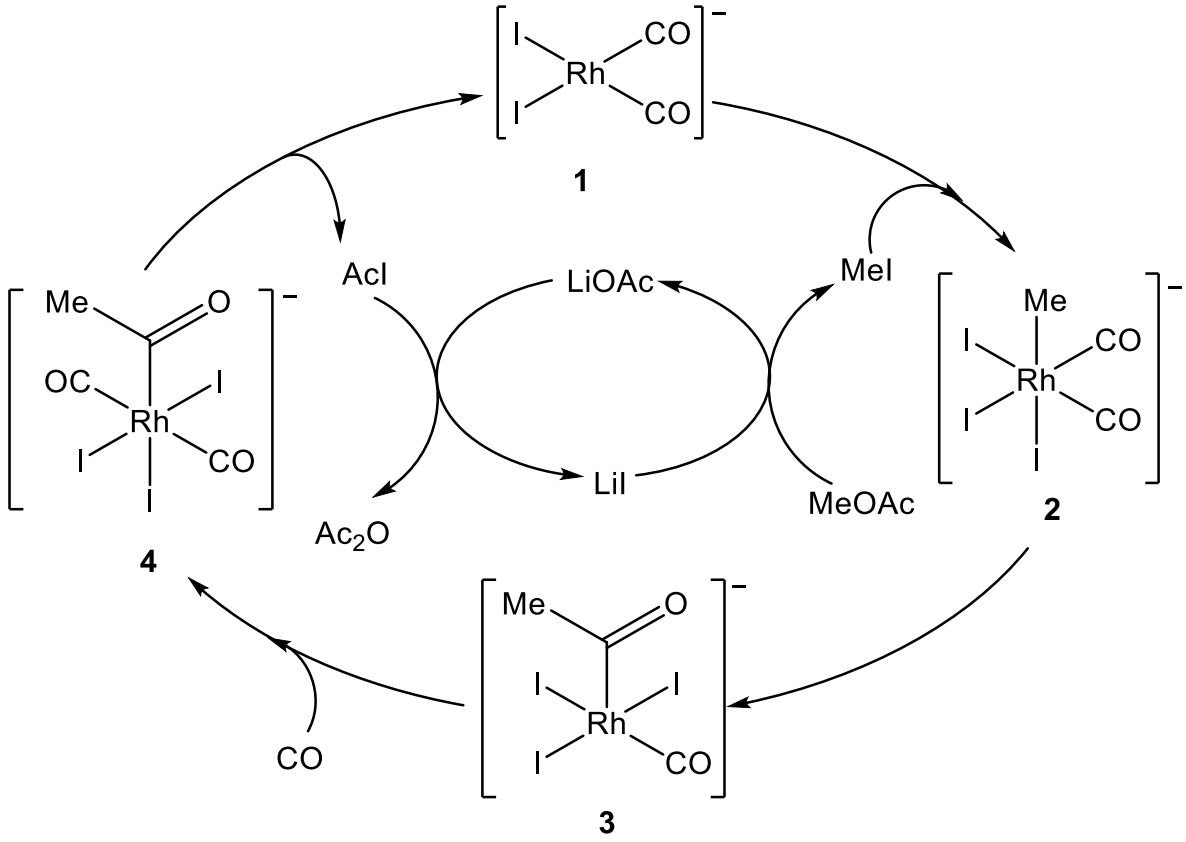

Scheme 1.4: Mechanism for methylacetate carbonylation in the Eastman process

Thermodynamically, the carbonylation of methyl acetate is less favourable than carbonylation of methanol. The calculated $\Delta G_{298\,K}$ and $\Delta H_{298\,K}$ are significantly less negative (ΔG_{298K} = -10.5 kJ mol^{-1} and ΔH_{298K} = -50.7 kJ mol^{-1}) compared to the corresponding values ($\Delta G_{298\,K}$ = -74.5 kJ mol^{-1} and $\Delta H_{298\,K}$ = -120.6 kJ mol^{-1}) for methanol carbonylation. As such the reaction operates at equilibrium, as opposed to completion in the Monsanto process.

1.2.3 Product formation in the Monsanto process

As previously discussed, the product formation mechanism is typically proposed to involve reductive elimination of acetyl iodide and subsequent hydrolysis to form acetic acid (Scheme

1.5, blue, I). Recently Kalck and co-workers proposed alternative routes of product formation in the Monsanto cycle, shown in Scheme 1.5.[25]

As previously mentioned, reductive elimination is rate limiting below 8 wt. % water.[7] Kalck studied the effect of water concentration on reductive elimination and found that below 5 wt. % only $[Rh(COMe)(CO)_2I_3]^-$ (**4**) is observed in solution, consistent with a change in rate determining step.[25,39] The potential role of water as a nucleophile (Scheme 1.5, green, II) was proposed.

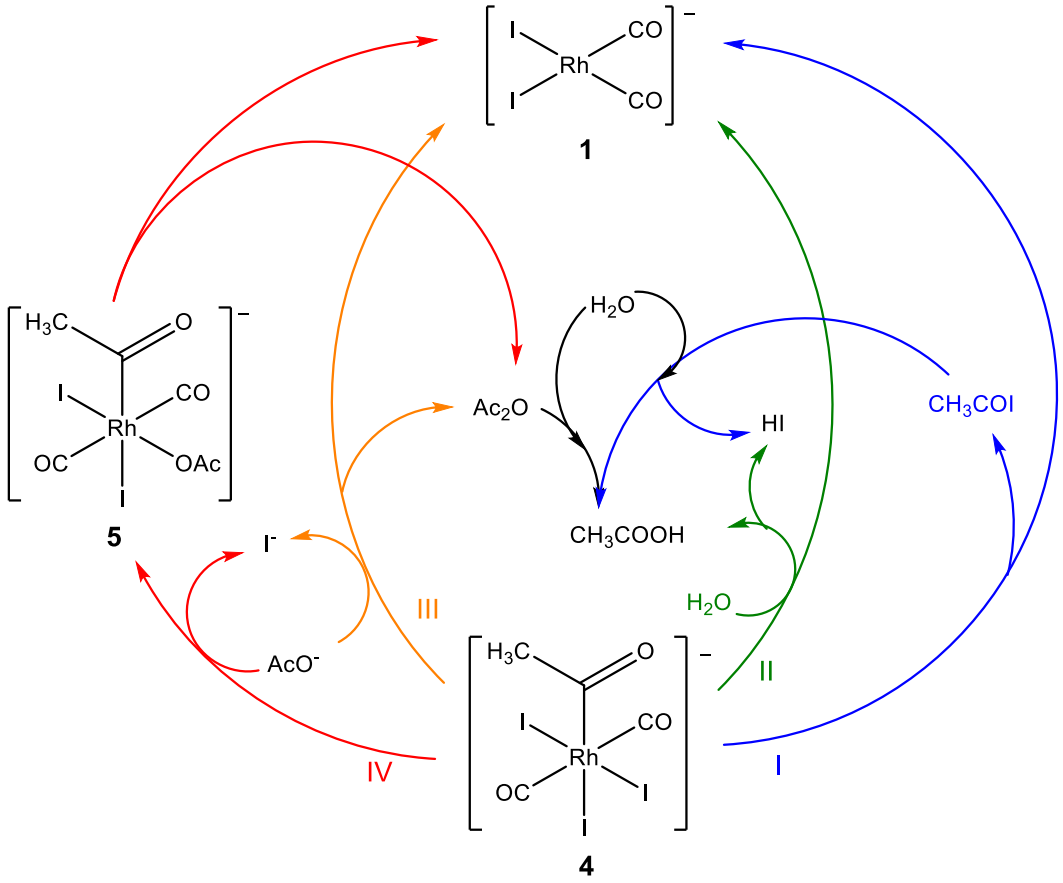

Scheme 1.5: Proposed routes of acetic acid formation from $[Rh(COMe)(CO)_2I_3]^-$ in methanol carbonylation adapted from Kalck[25]

The reductive elimination step, from $[Rh(COMe)(CO)_2I_3]^-$, was monitored by FTIR spectroscopy in the presence and absence of water. It was found that this reaction proceeded slowly regardless of water concentration. This was also supported by DFT calculations where attack of

water was exergonic (-21 kJ mol^{-1}) but had an energy barrier of 184 kJ mol^{-1}, making this pathway kinetically unlikely. It is known that the water concentration affects the equilibrium for formation of acetate in solution. Thus the involvement of an acetate anion was proposed by Kalck. Maitlis *et al*. observed that tetrabutylammonium acetate reacts rapidly with $[Rh(COMe)(CO)_2I_3]^-$ to produce $[Rh(CO)_2I_2]^-$ and acetic anhydride.[33] As such water content may affect the reductive elimination rate due to acetate concentration being dependent on water concentration.

Direct attack of acetate (Scheme 1.5, orange, III) on the acetyl ligand of **4** was investigated by DFT. However, whilst the reaction was indicated to be highly exergonic (-151 kJ mol^{-1}) a very high energy barrier to attack (234 kJ mol^{-1}) made this pathway unlikely. As such replacement of an iodide ligand by acetate to form $[Rh(COMe)(CO)_2(OAc)I_2]^-$ and subsequent reductive elimination of acetic anhydride was proposed (Scheme 1.5, red, IV). This acetic anhydride is then immediately hydrolysed to acetic acid. This mechanism was found to be exergonic (-192 kJ mol^{-1}) and has a barrier of 75 kJ mol^{-1} making this mechanism the most likely. Experimental evidence for an acetate coordinated intermediate was not observed by Kalck. However, in previous work in Sheffield, Lyons[40] conducted a stopped-flow IR spectroscopic investigation on the addition of $[Bu_4N][OAc]$ to $[Rh(COMe)(CO)_2I_3]^-$ and found evidence for formation of an acetate coordinated species $[Rh(COMe)(CO)_2I_2(OAc)]^-$.

1.2.4 Ligand effects in carbonylation reactions

Since oxidative addition of MeI has been found to be the rate limiting step, under industrial conditions, many studies have attempted to increase the nucleophilicity of the rhodium centre by introducing strongly donating ligands. The original communication from Monsanto included $[Rh(CO)(PPh_3)_2Cl]$ as a viable catalyst.[41] Cole-Hamilton *et al*. investigated the use of strongly electron-donating PEt_3 ligands.[42,43] However, these systems can lose activity due to phosphine

degradation forming by-products such as Et_3PI^+, Et_3PH^+, Et_3PMe and Et_3PO. The conventional Monsanto catalyst, $[Rh(CO)_2I_2]^-$ is reformed upon degradation of phosphine ligands.

Many diphosphine species in the presence of H_2 favour reductive carbonylation of methanol forming acetaldehyde and water ($MeOH + CO + H_2 \rightarrow MeCHO + H_2O$). Moloy and Wegman used diphosphine ligands of the type $Ar_2P(CH_2)_nPAr_2$ (n=2-4) to increase selectivity for reductive carbonylation of methanol to form acetaldehyde.[44,45] Using dppp ($Ph_2P(CH_2)_3PPh_2$) almost 90% selectivity for acetaldehyde was obtained. Diphosphine containing catalysts have been widely studied for methanol carbonylation; Scheme 1.6 shows a generic catalytic cycle observed with a Rh diphosphine species. The inorganic species in this cycle are neutral, in contrast to the anionic species in the "unmodified" Monsanto cycle (Scheme 1.2).

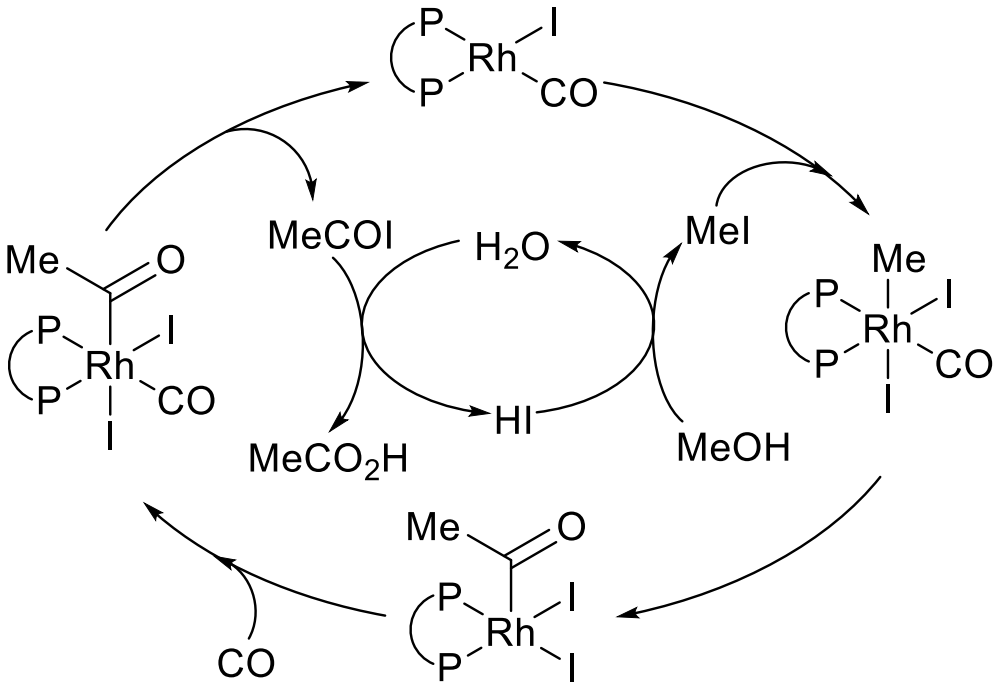

Scheme 1.6: Mechanism for Rh(P-P)(CO)I catalysed methanol carbonylation.

Clarke et al investigated H_2 tolerant catalysts based on diphosphine ligands,[46] in an attempt to reduce formation of by-products such as acetaldehyde and methane. It was found that dppb and dppx complexes [Rh(P-P)(CO)I] reacted readily with MeI to form $[Rh(P\text{-}P)(COMe)I_2]$ (ligands are shown in Scheme 1.7). However, the BINAP and dcpb complexes decomposed.

Only dppb was found to give a catalytic rate exceeding that of $[Rh(CO)_2I_2]^-$. Cole-Hamilton tested variants of C_4 diphosphines where the phenyl groups on dppx were replaced with ^tBu groups (dtbpx).[47] These were found to have higher reactivity than $[Rh(CO)_2I_2]^-$, however this phosphine was eventually quaternised and $[Rh(CO)_2I_2]^-$ formed.

A range of wide bite-angle diphosphines e.g. DPEphos, xantphos, Scheme 1.7, have also been utilised in methanol carbonylation.[21,48] It has been observed that both xantphos and DPEphos have a higher turn-over frequency than the unmodified $[Rh(CO)_2I_2]^-$ catalyst. Williams *et al* isolated and characterised the Rh(III) acetyl species $[Rh(xantphos)(COMe)I_2]$ and found that it adopts a pincer κ^3 - P,O,P coordination mode with oxygen trans to the acyl. This oxygen coordination enhances the nucleophilicity of the rhodium centre, Scheme 1.8.

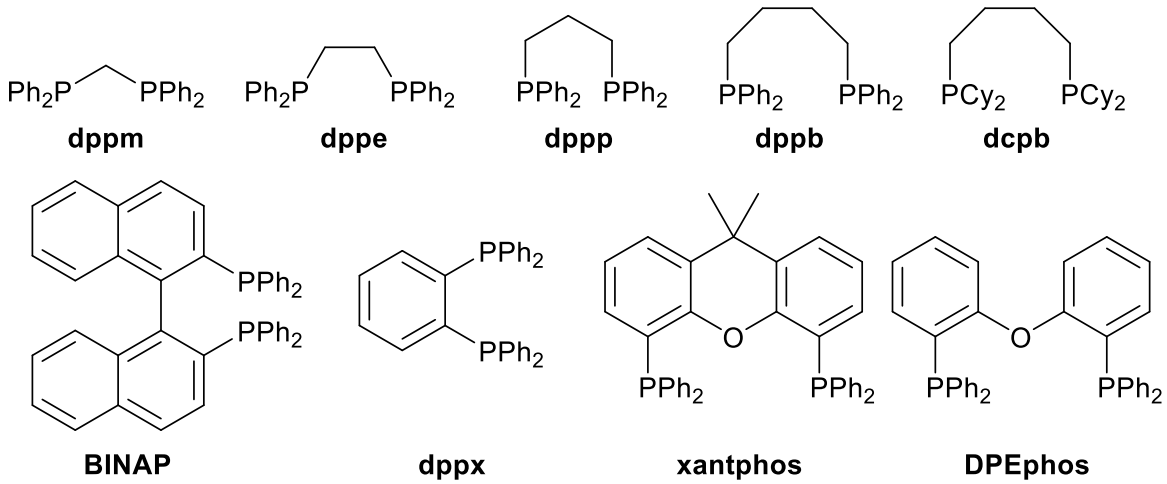

Scheme 1.7: Diphosphine ligands investigated in methanol carbonylation

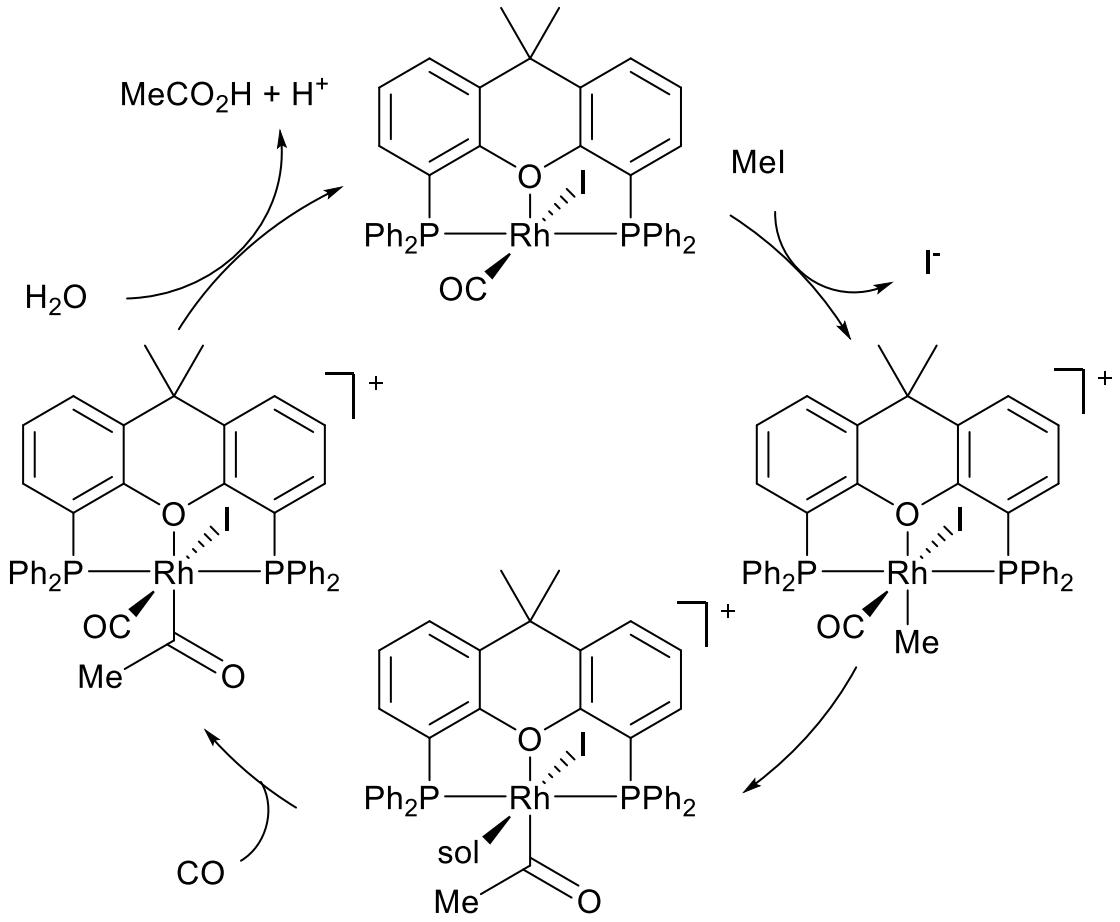

Scheme 1.8: Methanol carbonylation enhanced by xantphos ligand

Pringle et al. tested a range of unsymmetrical diphosphines of the type ($Ph_2P(CH_2)_2PAr_2$) where Ar= C_6H_5, 3-F-C_6H_4, 4-CF_3-C_6H_4 and 4-MeO-C_6H_4.[49] These systems gave high selectivity for acetic acid and had a higher activity than dppe, but were less active than $[Rh(CO)_2I_2]^-$.

A series of Rh(III) acetyl diphosphine species $[Rh(P\text{-}P)(COMe)I_2]$ have been isolated in studies of MeI addition to [Rh(P-P)(CO)I] by Haynes and co-workers,[48,50] Moloy et al[45] and Lamb et al.[46] Complexes with a cis chelating ligand have a distorted square-based pyramidal geometry, Scheme 1.9. The electron donating nature of these diphosphine ligands makes product formation steps slower, disfavouring reductive elimination.

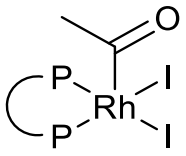

Scheme 1.9: Generic structure of [Rh(P-P)(COMe)I_2] with *cis* chelating diphosphine

The effects of other bidentate ligands on methanol carbonylation have also been studied. Lindner et al reviewed the application of a large range of difunctional ligands in a variety of catalytic processes.[51] Wegman found that dppeO, a derivative of dppe, gave good activity under mild conditions[52] (TOF 400 h^{-1}, 80°C, 3 bar CO). dppeO was found to be hemi-labile with [$Rh(CO)_2Cl(\kappa^1$-dppeO)] as the only species observed under catalytic conditions.

The effects of using dppmS as a ligand have been studied. Carbonylation rates up to 8.5 times faster than **1** were observed at 185°C, though activity was limited to around one hour.[53] Gonsalvi et al obtained evidence for the mechanism of [Rh(dppmS)(CO)I].[54] An MChem project in the Haynes group investigated oxidative addition of MeI to [Rh(dppmSe)(CO)I], the rate determining step for methanol carbonylation, and found a 74x rate increase relative to **1**.[55] An investigation of pyridyl imine and diimine complexes by Gonsalvi et al also showed a dramatic increase of up to 7000x in oxidative addition of MeI to [Rh(L-L)(CO)I], relative to **1**.[56] A series of iminophosphine complexes [Rh(PN-Ar)(CO)I] was also investigated by Best et al[50] and were found to catalyse methanol carbonylation up to 1.6 times the rate of the active catalytic species in the Monsanto process.

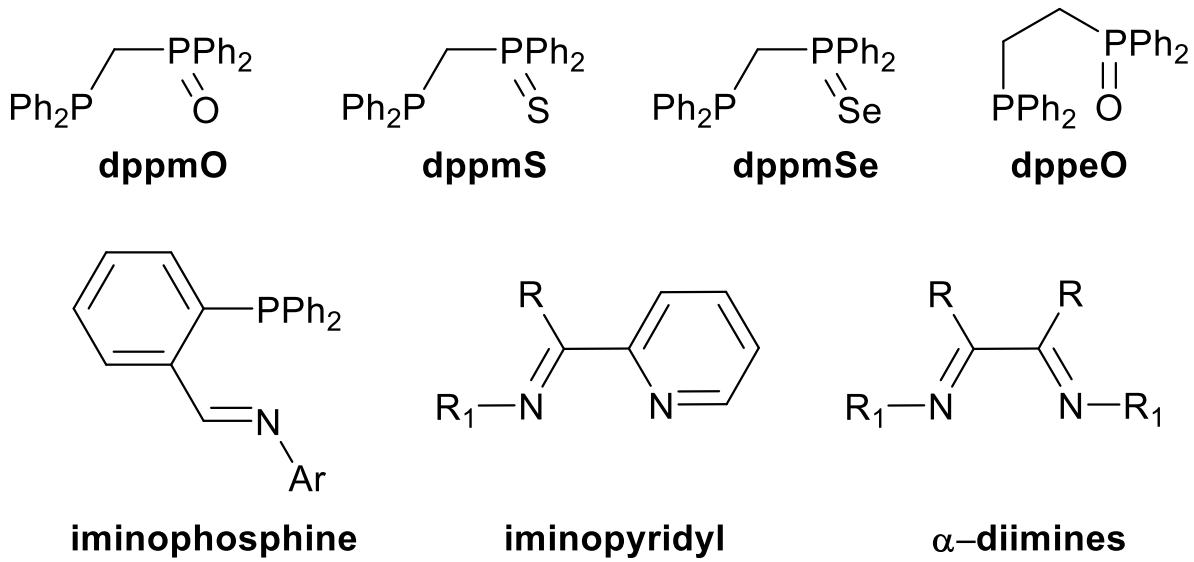

Scheme 1.10: Heterobifunctional ligands investigated in methanol carbonylation

This thesis will investigate the reactions of a range of [Rh(P-L)(COMe)I_2] acetyl complexes, previously isolated from the reaction of MeI and [Rh(P-L)(CO)I], with carboxylates to probe anhydride formation as proposed by Kalck,[25] as well as probing the reaction of these complexes with other nucleophiles.

1.2.5 Transition metal carboxylate acyl complexes

Some metal complexes with both acyl and carboxylate ligands (M(COR)(O_2CR)) are known. One method of synthesis of these complexes is substitution of a halide ligand by a carboxylate. Kovach et al isolated a [Rh(diimine)(COMe)$(TFA)_2(H_2O)$] complex as shown in Scheme 1.11.[57]

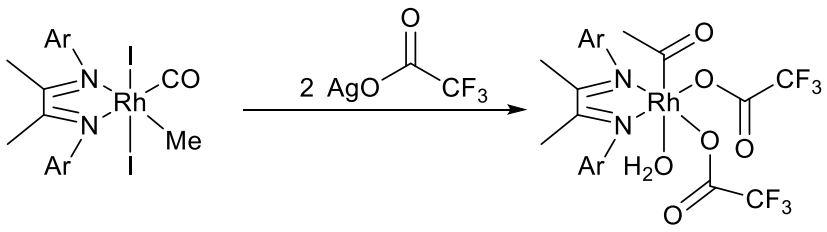

Scheme 1.11: Synthesis of a Rh(COMe)$(OCOCF_3)_2$ complex by Kovach et al.[57]

Matas et al[58] isolated a Ru complex with acyl carboxyl complexes by addition of NaO_2CR to a Ru acyl complex as shown in Scheme 1.12.

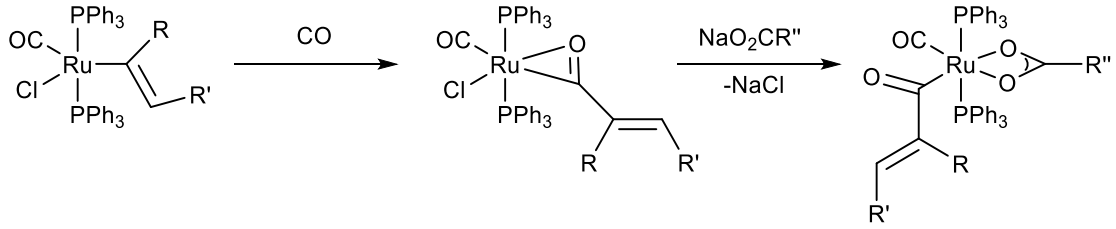

Scheme 1.12: Synthesis of Ru acyl carboxylate by Matas et al. [58]

Analogous Co[59] complexes have been made by addition of acetic acid to a cobalt hydride complex, Scheme 1.13, this was isolated and a crystal structure obtained.

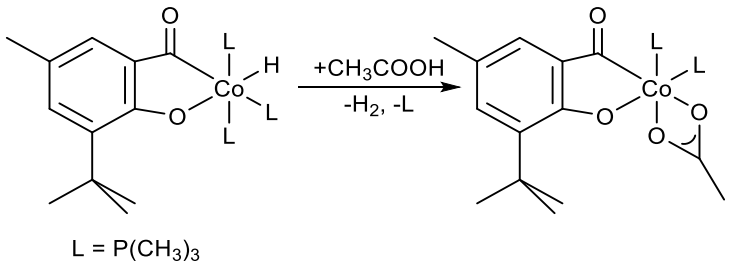

Scheme 1.13: Synthesis of Co carboxylate acyl complex by Klein et al. [59]

Hong *et al* synthesised a range of these complexes in reactions which proceeded by methyl migration, shown in Scheme 1.14. Crystal structures were obtained for several Ir(III)complexes with acetyl and carboxylates.[60]

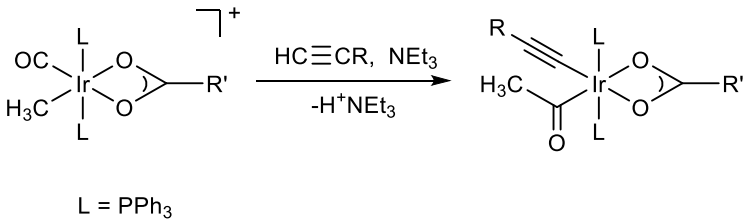

Scheme 1.14: Synthesis of Ir(O_2CR')(COMe) complex by Hong.[60]

Another route to formation of M(COR)(O_2CR) containing complexes is oxidative addition of an anhydride to a metal. Miller et al.[61] characterised the products from oxidative addition of

propionic anhydride to [Rh(PPh$_3$)$_3$Cl], Scheme 1.15. Coordination of carboxylates was assigned by carboxylate ν(CO$_2$) stretches as discussed by Deacon et al.[62]

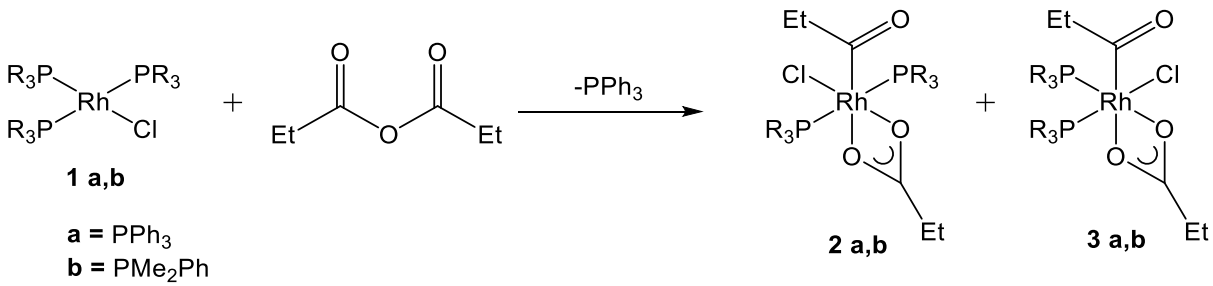

Scheme 1.15: Oxidative addition of propionic anhydride to [Rh(PPh$_3$)$_3$Cl] to form M(COR)(O$_2$CR).[62]

Oxidative addition of anhydrides to a range of square planar Ir(I) complexes has been observed by Blake[63], Scheme 1.16.

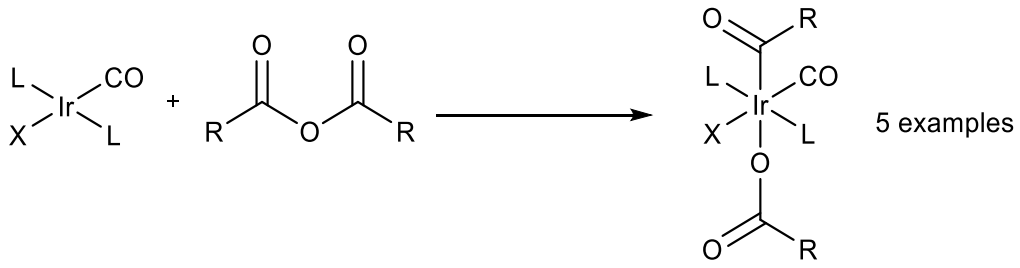

Scheme 1.16: Oxidative addition of anhydrides to Ir(I) square planar complexes by Blake[63]

Similar reactions have been observed for Ni(II) and Pt(II) by Sano et al.[64] for oxidative addition of succinic anhydride, shown in Scheme 1.17.

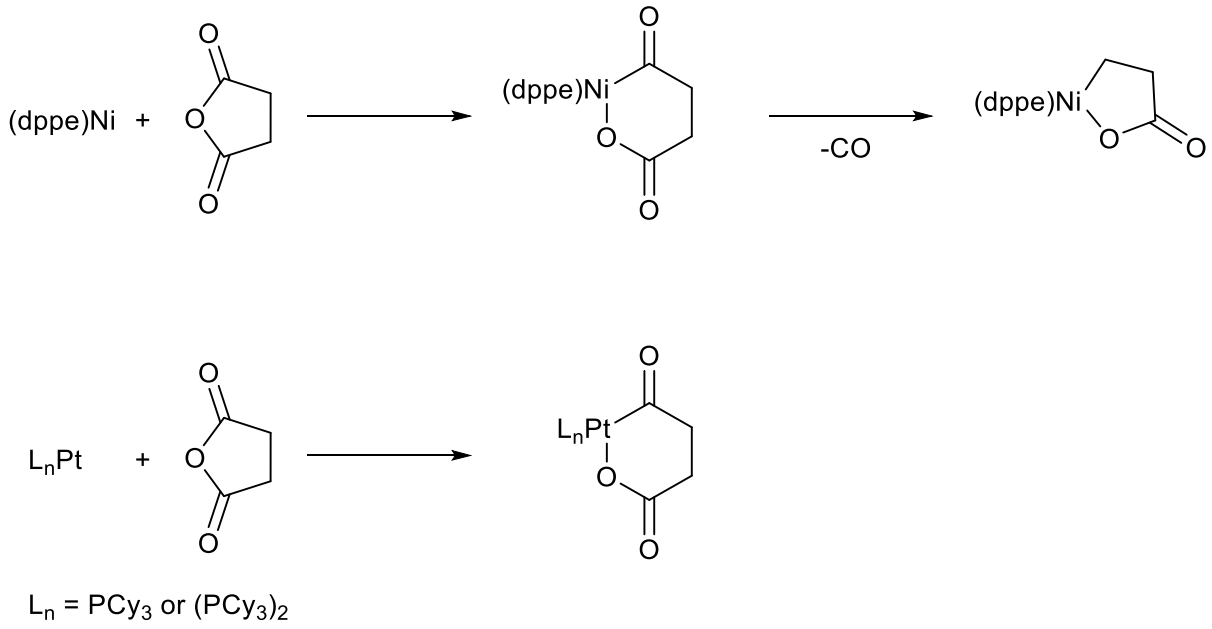

Scheme 1.17: Oxidative addition of succinic anhydrides to Ni and Pt complexes

The Ni acyl carboxylate complex underwent decarbonylation to give a Ni alkyl carboxylate complex. These M(COR)(O_2COR) complexes have been proposed as intermediates in decarbonylative dehydration reactions by Miller et al.[65] and Foglia et al.[66]

1.3 Decarbonylative dehydration

Linear alpha olefins (LAOs) are used in a wide range of synthesis and petrochemical processes.[67–69] Most LAOs are derived from fossil fuel sources. Naturally occurring long chain fatty acids are a possible renewable source of LAOs, [70,71] which can be accessed by transition metal catalysed decarbonylative dehydration, as shown in Scheme 1.18.

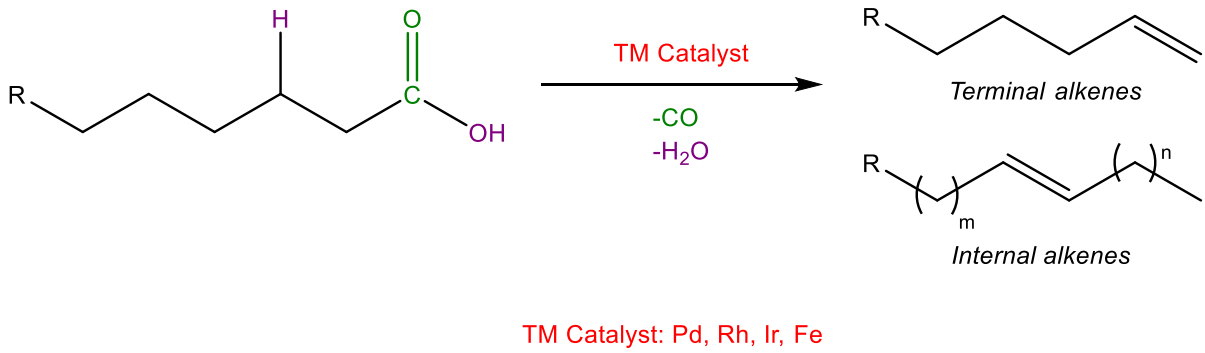

Scheme 1.18: Decarbonylative dehydration of a long chain fatty acid to alkene

Anhydrides are a commonly used additive in these processes and the catalytic cycle is thought to proceed via oxidative addition of anhydride to the metal, as shown in Scheme 1.19.[72]

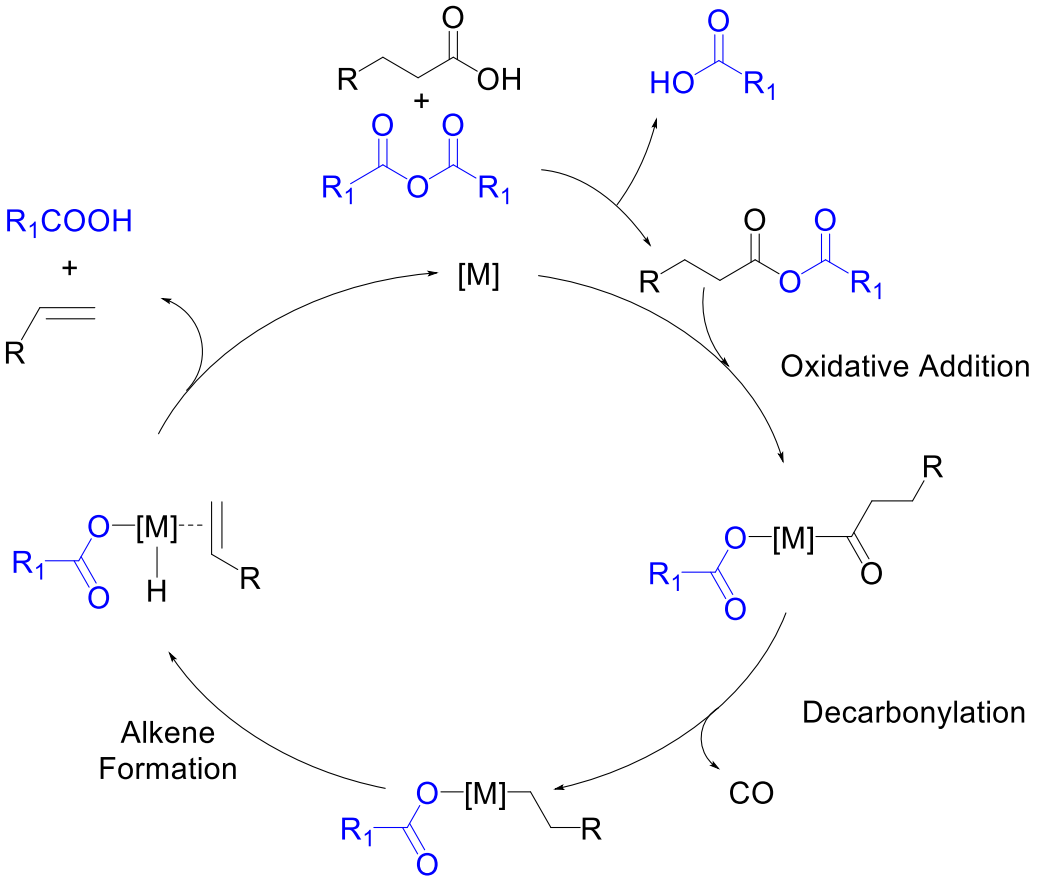

Scheme 1.19: General reaction scheme for decarbonylative dehydration of carboxylic acids to alkenes.

Formation of a mixed anhydride, which undergoes oxidative addition to the metal is proposed as the first step. The metal(acyl)(carboxylate) complex formed is analogous to that proposed by Kalck for product formation in the Monsanto cycle. This metal acyl then undergoes decarbonylation and β-hydride elimination to form the product and a carboxylic acid.

The catalysts used and mechanistic aspects of decarbonylative dehydration will be covered in detail in Chapter 6 of this thesis.

1.4 Project Aims

This project aims to investigate the proposed route of anhydride formation from the reactions of Rh(III) acetyl complexes with carboxylates, such as acetate, benzoate and trifluoroacetate. Two possible routes of reaction have been proposed, direct attack of carboxylate or coordination of carboxylate and subsequent reductive elimination of anhydride.

The reactions of a range of Rh(III) diphosphine complexes with carboxylates will be probed spectroscopically to determine the route of product formation (Chapter 3). Other Rh(III) acetyl complexes with heterobifunctional bidentate ligands will also be investigated (Chapter 4).

The reactivity of these Rh(III) acetyl complexes will be further probed in a study of their reactions with amines to form acetamides (Chapter 5).

Decarbonylative dehydration of fatty acids in principle provides a sustainable route to LAO formation. A range of new catalysts for decarbonylative dehydration will be tested. Mechanistic investigations will probe the incorporation of deuterium from $(CD_3CO)_2O$ into the alkene products and acylation of iminophosphine ligands, observed in a previous project in the group (Chapter 6).

1.5 References

(1) Jones, A.; McNicol, B. D. *J. Catal.* **1977**, *47*, 384–388.

(2) Dry, M. E. *J. Chem. Technol. Biotechnol.* **2002**, *77*, 43–50.

(3) Cecchin, G.; Morini, G.; Piemontesi, F. In *Kirk-Othmer Encyclopedia of Chemical Technology*; John Wiley & Sons, Inc.: Hoboken, NJ, USA, 2003.

(4) Gary, J. H.; Handwerk, G. E. *Petroleum refining : technology and economics*; 4th ed.; M. Dekker, 2001.

(5) Babich, I.; Moulijn, J. *Fuel* **2003**, *82*, 607–631.

(6) Haynes, A. In *Advances in Catalysis*; 2010; Vol. 53, pp. 1–45.

(7) Jones, J. *Platin. Met. Rev.* **2000**, *44*, 94–105.

(8) Zoeller, J. R.; Agreda, V. H.; Cook, S. L.; Lafferty, N. L.; Polichnowski, S. W.; Pond, D. M. *Catal. Today* **1992**, *13*, 73–91.

(9) Wolowska, J.; Eastham, G. R.; Heaton, B. T.; Iggo, J. A.; Jacob, C.; Whyman, R. *Chem. Commun.* **2002**, 2784–2785.

(10) Drent, E.; Van Broekhoven, J. A. M.; Doyle, M. J. *J. Organomet. Chem.* **1991**, *417*, 235–251.

(11) Brown, J. M.; Kent, A. G. *J. Chem. Soc. Perkin Trans. 2* **1987**, 1597.

(12) Evans, D.; Osborn, J. A.; Wilkinson, G. *J. Chem. Soc. A Inorganic, Phys. Theor.* **1968**, 3133.

(13) Hebrard, F.; Kalck, P. *Chem. Rev.* **2009**, *109*, 4272–4282.

(14) Keith, J. A.; Nielsen, R. J.; Oxgaard, J.; Goddard, W. A. *J. Am. Chem. Soc.* **2007**, *129*, 12342–12343.

(15) Crabtree, R. H.; Felkin, H.; Morris, G. E. *J. Organomet. Chem.* **1977**, *141*, 205–215.

(16) Osborn, J. A.; Jardine, F. H.; Young, J. F.; Wilkinson, G. *J. Chem. Soc. A Inorganic, Phys. Theor.* **1966**, 1711.

(17) Tolman, C. A. *J. Am. Chem. Soc.* **1970**, *92*, 2953–2956.

(18) Tolman, C. A. *J. Am. Chem. Soc.* **1970**, *92*, 2956–2965.

(19) Freixa, Z.; van Leeuwen, P. W. N. M.; Leeuwen, P. Van. *Dalton. Trans.* **2003**, 1890–1901.

(20) Kamer, P. C. J.; van Leeuwen, P. W. N. M.; Reek, J. N. H. *Acc. Chem. Res.* **2001**, *34*, 895–904.

(21) Deb, B.; Dutta, D. K. *J. Mol. Catal. A Chem.* **2010**, *326*, 21–28.

(22) Wakatsuki, K. *Acetyls Chain - World Market Overview*; 2015.

(23) Thomas, C.; Süss-Fink, G. *Coord. Chem. Rev.* **2003**, *243*, 125–142.

(24) Forster, D.; Singleton, T. C. *J. Mol. Catal.* **1982**, *17*, 299–314.

(25) Lassauque, N.; Davin, T.; Nguyen, D. H.; Adcock, R. J.; Coppel, Y.; Le Berre, C.; Serp, P.; Maron, L.; Kalck, P. *Inorg. Chem.* **2012**, *51*, 4–6.

(26) Fulford, A.; Hickey, C.; Maitlis, P. *J. Organomet. Chem.* **1990**, *398*, 311–323.

(27) Forster, D. *Ann. N. Y. Acad. Sci.* **1977**, *295*, 79–82.

(28) Haynes, A. *Carbonylation Reactions; Comprehensive Inorganic Chem II*; Elsevier Ltd., 2013; Vol. 6.

(29) Howard, M. J.; Sunley, G. J.; Poole, A. D.; Watt, R. J.; Sharma, B. K. *Stud. Surf. Sci. Catal.* **1999**, *121*, 61–68.

(30) Zhang, S.; Qian, Q.; Yuan, G. *Catal. Commun.* **2006**, *7*, 885–888.

(31) Qian, Q.; Zhang, S.; Yuan, G. *Catal. Commun.* **2007**, *8*, 483–487.

(32) Qian, Q.; Li, F.; Yuan, G. *Catal. Commun.* **2005**, *6*, 446–448.

(33) Maitlis, P.; Haynes, A. *J. Chem. Soc., Dalton Trans.* **1996**, 2187–2196.

(34) Schrod, M.; Luft, G.; Grobe, J. *J. Mol. Catal.* **1983**, *22*, 169–178.

(35) Zoeller, J. R. *Catal. Today* **2009**, *140*, 118–126.

(36) Smith, B. L.; Torrence, G. P.; Murphy, M. A.; Aguiló, A. *J. Mol. Catal.* **1987**, *39*, 115–136.

(37) Zoeller, J. R. *Org. Process Res. Dev.* **2016**, *20*, 1016–1025.

(38) Baker, E. C.; Hendriksen, D. E.; Eisenberg, R. *J. Am. Chem. Soc.* **1980**, *102*, 1020–1027.

(39) Nguyen, D. H.; Lassauque, N.; Vendier, L.; Mallet-Ladeira, S.; Le Berre, C.; Serp, P.; Kalck,

P. *Eur. J. Inorg. Chem.* **2014**, *2014*, 326–336.

(40) Lyons, J. R. Mechanistic Studies of Catalytic Carbonylation ; Reactivity of Iridium (III) and Rhodium (III) Complexes, PhD Thesis, University of Sheffield, 2008.

(41) Paulik, F.; Roth, J. *Chem. Commun.* **1968**, *11*, 2427.

(42) Rankin, J.; C. Benyei, A.; J. Cole-Hamilton, D.; D. Poole, A. *Chem. Commun.* **1997**, 1835.

(43) Rankin, J.; Benyei, A. C.; Poole, A. D.; Cole-Hamilton, D. J. *J. Chem. Soc. Dalton. Trans.* **1999**, *2*, 3771–3782.

(44) Moloy, K. G.; Wegman, R. W. *Organometallics* **1989**, *8*, 2883–2892.

(45) Moloy, K. G.; Petersen, J. L. *Organometallics* **1995**, *14*, 2931–2936.

(46) Lamb, G.; Clarke, M.; Slawin, A. M. Z.; Williams, B.; Key, L.; Roukoss, C.; Fiddy, S.; de Mallmann, A.; Rendón, N.; Basset, J.-M.; Kuntz, E.; Copéret, C. *Dalton Trans.* **2007**, 5582–5589.

(47) Jimenez-Rodriguez, C.; Pogorzelec, P. J.; Eastham, G. R.; Slawin, A. M. Z.; Cole-Hamilton, D. J. *Dalton. Trans.* **2007**, 4160.

(48) Williams, G. L.; Parks, C. M.; Smith, C. R.; Adams, H.; Haynes, A.; Meijer, A. J. H. M.; Sunley, G. J.; Gaemers, S. *Organometallics* **2011**, *30*, 6166–6179.

(49) Carraz, C.-A.; Orpen, A. G.; Ellis, D. D.; Pringle, P. G.; Ditzel, E. J.; Sunley, G. J. *Chem. Commun.* **2000**, 1277–1278.

(50) Best, J.; Wilson, J. M.; Adams, H.; Gonsalvi, L.; Peruzzini, M.; Haynes, A. *Organometallics* **2007**, *26*, 1960–1965.

(51) Bader, A.; Lindner, E. *Coord. Chem. Rev.* **1991**, *108*, 27–110.

(52) Wegman, R. W.; Abatjoglou, A. G.; Harrison, A. M. *J. Chem. Soc. Chem. Commun.* **1987**, 1891.

(53) Baker, M. J.; Giles, M. F.; Orpen, A. G.; Taylora, M. J.; Watta, R. J. *J. Chem. Soc. Chem. Commun.* **1995**, *1*, 197–198.

(54) Gonsalvi, L.; Adams, H.; Sunley, G. J.; Ditzel, E.; Haynes, A. *J. Am. Chem. Soc.* **1999**, *121*, 11233–11234.

(55) R. Rose, MChem Thesis, University of Sheffield, 2009.

(56) Gonsalvi, L.; Gaunt, J. A.; Adams, H.; Castro, A.; Sunley, G. J.; Haynes, A. *Organometallics* **2003**, *22*, 1047–1054.

(57) Kovach, J.; Brennessel, W. W.; Jones, W. D. *J. Organomet. Chem.* **2015**, *793*, 192–199.

(58) Matas, L.; Muniente, J.; Ros, J.; Alvarez-Larena, Á.; F. Piniella, J. *Inorg. Chem. Commun.* **1999**, *2*, 364–367.

(59) Klein, H.-F.; Haller, S.; Sun, H.; Li, X.; Jung, T.; Rohr, C.; Florke, U.; Haupt, H.-J. *Zeitschrift für Naturforsch. B* **2014**, *53*, 587–598.

(60) Chin, C. S.; Lee, H.; Lee, M. K.; Noh, S.; Eum, M.-S.; Hong, S. *J. Organomet. Chem.* **2005**, *690*, 1306–1313.

(61) Miller, J. A.; Nelson, J. A. *Organometallics* **1991**, *10*, 2958–2961.

(62) Deacon, G.; Phillips, R. *Coord. Chem. Rev.* **1980**, *33*, 227–250.

(63) Blake, D.; Shields, S.; Wyman, L. *Inorg. Chem.* **1974**, *13*, 1595–1600.

(64) Sano, K.; Yamamoto, T.; Yamamoto, A. *Bull. Chem. Soc. …* **1984**, *57*, 2741–2747.

(65) Miller, J. A.; Nelson, J. A.; Byrne, M. P. *J. Org. Chem.* **1993**, *58*, 18–20.

(66) Foglia, T. A.; Barr, P. A. *J. Am. Oil Chem. Soc.* **1976**, *53*, 737–741.

(67) Franke, R.; Selent, D.; Börner, A. *Chem. Rev.* **2012**, *112*, 5675–5732.

(68) Imokawa, G.; Tsutsumi, H.; Kurosaki, T.; Hayashi, M.; Kakuse, J. Detergent composition. US4139485A, February 22, 1977.

(69) Lengyel, S. P. Mixed ethoxylated alcohol/ethoxy sulfate surfactants and synthetic detergents incorporating the same. US4464292A, January 2, 1981.

(70) Petrus, L.; Noordermeer, M. A. *Green Chem.* **2006**, *8*, 861.

(71) Miao, X.; Wu, Q. *Bioresour. Technol.* **2006**, *97*, 841–846.

(72) Eliasson, S.; Chatterjee, A.; Occhipinti, G.; Jensen, V. *Inorganics* **2017**, *5*, 87.

Chapter 2

Experimental

2.1 Solvents and reagents

The solvents dichloromethane, acetonitrile and hexane were obtained from the departmental Grubbs dry solvent system, in which solvents are vigorously degassed before being passed through two sequential purification columns. Firstly, an activated alumina column removes protic contaminants, followed by a supported copper catalyst that removes trace oxygen from hydrocarbons.[1] The system is fitted with a Schlenk manifold that allows solvents to be collected and stored under a nitrogen atmosphere.

Methanol was purified by distillation after reflux over magnesium methoxide under a nitrogen atmosphere. Rhodium trichloride hydrate ($RhCl_3.xH_2O$) and iridium trichloride hydrate ($IrCl_3.xH_2O$) were supplied by Precious Metals Online, Monash University LPO, Melbourne, Australia.

Diphosphines bis(diphenylphosphino)methane (dppm), 1,2-bis(diphenylphosphino)ethane (dppe), 1,3-bis(diphenylphosphino)propane (dppp), 1,4-bis(diphenylphosphino)butane (dppb), 4,5-Bis(diphenylphosphino)-9,9'-dimethylxanthene (xantphos) and oxydi-2,1-phenylene bis(diphenylphosphine) (DPEphos), and ligand precursors 2-(diphenylphosphino)benzaldehyde, 2-acetylpyridine, 2-pyridinecarboxaldehyde, anilines, selenium and sulphur were supplied by Sigma-Aldrich or Alfa Aesar and used without further purification. All other standard reagents were supplied by Sigma-Aldrich and used as supplied, unless otherwise stated. Argon and carbon monoxide (99.9 % CP grade) gas was supplied by BOC.

2.2 Schlenk techniques

Due to the air sensitive nature of many rhodium/iridium complexes and phosphines all reactions were performed under inert conditions, in flame dried glassware using standard Schlenk techniques, unless otherwise stated. Solids were typically deposited in side-arm vessels and placed under vacuum before refilling with an argon, nitrogen or carbon monoxide

atmosphere. This was performed a minimum of three times. Syringes were degassed by filling with argon, nitrogen or carbon monoxide from a degassed vessel and expelling outside of the flask. This process was repeated a minimum of three times.

2.3 Instrumentation

NMR spectra were recorded on Bruker AV1400, AV3-400 or AC-250 spectrometers fitted with a Bruker B-ACS60 automated sample changer and analysed using MestReNova. Infrared solution spectra were recorded using a Nicolet Magna-IR 560 Spectrometer operated by Omnic software. Standard solution cells for IR spectroscopy had CaF_2 windows and a path length of 0.5 mm. Attenuated Total Reflectance Infrared spectra were recorded on a Perkin Elmer Spectrum Two FT-IR Spectrometer.

2.4 DFT Methods

All calculations were performed using the Gaussian 09 computational package on local high-performance computer *Jupiter*.

2.4.1 *Jupiter* high performance computer

Jupiter is a local Linux based high performance computer (HPC) cluster located in the theoretical chemistry group in the chemistry department at the University of Sheffield. The operating system is a 64-bit CentOS, with the Sun Grid Engine (SGE) utilised for job scheduling. In total the cluster contains 460 CPUs.

2.4.2 Gaussian 09 computational package

Gaussian is a quantum-chemical modelling program.[2] Each revision was compiled using the Portland compiler using Gaussian supplied BLAS libraries on the EMT64 architecture. The results from Gaussian are visualised using a GUI program, GaussView.

2.4.3 Computational methods

All calculations were performed at the DFT level of theory using B3LYP functional unless otherwise stated. The metal atoms were generally described using a Stuttgart/Dresden effective core potential (SDD). A mixed basis set was used consisting of SDD on the metal and 6-311G(d,p) on all other atoms. Reactants were optimised without symmetry constraints.

Frequency calculations were carried out on all optimised structures to confirm them as energy minima. Solvent effects were taken into account using the default PCM model implemented through Gaussian 09 using dichloromethane as solvent.

2.5 X-ray Crystallography

Crystallographic structures were obtained through the departmental service. Crystallographic data were collected on a Bruker Smart Apex II CCD area detector with Oxford Cryosystems low-temperature system (100 K) using Mo Kα radiation (λ = 0.71073 Å). The structures were solved by direct methods and refined by full-matrix least squares methods on F^2. Hydrogen atoms were placed geometrically and refined using a riding model (including torsional freedom for methyl groups). Complex scattering factors were taken from the SHELXTL program package. Full listings of crystallographic data are given in the Appendix.

2.6 Synthesis of literature reported organic compounds

Acetyl benzoic anhydride,[3] myristoyl iodide[4] and 2,2-dimethyl-5-propyl-1,3-dioxane-4,6-dione[5] were synthesised by literature methods. Characterisation obtained was consistent with reported literature data.

2.7 Synthesis of literature reported Rh and Ir complexes

The complexes $[Rh(CO)_2Cl]_2$,[6] $[Rh(CO)_2I]_2$, $[Rh(COMe)(NCMe)(CO)I_2]_2$,[7] $[Rh(CO)_2I_2][NBu_4]$,[8] $[Rh(CO)_2I_4][NBu_4]$,[9] $[Rh(COMe)(CO)I_3]_2[NBu_4]_2$,[10] $[Cp^*RhCl_2]_2$,[11] $Cp^*Rh(CO)_2$,[12] $[Rh(acac)(CO)_2]$,[13] $[Rh(acac)(CO)(PPh_3)]$,[12] $[Ir(COD)Cl]_2$,[14] $[Ir(CO)_2I_2][NBu_4]$ [15] were all synthesised by literature methods. Characterisation was in accordance with reported literature data.

2.8 Synthesis of literature reported ligands

The iminophosphine ligands PN-*o*Anis, PN-Me_2Ph, PN-$^i Pr_2$Ph, PN-Mes[16,17] and pyridyl imine ligands[18] were synthesised by literature methods. Characterisation was in accordance with reported literature data.

2.8.1 Synthesis of bis(diphenylphosphino)methane monosulfide (dppmS)

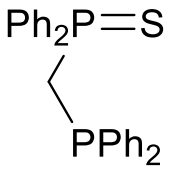

Bis(diphenylphosphino)methane monosulfide was prepared in the method described by Lobana.[19] Bis-(diphenylphosphino)methane (2.31 g, 6.0 mmol) was dissolved in toluene (30 mL) under N_2 in a two-neck round-bottom flask. The solution was cooled in an ice bath. Elemental sulfur (0.224 g, 7.0 mmol) was dissolved in toluene (30 mL) and added over 30 minutes with an addition funnel. The solution was stirred for 2 hours at 0 ^oC. Solvent was

removed *in vacuo* and the resultant solid dissolved in the minimum volume CH_2Cl_2 and products were separated by column chromatography using a mixture of 7:3 ethyl acetate: hexane to give dppmS (1.648 g, 4.0 mmol, 66 % yield) as a white solid.

^{1}H NMR δ/ppm ($CDCl_3$): 7.91 – 7.72 (m, 4H), 7.54 – 7.17 (m, 16H), 3.36 (dd, 2H, *J* = 12.7, 0.9 Hz).

^{31}P NMR δ/ppm ($CDCl_3$): 40.6 (d, J_{P-P} = 76 Hz), -27.8 (d, J_{P-P} = 76 Hz)

2.8.2 Synthesis of bis(diphenylphosphino)methane monoselenide (dppmSe)

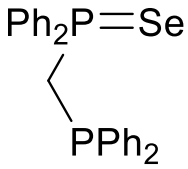

Bis(diphenylphosphino)methane monoselenide was synthesised using a modified method by Bond[20]. Bis(diphenylphosphino)methane (0.425 g, 1.11 mmol) and grey selenium (0.089 g, 1.12 mmol) were mixed and THF (10 mL) added giving a grey solution, which rapidly turned colourless upon stirring. The solution was stirred for 3 hours and solvent removed *in vacuo.* The resultant solid was recrystallised from CH_2Cl_2 and hexane giving dppmSe (0.28 g, 0.60 mmol, 54% yield) as an off-white solid.

^{1}H NMR δ/ppm ($CDCl_3$): 7.97 – 7.67 (m, 4H), 7.55 – 7.10 (m, 16H), 3.52 (d, 2H, *J* = 12.9 Hz)

^{31}P NMR δ/ppm ($CDCl_3$): -27.1 (d, J_{P-P} = 83 Hz), 30.7d (d, J_{P-P} = 83 Hz, J_{P-Se} = 727 Hz, 7.63 % ^{77}Se abundance)

2.9 Synthesis of Rh(I) complexes

2.9.1 Synthesis of Rh(I) iminophosphine complexes

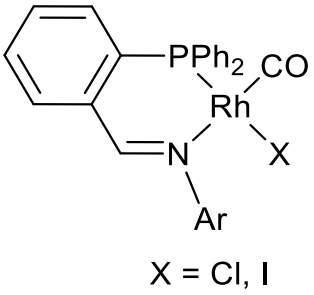

Rh(I) iminophosphines complexes were prepared in a method adapted from Best *et al*.[21] A solution of $[Rh(CO)_2I]_2$ or $[Rh(CO)_2Cl]_2$ and 2 equivalents of PN-ligand in CH_2Cl_2 (5 mL) was stirred under N_2 in CH_2Cl_2 (5 mL). A colour change from red to orange occurred after ~10 minutes. The solution was stirred for 2 hours, after which the solvent was removed *in vacuo* and the resultant solid washed with pentane (30 mL) and toluene (50 mL). An orange solid remained, which was recrystallised from CH_2Cl_2 and hexane yielding [Rh(PN)(CO)X] as an orange/red powder.

2.9.2 Synthesis of [Rh(PN-$^{i}Pr_2Ph$)(CO)Cl]

[Rh(PN-$^{i}Pr_2Ph$)(CO)Cl] was prepared according to the method in section 2.9.1 using $[Rh(CO)_2Cl]_2$ (0.122 g, mmol) and PN -2,6-$^{i}Pr_2Ph$ (0.119 g, 0.265 mmol) to give [Rh(PN-$^{i}Pr_2Ph$)(CO)Cl] as an orange powder 0.206 g (0.242 mmol, 93 %).

IR: ν(CO) (CH_2Cl_2): 2010 cm^{-1}

^{1}H NMR δ/ppm ($CDCl_3$): 8.09 (d, 1H, J = 2.5 Hz), 7.59 – 7.40 (m, 12H), 7.26 – 6.99 (m, 5H), 3.14 – 2.97 (sept, 2H), 1.33 (d, 6H, J = 6.8 Hz), 0.74 (d, 6H, *J* = 6.8 Hz)

^{31}P NMR δ/ppm ($CDCl_3$): 43.15 (d, J_{Rh-P} = 166.3 Hz)

2.9.3 Synthesis of [Rh(PN-Me_2Ph)(CO)Cl]

[Rh(PN-Me_2Ph)(CO)Cl] was prepared according to the method in section 2.9.1 using $[Rh(CO)_2Cl]_2$ (0.163 g, 0.420 mmol) and PN -2,6-Me_2Ph (0.332 g, 0.845 mmol) to give [Rh(PN-Me_2Ph)(CO)Cl] as an orange powder 0.461 g (0.823 mmol, 98 %).

IR: ν(CO) (CH_2Cl_2): 2009 cm^{-1}

^{1}H NMR δ/ppm ($CDCl_3$): 8.01 (d, 1H, *J* = 2.4 Hz), 7.73 – 7.64 (m, 1H), 7.59 (m, 2H, arom), 7.56 – 7.42 (m, 10H), 7.10 – 6.98 (m, 4H), 2.10 (s, 6H).

^{31}P NMR δ/ppm ($CDCl_3$): 43.96 (d, J_{Rh-P} = 166.5 Hz)

2.9.4 Synthesis of [Rh(PN-Mes)(CO)Cl]

[Rh(PN-Mes)(CO)Cl] was prepared according to the method in section 2.9.1 using $[Rh(CO)_2Cl]_2$ (0.112 g, 0.288 mmol) and PN -2,4,6-Me_3Ph (0.244, 0.599 mmol) to give [Rh(PN-Mes)(CO)Cl] as an orange powder (0.315 g, 0.549 mmol, 95 % yield).

IR: ν(CO) (CH_2Cl_2): 2008 cm^{-1}

^{1}H NMR δ/ppm ($CDCl_3$): 7.93 (d, 1H, J = 2.3 Hz), 7.73 – 6.79 (m, 16H), 2.29 (s, 3H), 2.06 (s, 6H).

^{31}P NMR δ/ppm ($CDCl_3$): 40.95 (d, J_{Rh-P} = 170.7 Hz)

2.9.5 Synthesis of [Rh(PN-Et_2Ph)(CO)Cl]

[Rh(PN-Et_2Ph)(CO)Cl] was prepared according to the method in section 2.9.1 using $[Rh(CO)_2Cl]_2$ (0.071 g, 0.183 mmol) and PN -2,6-Me_2Ph (0.019 g, 0.446 mmol) to give [Rh(PN-Et_2Ph)(CO)Cl] as an orange powder (0.165 g, 0.281 mmol, 77 % yield).

IR: ν(CO) (CH_2Cl_2): 2008 cm^{-1}

^{1}H NMR δ/ppm ($CDCl_3$): δ 8.05 (d, 1H, *J* = 2.5 Hz), 7.75 – 7.41 (m, 12H), 7.18 (m), 7.14 – 7.01 (m, 5H), 2.79 – 2.54 (m, 2H), 2.41 (m, 2H), 0.94 (t, 6H, *J* = 7.5 Hz)

^{31}P NMR δ/ppm ($CDCl_3$): δ 43.36 (d, J_{Rh-P} = 166.7 Hz)

2.9.6 Synthesis of [Rh(PN-*o*Anis)(CO)I]

[Rh(PN-oAnis)(CO)I] was prepared according to the standard method using $[Rh(CO)_2I]_2$ (0.157 g 0.275 mmol) and PN-oAnis ligand (0.226 g, 0.572 mmol) yielding [Rh(PN-oAnis)(CO)I] as an orange/red powder (0.209 g, 0.319 mmol, 58 % yield).

IR: ν(CO) (CH_2Cl_2): 1995 cm^{-1}

^{1}H NMR δ/ppm ($CDCl_3$): 7.99 (d, 1H, J = 2.1 Hz), 6.82-7.60 (m, 18H, Ar H),

3.76 (s, 3H, OMe)

^{31}P NMR δ/ppm ($CDCl_3$): 44.5 (d, J_{Rh-P} = 171.0 Hz)

2.9.7 Synthesis of [Rh(dipiep)(CO)I]

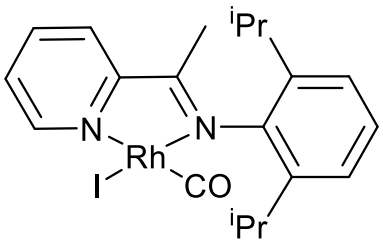

[Rh(dipiep)(CO)I] was synthesised in a modified method as used by Gaunt et al.[22] $[Rh(CO)_2I]_2$ (0.100 g, 0.29 mmol) was added to dipiep (0.133 g, 0.59 mmol) under N_2 atmosphere in 5 mL toluene. After 3 hours formation of dark purple crystals occurred. Once the solution was cooled these crystals were collected by filtration to yield [Rh(dipiep)(CO)I] (0.200 g, 0.45 mmol, 76 % yield).

IR: ν(CO) (CH_2Cl_2): 1987 cm^{-1}

^{1}H NMR δ/ppm ($CDCl_3$): 9.77 (m, 1H), 7.99 (m, 1H), 7.78 (m, 1H), 7.69 (m, 1H), 7.13-7.28 m (3H), 3.23 (sept, 1H, *J* = 7 Hz), 1.69 (s, 3H, N=C**CH_3**), 1.31 (d, 6H, *J* = 7 Hz), 1.06 (d, 6H, *J* = 7 Hz)

2.9.8 Synthesis of [Rh(dipimp)(CO)I]

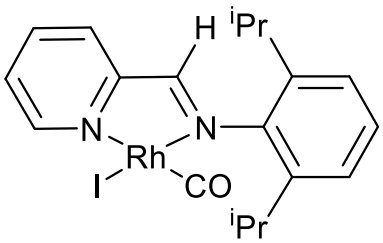

[Rh(dipimp)(CO)I] was prepared in a modified method as used by Gaunt et al.[22] $[Rh(CO)_2I]_2$ (0.102 g, 0.261 mmol) was added to dipimp (0.145 g, 0.544 mmol) under an N_2 atmosphere in toluene (5 mL). After 3 hours formation of dark purple crystals occurred, which were collected by filtration to yield [Rh(dipimp)(CO)I] (0.201 g, 0.464 mmol, 88.6 % yield).

IR: ν(CO) (CH_2Cl_2): 1993 cm^{-1}

^{1}H NMR δ/ppm ($CDCl_3$): 9.90 (m, 1H), 8.67 (d, 1H, J = , N=C(**H**)), 8.03 (m, 1H), 7.78-7.86 (m, 2H), 7.21-7.34 (m ,3H), 3.52 (sept, 2H, *J* = 6.8 Hz), 1.36 (d, 6H, *J* = 6.8 Hz), 1.14 (d, 6H, *J* = 6.8 Hz)

2.9.9 Synthesis of [Rh(xantphos)(CO)Cl]

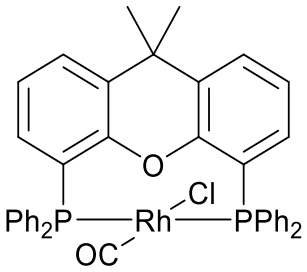

[Rh(xantphos)(CO)Cl] was prepared as described by Williams *et al*.[23] $[Rh(CO)_2Cl]_2$ (0.212 g, 0.546 mmol) and xantphos (0.634 g, 1.10 mmol) were dissolved in ethanol (10 mL) under an N_2 atmosphere. Immediate formation of a yellow precipitate was observed. The solution was stirred for 10 minutes. The yellow solid was isolated by filtration and washed with ethanol and diethylether to yield [Rh(xantphos)(CO)Cl] (0.674 g, 0.905 mmol, 82 % yield).

IR: ν(CO) (CH_2Cl_2): 1967 cm^{-1}

^{31}P NMR δ/ppm($CDCl_3$): 21.5 (d, $J_{Rh\text{-}P}$ =130.2 Hz)

2.9.10 Synthesis of $[Rh_2(\mu\text{-dppm})_2(\mu\text{-CO})(\mu\text{-I})(CO)_2][I]$

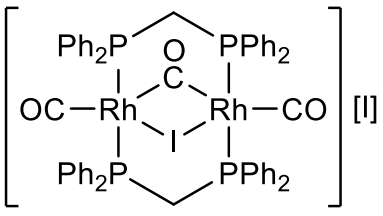

$[Rh_2(\mu\text{-dppm})_2(\mu\text{-CO})(\mu\text{-I})(CO)_2][I]$ was made in the method according to Kubiak.[24] $[Rh(CO)_2I]_2$ (0.050 g, 0.087 mmol) was dissolved in 3 mL CH_2Cl_2 under CO atmosphere.

Bis(diphenylphosphino)methane (0.067 g, 0.17 mmol) was added in 2 mL CH_2Cl_2. The reaction was monitored by IR spectroscopy until formation of product was observed, 10 minutes. Solvent was reduced to ~30 % by rotary evaporation and diethyl ether added. The solution was stored at -10 ^oC overnight to induce formation of red crystals yielding $[Rh_2(\mu\text{-dppm})_2(\mu\text{-CO})(\mu\text{-I})(CO)_2][I]$ 0.142 g (0.12 mmol, 69 % yield).

IR ν(CO) (CH_2Cl_2): 1986, 1866 cm^{-1}

^{1}H NMR δ/ppm ($CDCl_3$): 7.64 (m, 16H), 7.44 (m, 16H), 7.32 (m, 8H), 4.58 (m, 2H), 4.50 – 4.34 (m, 2H)

^{31}P NMR δ/ppm($CDCl_3$): 27.04 m

2.9.11 Synthesis of Vaska's complex $[Ir(PPh_3)_2(CO)Cl]$

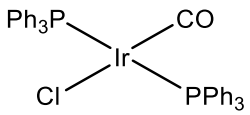

$[Ir(COD)Cl]_2$ (0.333 g, 0.496 mmol) and triphenylphosphine (PPh_3) (0.529 g, 2 mmol) were dissolved in 1:1 mixture of hexane: dichloromethane (10 mL) the resulting solution stirred for 30 minutes. CO was bubbled through the solution affording a yellow precipitate. The precipitate was filtered and washed with hexane and dried under vacuum to give $[Ir(PPh_3)_2(CO)Cl]$ (0.82 g, 1.0 mmol, 99% yield).

IR: ν(CO) (CH_2Cl_2): 1967 cm^{-1}

^{31}P NMR δ/ppm($CDCl_3$): 23.91 s

2.10 Synthesis of Rh(III) acetyl complexes

Method A

Rh(III) acetyl complexes were prepared in a variation of the method described by Haynes *et al*.[25] $[Rh(CO)(COMe)(NCMe)I_2]_2$ (0.2 mmol)and the bidentate ligand (L-L) (0.4 mmol) were dissolved in toluene under N_2 and stirred for 1 hour. The precipitate formed was filtered off and dried under vacuum giving the Rh(III) acyl complex as a yellow/orange/brown powder with no further purification required. The toluene filtrate was concentrated *in vacuo* and stored at –10 ^oC for 24 hours before filtering to yield a second crop of product.

Method B

$[Rh(CO)_2I]_2$ (0.2 mmol) and bidentate ligand L-L (0.4 mmol) were dissolved in CH_2Cl_2 under N_2 and monitored by IR spectroscopy until formation of [Rh(L-L)(CO)I] was observed . An excess of iodomethane (0.1 mL) was then added and the solution stirred for 2 hours, or until IR spectra indicated formation of $[Rh(COMe)(L\text{-}L)I_2]$. The volume of the solution was reduced to ~20% and diethyl ether (0.5 mL) added to induce crystal formation. The solution was stored at -10 ^oC for 24 hours. The resultant precipitate was filtered and washed with diethyl ether (10 mL).

2.10.1 Synthesis of $[Rh(dppm)(COMe)I_2]$ 3a

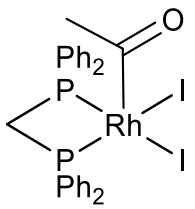

$[Rh(dppm)(COMe)I_2]$ was prepared using method A with $[Rh(CO)(COMe)(NCMe)I_2]_2$ (0.216 g, 0.230 mmol) and bis(diphenylphosphino)methane (0.181 g, 0.471 mmol) giving $[Rh(dppm)(COMe)I_2]$ as an orange powder (0.322 g, 0.410 mmol, 89 % yield). Spectroscopic data was consistent with literature values and indicated satisfactory purity. [26]

IR ν(CO) (CH_2Cl_2): 1709 cm^{-1}

^{1}H NMR δ/ppm ($CDCl_3$): 7.82-7.73 (m, 4H), 7.52-7.23 (m, 16H), 5.22 (m, P-C***H***H-P, 1H), 4.63 (m, P-C***H***H-P, 1H), 3.10s (s, COC***H***$_3$)

^{31}P NMR δ/ppm ($CDCl_3$): -25.65 (d, J_{Rh-P} = 119.5 Hz)

2.10.2 Synthesis of [Rh(dppe)(COMe)I_2] 3b

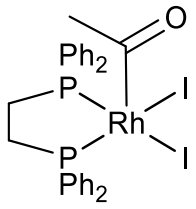

[Rh(dppe)(COMe)I_2] was prepared by method A in the quantities: [Rh(CO)(COMe)(NCMe)I_2]$_2$ (0208 g, 0.222 mmol) and 1,2-bis(diphenylphosphino)ethane (dppe) (0.184 g, 0.461 mmol). [Rh(dppe)(COMe)I_2] was isolated as an orange powder (0308 g, 0.385 mmol, 87% yield). Spectroscopic data was consistent with literature values and indicated satisfactory purity.[27]

IR ν(CO) (CH_2Cl_2): 1710 cm^{-1}

^{1}H NMR δ/ppm ($CDCl_3$): 7.82-7.73 (m, 4H), 7.52-7.23 (m, 16H), 3.17-2.96 (m, 2H, P-CH_2-C***H***$_2$-P), 2.28-2.07 (m, 2H, P-C***H***$_2$-CH_2-P), 2.80 (s, 3H, COC***H***$_3$)

^{31}P NMR δ/ppm ($CDCl_3$): 70.02 (d, J_{Rh-P} =139.0 Hz)

2.10.3 Synthesis of [Rh(dppp)(COMe)I_2] 3c

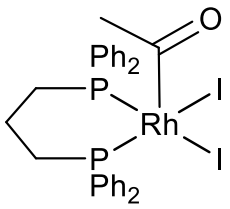

[Rh(dppp)(COMe)I_2] was prepared by method A using the quantities: [Rh(CO)(COMe)(NCMe)I_2]$_2$ (0.105 g, 0.129 mmol) and 1,3-bis(diphenylphosphino)propane (dppp) (0.092 g, 0.22mmol) giving [Rh(dppp)(COMe)I_2] as yellow/brown crystals (0.145 g, 0.18 mmol, 82 % yield). Spectroscopic data was consistent with literature values and indicated satisfactory purity.[28]

IR ν(CO) (CH_2Cl_2): 1701 cm^{-1}

^{1}H NMR δ/ppm ($CDCl_3$): 7.74 – 7.65 (m, 4H), 7.49 – 7.24 (m, 16H), 3.16 (m, 2H), 3.09 (s, 3H), 2.59 – 2.39 (m, 2H), 1.78 – 1.62 (m, 3H).

^{31}P NMR δ/ppm ($CDCl_3$): 17.9 (d, J_{Rh-P} = 131.5 Hz).

2.10.4 Synthesis of [Rh(dppb)(COMe)I_2] 3d

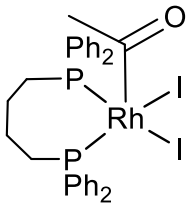

[Rh(dppb)(COMe)I_2] was prepared by method B using the quantities: [Rh(CO)$_2$I]$_2$ (0.173 g, 0.3 mmol), bis(diphenylphosphino)butane (dppb) (0.262 g, 0.61 mmol), dichloromethane (5 mL) and iodomethane (1 mL, 0.016 mol) giving [Rh(dppb)(COMe)I_2] as a dark red solid 0.410 g (0.5

mmol, 82% yield). Spectroscopic data was consistent with literature values and indicated satisfactory purity.[29]

IR ν(CO) (CH_2Cl_2): 1700 cm^{-1}

^{1}H NMR δ/ppm ($CDCl_3$): 7.58 (dt, 4H), 7.23–7.41 (m, 12H), 3.19 (m, 2H), 2.76 (s, 3H, COC***H₃***), 2.35 (2H, m),1.49 (m, 2H), 0.98 (m, 2H).

^{31}P NMR δ/ppm ($CDCl_3$): 31.61 (d, J_{Rh-P} = 139.1 Hz).

2.10.5 Synthesis of [Rh(xantphos)(COMe)I_2] 3e

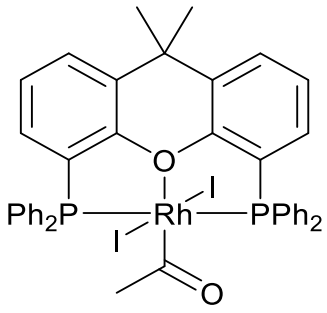

[Rh(xantphos)(COMe)I_2] was prepared by method A, a variation on the method as described by Williams,[23] using [Rh(CO)(COMe)(NCMe)I_2]$_2$ (0.120 g, 0.13 mmol) and 4,5-Bis(diphenylphosphino)-9,9-dimethylxanthene (0.150 g, 0.26 mmol) yielding [Rh(xantphos)(COMe)I_2] as dark red crystals (0.202 g, 0.21 mmol 81 % yield). Spectroscopic data was consistent with literature values and indicated satisfactory purity.

IR ν(CO) (CH_2Cl_2): 1683, 1666 cm^{-1}

^{1}H NMR δ/ppm ($CDCl_3$): 7.93 – 7.21 (m, 26H), 2.90 (t, 3H, *J* = 1.7 Hz, C=O***CH₃***), 1.77 (s, 6H, C***Me₂***).

^{31}P NMR δ/ppm ($CDCl_3$): 9.72 (d, J_{Rh-P} = 108.7 Hz).

2.10.6 Synthesis of [Rh(DPEphos)(COMe)I_2] 3f

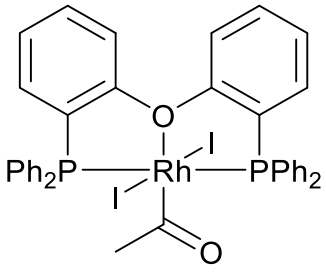

[Rh(DPEphos)(COMe)I_2] was prepared as described by Williams.[30] [Rh(CO)(COMe)(NCMe)I_2]$_2$ (0.095 g, 0.10 mmol) was dissolved in CH_2Cl_2 (5 mL) under N_2 giving a red solution. (Oxydi-2,1-phenylene)bis(diphenylphosphine) (DPEphos) (0.109 g, 0.20 mmol) was added to solution and stirred for 3 hours, during this time a colour change from red to orange was observed. The solution was then concentrated *in vacuo* and diethyl ether added until precipitation began to occur. The solution was stored at -10 ^oC overnight to induce formation of orange/brown crystals of [Rh(DPEphos)(COMe)I_2] (0.1499 g, 0.16 mmol, 79 % yield).

IR ν(CO) (CH_2Cl_2):1686, 1664 cm^{-1}

^{1}H NMR δ/ppm ($CDCl_3$): 7.75 (s, 8H), 7.48 – 7.35 (m, 6H), 7.35 – 7.26 (m, 12H), 7.10 – 7.03 (m, 2H), 2.90 (t, 3H, *J* = 1.7 Hz, 3H, C=O***CH$_3$***).

^{31}P NMR δ/ppm ($CDCl_3$): 7.49 (d, J_{Rh-P}= 112.0 Hz).

2.10.7 Synthesis of [Rh(xantphos)(COMe)(NCMe)I][BF_4]

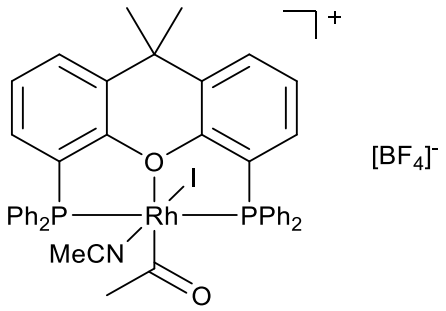

The procedure to make[Rh(xantphos)(COMe)(NCMe)I][BF_4] was based on the method described by Williams.[23] [Rh(xantphos)(COMe)I_2] (0.182 g, 0.18 mmol) was dissolved in 2:1 CH_2Cl_2/MeCN (15 mL) giving an orange solution. $AgBF_4$ (0.037 g, 0.19 mmol) was added leading to rapid formation of AgI and a yellow/orange solution. The solution was monitored by IR spectroscopy, upon indication of product formation the solution was filtered through Celite and the solvent removed *in vacuo* to give [Rh(xantphos)(COMe)(NCMe)I][BF_4] as a yellow/orange crystalline powder (0.159 g, 0.16 mmol 89% yield). Spectroscopic data was consistent with literature values and indicated satisfactory purity.

IR ν(CO) (CH_2Cl_2): 1708 cm^{-1}

^{1}H NMR δ/ppm ($CDCl_3$): 7.3−8.1 (m, 26H, aromatics), 2.80 (t, 3H, J_{Me-P} =1.4 Hz, CO***CH_3***), 1.92 and 1.76 (each s, 3H, xantphos-C***Me_2***)

^{31}P NMR δ/ppm ($CDCl_3$): 16.02 (d, J_{Rh-P} = 100.6 Hz)

2.10.8 Synthesis of [Rh(PN-^{i}Pr$_2$Ph)(COMe)I$_2$] 3g

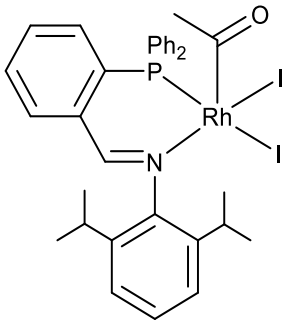

[Rh(PN-^{i}Pr$_2$Ph)(COMe)I$_2$] was synthesised according to method A from [Rh(NCMe)(COMe)(CO)I$_2$]$_2$ (0.122 g, 0.13 mmol), PN-^{i}Pr$_2$Ph (0.119 g, 0.26 mmol) and toluene (5 mL) giving [Rh(PN-^{i}Pr$_2$Ph)(COMe)I$_2$] as an orange powder (0.206 g, 0.24 mmol, 93 % yield). Spectroscopic data was consistent with literature values and indicated satisfactory purity.[21]

IR ν(CO) (CH_2Cl_2): 1714 cm^{-1}

^{1}H NMR δ/ppm ($CDCl_3$): 8.17 (d, 1H, *J* = 3.7 Hz, N=C***H***), 6.93-7.86 (m, 17H, Ar-***H***), 3.44 (s, 3H, CO***CH$_3$***), 1.73, 2.55 (each sept, 1H, $^{3}J_{HH}$ = 7.6 Hz, C***H***Me$_2$), 0.96, 1.13, 1.16, 1.29 (each d, 3H, $^{3}J_{HH}$ = 7.6 Hz, CH-(***CH$_3$***)$_2$)

^{31}P NMR δ/ppm($CDCl_3$): 45.92 (d, $J_{Rh\text{-}P}$= 129.0 Hz)

2.10.9 Synthesis of [Rh(PN-Me$_2$Ph)(COMe)I$_2$] 3h

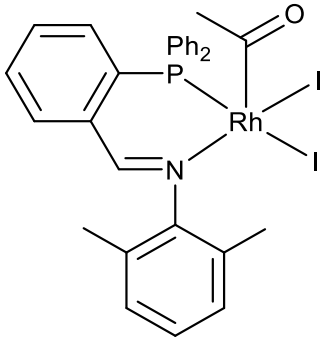

[Rh(PN-Me_2Ph)(COMe)I_2] was synthesised according to method A using [Rh(NCMe)(COMe)(CO)I_2]$_2$ (0.147 g, 0.16 mmol) and PN-Me_2Ph (0.128 g, 0.32 mmol) giving [Rh(PN-Me_2Ph)(COMe)I_2] as an orange/red powder (0.185 g, 0.23 mmol, 74 % yield). Spectroscopic data was consistent with literature values and indicated satisfactory purity.[21]

IR ν(CO) (CH_2Cl_2): 1716 cm^{-1}

^{1}H NMR δ/ppm ($CDCl_3$): 8.14 (d, 1H, *J* = 3.7 Hz, N=C***H***), 6.8-7.9 (m, 17H), 3.48 (s, 3H, CO***CH_3***), 2.14 (s, 3H), 1.30 (s, 3H),

^{31}P NMR δ/ppm($CDCl_3$): 46.47 (d, J_{Rh-P}= 129 Hz)

2.10.10 Synthesis of [Rh(PN-Mes)(COMe)I_2] 3i

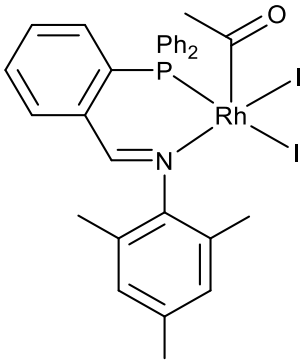

[Rh(PN-Mes)(COMe)I_2] was synthesised according to method A with [Rh(NCMe)(COMe)(CO)I_2]$_2$ (0.143 g, 0.15 mmol) and PN-Mes (0.133 g, 0.33 mmol) and toluene (5 mL) giving [Rh(PN-Mes)(COMe)I_2] (0.177 g, 0.22 mmol, 72 % yield). Spectroscopic data was consistent with literature values and indicated satisfactory purity.[21]

IR ν(CO) (CH_2Cl_2): 1716 cm^{-1}

^{1}H NMR δ/ppm ($CDCl_3$): 8.03 (d, 1H, *J* = 3.7 Hz), 7.66 – 7.42 (m, 10H), 7.37 (m, 2H), 7.28 – 7.15 (m, 3H), 7.07 – 6.97 (m, 1H), 3.45 (s, 3H, CO***CH_3***), 2.19 (s, 3H), 1.94 (s, 6H)

^{31}P NMR δ/ppm($CDCl_3$): 46.3 (d, J_{Rh-P} = 138.2 Hz)

A crystal of **3i** suitable for X-ray crystallography was obtained by slow evaporation of $CHCl_3$ from a concentrated solution of **3i** in $CHCl_3$.

2.10.11 Synthesis of [Rh(PN-oAnis)(COMe)I_2] 3j

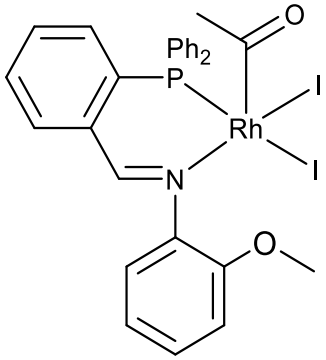

[Rh(PN-oAnis)(COMe)I_2] was synthesised according to method A using [Rh(NCMe)(COMe)(CO)I_2]$_2$ (0.143 g, 0.15 mmol) and PN-oAnis (0.133 g, 0.33 mmol) giving [Rh(PN-Mes)(COMe)I_2] as an orange powder (0.177 g, 0.22 mmol, 72 % yield). Spectroscopic data was consistent with literature values and indicated satisfactory purity.[21]

IR ν(CO) (CH_2Cl_2): 1703 cm^{-1}

^{1}H NMR δ/ppm ($CDCl_3$): 8.28 (s, 1H), 6.7-7.9 (m, 18H, arom), 3.98 (3H, OMe), 3.37s (3H, CO**CH_3**)

^{31}P NMR δ/ppm($CDCl_3$): 44.40d (J_{Rh-P} = 132.2 Hz)

2.10.12 Synthesis of [Rh(dppms)(COMe)I_2] 3k

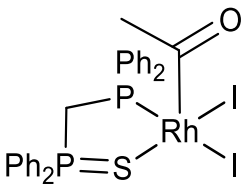

[Rh(dppms)(COMe)I_2] was synthesised using method A using [Rh(NCMe)(COMe)(CO)I_2]$_2$ (0.200 g, 0.21 mmol) and dppms (0.182 g, 0.44 mmol) giving [Rh(dppms)(COMe)I_2] as an orange powder (0.290 g, 0.35 mmol, 81 % yield). Spectroscopic data was consistent with literature values and indicated satisfactory purity.

IR ν(CO) (CH_2Cl_2): 1701 cm^{-1}

^{1}H NMR δ/ppm ($CDCl_3$): 7.80-6.90 (m, 20H, arom), 4.88 (ddd, 1H, *J* = 13, 8, 4 Hz) 3.58 (ddd, 1H, *J* = 13, 5, 2 Hz), 3.34 (s, 3H, CO**CH_3**)

^{31}P NMR δ/ppm($CDCl_3$): 57.9 (dd, $J_{Rh\text{-}P}$ = 4 Hz, $J_{P\text{-}P}$ = 47 Hz) 54.6 (dd, $J_{Rh\text{-}P}$ = 137 Hz, $J_{P\text{-}P}$ = 47 Hz)

2.10.13 Synthesis of [Rh(dppmSe)(COMe)I_2] 3l

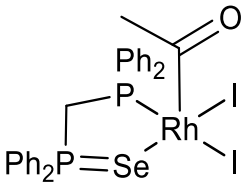

[Rh(dppmSe)(COMe)I_2] was synthesised using method A using [Rh(NCMe)(COMe)(CO)I_2]$_2$ (0.146 g, 0.16 mmol) and dppmSe (0.176 g, 0.38 mmol) giving [Rh(dppmSe)(COMe)I_2] as an orange powder (0.248 g, 0.29 mmol, 90 % yield). Spectroscopic data was consistent with literature values and indicated satisfactory purity. [31]

IR ν(CO) (CH_2Cl_2): 1698 cm^{-1}

^{1}H NMR δ/ppm ($CDCl_3$): 7.85 – 7.34 (m, 18H), 7.04 (m, 2H), 5.02 (m, 1H), 3.79 (m, 1H), 3.32 (s, 3H, CO**CH_3**).

^{31}P NMR δ/ppm($CDCl_3$): 58.88 (dd, $J_{Rh\text{-}P}$ = 142.7, $J_{P\text{-}P}$ = 55.8 Hz), 37.61 (dd, $J_{P\text{-}P}$ 55.8, $J_{Rh\text{-}P}$ = 4.0 Hz)

2.11 Reaction of Rh(III) acetyl complexes with carboxylates

2.11.1 General reaction of Rh(III) acetyl complexes and carboxylates, monitored spectroscopically

[Rh(L-L)(COMe)I_2] (~20 mg) was dissolved in CH_2Cl_2 (3 mL) for IR spectroscopy or $CDCl_3$ (1 mL) for NMR spectroscopy under an N_2 or CO atmosphere. To this solution 1 molar equivalent [Bu_4N][OAc] or [Bu_4N][OBz] was added in CH_2Cl_2 or $CDCl_3$ (1 mL). The reaction was monitored by IR and NMR spectroscopy periodically to determine the species formed before elimination of anhydride.

2.11.2 General synthesis of Rh(III) acetyl carboxylate complexes

[Rh(L-L)(COMe)I_2] (~60 mg) was dissolved in CH_2Cl_2 (5 mL) under an N_2 atmosphere. To this solution 1 molar equivalent [Bu_4N][OAc] or [Bu_4N][OBz] was added in CH_2Cl_2 (1 mL). The solution was stirred for one hour. The volume of solution was reduced to ~30 % *in vacuo* and remaining solution placed at -10 ^{o}C for 24 hours to induce crystallisation. The resultant solid was isolated by filtration.

2.11.3 Synthesis of [Rh(dppms)(COMe)(OAc)I] 4k

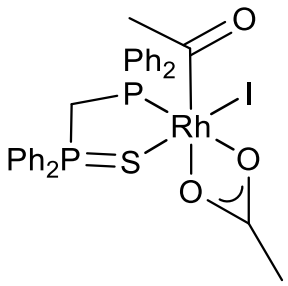

[Rh(dppms)(COMe)I_2] (60 mg, 0.074 mmol) was dissolved in CH_2Cl_2 under nitrogen. 1 equivalent [NBu_4][OAc] (23 mg, 0.077 mmol) was added. A colour change from orange to yellow was observed. After 5 minutes a yellow precipitate formed, the solution was filtered to give [Rh(dppms)(COMe)(OAc)I] (23 mg, 0.03 mmol, 42 % yield).

IR ν(CO) (CH_2Cl_2): 1690, 1668 (**C=O**CH_3), 1551 $\nu(CO_2)_{sym}$, 1434 $\nu(CO_2)_{asym}$ cm^{-1}

^{1}H NMR δ/ppm ($CDCl_3$): 7.90 – 7.03 (m, 20H, arom), 5.09 (ddd, 1H, *J* = 17.9, 13.7, 11.25 Hz, PC**H**HP), 3.87 (ddd, 1H, *J* = 13.7, 11.5, 4.8 Hz, PCH**H**P), 3.04 (s, 3H, COC**H$_3$**), 2.26 (s, 3H, OC(O)C**H$_3$**,)

^{31}P NMR δ/ppm ($CDCl_3$): 50.42 (dd, $J_{P\text{-}P}$ = 31.9, $J_{Rh\text{-}P}$ = 1.8 Hz), 43.90 (dd, $J_{Rh\text{-}P}$ = 139.8, $J_{P\text{-}P}$ 31.9 Hz)

Elemental analysis: expected for $C_{29}H_{29}IO_3P_2SRh$; C: 46.48, H: 3.9, S: 4.28

found C: 46.00, H: 4.17, S: 4.48

Crystals of **4k** suitable for X-ray crystallography were obtained by slow evaporation of diethyl ether into a concentrated solution of **4k** in CH_2Cl_2.

2.11.4 Synthesis of [Rh(dppms)(COMe)(OBz)I] 5k

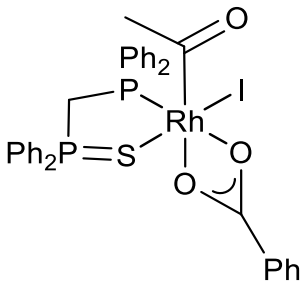

[Rh(dppms)(COMe)I_2] (22 mg, 0.028 mmol) was dissolved in CH_2Cl_2 under nitrogen. 1 equivalent [NBu_4][OBz] (10 mg, 0.028 mmol) was added. A colour change from orange to yellow was observed after 5 minutes and formation of a yellow precipitate, the solution was filtered to give [Rh(dppms)(COMe)(OCOPh)I] (16 mg, 0.02 mmol, 73% yield).

IR ν(CO) (CH_2Cl_2): 1692, 1673, 1552, 1436 cm^{-1}

^{1}H NMR δ/ppm ($CDCl_3$): 8.21 (d, 1H, *J* = 6.7 Hz), 7.77 – 7.00 (m, 24H, arom), 5.05 (ddd, 1H *J* = 17.9, 13.7, 11.2 Hz, PC**H**HP), 3.91 (ddd, 1H, *J* = 13.7, 5.0, 2.3 Hz, PCH**H**P,), 3.07 (s, 3H, COC**H$_3$**).

^{31}P NMR δ/ppm ($CDCl_3$): 50.2 (dd, $J_{P\text{-}P}$ = 31.7, $J_{Rh\text{-}P}$ = 1.3 Hz) 43.4 (dd, $J_{Rh\text{-}P}$ = 140.6, $J_{P\text{-}P}$ = 31.7 Hz)

Elemental analysis: expected for $C_{34}H_{30}IO_3P_2RhS$; C, 50.39, H, 3.73, S, 3.96

found C, 47.72, H, 3.73, S, 4.22

Crystals of **5k** suitable for X-ray crystallography were obtained by slow evaporation of diethyl ether into a concentrated solution of **5k** in CH_2Cl_2.

2.11.5 Synthesis of [Rh(dppmSe)(COMe)(OAc)I] 4l

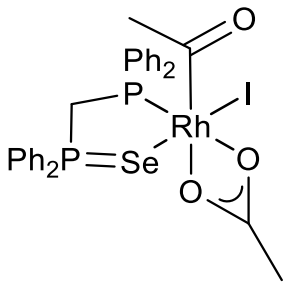

[Rh(dppmSe)(COMe)I_2] (43 mg, 0.050 mmol) was dissolved in CH_2Cl_2 under nitrogen. 1 equivalent [NBu_4][OAc] (16 mg, 0.053 mmol) was added. A colour change from orange to yellow was observed, after 5 minutes a yellow precipitate formed, the solution was filtered to give [Rh(dppmSe)(COMe)(OAc)I] (23 mg, 0.029 mmol, 58 % yield).

IR ν(CO) (ATR): 1689, 1666, 1552, 1435 cm^{-1}

^{1}H NMR δ/ppm ($CDCl_3$): 7.90 – 7.03 (m, 20H, arom), 5.22 (ddd, 1H, *J* = 17.1, 13.8, 11.5 Hz, PC**H**HP), 3.87 (ddd, 1H, *J* = 13.7, 11.5, 4.8 Hz, PCH**H**P), 3.02 (s, 3H, COC**H$_3$**), 2.22 (s, 3H, OC(O)C**H$_3$**).

^{31}P NMR δ/ppm ($CDCl_3$): 44.9 (dd, , J_{Rh-P} = 141.9 J_{P-P} = 36.6 Hz), 29.71 (dd, J_{P-P} = 36.6, J_{Rh-P} = 1.7 Hz)

High resolution MS (TOF ES + m/z): 818.86 [M][Na^+]

Elemental analysis: expected for $C_{29}H_{28}IO_3P_2SeRh$; C, 43.80; H, 3.55; I, 15.96

Found C, 43.59; H, 3.68; I, 16.46

Crystals of **4l** suitable for X-ray crystallography were obtained by slow evaporation of diethyl ether into a concentrated solution of **4l** in CH_2Cl_2.

2.11.6 Synthesis of [Rh(dppmSe)(COMe)(OBz)I] 5l

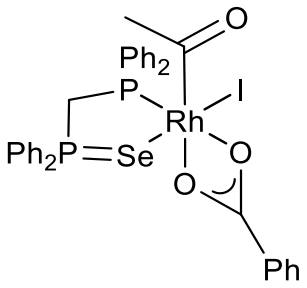

[Rh(dppmSe)(COMe)I_2] (41 mg, 0.047 mmol) was dissolved in CH_2Cl_2 (3 mL) under nitrogen. 1 equivalent [NBu_4][OBz] (15 mg, 0.049 mmol) was added and solution was stirred. A colour change from orange to yellow was observed. After 5 minutes a yellow precipitate formed, which was filtered to give [Rh(dppmSe)(COMe)(OBz)I] (16 mg, 0.019 mmol, 40 % yield).

IR ν(CO) (CH_2Cl_2): 1693, 1667, 1551, 1434 cm^{-1}

^{1}H NMR δ/ppm ($CDCl_3$): 8.21 (d, 1H, *J* = 6.7 Hz, arom), 7.77 – 7.00 (m, 24H, arom), 5.24 (ddd, 1H , *J* = 17.2, 13.7, 11.4 Hz, PC**H**HP), 3.79 (ddd, 1H, *J* = 13.7, 11.4, 4.7 Hz, PC**H**HP), 3.18 (s, 3H, COC**H$_3$**).

^{31}P NMR δ/ppm ($CDCl_3$): 45.0 (dd, J_{Rh-P} = 142.1 Hz, J_{P-P} = 36.7 Hz) 29.61 (d, J_{P-P} = 36.7 Hz)

High resolution MS (TOF ES + m/z): 880.88 [M][Na^+]

Elemental analysis: expected for $C_{34}H_{30}IO_3P_2RhSe$: C, 47.63; H, 3.53; I, 14.80

Found C, 47.21; H, 3.68; I, 15.18

2.12 Reaction of Rh(III) acetyl complexes with [Ag][TFA]

2.12.1 General reaction of Rh(III) acetyl complexes and AgTFA, monitored spectroscopically

[Rh(L-L)(COMe)I_2] **3a-d,g-l** were dissolved in MeCN (3 mL) for IR spectroscopy or CD_3CN (1 mL) for NMR spectroscopy under an N_2 or CO atmosphere and a spectrum of starting material taken. To this solution one molar equivalent of AgTFA was added. Rapid formation of a grey precipitate was observed. The reaction was monitored by IR and NMR spectroscopy periodically to determine the species formed before elimination of an anhydride.

2.12.2 Synthesis of Rh(III) acyl trifluoroacetate complexes

[Rh(L-L)(COMe)I_2] (0.1 mmol) was dissolved in MeCN (3 mL) under N_2 or CO. One molar equivalent of [Ag][TFA] (0.1 mmol) was added in MeCN (1 mL). Rapid formation of a grey precipitate was observed alongside a colour change of the solution from orange to yellow. The solution was stirred for 1 hour and then filtered through celite, to remove AgI, and the solvent was removed *in vacuo*. The resulting solid was recrystallised from CH_2Cl_2 and hexane.

2.12.3 Synthesis of [Rh(PN-^{i}Pr$_2$Ph)(COMe)(TFA)I] 6g

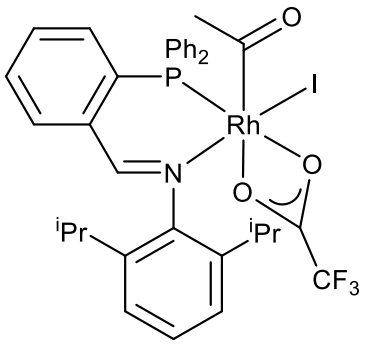

[Rh(PN-^{i}Pr$_2$Ph)(COMe)(TFA)I] was prepared using the method described above with [Rh(PN-^{i}Pr$_2$Ph)(COMe)I$_2$] (0.122 g, 0.143 mmol) and AgTFA (0.032 g, 0.144 mmol) giving **6g** as an orange powder (0.064 g, 0.077 mmol, 54 % yield).

IR ν(CO) (CH_2Cl_2): 1706 cm^{-1}

^{1}H NMR δ/ppm ($CDCl_3$): 8.18 (d, 1H, J = 3.7 Hz, Ar-N=C**H**), 7.90 – 7.32 (m, 14H, arom), 7.25 – 6.91 (m, 3H, arom), 3.25 (s, 3H, COC**H$_3$**), 2.59 (sept, 1H, $CH_3(R_1)C\mathbf{H}CH_3$), 1.79 – 1.66 (sept, 1H, $CH_3(R_2)C\mathbf{H}CH_3$), 1.42 (d, 3H, $\mathbf{H_3}C(R_1)HCH_3$, *J* = 6.8 Hz), 1.08 (d, 3H, $CH_3C(R_1)HC\mathbf{H_3}$, *J* = 6.8 Hz), 0.86 (d, 3H, $\mathbf{H_3}C(R_2)HCH_3$, *J* = 6.6 Hz), 0.28 (d, 3H, $CH_3C(R_2)HC\mathbf{H_3}$, *J* = 6.8 Hz)

^{31}P NMR δ/ppm($CDCl_3$): 49.31 (d, $J_{Rh\text{-}P}$ = 145.5 Hz)

Crystals of **6g** suitable for X-ray crystallography were obtained by slow evaporation of diethyl ether into a concentrated solution of **6g** in CH_2Cl_2.

2.12.4 Synthesis of [Rh(PN-Me_2Ph)(COMe)(TFA)I] 6h

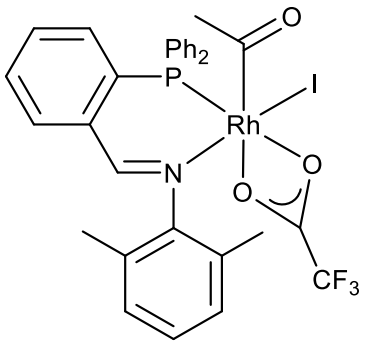

[Rh(PN-Me_2Ph)(COMe)(TFA)I] was prepared using the method described above with [Rh(PN-Me_2Ph)(COMe)I_2] (0.084 g, 0.105 mmol) and AgTFA (0.024 g, 0.109 mmol) giving **6h** as an orange powder (0.039 g, 0.047 mmol, 45 % yield).

IR ν(CO) (CH_2Cl_2): 1708 cm^{-1}

^{1}H NMR δ/ppm ($CDCl_3$): 8.17 (d, 1H, *J* = 3.8 Hz, Ar-N=C**H**), 7.90 – 7.31 (m, 14H, arom), 7.19 – 6.81 (m, 3H, arom), 3.28 (s, 3H, COC**H_3**), 2.09 (s, 3H, ArC**H_3**), 1.24 (s, 3H, ArC**H_3**)

^{31}P NMR δ/ppm($CDCl_3$): 49.34 (d, $J_{Rh\text{-}P}$ = 145.0 Hz)

2.12.5 Synthesis of [Rh(PN-Mes)(COMe)(TFA)I] 6i

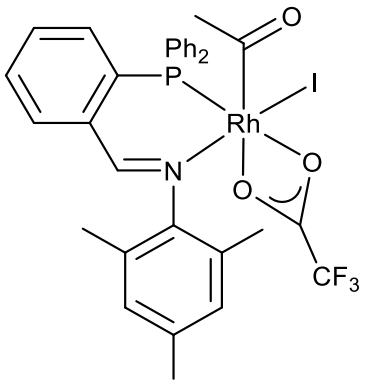

[Rh(PN-Mes)(COMe)(TFA)I] was prepared using the method described above with [Rh(PN-Mes)(COMe)I_2] (0.088 g, 0.109 mmol) and AgTFA (0.025 g, 0.111 mmol) giving **6i** as an orange powder (0.041 g, 0.052 mmol, 48 % yield).

IR ν(CO) (ATR): 1707, 1641, 1564, 1437 cm^{-1}

^{1}H NMR δ/ppm ($CDCl_3$): 8.17 (d, 1H, *J* = 3.8 Hz, Ar-N=C**H**), 7.86 – 7.30 (m, 16H, arom), 3.27 (s, 3H, COC**H_3**), 2.24 (s, 3H, ArC**H_3**), 2.05 (s, 3H, ArC**H_3**), 1.19 (s, 3H, ArC**H_3**)

^{31}P NMR δ/ppm($CDCl_3$): 49.31 (d, $J_{Rh\text{-}P}$ = 145.2 Hz)

Elemental analysis: expected for $C_{32}H_{29}F_3INO_3PRh$: C,48.45; H, 3.68; N, 1.77; I, 16.00

Found C, 48.07; H, 3.74; N, 1.70; I, 15.21

2.12.6 Synthesis of [Rh(dppms)(COMe)(TFA)I] 6k

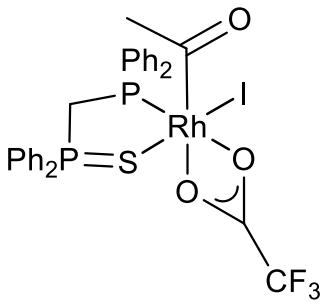

6k was prepared according to general synthetic procedure using [Rh(dppms)(COMe)I_2] (91 mg, 0.115 mmol) and AgTFA (24 mg, 0.111 mmol) yielding **6k** as yellow solid **(**37 mg, 0.047 mmol, 42 % yield).

IR ν(CO) (ATR): 1686, 1663, 1574, 1435 cm^{-1}

^{1}H NMR δ/ppm ($CDCl_3$): 8.21 (d, 2H, *J* = 6.7 Hz, arom), 7.77 – 7.00 (m, 18H, arom), 4.98 (ddd, 1H, *J* = 17.7, 13.8, 11.3 Hz, PC**H**HP), 3.79 (ddd, 1H, *J* = 13.8, 4.9, 2.4 Hz, PC**H**HP), 3.10 (s, 3H, COC**H_3**).

^{19}F NMR δ/ppm ($CDCl_3$): -74.65 s

^{31}P NMR δ/ppm ($CDCl_3$): 49.70 (dd, $J_{P\text{-}P}$ = 28.5, $J_{Rh\text{-}P}$ = 1.8 Hz), 44.89 (dd, $J_{Rh\text{-}P}$ = 146.8, $J_{P\text{-}P}$ = 28.5 Hz)

High resolution MS (TOF ES + m/z): 688.9 $[M]^+$-$[TFA]^-$

Crystals of **6k** suitable for X-ray crystallography were obtained by slow evaporation of diethyl ether into a concentrated solution of **6k** in CH_2Cl_2.

2.12.7 Synthesis of [Rh(dppmSe)(COMe)(TFA)I] 6l

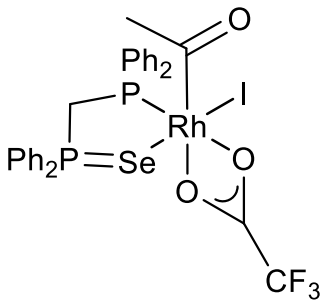

6l was prepared according to the general synthetic procedure using **3l** (0.180 g, 0.208 mmol) and AgTFA (0.047 g, 0.213 mmol) under N_2. Yielding **6l** as an orange/yellow powder (0.111 g, 0.131 mmol, 63 % yield).

IR ν(CO) (ATR): 1699, 1660, 1437, 1196cm^{-1}

^{1}H NMR δ/ppm ($CDCl_3$): 7.72 - 7.10 (m, 20H, arom), 5.12 (ddd, 1H, J = 16.8, 13.8, 11.5 Hz, PC**H**HP), 4.28 (ddd, 1H, *J* = 13.8, 7.1, 2.7 Hz, PC**H**HP), 3.08 (s, 3H, COC**H$_3$**)

^{31}P NMR δ/ppm ($CDCl_3$): 45.38 (dd, $J_{Rh\text{-}P}$ = 148.7, $J_{P\text{-}P}$ = 33.0 Hz), 28.85 (dd, $J_{P\text{-}P}$ = 33.0, $J_{Rh\text{-}P}$ = 4.0 Hz)

2.12.8 Synthesis of [Rh(dppe)(COMe)(TFA)$_2$]

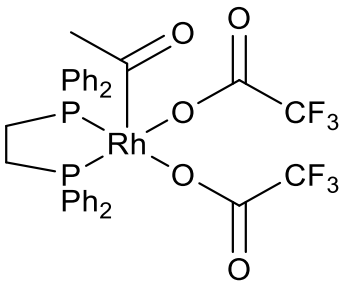

[Rh(dppe)(COMe)I_2] (0.152 g, 0.190 mmol) was dissolved in CH_2Cl_2 (5 mL) under N_2 atmosphere, to this a solution of AgTFA (0.087 g, 0.394 mmol) in MeCN (2 mL) was added. This solution was stirred for 2 hours, formation of a grey precipitate was observed as well as a

colour change of the solution from yellow-orange to a very pale yellow. The solution was filtered through celite and solvent removed *in vacuo*. The resulting solid was recrystallised in CH_2Cl_2 and hexane giving [Rh(dppe)(COMe)$(TFA)_2$] (0.061 g, 0.079 mmol, 41 % yield) as a pale yellow solid.

IR ν(CO) (ATR): 1730, 1709, 1642, 1183 cm^{-1}

^{1}H NMR δ/ppm ($CDCl_3$): 7.85-7.35 (m, 20H, arom), 3.24 (m, 2H, PCH_2CH_2P), 2.41 (m, 2H, PCH_2CH_2P) 2.38 (s, 3H, CO***CH_3***)

^{19}F NMR δ/ppm ($CDCl_3$): -79.94 s

^{31}P NMR δ/ppm ($CDCl_3$): 67.23 (d, $J_{Rh\text{-}P}$ = 154.6 Hz)

High resolution MS (TOF ES + m/z): 657.2 [M+]-$[TFA]^-$

Elemental analysis: expected for $C_{32}H_{27}F_6O_5P_2Rh$; C,49.89; H, 3.53

Found C, 49.88; H, 3.69

2.13 Reaction of Rh (III) acetyl complexes with amines

2.13.1 General reaction of Rh (III) acetyl complexes with N-methyl aniline

[Rh(L-L)(COMe)I_2] (~20 mg) was dissolved in CH_2Cl_2 (3 mL) under CO, to this solution 10 molar equivalents N-methyl aniline were added. This solution was stirred at 25 °C for 2 days and monitored by IR spectroscopy periodically.

2.13.1 General reaction of Rh (III) acetyl complexes with diethylamine

[Rh(L-L)(COMe)I_2] (~20 mg) was dissolved in CH_2Cl_2 (3 mL) under CO, to this solution 10 molar equivalents diethylamine were added. This solution was stirred at 25 °C for 3 hours and monitored by IR spectroscopy periodically.

2.14 General procedure for IR kinetic studies

Samples for kinetic analysis were prepared by placing 33-165 µL diethylamine into a 5-10 mL volumetric flask and making up to the mark with dichloromethane. This solution was used to generate a background spectrum. Typically around 5-6 mg of the complex to be studied was weighed into a sample tube, to which 1000 µL of diethylamine solution was added. This solution was mixed rapidly with a pipette and transferred into a solution cell (0.5 mm path length with CaF_2 windows) before the experiment started. The cylindrical IR cell was placed inside a fitted thermostatted jacket, which was used to maintain a constant temperature throughout the experiment. Data collection was controlled using the Omnic package and analysed using Omnic and Kaleidagraph software.

2.15 Decarbonylative dehydration reactions

2.15.1 General procedure for catalytic decarbonylative dehydration reactions

To a 10 mL snap cap microwave tube myristic acid (~0.7 g, 3.0 mmol), potassium iodide (~0.25 g, 1.5 mmol), acetic anhydride (0.7 mL, 7.4 mmol) metal complex (0.15 mmol) and a magnetic stirrer bar were added. The tube was placed under a protective atmosphere of nitrogen or argon by purging with a syringe attached to a Schlenk line for 10 minutes. The vessel was sealed with the snap cap and heated in a pre-heated oil bath at 160 °C for 4 hours. After this

time the reaction vessel was cooled to room temperature. Alkene products were isolated by column chromatography on silica using hexane solvent. Products were visualised using a potassium permanganate dip. Hexane was removed by rotary evaporation and product weighed to obtain the yield. ^{1}H NMR spectroscopy was used to determine terminal/internal alkene selectivity for products.

2.15.2 General procedure for catalytic decarbonylative dehydration reactions using d^{6}-Ac_2O

General synthetic procedure was as above using ½ molar scale and d^{6}-Ac_2O. One molar equivalent of methyl benzoate was added to the isolated alkene product, determined by mass, and a ^{1}H NMR spectrum obtained to determine deuterium incorporation by comparison of integrals to the methyl peak of methyl benzoate, an example calculation is in the appendix section of this thiesis.

2.15.3 Addition of myristoyl iodide to [Rh(PN-Ar)(CO)I] complexes

Myristoyl iodide was prepared from myristic acid as described by Keinan et al.[4] and distilled under vacuum 175 ^{o}C/ 0.67 mbar. Myristoyl iodide was then placed under an Ar atmosphere and a solution of [Rh(PN-Ar)(CO)I] (~0.1 g, ~0.15 mmol) in CH_2Cl_2 (5 mL) was added. This solution was monitored periodically by IR spectroscopy.

2.16 Preparation of *N*-[[2-(diphenylphosphinyl)phenyl]methyl]-*N*-(aryl)-acetamides

Phosphinyl acetamide compounds were prepared by mixing PN-Ar (0.5 mmol), myristic acid 0.338 g (1.48 mmol), potassium iodide (0.150 g, 0.904 mmol) and acetic anhydride 0.35 mL

(3.70 mmol) in a snap cap microwave tube and purging with N_2 for 10 minutes. This solution was heated to 160 °C for 3 hours. After 3 hours the solution was cooled to room temperature and the mixture separated by column chromatography 7:3 ethyl acetate:40-60 petroleum ether, yielding phosphinyl acetamides as yellow powders.

2.16.1 Synthesis of *N*-[[2-(diphenylphosphinyl)phenyl]methyl]-*N*-(2,6 diisopropylbenzyl)-acetamide

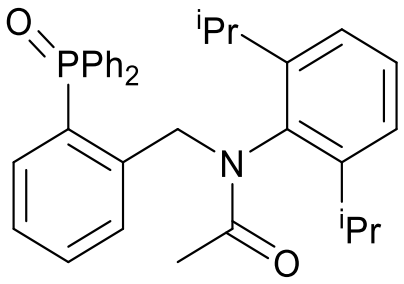

N-[[2-(diphenylphosphinyl)phenyl]methyl]-N-(2,6 diisopropylbenzyl)-acetamide was prepared using the method outlined above using PN-$^{i}Pr_2$Ph (0.184 g, 0.41 mmol), myristic acid (0.353 g, 1.55 mmol), potassium iodide (0.125 g, 0.75 mmol) and acetic anhydride (0.35 mL, 3.70 mmol). giving OPCO-Me_2Ph as a yellow powder (0.063 g, 0.138 mmol, 27.5% yield).

IR ν(CO) (CH_2Cl_2): 1648 cm^{-1}

^{1}H NMR δ/ppm ($CDCl_3$): 7.95 (dd, 1H, J = 7.6, 4.1 Hz, arom), 7.59 – 7.50 (m, 1H, arom), 7.50 – 7.39 (m, 5H, arom), 7.37 – 7.26 (m, 5H, arom), 7.25 – 7.15 (m, 2H, arom), 7.02 – 6.93 (m, 3H, arom), 5.26 (s, 2H, NC**H$_2$**Ar), 2.85 (sept, 2H, J = 6.8 Hz, CH_3(R)C**H**CH_3), 1.84 (s, 3H, N-COC**H$_3$**), 1.11 (d, 6H, J = 6.8 Hz, C**H$_3$**(R)CHCH_3), 0.77 (d, 6H, J = 6.8 Hz, CH_3(R)CHC**H$_3$**)

^{31}P NMR δ/ppm ($CDCl_3$): 31.9 s

High resolution MS (TOF ES + m/z): 508.25 [M] – H^+

2.16.2 Synthesis of *N*-[[2-(diphenylphosphinyl)phenyl]methyl]-*N*-(2,6 dimethylbenzyl)-acetamide

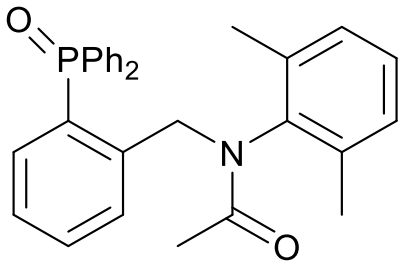

N-[[2-(diphenylphosphinyl)phenyl]methyl]-N-(2,6 dimethylbenzyl)-acetamide was prepared using the method outlined above using PN-Me_2Ph (0.201 g, 0.510 mmol), myristic acid (0.338 g, 1.48 mmol), potassium iodide (0.150 g, 0.904 mmol) and acetic anhydride (0.35 mL, 3.70 mmol) giving OPCO-Me_2Ph as a yellow powder (0.074 g, 0.163 mmol, 32 % yield).

IR ν(CO) (CH_2Cl_2): 1649 cm^{-1}

^{1}H NMR δ/ppm ($CDCl_3$): 7.99 (dd, 1H, J = 7.6, 4.1 Hz, arom), 7.63 – 7.31 (m, 10H, arom), 7.22 (dd, 2H, J = 10.8, 4.3 Hz, arom), 7.12 – 6.80 (m, 4H, arom), 5.33 (s, 2H, NC**H_2**Ar), 1.93 (s, 6H, C**H_3**Ar), 1.75 (s, 3H, N-COC**H_3**)

^{31}P NMR δ/ppm ($CDCl_3$): 31.8 s

High resolution MS (TOF ES + m/z): 452.19 [M] – H^+

2.17 References

(1) Pangborn, A. B.; Giardello, M. A.; Grubbs, R. H.; Rosen, R. K.; Timmers, F. J. *Organometallics* **1996**, *15*, 1518–1520.

(2) Frisch, M. J.; Trucks, G. W.; Schlegel, H. B.; Scuseria, G. E.; Robb, M. A.; Cheeseman, J. R.; Scalmani, G.; Barone, V.; Mennucci, B.; Petersson, G. A.; Nakatsuji, H.; Caricato, M.; Li, X.; Hratchian, H. P.; Izmaylov, A. F.; Bloino, J.; Zheng, G.; Sonnenberg, J. L.; Hada, M.; Ehara, M. K.; Toyota; Fukuda, R.; Hasegawa, J.; Ishida, M.; Nakajima, T.; Honda, Y.; Kitao, O.; Nakai, H.; Vreven, T.; Montgomery, J. A. J.; Peralta, J. E.; Ogliaro, F.; Bearpark, M.; Heyd, J. J.; Brothers, E.; Kudin, K. N.; Staroverov, V. N.; Keith, T.; Kobayashi, R.; Normand, J.; Raghavachari, K.; Rendell, A.; Burant, J. C.; Iyengar, S. S.; Tomasi, J.; Cossi, M.; Rega, N.; Millam, J. M.; Klene, M.; Knox, J. E.; Cross, J. B.; Bakken, V.; Adamo, C.; Jaramillo, J.; Gomperts, R.; Stratmann, R. E.; Yazyev, O.; Austin, A. J.; Cammi, R.; Pomelli, C.; Ochterski, J. W.; Martin, R. L.; Morokuma, K.; Zakrzewski, V. G.; Voth, G. A.; Salvador, P.; Dannenberg, J. J.; Dapprich, S.; Daniels, A. D.; Farkas, O.; Foresman, J. B.; Ortiz, J. V.; Cioslowski, J.; Fox, and D. J.; Gaussian, Inc., W. C. Gaussian 09, Revision D.01, 2013.

(3) Pasha, M. A.; Rizwana, S. *Indian J. Chem.* **2005**, *44*, 420–421.

(4) Keinan, E.; Sahai ', M. *J . Org. Chem* **1990**, *55*, 3922–3926.

(5) Fortner, K. C.; Shair, M. D. *J. Am. Chem. Soc.* **2007**, *129*, 1032–1033.

(6) McCleverty, J. A.; Wilkinson, G. *Inorg. Synth.* **1966**, *8*, 211.

(7) Haynes, A.; Maitlis, P. M.; Stanbridge, I. a.; Haak, S.; Pearson, J. M.; Adams, H.; Bailey, N. a. *Inorganica Chim. Acta* **2004**, *357*, 3027–3037.

(8) Fulford, A.; Hickey, C.; Maitlis, P. *J. Organomet. Chem.* **1990**, *398*, 311–323.

(9) Heaton, B. T.; Jacob, C.; Moffet, S. *J. Organomet. Chem.* **1993**, *462*, 347–352.

(10) Adamson, G. W.; Daly, J. J.; Forster, D. *J. Organomet. Chem.* **1974**, *71*, C17–C19.

(11) White, C.; Yates, A.; Maitlis, P. M.; Heinekey, D. M. John Wiley & Sons, Inc.; pp. 228–234.

(12) Kang, J.; Maitlis, P. *J. Organomet. Chem* **1971**, *30,* 127-133.

(13) Otto, S.; Roodt, A.; Erasmus, J. J. C.; Swarts, J. C. *Polyhedron* **1998**, *17*, 2447–2453.

(14) Pearson, J. M. PhD Thesis, University of Sheffield, 1994.

(15) Forster, D. *Synth. React. Inorg. Met. Chem.* **1971**, *1*, 221–226.

(16) Crochet, P.; Gimeno, J.; Borge, J.; García-Granda, S. *New J. Chem.* **2003**, *27*, 414–420.

(17) Cocker, D. Synthesis and reactivity of Rh(I) and Ir(I) complexes and their application in catalytic decarbonylative dehydration reactions, PhD Thesis, University of Sheffield, 2015.

(18) Tian, M.; Li, J.; Zhang, S.; Guo, L.; He, X.; Kong, D.; Zhang, H.; Liu, Z. *Chem. Commun.* **2017**, *53*, 12810–12813.

(19) Lobana, T.; Sharma, P. *Ind. J. Chem.* **1987**, *26*, 784–785.

(20) Bond, A. M.; Colton, R.; Panagiotidou, P. *Organometallics* **1988**, *7*, 1774–1782.

(21) Best, J.; Wilson, J. M.; Adams, H.; Gonsalvi, L.; Peruzzini, M.; Haynes, A. *Organometallics* **2007**, *26*, 1960–1965.

(22) Gonsalvi, L.; Gaunt, J. A.; Adams, H.; Castro, A.; Sunley, G. J.; Haynes, A. *Organometallics* **2003**, *22*, 1047–1054.

(23) Williams, G. L.; Parks, C. M.; Smith, C. R.; Adams, H.; Haynes, A.; Meijer, A. J. H. M.; Sunley, G. J.; Gaemers, S. *Organometallics* **2011**, *30*, 6166–6179.

(24) Kubiak, C.; Woodcock, C.; Eisenberg, R. *Inorg. Chem.* **1982**, *21*, 2119.

(25) Haynes, A.; Maitlis, P. M.; Stanbridge, I. A.; Haak, S.; Pearson, J. M.; Adams, H.; Bailey, N. A. *Inorg Chim. Acta* **2004**, *357*, 3027–3037.

(26) Adams, H.; Bailey, N. A.; Mann, B. E.; Manuel, C. P. *Inorg. Chim. Acta* **1992**, *198–200*, 111–118.

(27) Gonsalvi, L.; Adams, H.; Sunley, G. J.; Ditzel, E.; Haynes, A. *J. Am. Chem. Soc.* **2002**, *124*, 13597–13612.

(28) Moloy, K. G.; Petersen, J. L. *Organometallics* **1995**, *14*, 2931–2936.

(29) Lamb, G.; Clarke, M.; Slawin, A. M. Z.; Williams, B.; Key, L.; Roukoss, C.; Fiddy, S.; de Mallmann, A.; Rendón, N.; Basset, J.-M.; Kuntz, E.; Copéret, C. *Dalton Trans.* **2007**, 5582–5589.

(30) Williams, G. L. A Mechanistic Study of Rhodium / Xantphos Catalysed Methanol

Carbonylation, PhD Thesis, University of Sheffield, 2008.

(31) Rose, R. Reactivity of P-Se Chelate Complexes of Rhodium, MChem Thesis, University of Sheffield, 2009.

Chapter 3

Reactions of Rh(III) diphosphine acetyl complexes with carboxylates

Complexes

1) [Rh(P-P)(CO)I]

1a	dppm
1b	dppe
1c	dppp
1d	dppb

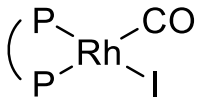

3) [Rh(P-P)(COMe)I_2]

3a	dppm
3b	dppe
3c	dppp
3d	dppb
3e	xantphos
3f	DPEphos

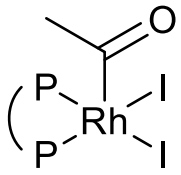

4) [Rh(P-P)(COMe)(OAc)I]

4a	dppm
4b	dppe
4c	dppp
4d	dppb
4e	xantphos

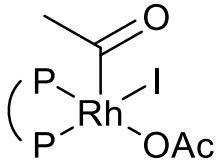

5) [Rh(P-P)(COMe)(OBz)I]

5a	dppm
5b	dppe
5c	dppp
5d	dppb
5e	xantphos

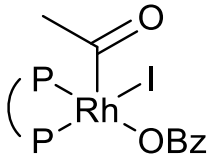

6) [Rh(P-P)(COMe)(TFA)I]

6a	dppm
6b	dppe
6c	dppp
6d	dppb

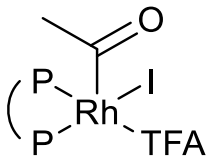

3.0 Introduction

The effects of diphosphine ligands on the rate of rhodium catalysed methanol carbonylation have been widely studied.[1–4] Primarily, the effect of these ligands on enhancing the rate of oxidative addition of MeI to Rh(I) complexes has been investigated. In the original communication from Monsanto [$Rh(CO)(PPh_3)_2Cl$] was found to be a viable catalyst precursor.[5] Diphosphine ligands are potentially attractive as they are strongly donating and so can increase the nucleophilicity of the Rh(I) species. A general scheme for methanol carbonylation when using a rhodium/diphosphine catalyst is shown in Scheme 3.1. Product formation is typically proposed to occur via reductive elimination of acetyl iodide and subsequent hydrolysis to form acetic acid. As discussed in Chapter 1 Kalck and co-workers[6,7] proposed that in the Monsanto system, an alternative mechanism may involve formation of acetate in solution. The acetate then reacts with a rhodium acetyl complex to give acetic anhydride which is subsequently hydrolysed to give acetic acid.

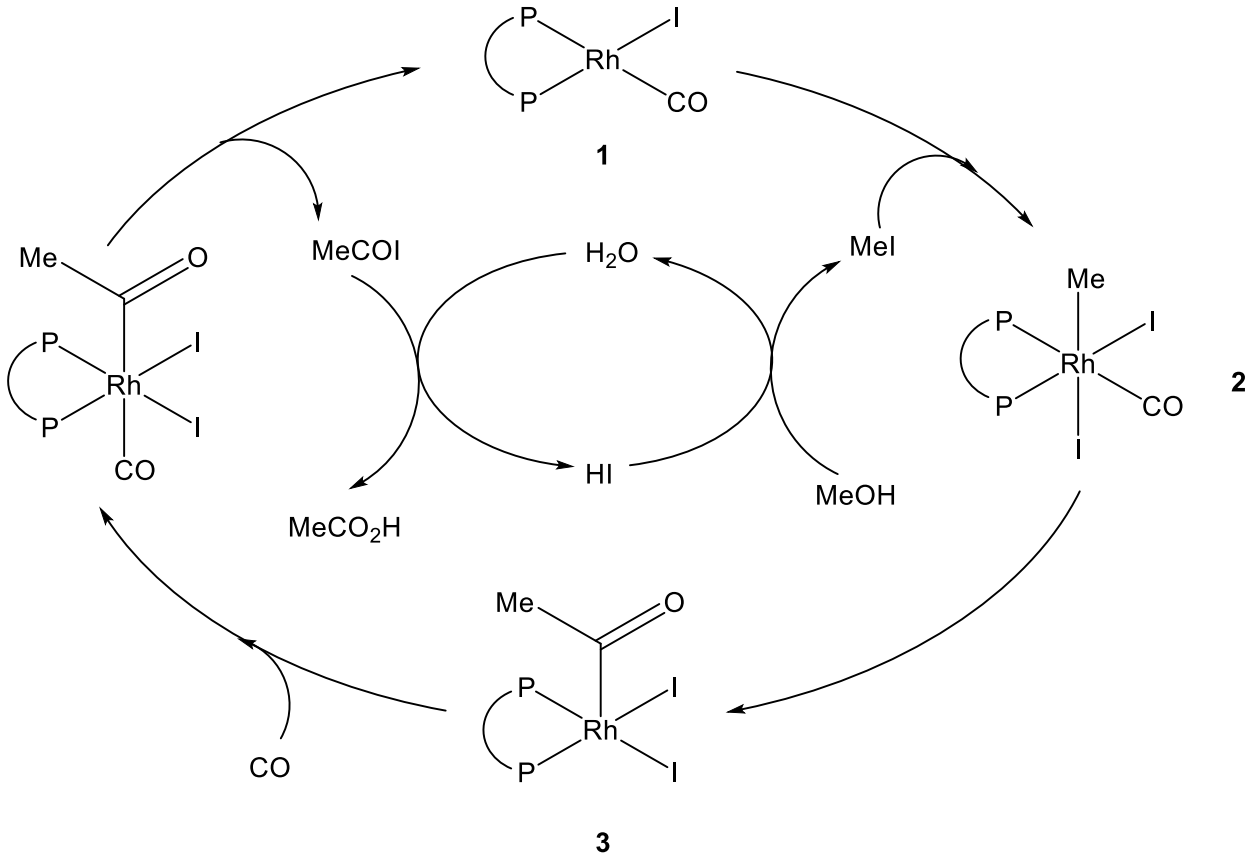

Scheme 3.1: General mechanism of methanol carbonylation using diphosphine ligands.

Many stable rhodium(III) acetyl complexes of formula [Rh(P-P)(COMe)I_2] (**3**) have been isolated and characterised.[2–4,8] Due to their greater stability and higher electron density on rhodium it may be expected that the reaction of these complexes with carboxylates would be slower than for [Rh(COMe)$(CO)_2I_3$]$^-$, enabling mechanistic investigations.

This chapter reports an investigation of the reactions of carboxylates with a series of rhodium acetyl diphosphine complexes of formula [Rh(P-P)(COMe)I_2] (**3**) containing ligands **a-f**, Scheme 3.2.

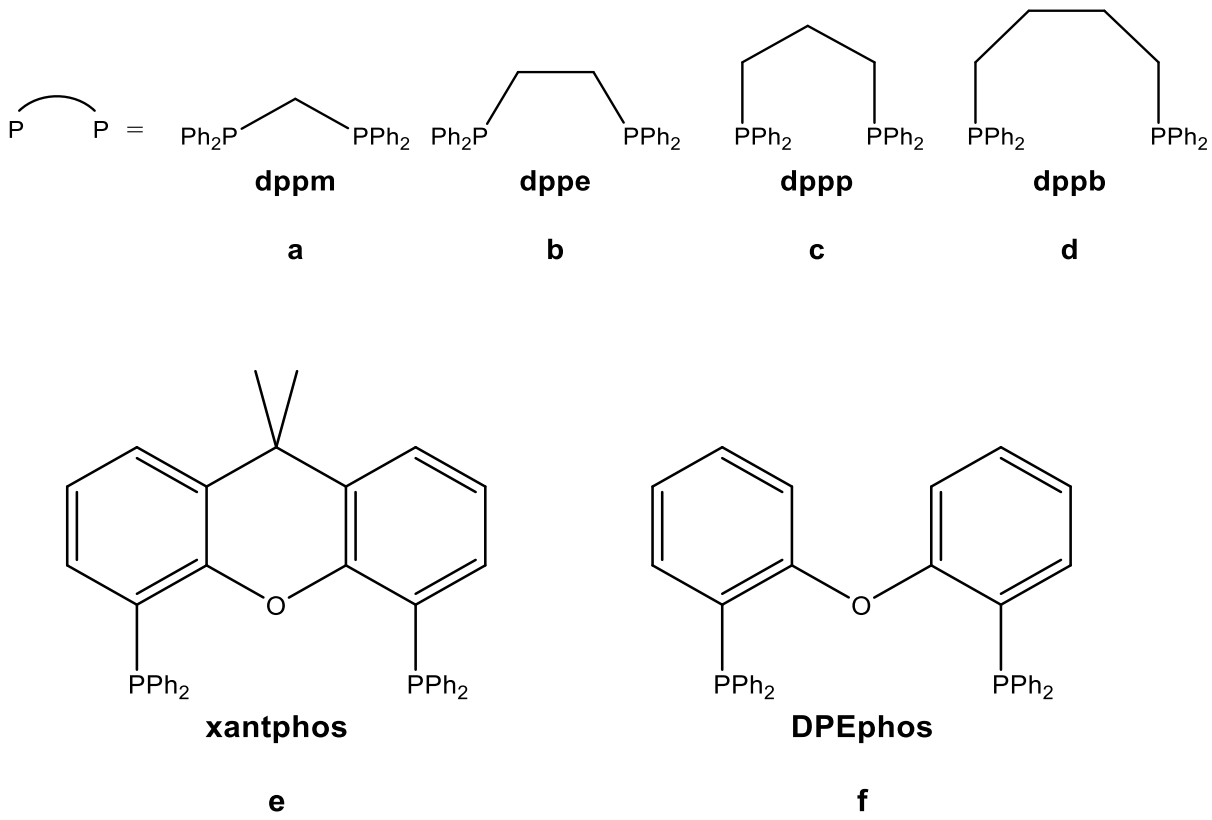

Scheme 3.2: Diphosphine ligands used in this chapter

Reactions of complexes **3a-f** with [Bu_4N][OAc], [Bu_4N][OBz] and [Ag][TFA] were monitored spectroscopically to determine if anhydrides are formed and whether intermediates in the reaction mechanism can be detected.

3.1 Results and discussion

3.1.1 Synthesis of [Rh(P-P)(COMe)I_2] complexes

Rhodium(III) acetyl complexes of general formula [Rh(P-P)(COMe)I_2] (**3a-f**) were synthesised using methods reported previously by Haynes and coworkers.[4,9] Scheme 3.3 shows the two routes used. For complexes **3a-c,e,f** reaction of the Rh(I) precursor [Rh(CO)$_2$I]$_2$ with MeI in MeCN initially gave the dimeric Rh(III) acetyl complex, [Rh(COMe)(NCMe)(CO)I_2]$_2$, isolated as a red powder. Reaction of this complex with two equivalents of diphosphine ligand in toluene resulted in cleavage of the dimer and substitution of CO and MeCN ligands to yield the chelate product [Rh(P-P)(COMe)I_2]. In the case of **3d**, the reaction of [Rh(CO)$_2$I]$_2$ and dppb (**d**) in CH_2Cl_2 formed [Rh(dppb)(CO)I] **1d** *in situ* and subsequent addition of iodomethane gave the product, **3d**.

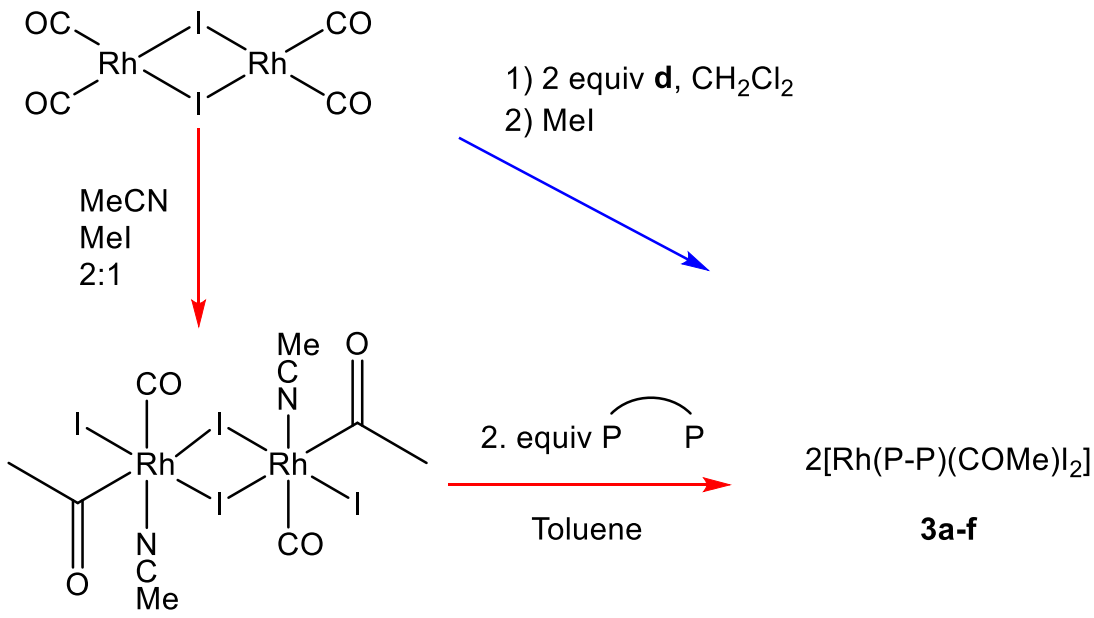

Scheme 3.3: Two synthetic pathways used to synthesise [Rh(P-P)(COMe)I_2] complexes 3a-f

Table 3.1 shows selected spectroscopic data for complexes **3a-f**. The ^{31}P ,^{1}H NMR and IR spectra are consistent with data reported in the literature.[4,10] Each complex shows a doublet in the ^{31}P NMR spectrum due to equivalent P atoms and coupling to ^{103}Rh. The ^{1}H NMR spectra

display singlets near 3 ppm due to the acetyl ligand and the IR spectra show the expected ν(C=O) absorption around 1700 cm^{-1}.

Table 3.1: Selected spectroscopic data for complexes 3a-f

	[Rh(P-P)(COMe)I_2]	ν(CO) /cm^{-1} (CH_2Cl_2)	δ ^{1}H COCH_3 ($CDCl_3$) /ppm	δ ^{31}P (J_{P-Rh})($CDCl_3$) /ppm
3a	dppm	1709	3.10s	-25.7d (119.5 Hz)
3b	dppe	1711	2.80s	70.5d (139.0 Hz)
3c	dppp	1701	3.09s	17.9d (131.5 Hz)
3d	dppb	1700	2.76s	31.61d (139.1Hz)
3e	xantphos	1683, 1666	2.90t	9.7d (108.5 Hz)
3f	DPEphos	1686, 1664	2.90t	7.5d (113.0Hz)

The reactions of these complexes with carboxylates under either an N_2 or CO atmosphere were monitored by *in situ* IR, ^{31}P and ^{1}H NMR spectroscopy to investigate the formation of anhydrides by coupling of the acetyl ligand with carboxylate.

3.1.2 Reaction of [Rh(dppe)(COMe)I_2] (3b) with [Bu_4N][OAc]

The reaction of **3b** with [Bu_4N][OAc] will be treated as a representative example and discussed in detail in this section.

Figure 3.1 shows several IR spectra obtained over 3 hours during the reaction of [Bu_4N][OAc] with **3b** under N_2 in CH_2Cl_2. After one minute the ν(CO) band for [Rh(dppe)(COMe)I_2] at 1711 cm^{-1} has almost completely decayed. The band for [Bu_4N][OAc] at 1577 cm^{-1} also decays over this time. As starting material bands decay, rapid formation of a band at 1687 cm^{-1} is observed, assigned as an intermediate complex, [Rh(dppe)(COMe)(OAc)I] **4b**. This species then decays

with growth of bands at 1825 and 1756 cm^{-1} that indicate formation of acetic anhydride. No Rh(I) carbonyls species were observed to form by IR spectroscopy in the absence of CO.

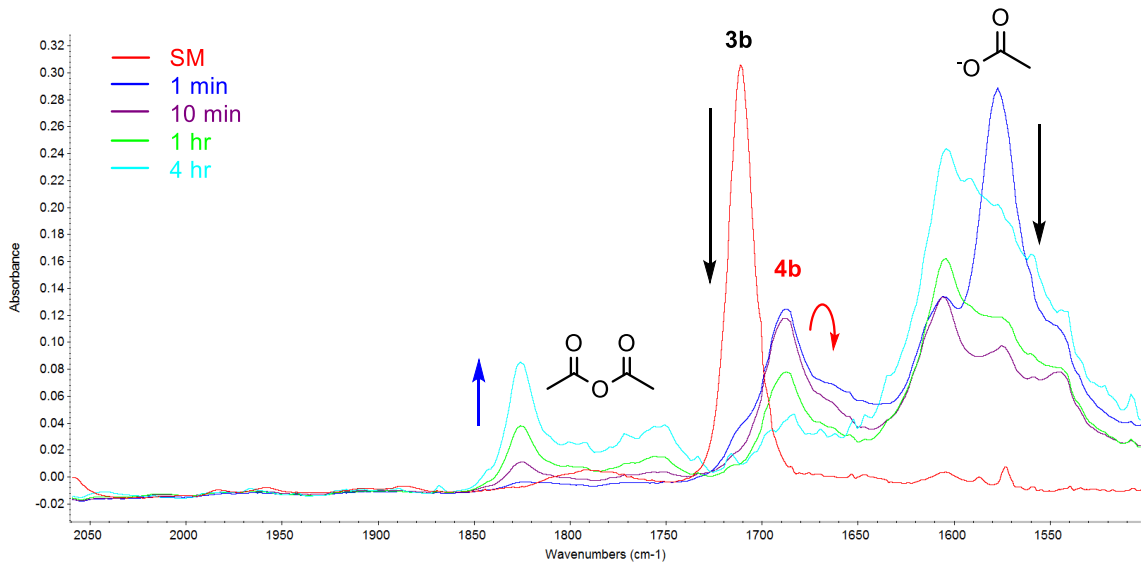

Figure 3.1: IR spectra obtained for the reaction of $[Bu_4N][OAc]$ with 3b in CH_2Cl_2 over 3 h under N_2.

The reaction of acetate with **3b** was also conducted under a CO atmosphere. Figure 3.2 shows a series of spectra obtained over 4 hours during this experiment. After two minutes, rapid decay of bands for **3b** and acetate at 1711 and 1577 cm^{-1} respectively coincides with formation of a new band at 1687 cm^{-1} corresponding to **4b**, as observed under N_2. Decay of this intermediate is accompanied by formation of acetic anhydride (1825, 1756 cm^{-1}) and a ν(CO) band at 2010 cm^{-1} which is assigned to [Rh(dppe)(CO)I] (**1b**). Weak bands at 2059, 1988 cm^{-1} indicate formation of a small amount of $[Rh(CO)_2I_2]^-$.

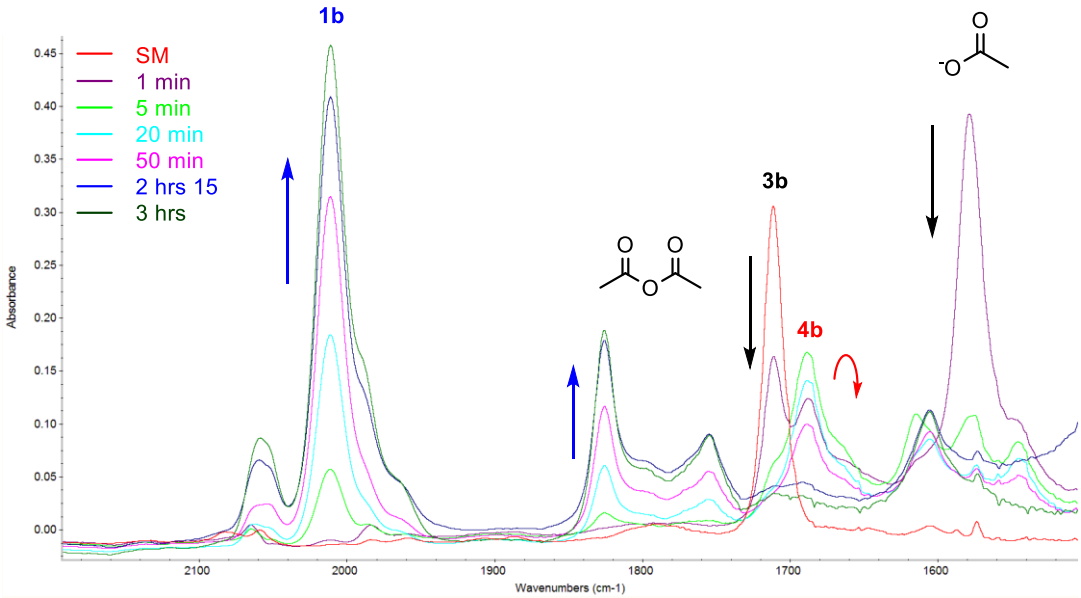

Figure 3.2: IR spectra obtained for the reaction of $[Bu_4N][OAc]$ with 3b in CH_2Cl_2 over 4 h under CO.

Coordinated acetate should show absorptions between 1300 – 1700 cm^{-1}, but IR absorptions of the solvent, CH_2Cl_2, make it difficult to discern peaks in this region.

Phillips and Deacon [11]discussed the relationship between carbon-oxygen stretching frequencies of carboxylato complexes and the type of carboxylate coordination. Scheme 3.4 shows several possible ways carboxylate can coordinate to metals; I) as a monodentate ligand, II) as a chelating ligand, III) as a bridging bidentate ligand and IV) as a mono atomic bridging ligand.

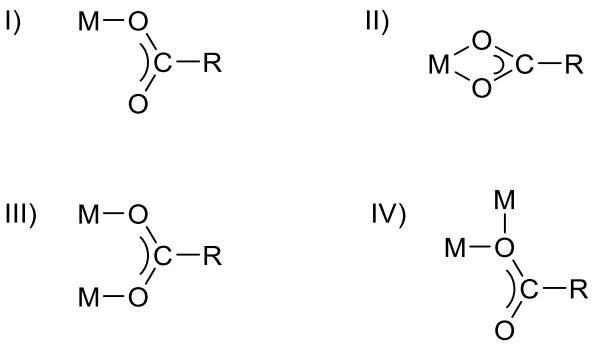

Scheme 3.4: Coordination modes of carboxylate ligands

By analysis of IR spectra and crystallographic structures for a large range of complexes, Phillips and Deacon determined empirical relationships between carbon-oxygen stretching frequencies and the type of carboxylate coordination were discerned. A large separation ($\Delta \geq 200$ cm^{-1}) between $\nu_{asym}(CO_2)$ and $\nu_{sym}(CO_2)$ is indicative of monodentate coordination. Complexes with a small separation ($\Delta \leq 150$ cm^{-1}) are indicative of chelating acetate groups, or acetate groups which are both chelating and bridging.

In order to determine the coordination mode of acetate using IR spectroscopy a solid-state IR spectrum was obtained. The reaction of **3b** with one equivalent of $[Bu_4N][OAc]$ in CH_2Cl_2 was monitored *in-situ* until the complete conversion of **3b** into **4b**. The solvent was then removed *in vacuo* and an ATR-IR spectrum of the resulting solid recorded, given in the appendix of this thesis. This showed $\nu(CO_2)$ bands for coordinated acetate at 1545 and 1435 cm^{-1}. The separation between $\nu_{asym}(CO_2)$ and $\nu_{sym}(CO_2)$ of 110 cm^{-1} is consistent with chelate coordination of a carboxylate as discussed by Phillips.[11]

The reaction of **3b** and $[Bu_4N][OAc]$ in $CDCl_3$ under N_2 was monitored by ^1H NMR spectroscopy. Figure 3.3 shows a ^1H NMR spectrum obtained 15 minutes after the addition of $[Bu_4N][OAc]$ to a solution of **3b**. A small peak for $COCH_3$ of **3b** at 2.81 ppm can still be observed, as well as two new singlets at 2.54 ($COCH_3$) and 1.69 ppm ($OCOCH_3$), assigned to intermediate **4b**. As these peaks decay, growth of a peak at 2.25 ppm is consistent with formation of acetic anhydride.

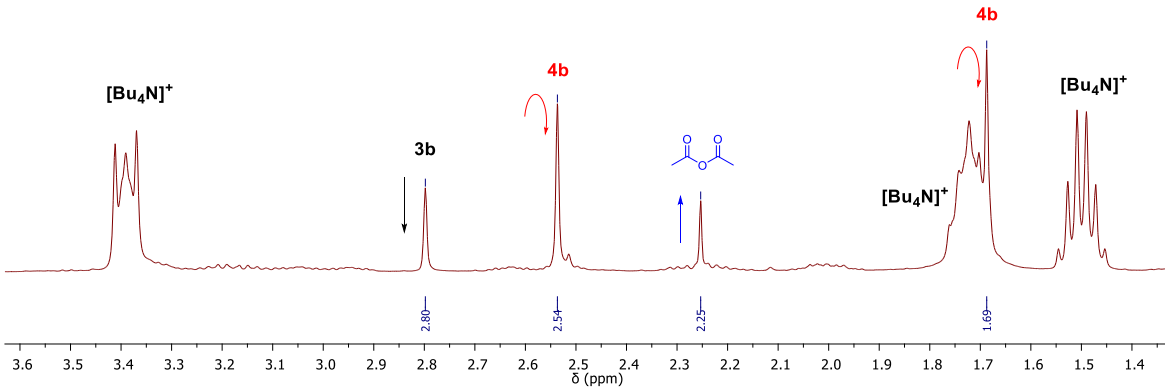

Figure 3.3: ^{1}H NMR spectrum obtained 15 min after addition of [Bu$_4$N][OAc] to 3b in CDCl$_3$ under N$_2$.

Figure 3.4 shows a ^{31}P{^{1}H} NMR spectrum taken 5 minutes after addition of [Bu$_4$N][OAc] to **3b** in CDCl$_3$ under N$_2$. Some of the reactant complex is still present, however two new doublets of doublets at 66.46 and 60.84 ppm are assigned to intermediate **4b**, indicating inequivalence of the phosphorus atoms of the dppe ligand, due to a loss of symmetry of the molecule. This is consistent with acetate replacing an iodide ligand of **3b** to form intermediate **4b**. As this species decays formation of acetic anhydride is observed in the ^{1}H NMR spectrum. A ^{31}P peak at 32.60 ppm indicates that some oxidised dppe is present after the formation of acetic anhydride, however no rhodium(I) product was observed.

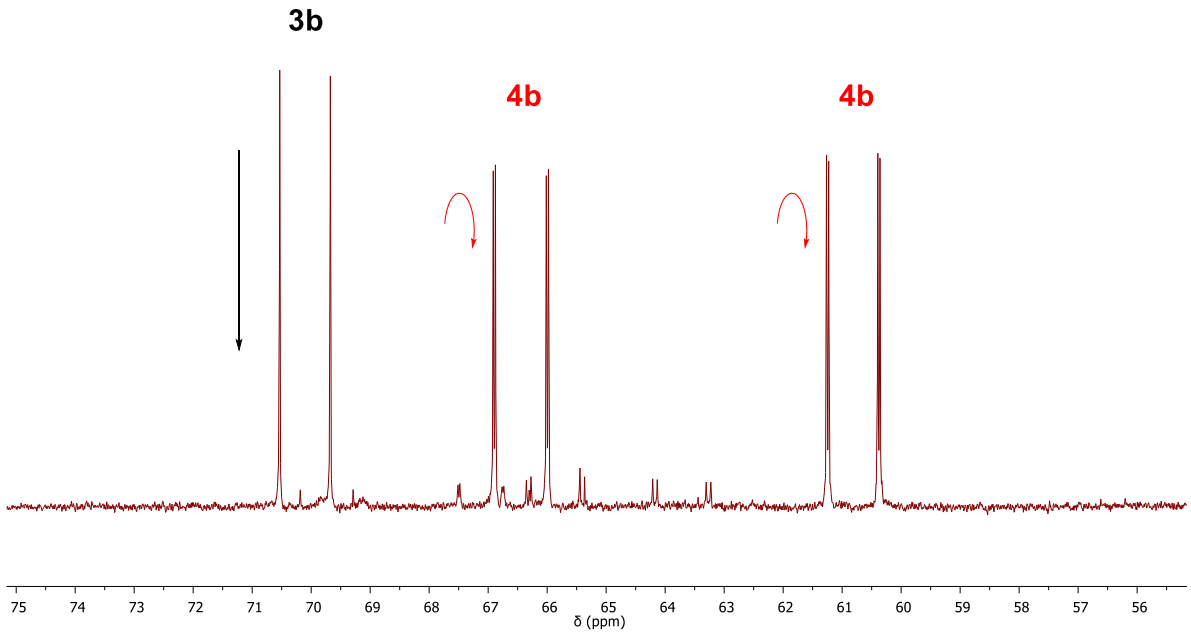

Figure 3.4: $^{31}P\{^{1}H\}$ NMR spectrum 5 minutes after addition of $[Bu_4N][OAc]$ to 3b in $CDCl_3$

Some minor doublets are also apparent in Figure 3.4 and a small singlet at 2.51 ppm in Figure 3.3. These may be due to species arising from exchange of iodide ligands with chloride ions in solution. A spectrum in d^6 acetone showed no minor peaks in these regions, indicating that the chlorinated solvent could be responsible for them, possibly due to traces of HCl or the reaction of free acetate with chloroform (Scheme 3.5). An experiment with acetate in CH_2Cl_2 showed that over 2 days a band appeared at 1764 cm^{-1}, indicating formation of chloromethyl acetate.

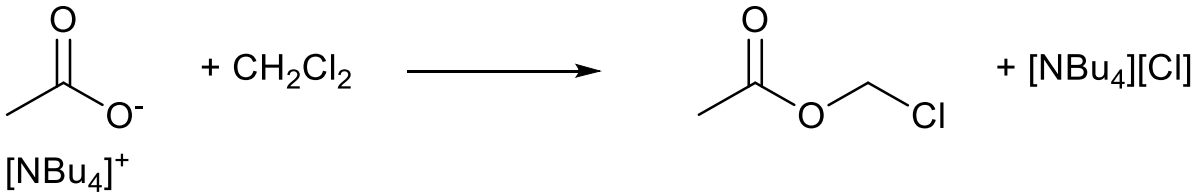

Scheme 3.5: Reaction of CH_2Cl_2 and acetate

When conducted under a CO atmosphere, as intermediate **4b** decays and acetic anhydride is observed in the ^{1}H NMR spectrum, two doublets of doublets in the ^{31}P {^{1}H} NMR at δ 70.42 and 51.92 indicate formation of [Rh(dppe)(CO)I] (**1b**), as observed by IR.

Based on the spectroscopic data, reaction of [Bu_4N][OAc] with **3b** leads to formation of an intermediate **4b** with acetate replacing an iodide ligand. A solid-state IR spectrum indicates chelate coordination of acetate. As the intermediate **4b** decays, formation of acetic anhydride is observed, accompanied by formation of **1b** when under a CO atmosphere. Intermediate **4b** eliminates anhydride readily and so could not be isolated as a pure solid.

Several structural isomers that can be considered for **4b** are shown in Scheme 3.6. Both **4b$_1$** and **4b$_2$** are unsymmetrical complexes, with either chelate or monodentate coordination of acetate. This is consistent with the evidence obtained from ^{31}P NMR spectroscopy for an unsymmetrical complex. Isomer **4b$_3$**, however, is a symmetrical complex with equivalent P atoms so cannot be the intermediate observed. ATR IR spectroscopy indicates chelate coordination of acetate in **4b**, suggesting that conformer **4b$_1$** is most likely.

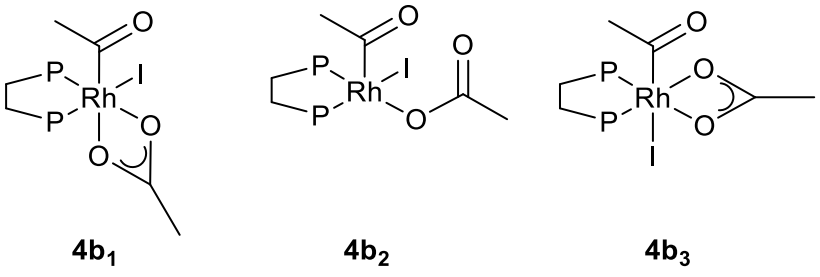

Scheme 3.6: Possible structural isomers of 4b (Ph groups omitted for clarity)

DFT modelling (*Gaussian09,* B3LYP, 6-311G, SDD on Rh, solvent CH_2Cl_2 modelled by PCM) was used to determine the most likely coordination mode of acetate in **4b**. Relative energies for **4b$_{1-3}$** are given in Table 3.2. Isomer **4b$_1$** is lower in energy (ΔG) than both **4b$_2$** and **4b$_3$**. This supports the suggestion that **4b$_1$** is the isomer formed upon addition of acetate to **3b** before reductive elimination of acetic anhydride.

Table 3.2: Relative Gibbs energies (ΔG) and calculated ν(CO) frequencies of acetyl and acetate ligands from DFT calculations.

Isomer	ΔG/ kJ mol^{-1}	Acetyl ν(CO)	ν $_{asym}$(CO_2)	ν $_{sym}$(CO_2)
3b	-	1756	-	-
4b$_1$	0	1741	1578	1423
4b$_2$	26.9	1753	1661	1322
4b$_3$	44.0	1727	1488	1456

The calculated acetyl and acetate ligand IR frequencies are also given in Table 3.2. The decrease in wavenumber for the acetyl ν(CO) observed for **4b$_1$** relative to **3b** supports the experimentally observed wavenumber decrease. Predicted carboxylate ν(CO_2) values for **4b$_1$** are typical for chelate coordinated carboxylates as observed in the ATR-IR spectrum for **4b**.

Scheme 3.7 shows the overall proposed reaction for reaction of acetate with **3b**. An iodide ligand is substituted by acetate forming **4b** with chelate coordination of the acetate ligand. This complex then undergoes reductive elimination to form acetic anhydride. In the presence of CO, **1b** and minor traces of $[Rh(CO)_2I_2]^-$ form after elimination of anhydride, whereas under N_2 no identifiable Rh(I) product was observed.

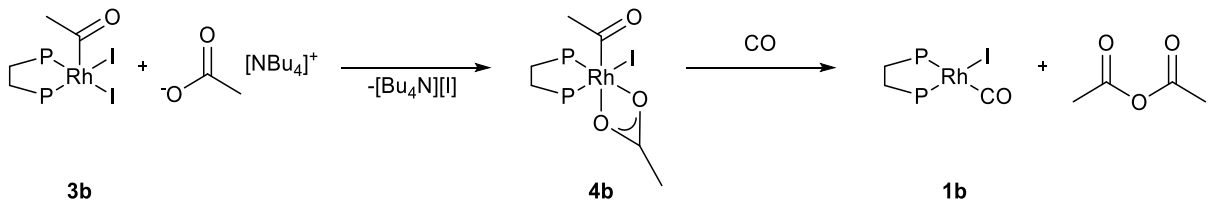

Scheme 3.7: Proposed scheme for reaction of 3b with [Bu$_4$N][OAc] under CO (Ph groups omitted for clarity)

3.1.3 Reaction of [Rh(dppe)(COMe)I_2] (3b) with [Bu_4N][OBz]

The reaction of **3b** with benzoate will be discussed in detail here as a representative example for the reactions of **3a-d**.

The addition of one equivalent of [Bu_4N][OBz] to **3b** in CH_2Cl_2, under a N_2 atmosphere, was monitored by *in-situ* IR spectroscopy. Rapid depletion of the bands at 1711 and 1563 cm^{-1}, due to **3b** and benzoate respectively, occurs over the first 2 minutes. This corresponds with growth of a band at 1690 cm^{-1}, consistent with formation of a carboxylate coordinated intermediate [Rh(dppe)(COMe)(OBz)I] **5b**, similar to the reaction of acetate with **3b**. As this intermediate decays, bands grow at 1810 and 1734 cm^{-1} that match those for the mixed anhydride, AcOBz, synthesised separately by the reaction of zinc acetate with benzoyl chloride. As for the reaction of **3b** and acetate under N_2, no discernible rhodium product was observed.

Figure 3.5 shows a series of IR spectra obtained over 3 hours upon addition of [Bu_4N][OBz] to **3b** in CH_2Cl_2 under a CO atmosphere. Intermediate **5b** at 1690 cm^{-1} is observed after 2 minutes. As AcOBz (1810, 1734 cm^{-1}) grows, a band appears at 2011 cm^{-1} corresponding to [Rh(dppe)(CO)I] **1b** as well as weak absorptions due to $[Rh(CO)_2I_2]^-$.

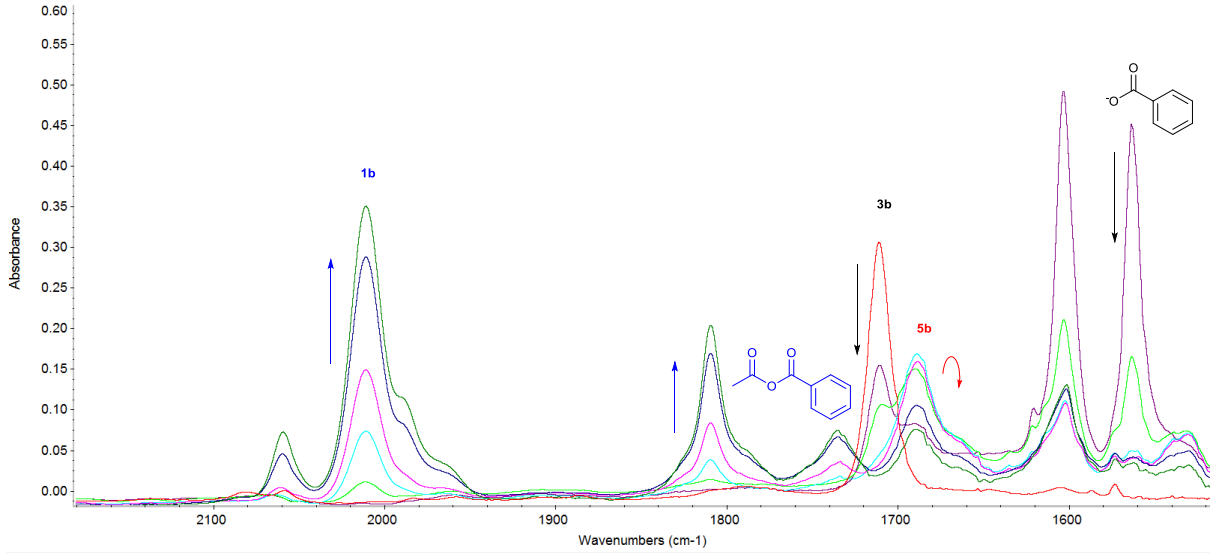

Figure 3.5: IR spectra obtained after addition of $[Bu_4N][OBz]$ to 3b under CO, CH_2Cl_2 over 3 hours

After ~5 hours bands at 1825, 1756 and 1789, 1725 cm^{-1} were observed, corresponding with formation of Ac_2O and Bz_2O respectively, presumably arising from scrambling of the mixed anhydride, AcOBz. To test this, a solution of AcOBz in CH_2Cl_2 was monitored by *in-situ* IR spectroscopy. After an hour a mixture of Ac_2O, Bz_2O and AcOBz was observed indicating that scrambling of anhydrides can occur in the absence of a metal catalyst, as shown in Scheme 3.8.

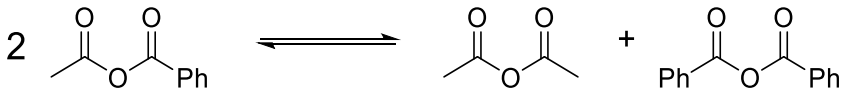

Scheme 3.8: AcOBz scrambling in solution to form Ac_2O and Bz_2O

Figure 3.6 shows a ^1H NMR spectrum obtained 1 hour after addition of $[Bu_4N][OBz]$ to a solution of **3b** in $CDCl_3$ under CO. Immediately after addition of benzoate, formation of a singlet at 2.61 ppm was observed, consistent with formation of a benzoate coordinated intermediate **5b**. As this intermediate decayed a peak appeared at δ 2.42 ppm, which matches

the separately synthesised acetic benzoic anhydride. However, minor species were also observed at 2.25 ppm and 2.54 ppm which correspond to acetic anhydride and [Rh(dppe)(COMe)(OAc)I] (**4b**) respectively. The presence of acetic anhydride was also observed by IR spectroscopy and is likely due to anhydride scrambling in solution, as discussed above.

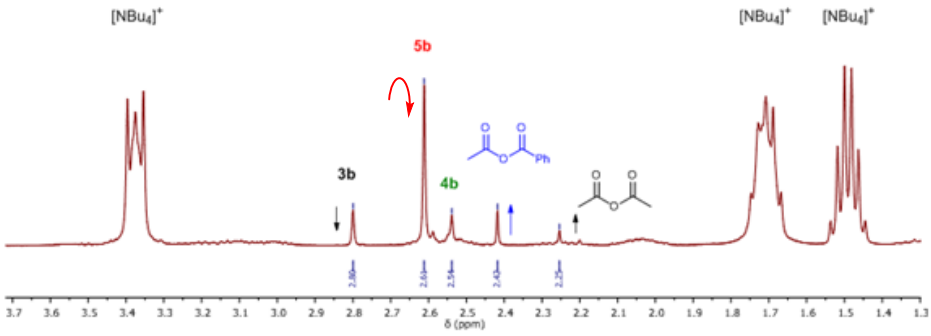

Figure 3.6: ^{1}H NMR spectrum obtained 1 hour after addition of [Bu$_4$N][OBz] to 3b in CDCl$_3$ under CO

A ^{31}P{^{1}H} NMR spectrum obtained 1 hour after addition of benzoate to **3b** under CO is shown in Figure 3.7. Two signals observed at δ 66.69 and 61.53 ppm (both dd) are assigned to intermediate **5b**, analogous to **4b** discussed above. As this intermediate decayed formation of AcOBz was observed in the ^{1}H NMR spectrum. As AcOBz is eliminated, appearance of peaks in the ^{31}P{^{1}H} NMR spectrum at δ 70.42 and 51.92 (both dd) is consistent with formation of **1b**. Minor signals were also observed at 66.46 (dd, *J* = 145.8, 5.9 Hz) and 60.84 (dd, *J* = 140.7, 5.9 Hz) ppm which indicate formation of **4b**, as observed in the ^{1}H NMR spectrum.

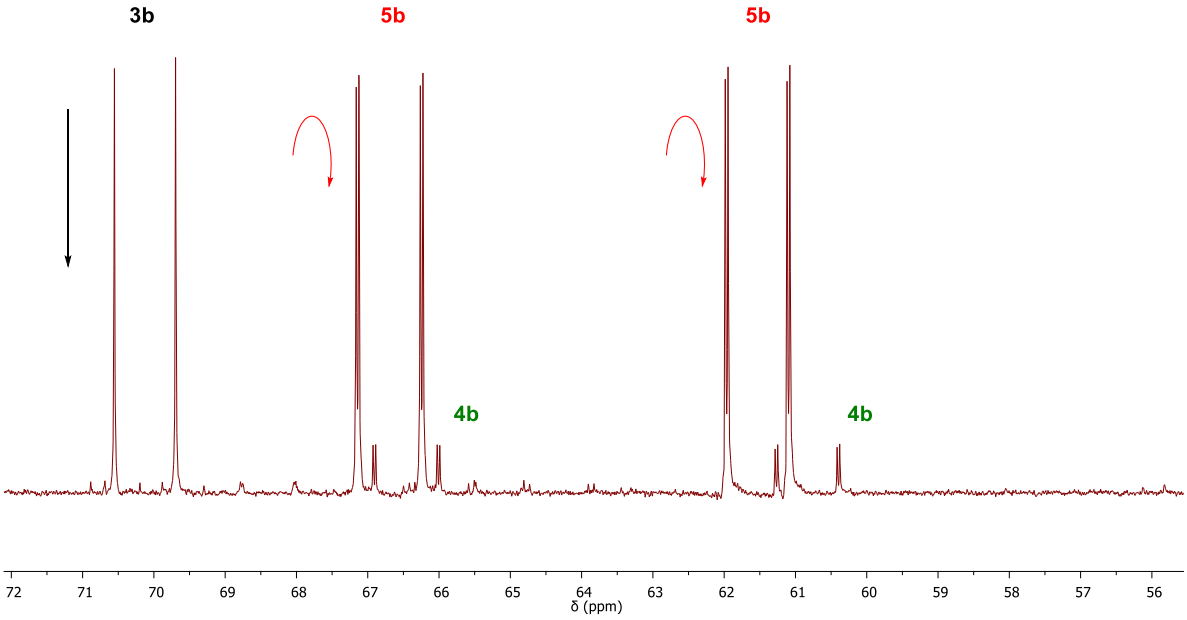

Figure 3.7: $^{31}P\{^{1}H\}$ NMR spectrum obtained 15 min after addition of $[Bu_4N][OBz]$ to 3b in $CDCl_3$

In order to explain the presence of **4b** in the ^{1}H and ^{31}P NMR spectra, the role of acetic anhydride, generated by scrambling of acetic benzoic anhydride, was considered. In principle, **4b** could be formed by oxidative addition of acetic anhydride to a Rh(I)-dppe complex. Oxidative addition of anhydrides to Rh(I)[12], Ir (I)[13] and Ni(II)/Pt(II)[14] complexes to give $M(COR)(O_2CR)$ has previously been reported. To test the reversibility of anhydride reductive elimination, a solution of [Rh(dppe)(CO)I] and acetic anhydride in $CDCl_3$ was heated to 333 K for 2 hours. A $^{31}P\{^{1}H\}$ NMR spectrum indicated formation of **4b** as well as some oxidised phosphine. Scheme 3.9 shows the reaction of **1b** and acetic anhydride leading to formation of **4b**.

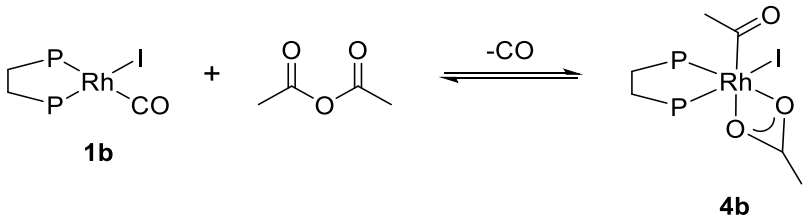

Scheme 3.9: Reaction of 1b and Ac_2O forming 4b, Ph groups omitted for clarity

The overall proposed mechanism for formation of **4b** upon addition of benzoate to **3b** is shown in Scheme 3.10. The Rh(I) species that participates is not precisely defined, as formation of **4b** occurs both under CO or N_2 atmospheres.

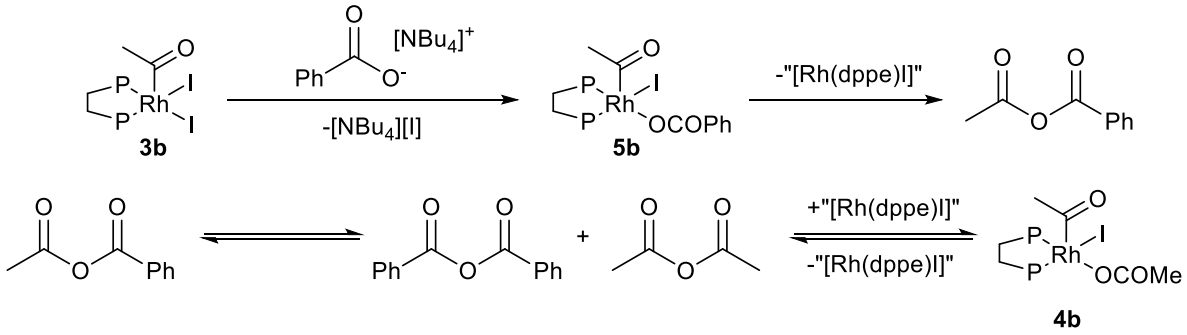

Scheme 3.10: Proposed mechanism for formation of [Rh(dppe)(COMe)(OAc)I] 4b upon addition of $[Bu_4N][OBz]$ to 3b, Ph groups on dppe omitted for clarity.

DFT calculations were performed on the structural isomers of **5b**, analogous to those investigated for **4b**. The presence of two inequivalent phosphorus atoms in the ^{31}P NMR spectrum indicates an unsymmetrical complex. The isomers are shown in Scheme 3.11 and relative energies are given in Table 3.3. It was found that the chelate complex $\mathbf{5b_1}$ is 17.6 kJ mol^{-1} lower in energy (ΔG) than $\mathbf{5b_2}$ with a monodentate benzoate ligand and 45.3 kJ mol^{-1} lower in energy than $\mathbf{5b_3}$. These results are comparable to the calculations for isomers of **4b**.

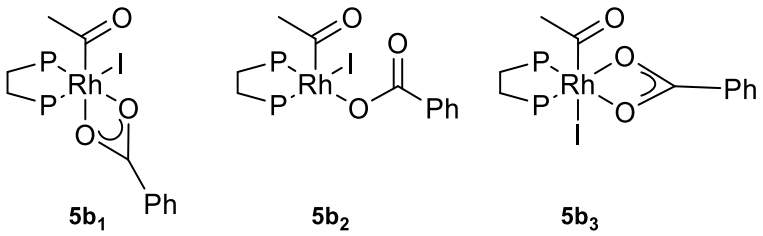

5b$_1$ **5b$_2$** **5b$_3$**

Scheme 3.11: Possible structural isomers for coordination of benzoate to 5b, Ph groups omitted for clarity

Table 3.3: Relative Gibbs energies (ΔG) and acetyl ν(CO) frequencies for isomers of 5b from DFT calculations.

Isomer	ΔG/ kJ mol^{-1}	Acetyl ν(CO)
3b	-	1756
5b$_1$	0	1744
5b$_2$	17.6	1760
5b$_3$	45.3	1727

The calculated acetyl ν(CO) frequency in **5b$_1$** shows a decrease relative to **3b** as observed experimentally. For isomer **5b$_2$** a higher frequency is predicted, further supporting the assignment of **5b$_1$** as the experimentally observed species.

Scheme 3.12 shows the overall proposed mechanism for the reaction. As for the reaction of **3b** and acetate, an iodide ligand is replaced by a chelate carboxylate ligand, in this case benzoate. This intermediate reductively eliminates AcOBz and in the presence of CO forms **1b**. The anhydride can then scramble in solution forming acetic anhydride and benzoic anhydride.

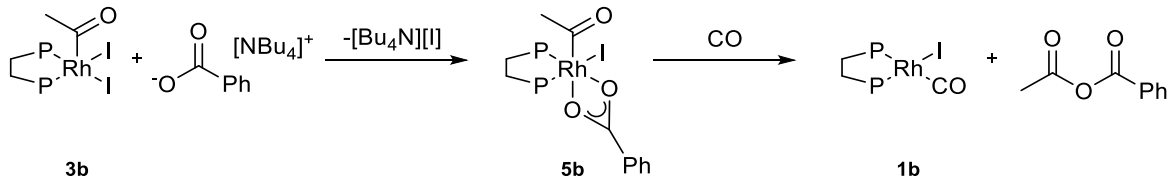

Scheme 3.12: Reaction of benzoate with [Rh(dppe)(COMe)I_2] 3b

3.1.4 Reaction of 3b [Rh(dppe)(COMe)I_2] with trifluoroacetate

As neither intermediate **4b** nor **5b** were isolable, the reaction of trifluoroacetate with **3b** was considered. It was thought that a less electron donating carboxylate may not eliminate an anhydride as rapidly. The reaction of **3b** and [$HNEt_3$][TFA] was monitored by IR, ^{31}P and ^{1}H NMR spectroscopy. However, after 2 days reflux no reaction was observed. Therefore, AgTFA was used to abstract an iodide ligand forming AgI and allowing trifluoroacetate to react with **3b**.

The reaction of **3b** and AgTFA (1 equivalent) was monitored over 30 hours, in MeCN under CO. As the band for **3b** at 1711 cm^{-1} decays in intensity, growth of a band is observed at 1695 cm^{-1} consistent with formation of species **6b**, analogous to the species observed for the reaction of **3b** with acetate and benzoate. After 24 hours the appearance of bands around 1830-1750 cm^{-1} indicates formation of anhydrides and bands in the range 2100-1950 cm^{-1} are consistent with formation of rhodium carbonyl complexes. Unfortunately, no single isolable rhodium carbonyl species was observed. A strong absorption for starting material **3b** was still present in the IR spectrum after addition of AgTFA.

The addition of AgTFA to **3b** was monitored *in-situ* by $^{31}P\{^{1}H\}$ and ^{1}H NMR spectroscopy, in d_3-MeCN. Figure 3.8 shows a $^{31}P\{^{1}H\}$ NMR spectrum obtained 10 minutes after addition of 1.5 equivalents of AgTFA to **3b**. Two dd signals at 69.20 and 62.18 ppm are consistent with a

carboxylate coordinated complex [Rh(dppe)(COMe)(TFA)I] **6b**, analogous to the previously observed species **4b** and **5b.**

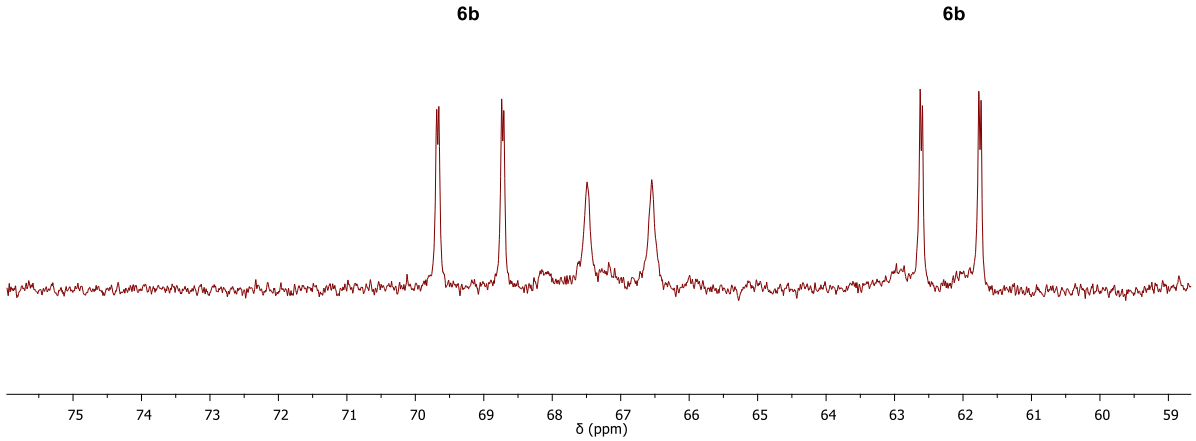

Figure 3.8: ^{31}P {H} NMR spectrum obtained 10 minutes after addition of 1.5 equivalents AgTFA to 3b in d_3-MeCN

The doublet at 67.02 ppm indicates formation of a symmetrical complex, probably arising from disubstitution of iodide ligands by TFA, to form [Rh(dppe)(COMe)$(TFA)_2$]. To test this, two equivalents of AgTFA were added to **3b** [Rh(dppe)(COMe)I_2] resulting in one species in the ^{31}P NMR spectrum, a doublet at δ 67.02 ppm corresponding to [Rh(dppe)(COMe)$(TFA)_2$]. This may also explain the presence of starting material in the IR spectrum obtained after addition of one equivalent AgTFA to **3b**.

It was thought that exchange between iodide and TFA ligands in **6b** to form **3b** and [Rh(dppe)(COMe)$(TFA)_2$] in solution may occur. To test if these ligands could exchange, a d_3-MeCN solution containing [Rh(dppe)(COMe)$(TFA)_2$] was generated *in-situ* by addition of 2 equivalents AgTFA to **3b.** After filtering the solution through celite to remove AgI, a ^{31}P NMR spectrum was obtained to determine [Rh(dppe)(COMe)$(TFA)_2$] formation. To this solution **3b** was added and the reaction observed by IR and NMR spectroscopy. After 10 minutes the ^{31}P

NMR spectrum indicated formation of **6b** showing that the TFA^- and I^- ligands are labile and exchange readily between **3b**, **6b** and [Rh(dppe)(COMe)$(TFA)_2$] as shown in Scheme 3.13.

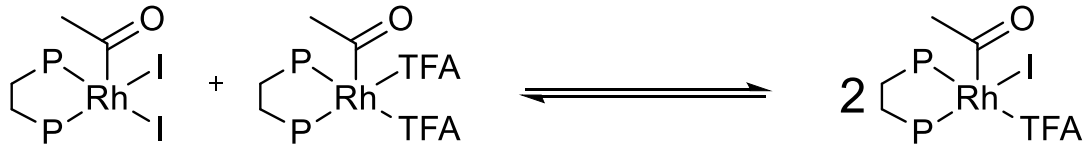

3b **6b**

Scheme 3.13: Mixing of ligands in solution between [Rh(dppe)(COMe)I_2 and [Rh(dppe)(COMe)$(TFA)_2$]

Due to the mixture of complexes produced upon addition of AgTFA to **3b** the intermediate **6b** could not be isolated. However, the doubly substituted complex [Rh(dppe)(COMe)$(TFA)_2$] was isolated and a crystal suitable for X-ray crystallography was obtained by slow evaporation of diethyl ether into a concentrated solution of the complex in CH_2Cl_2. The crystal structure is shown in Figure 3.9 and selected bond lengths are listed in Table 3.4.

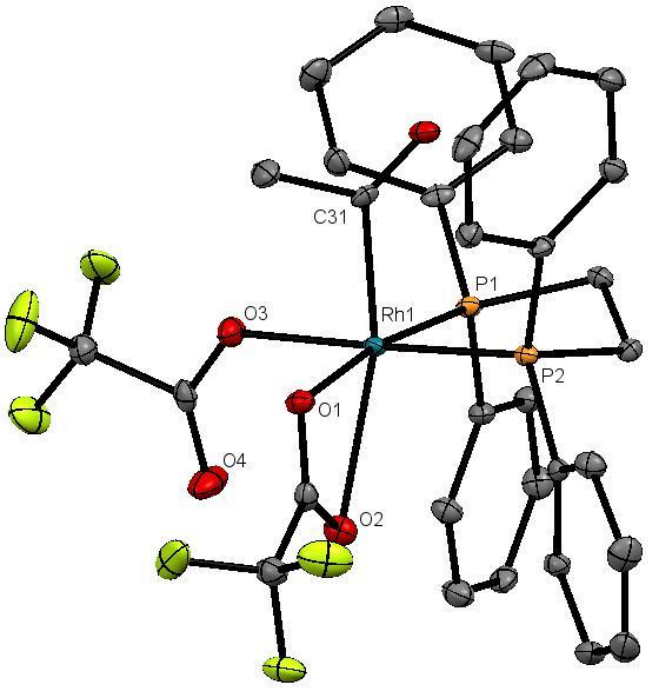

Figure 3.9: X-ray crystal structure for [Rh(dppe)(COMe)(TFA)$_2$] with thermal ellipsoids shown at 50% probability level. Hydrogen atoms omitted for clarity.

Table 3.4: Selected bond lengths (Å) and angles (deg) for [Rh(dppe)(COMe)(TFA)$_2$]

Bond Length		Angle	
Rh(1)-P(1)	2.255(1)	P(1)-Rh(1)-P(2)	86.08(5)
Rh(1)-P(2)	2.274(1)	O(1)-Rh(1)-O(2)	56.3(1)
Rh(1)-C(31)	1.995(6)	C(31)-Rh(1)-O(1)	98.2(2)
Rh(1)-O(1)	2.177(3)	C(31)-Rh(1)-P(1)	88.2(1)
Rh(1)-O(2)	2.490(5)	C(31)-Rh(1)-P(2)	91.0(1)
Rh(1)-O(3)	2.117(3)	C(31)-Rh(1)-O(3)	86.6(2)
Rh(1)-O(4)	3.489(5)	C(31)-Rh(1)-O(2)	154.2(2)
C(27)-O(1)	1.266(6)		
C(27)-O(2)	1.233(6)		
C(29)-O(3)	1.272(6)		
C(29)-O(4)	1.219(6)		

The structure shows a distorted octahedral geometry with two trifluoroacetate ligands, one coordinated bidentate, the other monodentate. Although this structure is unsymmetrical, the ^{31}P NMR spectrum of the complex in $CDCl_3$ possesses only one doublet, indicating that the phosphorus atoms are equivalent. This suggests a fluxional process with the two TFA ligands able to exchange between coordination modes. The dppe ligand bite angle is slightly greater than that observed in **3b** (84.73(7)),[9] possibly due to the bulkier iodide ligands in **3b**.

Some metal acyl complexes containing a chelate coordinated carboxylate that have been observed previously are shown in Scheme 3.14. Hong *et al* made a variety of Ir compounds containing this structural motif, for which X-ray crystal structures were obtained.[15] Piniella *et al* also obtained a crystal structure of an analogous ruthenium compound.[16] Klein et al discerned the structure of an analogous cobalt compound containing acetyl and carboxylate ligands. [17] All

of these complexes contain two phosphine ligands, two examples of which are trans coordinated, whereas the intermediate **4b** contains a cis-chelating diphosphine.

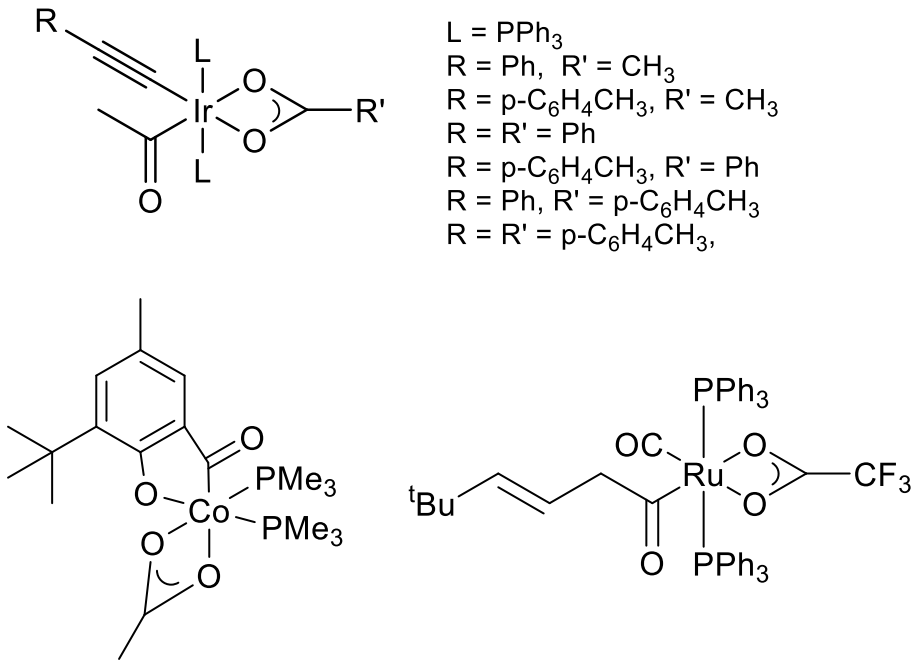

Scheme 3.14: Ir acetyl carboxylate complexes synthesised by Hong et al,[15] Ru acetyl carboxylate complex isolated by Piniella et al,[16] Cobalt acetyl carboxylate complex isolated by Klein et al.[17]

3.1.5 Reactions of 3a-d with carboxylates

The reactions of complexes **3a,c,d** with $[Bu_4N][OAc]$, $[Bu_4N][OBz]$ and [Ag][TFA] all showed similar behaviour to that described above for **3b**. For the reactions with $[Bu_4N][OAc]$, formation of an acetate coordinated intermediate **4a-d** followed by elimination of acetic anhydride was observed by IR, ^{1}H and ^{31}P NMR spectroscopy. Selected spectroscopic data for intermediates **4a-d** are displayed in Table 3.5. For reactions under a CO atmosphere, Rh(I) carbonyl species were formed alongside reductive elimination of anhydride. These will be discussed in more detail later in the chapter. Representative spectra for these species are given in the appendix of this thesis.

Table 3.5: Select spectroscopic data for intermediates 4a-d

Complex	ν(CO) /cm^{-1} (CH_2Cl_2)	δ ^{1}H COC*H*$_3$ ($CDCl_3$)	δ ^{31}P ($CDCl_3$)	(J_{P-Rh}) /Hz	(J_{P-P}) /Hz
4a [Rh(dppm)(COMe)(OAc)I]	1684	1.92, 2.85	-19.44, -21.75	123.4, 123.7	69.4
4b [Rh(dppe)(COMe)(OAc)I]	1687	1.69, 2.54	66.40, 60.83	145.9, 140.7	5.9
4c [Rh(dppp)(COMe)(OAc)I]	1684	2.06, 2.52	19.69, 18.75	130.7, 134.9	30.6
4d [Rh(dppb)(COMe)(OAc)I]	1689	1.81, 2.51	40.33, 26.09	141.3, 135.7	20.9

Similarly, the reactions of **3a-d** with one equivalent of [Bu_4N][OBz] resulted in formation of a benzoate-coordinated complexes **5a-d** and subsequent reductive elimination of a mixed anhydride. Select spectroscopic data for intermediates **5a-d** are shown in Table 3.6. Scrambling of the anhydride product to give a mixture of Ac_2O, AcOBz and Bz_2O occurred as was the case with **3b**. Minor traces of the acetate coordinated intermediate **4a-d** were also observed *in-situ,* attributed to oxidative addition of Ac_2O, formed by scrambling, to the Rh(I) product of AcOBz elimination.

Table 3.6: Select spectroscopic data for intermediate 5a-d

Complex	ν(CO) /cm^{-1} (CH_2Cl_2)	δ ^{1}H COC*H*$_3$ ($CDCl_3$)	δ ^{31}P ($CDCl_3$)	(J_{P-Rh}) Hz	(J_{P-P}) Hz
5a [Rh(dppm)(COMe)(OBz)I]	1685	2.96	-19.24, -21.00	123.5, 123.4	69.9
5b [Rh(dppe)(COMe)(OBz)I]	1690	2.61	61.50, 66.65	145.7, 140.5	6.3
5c [Rh(dppp)(COMe)(OBz)I]	1686	2.60	19.39, 18.95	130.0, 135.9	30.5
5d [Rh(dppb)(COMe)(OBz)I]	1686	2.58	40.63, 25.65	142.4, 135.4	20.3

Scheme 3.15 shows the reaction scheme observed upon addition of [Bu_4N][OAc] and [Bu_4N][OBz] to **3a-d**.

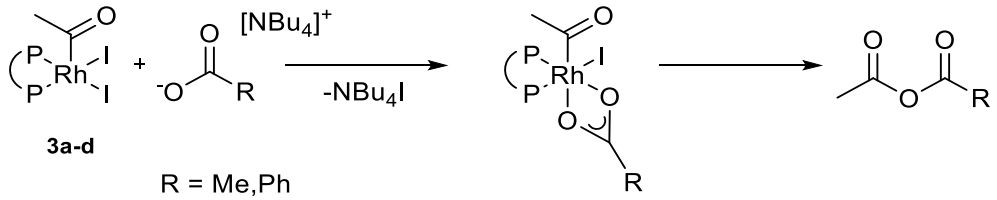

Scheme 3.15: Reaction of 3a-d with carboxylates, forming an intermediate which then eliminates an anhydride

For the reactions of **3a-d** with one equivalent of AgTFA, mixtures of reactant complex, [Rh(P-P)(COMe)(TFA)I] (**6a-d**) and [Rh(P-P)(COMe)$(TFA)_2$] were formed. Selected spectroscopic data are given in Table 3.7 for complexes **6a-d**. Unfortunately, **6d** was not characterised by ^{31}P or ^{1}H

NMR due to rapid elimination of anhydride product, which reacted rapidly leading to the observation of acetic acid in the ^{1}H NMR spectrum.

Table 3.7: Selected spectroscopic data for intermediate 6a-d

	Complex	ν(CO) /cm^{-1} (CH_2Cl_2)	δ ^{1}H COC*H*$_3$ ($CDCl_3$)	δ ^{31}P ($CDCl_3$)	(J_{P-Rh}) Hz	(J_{P-P}) Hz
6a	**[Rh(dppm)(COMe)(TFA)I]**	1694	2.96	-17.47, -23.86	130.4, 121.2	68.1
6b	**[Rh(dppe)(COMe)(TFA)I]**	1695	2.56	60.94, 68.44	138.8, 153.0	5.2
6c	**[Rh(dppp)(COMe)(TFA)I]**	1693	2.63	18.10, 20.44	128.7, 142.5	29.2
6d	**[Rh(dppb)(COMe)(TFA)I]**	1695	-	-	-	-

Around 24 hours after treatment of **3a-c** with AgTFA elimination of a range of products with ν(CO) in the range 1850-1700 cm^{-1} indicated formation of anhydride species. Scheme 3.16 shows the observed species upon addition of AgTFA to **3a-c**.

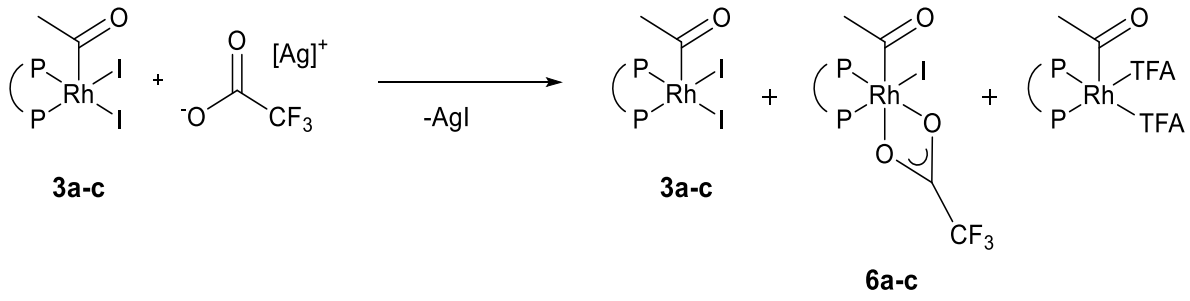

Scheme 3.16: Reaction scheme observed for addition of 1eq AgTFA to 3a-d

3.1.6 Determining coordination mode of carboxylate

As for **4b** and **5b**, DFT calculations were used to determine the most likely structures for the carboxylate coordinated intermediates **4c** and **5c**. Scheme 3.17 shows the structural isomers modelled and Table 3.8 shows the relative ΔG (kJ mol^{-1}) values obtained.

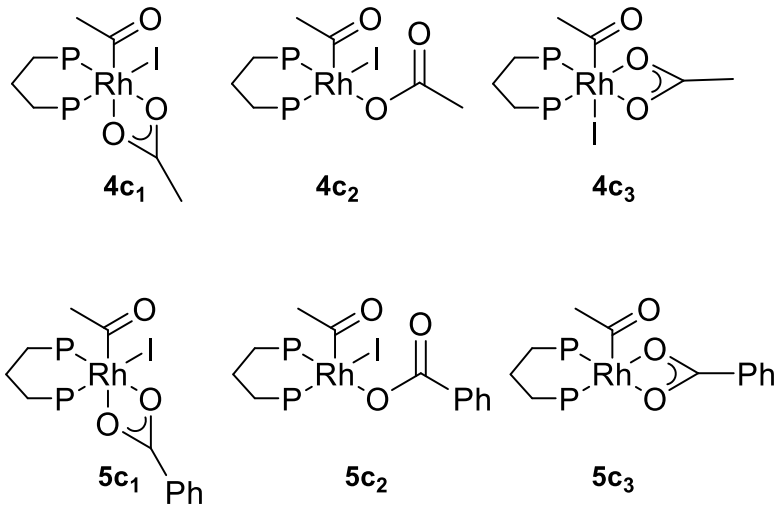

Scheme 3.17: Isomers of 4c and 5c modelled by DFT (ligand Ph groups omitted for clarity).

Table 3.8: Relative Gibbs energies (ΔG) and vibrational frequencies for acetyl and carboxylate ligands of structural isomers of 4c and 5c calculated by DFT.

Isomer	ΔG/ kJ mol^{-1}	Acetyl ν(CO)	$\nu_{asym}(CO_2)$	$\nu_{sym}(CO_2)$
3c	-	1737	-	-
$4c_1$	0	1726	1586	1419
$4c_2$	22.3	1734	1659	1325
$4c_3$	52.1	1713	1529	1490
$5c_1$	0	1728	1571	1405
$5c_2$	16.8	1748	1657	1338
$5c_3$	55.5	1712	1514	1443

For both complexes the unsymmetrical isomer with chelate coordinated carboxylate (**4c$_1$** and **5c$_1$**) was determined to be energetically favourable, as found for **4b**. Calculated ν(CO) absorptions for isomers of **4c** and **5c** are given in Table 3.8. For isomers with chelate coordinated carboxylate (**4c$_1$** and **5c$_1$**) a decrease in predicted acetyl ν(CO), relative to **3c**, is consistent with experimental observations. These complexes also have a smaller difference between predicted ν(CO_2) values than those predicted for **4c$_2$** and **5c$_2$** as would be expected for chelate coordination.

3.1.7 Interpretation of the $^{31}P\{^1H\}$ NMR spectra for 4c and 5c

On substitution of an iodide ligand in complexes **3a-d** by a carboxylate, the phosphorus atoms of the diphosphine ligand become inequivalent. In most cases this results in a pair of doublets of doublets in the $^{31}P\{^1H\}$ NMR spectrum (exemplified by the spectra of the dppe complexes **4b** and **5b** in Figures 3.4 and 3.7 respectively). By contrast, the dppp complexes **4c** and **5c** each displayed a more complex multiplet, indicative of an AB component of an ABX splitting pattern. This arises when the frequency difference between two resonances is of a similar magnitude to the coupling constant between them. An ABX splitting pattern is typically composed of two parts; an AB component, which appears as two overlapping doublets of doublets, and an X component that usually appears as an apparent doublet of doublets. ABX patterns cannot be solved by first-order NMR analysis. For **4c** and **5c** no X component is observed in the ^{31}P NMR spectrum as the X nucleus is ^{103}Rh.

The observed spectra were modelled to determine the ^{31}P chemical shifts and coupling constants. Figure 3.10 shows the $^{31}P\{^1H\}$ NMR spectrum of **4c** and the modelled AB component of the ABX splitting overlaid, giving the parameters δ 19.69 ($J_{P\text{-}Rh}$ = 130.7 Hz) and 18.75 ($J_{P\text{-}Rh}$ = 134.9 Hz) with $J_{P\text{-}P}$ = 30.6 Hz. Similarly, for the $^{31}P\{^1H\}$ NMR spectrum for **5c** and modelled splitting pattern are shown in Figure 3.11, giving the parameters δ 19.39 ($J_{P\text{-}Rh}$ = 130.0 Hz) and

18.95 ($J_{P\text{-}Rh}$ = 135.9 Hz) with $J_{P\text{-}P}$ = 30.5 Hz.), displayed in Figure 3.11. A sample calculation is given in the appendix of this thesis.

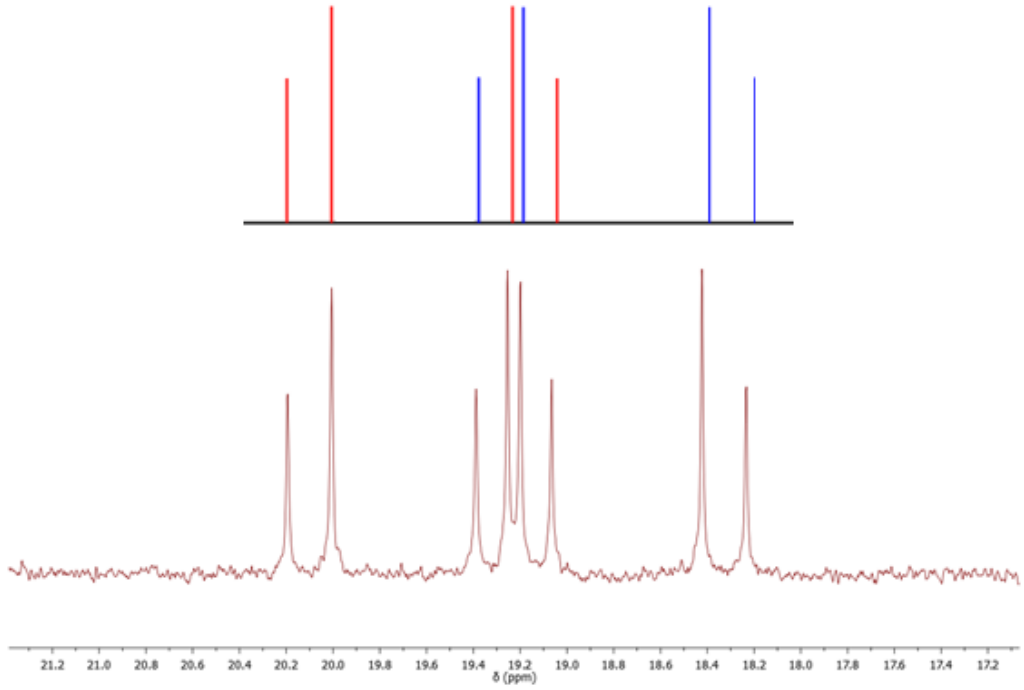

Figure 3.10: $^{31}P\{^{1}H\}$ NMR spectrum and ABX modelled peaks for 4c.

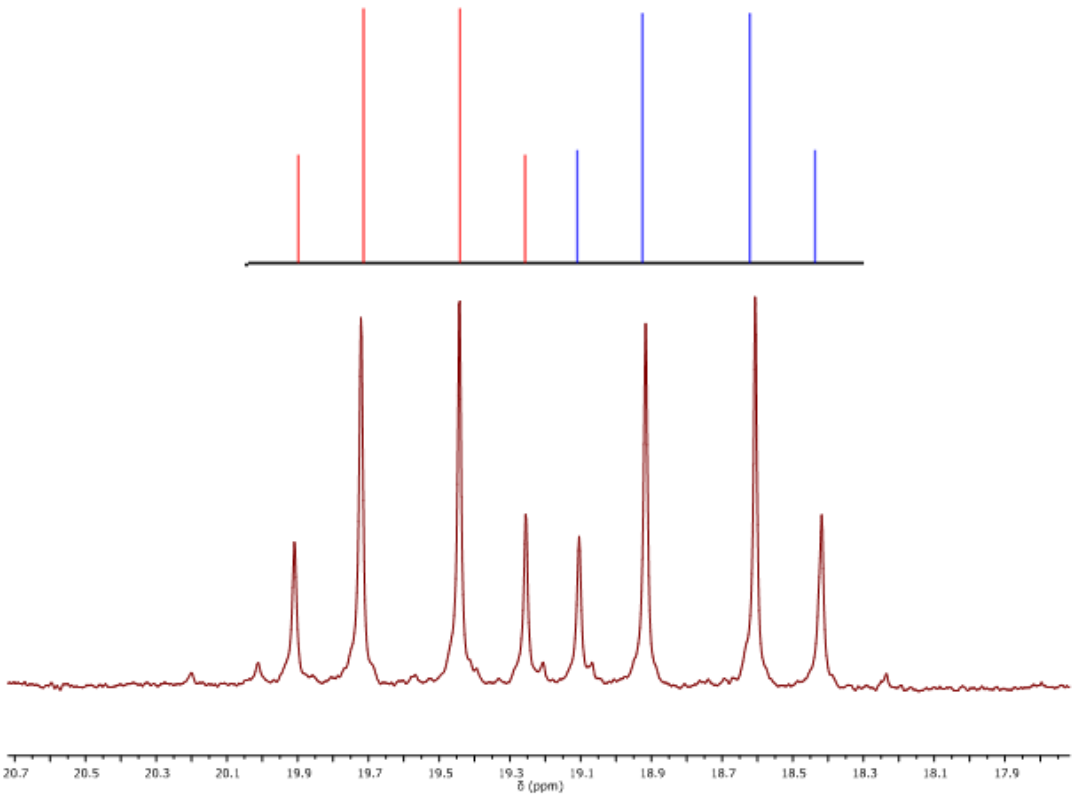

Figure 3.11: $^{31}P\{^{1}H\}$ NMR spectrum and ABX modelled peaks for 5c. (Minor peaks correspond to traces of 4c).

The magnitude of $J_{P\text{-}P}$ differs for complexes containing ligands **a-d** (see Tables 3.5-7) This is influenced by size of chelate ring formed upon coordination of the diphosphine ligand.[18] Grim and co-workers found that $J_{P\text{-}P}$ values are determined by two factors; a backbone contribution $^{B}J_{P\text{-}P}$ and a through-the-metal contribution $^{M}J_{P\text{-}P}$.[19] For 5-membered rings (e.g. **4b**, **5b**) these contributions are roughly equal but of opposite sign, leading to small values for $J_{P\text{-}P}$. For 6-membered rings (e.g. **4c**, **5c**) $^{B}J_{P\text{-}P}$ is negligible which means that $J_{P\text{-}P}$ is mainly attributed to through-the-metal coupling. The larger observed $J_{P\text{-}P}$ for **4c/5c** is therefore due to the backbone coupling contribution being negligible for a 6-membered Rh-dppp chelate ring.

3.1.8 Characterisation of Rh(I) products formed upon anhydride elimination

Under an N_2 atmosphere none of the reactions of **3a-d** with carboxylates produced identifiable Rh(I) species after reductive elimination of an anhydride. However, in the presence of CO, known Rh(I) carbonyl species were formed.

For the reaction of **3a** with acetate or benzoate under CO, formation of ν(CO) bands at 1993 and 1866 cm^{-1} indicated formation of a Rh(I) complex with terminal and bridging carbonyl ligands upon elimination of anhydride. The ^{31}P NMR spectrum of this product displayed a resonance with A_4X_2 splitting pattern, Figure 3.12.

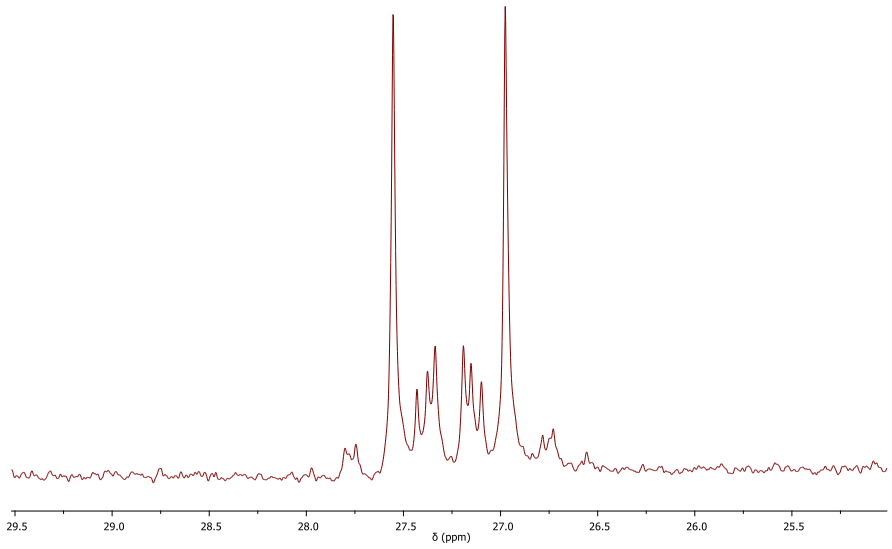

Figure 3.12: $^{31}P\{H\}$ NMR spectrum for the product for reaction of 3a with $[NBu_4][OAc]$ under CO

These spectroscopic data are consistent with formation of a Rh(I) dimer, $[Rh_2(\mu\text{-dppm})_2(\mu\text{-CO})(\mu\text{-I})(CO)_2]I$, previously synthesised by Sanger *et al.*[20] In order to fully characterise this Rh(I) product it was synthesised separately as shown in Scheme 3.18.

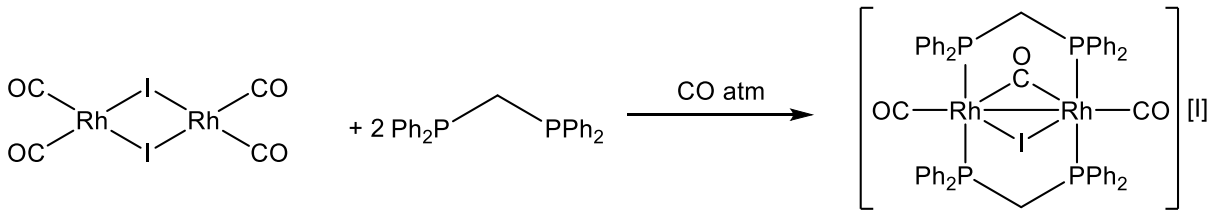

Scheme 3.18: Synthesis of $[Rh_2(\mu\text{-dppm})_2(\mu\text{-CO})(\mu\text{-I})(CO)_2][I]$

A crystal of $[Rh_2(\mu\text{-dppm})_2(\mu\text{-CO})(\mu\text{-I})(CO)_2]I.3CH_2Cl_2$ suitable for single crystal X-ray crystallography was obtained, by slow evaporation of diethyl ether into a concentrated CH_2Cl_2 solution. The structure is shown in Figure 3.13, with selected bond lengths and angles given in

Table 3.9.

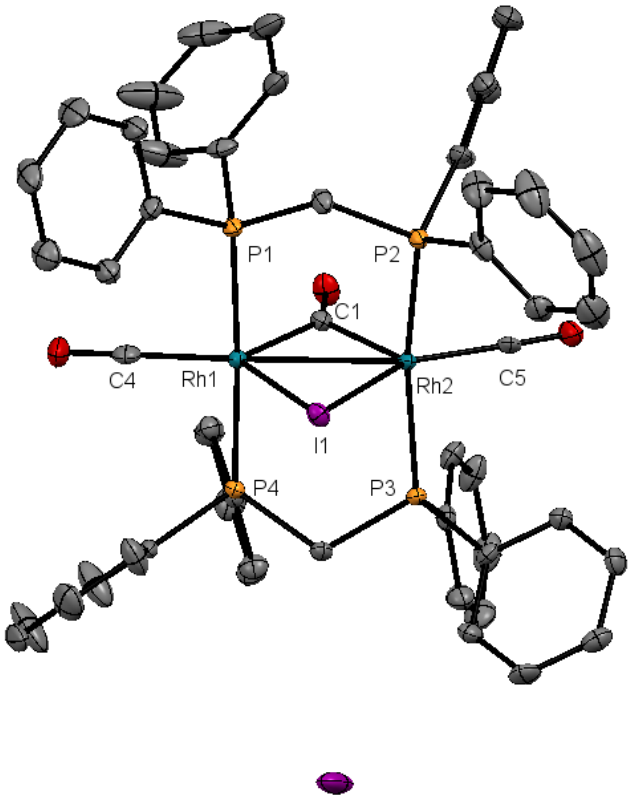

Figure 3.13: X-ray crystal structure for $[Rh_2(\mu\text{-dppm})_2(\mu\text{-CO})(\mu\text{-I})(CO)_2]I.3CH_2Cl_2$ with thermal ellipsoids shown at 50% probability level. Hydrogen atoms and CH_2Cl_2 omitted for clarity

Table 3.9: Selected bond lengths (Å) and angles (deg) for $[Rh_2(\mu\text{-dppm})_2(\mu\text{-CO})(\mu\text{-I})(CO)_2][I]$

Bond Length		Angle	
Rh(1)-C(4)	1.864(4)	C(4)-Rh(1)-Rh(2)	170.70(13)
Rh(1)-C(1)	2.041(4)	C(5)-Rh(2)-Rh(1)	154.6(1)
Rh(1)-P(4)	2.3363(9)	C(1)-Rh(1)-Rh(2)	48.48(11)
Rh(1)-P(1)	2.3415(9)	P(4)-Rh(1)-P(1)	176.80(3)
Rh(1)-Rh(2)	2.8021(4)	P(2)-Rh(2)-P(3)	164.99(4)
Rh(1)-I(1)	2.8079(4)		
Rh(2)-C(5)	1.847(4)		
Rh(2)-C(1)	2.106(4)		
Rh(2)-P(2)	2.3246(9)		
Rh(2)-P(3)	2.3312(9)		
Rh(2)-I(1)	2.8135(4)		

A structure of the cation, $[Rh_2(\mu\text{-dppm})_2(\mu\text{-CO})(\mu\text{-I})(CO)_2]^+$, was recently published by Chen *et al*[21] but appears to lack a counter ion so should be treated with caution.

The structure reported here, with an iodide counter ion, has bond lengths and angles very similar to those in the reported structure. It has an "A-frame" structure, with two rhodium centres bridged by carbon monoxide, iodide and two dppm ligands. The terminal Rh-C-O angles deviate significantly from 180°, being 170.70(13) and 154.6(1)° respectively which may be due to the bulk of the bridging iodide. The Rh-Rh distance, 2.8021(4) Å, indicates a single bond between the two atoms. This is similar to previously reported Rh(I) "A-frame" structures $[Rh_2(\mu\text{-dppm})_2(\mu\text{-CO})(\mu\text{-Cl})(CO)_2][X]$,[22,23] and $[Rh_2(\mu\text{-dppm})_2(\mu\text{-CO})(\mu\text{-H})(CO)_2][p\text{-tosyl}]$.[24] Some similarities, such as the A-frame structure can also be seen with the Rh(0) complex $[Rh_2(\mu\text{-dppm})_2(\mu\text{-CO})(CO)_2]$ isolated by Woodcock *et al.*[25]

The overall reaction scheme for addition of carboxylates to **3a** is shown in Scheme 3.19.

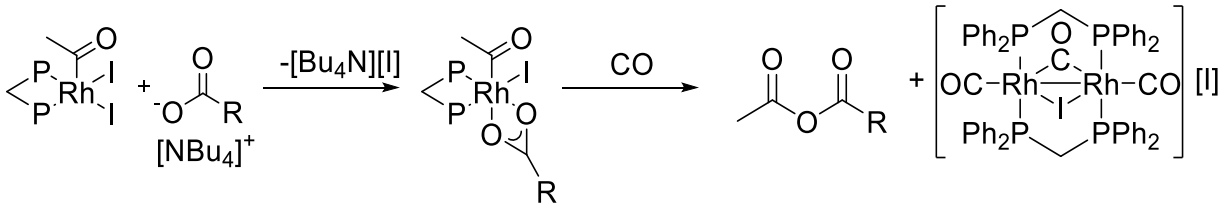

Scheme 3.19: Reaction observed upon addition of carboxylate to 3a under CO atmosphere, Ph ommited for clarity

For the reaction of **3c** with carboxylates under CO, a variety of Rh(I) species were observed via IR spectroscopy after elimination of anhydride. ν(CO) values at 2010, 1968 and 2055/1995 cm^{-1} are indicative of formation of $[Rh(dppp)(CO)I]$, $[Rh(dppp)(CO)I]_2$ and $[Rh(CO)_2I_2]^-$ respectively shown in Scheme 3.20.

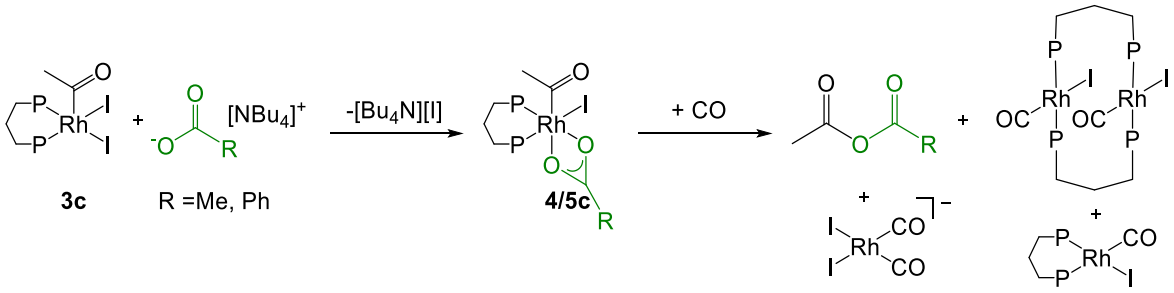

Scheme 3.20: Reaction observed upon addition of carboxylate to 3c under CO, Ph groups ommited for clarity

For the reactions of **3d** with carboxylates under CO, ν(CO) bands were observed by IR spectroscopy at 1963 and 2055/1995 cm^{-1}, indicating formation of $[Rh(dppb)(CO)I]_2$ and $[Rh(CO)_2I_2]^-$ respectively. The overall reaction scheme for addition of carboxylate to **3d** under CO atmosphere is shown in Scheme 3.21.

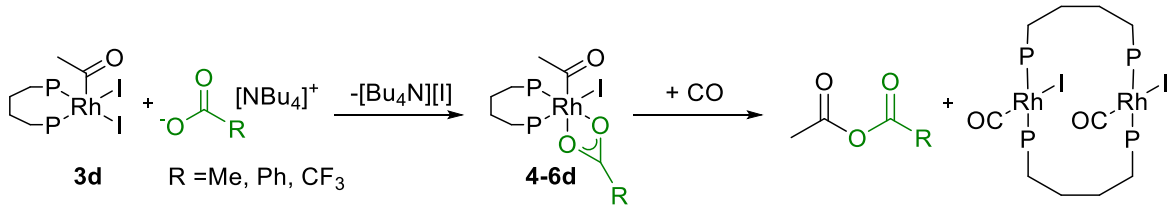

Scheme 3.21: Reaction observed upon addition of carboxylate to 3d under CO, Ph groups ommited for clarity

Upon elimination of anhydride under CO evidence for a Rh(I) carbonyl species was observed for each reaction. The major species observed in each reaction was a Rh(I) phosphine species, however some formed bridging complexes others were cis chelating, and minor traces of $[Rh(CO)_2I_2]^-$ were observed by IR spectroscopy for all of these reactions. The difference outcomes presumably reflect the relative stability of different Rh(I) product species.

3.1.9 Reactions of [Rh(xantphos)(COMe)I_2] (3e) and [Rh(DPEphos)(COMe)I_2] (3f) with carboxylates

Xantphos and DPEphos are "wide bite-angle" diphosphine complexes that are used in a wide range of catalytic processes.[26] Haynes and co-workers have previously studied the mechanistic behaviour of rhodium xantphos complexes in methanol carbonylation.[4] Complex **3e** was isolated from these reactions and structurally characterised as having a mer-tridentate coordination mode for xantphos with O coordinated in the site trans to the acetyl ligand. An analogous DPEphos complex (**3f**) was also made.

Upon addition of acetate, benzoate or trifluoroacetate to **3e** and **3f**, no change was observed by IR or NMR spectroscopy.

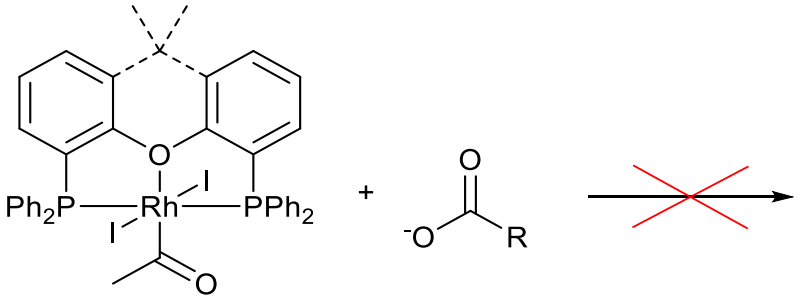

3e-f

Scheme 3.22: Addition of carboxylate to [Rh(POP)(COMe)I$_2$]

It has been found previously that an iodide ligand can be abstracted from **3e** by Ag^+ and replaced by acetonitrile to give [Rh(xantphos)(COMe)(NCMe)I][BF_4] **7e**, Scheme 3.23.[4] It was postulated that this complex might react more readily with a carboxylate than **3e** as acetonitrile is a much more labile ligand than iodide.

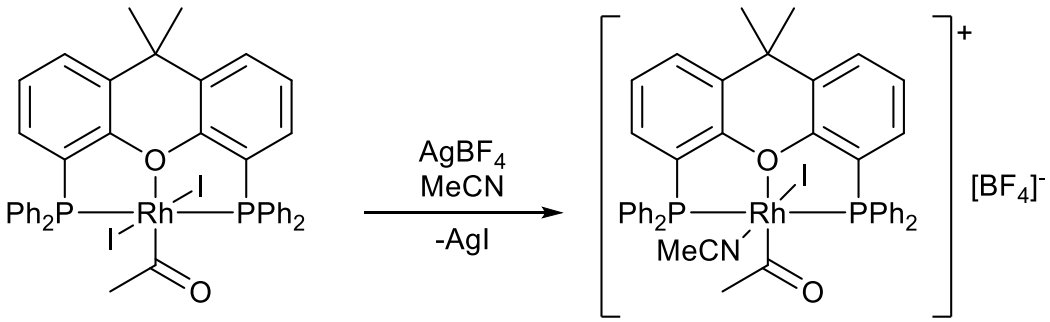

3e **7e**

Scheme 3.23: Synthesis of [Rh(xantphos)(COMe)(NCMe)I][BF_4]

After addition of [Bu_4N][OAc] to a solution of **7e** in CH_2Cl_2, an immediate colour change from yellow to red was observed. An IR spectrum taken after one minute showed complete disappearance of starting material at 2096, 1728 cm^{-1} and formation of ν(CO) bands at 1825 and 1756 cm^{-1} due to acetic anhydride. A ^{1}H NMR spectrum five minutes after addition showed complete disappearance of **7e** and acetate alongside formation of a peak at 2.25 ppm indicating formation of acetic anhydride. A number of Rh phosphine species were observed by ^{31}P NMR spectroscopy, under either N_2 or CO, which could not be identified.

Similarly, after addition of $[Bu_4N][OBz]$ to **7e**, an immediate colour change was observed from yellow to red. After one-minute IR spectroscopy indicated loss of starting material (2096, 1728 cm^{-1}) and formation of peaks at 1810, 1734 cm^{-1} indicative of formation of AcOBz. A ^{1}H NMR spectrum obtained 5 minutes after addition of benzoate to **7e** showed a peak at 2.41 ppm indicating formation of AcOBz. A wide range of doublets indicating a Rh phosphine species were observed by ^{31}P NMR spectroscopy under either N_2 or CO atmosphere, which could not be identified, like those observed for the reaction of **7e** and acetate.

Evidence for a carboxylate coordinated intermediate was not observed for the reaction of **7e** with acetate or benzoate at room temperature, due to the rapid elimination of anhydride. In order to determine if a carboxylate coordinated intermediate forms, as observed for the reactions of **3a-d**, the reaction of **7e** with one equivalent of $[Bu_4N][OAc]$ was monitored at low temperature by ^{31}P NMR spectroscopy.

$[Bu_4N][OAc]$ was added to **7e** at -78 °C in $CDCl_3$ in a Youngs NMR tube under a CO atmosphere. The sample was warmed in 5 °C increments and held at each temperature for 10 minutes while a ^{31}P NMR spectrum was taken. Several of these spectra at different temperatures are presented in Figure 3.14.

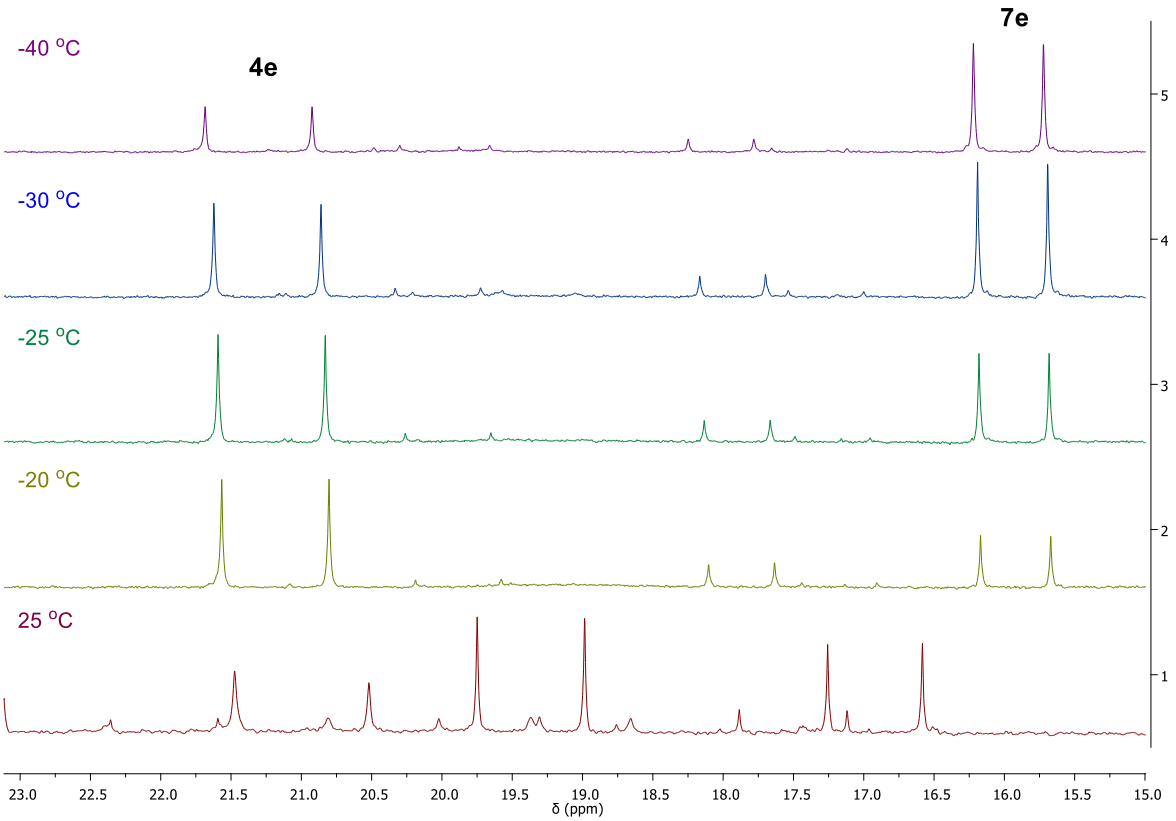

Figure 3.14: ^{31}P {H} NMR spectra obtained at low temperature for the reaction of 7e and [Bu$_4$N][OAc]

As the doublet for the reactant complex **7e** (16.02 ppm) decays, the growth of a doublet at 21.30 ppm is consistent with coordination of acetate giving [Rh(xantphos)(COMe)(OAc)I] **4e**. On warming to 25 °C, this species decays and a number of doublets appear, indicating formation of unidentified Rh(xantphos) complexes. Under N_2 fewer species are formed, but these products could not be assigned. The overall proposed reaction scheme for reaction of acetate with **7e** is shown in Scheme 3.24. The proposed structure for **4e** is replacement of MeCN by acetate. Due to its flexible nature xantphos can coordinate cis bidentate, as such other structures are possible.

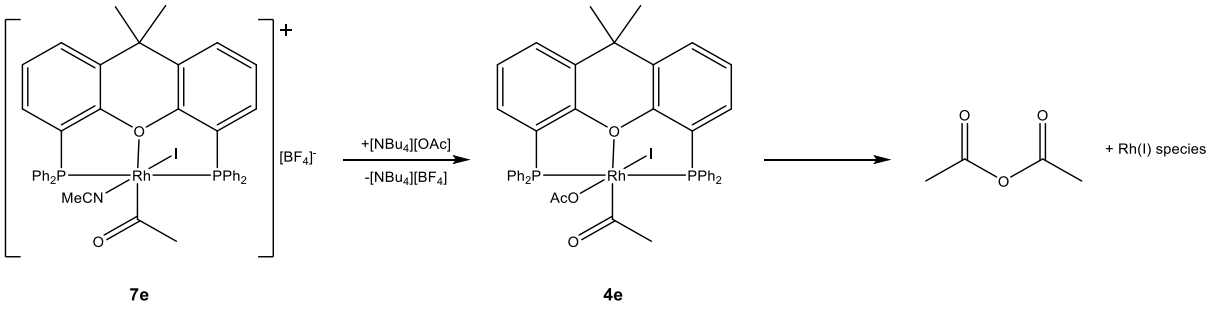

7e 4e

Scheme 3.24: Proposed reaction of 7e and [Bu$_4$N][OAc] forming acetic anhydride

3.2 Summary

The reactions of a series of rhodium diphosphine complexes of formula [Rh(P-P)(COMe)I$_2$] (**3a-f**) with carboxylates; [Bu$_4$N][OAc] and [Bu$_4$N][OBz] were monitored by IR, ^{31}P and ^{1}H NMR spectroscopy to investigate the formation of anhydrides. The reactions of cis chelate complexes **3a-d** were found to proceed via carboxylate coordination, replacing an iodide ligand, and subsequent reductive elimination of an anhydride. In the presence of CO, known Rh(I) carbonyl species were formed. Carboxylate coordinated intermediates [Rh(P-P)(COMe)(O$_2$CR)I] were observed and characterised *in situ*, but could not be isolated. ATR-IR spectra of these intermediates indicated chelate coordinate of the carboxylate ligand, this was supported by DFT calculations.

Complexes **3e** and **3f** with mer-tridentate coordinated ligands (xantphos and DPEphos) did not readily react to form anhydrides. However, [Rh(xantphos)(COMe)(NCMe)I][BF$_4$] was found to rapidly react with [NBu$_4$][OAc] and [NBu$_4$][OBz] to give an anhydride. Low temperature ^{31}P NMR spectroscopy experiments indicated formation of a carboxylate coordinated intermediate before elimination of an anhydride.

Addition of one equivalent of [Ag][TFA] to rhodium diphosphine complexes [Rh(P-P)(COMe)I$_2$] gave a mixture of [Rh(P-P)(COMe)I$_2$], [Rh(P-P)(COMe)(TFA)I] and [Rh(P-P)(COMe)(TFA)$_2$]. Exchange of ligands between these complexes was observed to occur in solution, and the

mono-substituted [Rh(P-P)(COMe)(TFA)I] could not be isolated. Elimination of anhydrides from [Rh(P-P)(COMe)(TFA)I] was slow, with the exception of [Rh(dppb)(COMe)(TFA)I]. Addition of two equivalents of [Ag][TFA] to [Rh(dppe)(COMe)I_2] yielded [Rh(dppe)(COMe)$(TFA)_2$] which was isolated and structurally characterised by X-ray crystallography, showing one TFA ligand chelating and the other monodentate.

3.3 References

(1) Moloy, K. G.; Wegman, R. W. *Organometallics* **1989**, *8*, 2883–2892.

(2) Moloy, K. G.; Petersen, J. L. *Organometallics* **1995**, *14*, 2931–2936.

(3) Lamb, G.; Clarke, M.; Slawin, A. M. Z.; Williams, B.; Key, L.; Roukoss, C.; Fiddy, S.; de Mallmann, A.; Rendón, N.; Basset, J.-M.; Kuntz, E.; Copéret, C. *Dalton Trans.* **2007**, 5582–5589.

(4) Williams, G. L.; Parks, C. M.; Smith, C. R.; Adams, H.; Haynes, A.; Meijer, A. J. H. M.; Sunley, G. J.; Gaemers, S. *Organometallics* **2011**, *30*, 6166–6179.

(5) Paulik, F. E.; Roth, J. F. *J. Chem. Soc, Chem. Commun.* **1968**, 1578a.

(6) Lassauque, N.; Davin, T.; Nguyen, D. H.; Adcock, R. J.; Coppel, Y.; Le Berre, C.; Serp, P.; Maron, L.; Kalck, P. *Inorg. Chem.* **2012**, *51*, 4–6.

(7) Nguyen, D. H.; Lassauque, N.; Vendier, L.; Mallet-Ladeira, S.; Le Berre, C.; Serp, P.; Kalck, P. *Eur. J. Inorg. Chem.* **2014**, 326–336.

(8) Best, J.; Wilson, J. M.; Adams, H.; Gonsalvi, L.; Peruzzini, M.; Haynes, A. *Organometallics* **2007**, *26*, 1960–1965.

(9) Gonsalvi, L.; Adams, H.; Sunley, G. J.; Ditzel, E.; Haynes, A. *J. Am. Chem. Soc.* **2002**, *124*, 13597–13612.

(10) Haynes, A.; Maitlis, P. M.; Stanbridge, I. a.; Haak, S.; Pearson, J. M.; Adams, H.; Bailey, N. *Inorg. Chim. Acta* **2004**, *357*, 3027–3037.

(11) Deacon, G.; Phillips, R. *Coord. Chem. Rev.* **1980**, *33*, 227–250.

(12) Miller, J. A.; Nelson, J. A. *Organometallics* **1991**, *10*, 2958–2961.

(13) Blake, D.; Shields, S.; Wyman, L. *Inorg. Chem.* **1974**, *13*, 1595–1600.

(14) Sano, K.; Yamamoto, T.; Yamamoto, A. *Bull. Chem. Soc.* **1984**, *57*, 2741–2747.

(15) Chin, C. S.; Lee, H.; Lee, M. K.; Noh, S.; Eum, M.-S.; Hong, S. *J. Organomet. Chem.* **2005**, *690*, 1306–1313.

(16) Matas, L.; Muniente, J.; Ros, J.; Alvarez-Larena, Á.; F. Piniella, J. *Inorg. Chem. Commun.* **1999**, *2*, 364–367.

(17) Klein, H.-F.; Haller, S.; Sun, H.; Li, X.; Jung, T.; Rohr, C.; Florke, U.; Haupt, H.-J. *Zeitschrift für Naturforsch. B* **2014**, *53*, 587–598.

(18) Garrou, P. E. *Chem. Rev.* **1981**, *81*, 229–266.

(19) Grim, S.; Barth, R.; Mitchell, J. D.; Del Gaudio, J. *Inorg. Chem.* **1977**, *16*.

(20) Sanger, A. R. *J. Chem. Soc, Dalton. Trans.* **1981**, 228.

(21) Chen, Y.; Liu, D.; Yu, Y. *RSC Adv.* **2017**, *7*, 49875–49882.

(22) Cowie, M. *Inorg. Chem.* **1979**, *18*.

(23) Olmstead, M. M.; Lindsay, C. H.; Benner, L. S.; Balch, A. L. *J. Organomet. Chem.* **1979**, *179*, 289–300.

(24) Kubiak, C.; Woodcock, C.; Eisenberg, R. *Inorg. Chem.* **1982**, *21*, 2119.

(25) Woodcock, C.; Eisenberg, R. *Inorg. Chem* **1985**, *24*, 1285–1287.

(26) Kamer, P. C. J.; van Leeuwen, P. W. N. M.; Reek, J. N. H. *Acc. Chem. Res.* **2001**, 895–904.

Chapter 4

Reactions of Rh(III)(P-L chelate) acetyl complexes with carboxylates

Complexes

1) [Rh(P-L)(CO)I]
   - 1g PN-$^{i}Pr_2Ph$
   - 1h PN- Me_2Ph
   - 1i PN- Mes
   - 1j PN-*o*Anis
   - 1k dppmS
   - 1l dppmSe

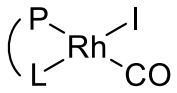

3) [Rh(P-L)(COMe)I_2]
   - 3g PN-$^{i}Pr_2Ph$
   - 3h PN- Me_2Ph
   - 3i PN- Mes
   - 3j PN-oAnis
   - 3k dppmS
   - 3l dppmSe

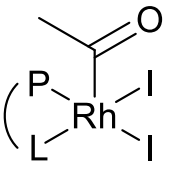

4) [Rh(P-L)(COMe)(OAc)I]
   - 4g PN-$^{i}Pr_2Ph$
   - 4h PN- Me_2Ph
   - 4i PN- Mes
   - 4j PN-oAnis
   - 4k dppmS
   - 4l dppmSe

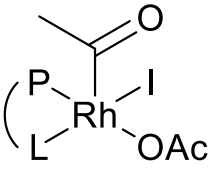

5) [Rh(P-L)(COMe)(OBz)I]
   - 5g PN-$^{i}Pr_2Ph$
   - 5h PN- Me_2Ph
   - 5i PN- Mes
   - 5j PN-oAnis
   - 5k dppmS
   - 5l dppmSe

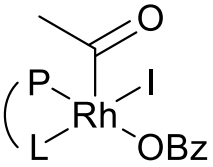

6) [Rh(P-L)(COMe)(TFA)I]
   - 6g PN-$^{i}Pr_2Ph$
   - 6h PN- Me_2Ph
   - 6i PN- Mes
   - 6j PN-oAnis
   - 6k dppmS
   - 6l dppmSe

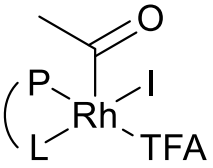

4.0 Introduction

Ligand effects on catalytic cycles and the reactivity of organometallic complexes have been widely studied. Methanol carbonylation is one area in which ligand effects have received great attention. [1–4] The previous chapter looked at the reactivity of Rh-acetyl complexes containing symmetrical diphosphine ligands. However, the use of unsymmetrical difunctional ligands in accelerating the rate of methanol carbonylation has also been investigated. [5–9] Ligands which increase the nucleophilicity of rhodium have been successfully used to enhance the rate of MeI oxidative addition. Scheme 4.1 shows a generic catalytic cycle for methanol carbonylation with heterodifunctional ligands. This is analogous to the cycle shown in Chapter 3 for Rh-diphosphine catalysts and Rh(III)-acetyl complexes [Rh(P-L)(COMe)I_2] (**3**) with a range of heterodifunctional ligands are known. This Chapter deals with the reactivity of such complexes where P-L is a bidentate (P,N) (P,S) or (P,Se) donor ligand.

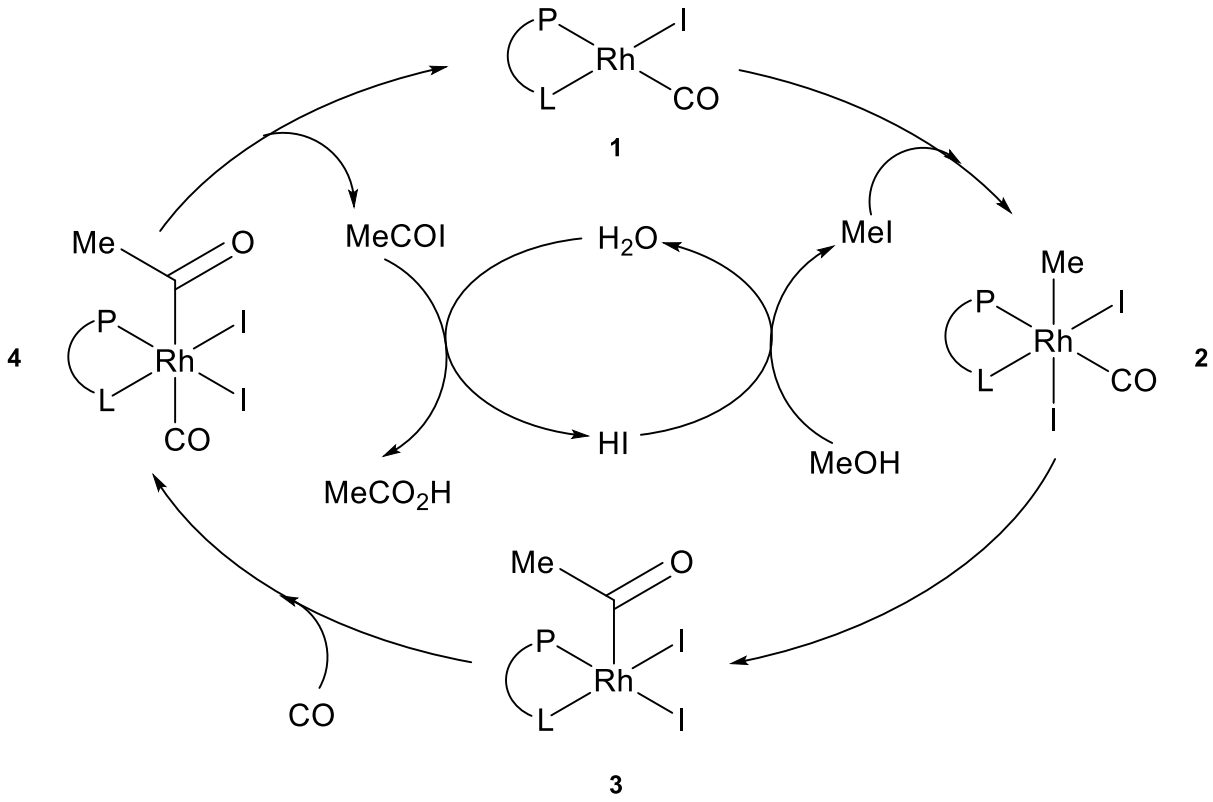

Scheme 4.1: General catalytic cycle for methanol carbonylation with heterodifunctional spectator ligand

Iminophosphines have been used in a wide range of transition metal catalysed reactions such as carbostannylation,[10,11] oligomerisation of ethene[12] and cross-coupling reactions.[13,14] Best *et al*.[15] investigated the reaction of a range of iminophosphine complexes of formula [Rh(PN-R)(CO)I] with MeI and found oxidative addition readily occurred. The product from this oxidative addition varied based on the ligand used. Some formed stable acetyl complexes [Rh(PN-R)(COMe)I_2] (**3**) whereas others resulted in equilibria between methyl (**2**) and acetyl species (**3**), as shown in Scheme 4.2.

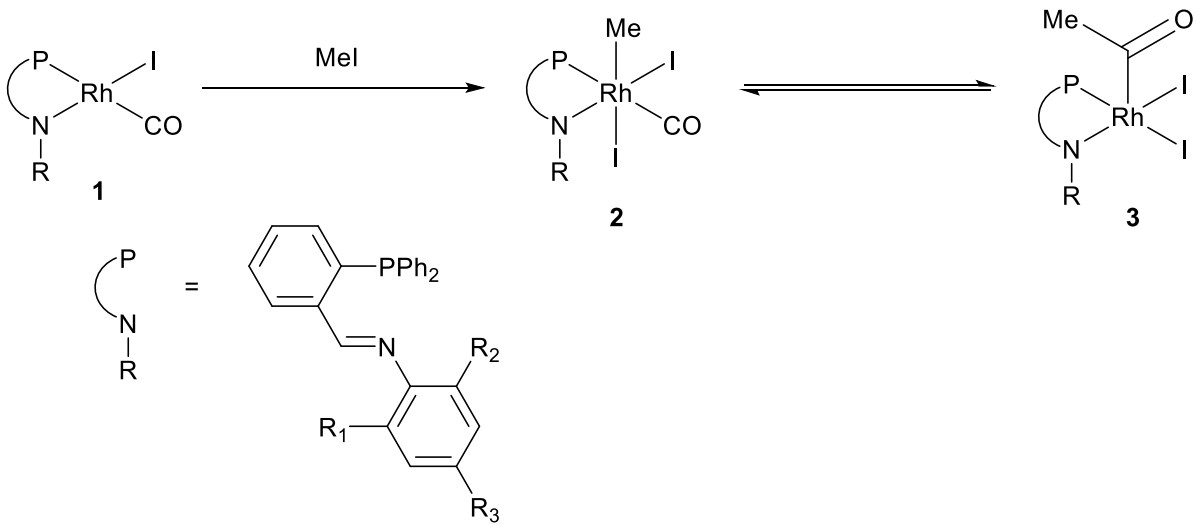

Scheme 4.2: Products formed upon oxidative addition of MeI to [Rh(PN-R)(CO)I]

Other heterodifunctional ligands investigated for enhancement of the rate of methanol carbonylation include derivatives of dppm containing a heteroatom, such as dppmO,[16] dppmS[7,17] or dppmSe.[18] These ligands accelerated the oxidative addition of MeI to Rh(I) by up to 30 to 50 times relative to $[Rh(CO)_2I_2]^-$ due to their good donor properties. Complexes of formula $[Rh(dppmX)(COMe)I_2]$ were isolated and characterised by X-ray crystallography for dppmS and dppmSe.

This chapter reports an investigation of reactions of carboxylates with Rh(III) acetyl complexes of general formula $[Rh(P\text{-}L)(COMe)I_2]$ (**3g-l**) where P-L is a heterodifunctional phosphine ligand. This extends the work on diphosphine analogues in Chapter 3 and provides a further opportunity to probe the mechanism for product formation in methanol carbonylation proposed by Kalck.[19,20]

The reactions of **3** with carboxylates, $[Bu_4N][OAc]$, $[Bu_4N][OBz]$ and [Ag][TFA] were monitored spectroscopically to determine if anhydride formation occurs and its mechanism of formation. A point of interest is how ligand properties affect the formation and reactivity of intermediate species with coordinated carboxylate, as identified in Chapter 3.

4.1 Reaction of Rh(III) iminophosphine acetyl complexes with carboxylates

4.1.1 Synthesis of ligands g-j

Iminophosphine ligands **g-j** were synthesised as described by Best *et al*,[15] via condensation reactions between 2-(diphenylphosphino)benzaldehyde and the corresponding aniline (Scheme 4.3). These ligands were isolated as yellow solids and characterised by ^{31}P and ^{1}H NMR spectroscopy and mass spectrometry.

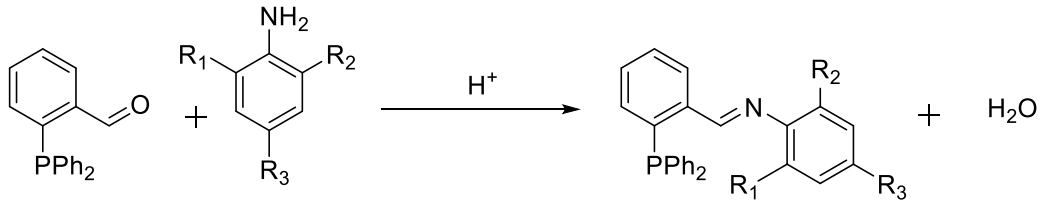

g $R_1, R_2 = {}^{i}Pr, R_3 = H$
h $R_1, R_2 = Me, R_3 = H$
i $R_1, R_2 = Me, R_3 = Me$
j $R_1 = OMe, R_2, R_3 = H$

Scheme 4.3: Synthesis of iminophosphine ligands g-j

Synthesis of complexes **3g-j** followed an analogous method to that used in Chapter 3 for **3a-f**, Scheme 4.4. Two equivalents of the iminophosphine ligand were added to $[Rh(COMe)(NCMe)(CO)I_2]_2$ in toluene to give $[Rh(COMe)(PN)I_2]$ **3g-j**. These complexes were isolated as orange powders and purified by recrystallisation.

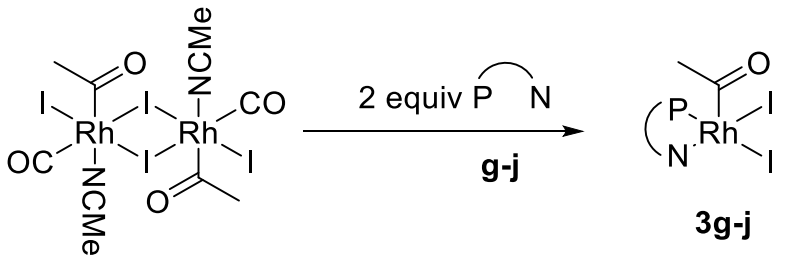

Scheme 4.4: Synthesis of iminophosphine complexes 3g-j

Selected spectroscopic data for compounds **3g-j** are listed in Table 4.1. The ^{31}P, ^{1}H NMR and IR spectroscopy data are consistent with literature data.[15,16,21] Bands for ν(CO) around 1700 cm^{-1} in the IR spectra and singlets in the ^{1}H NMR spectra around 3.4 ppm are indicative of an acetyl ligand. The ^{31}P NMR spectrum of each complex shows a doublet due to coupling to ^{103}Rh.

Table 4.1: Selected spectroscopic data for complexes 3g-j

[Rh(P-L)(COMe)I_2]	ν(CO) /cm^{-1} (CH_2Cl_2)	δ ^{1}H COCH_3 ($CDCl_3$)	δ ^{31}P ($J_{P\text{-}Rh}$)($CDCl_3$)	Yield %
PN-iPr_2Ph (3g)	1714	3.44s	45.92 (d, *J* = 129.0 Hz)	93
PN-Me_2Ph (3h)	1716	3.48s	46.47 (d, *J* = 129.0 Hz)	74
PN-Mes (3i)	1716	3.45s	46.34 (d, *J* = 138.2 Hz)	72
PN-oAnis (3j)	1703	3.37s	44.40 (d, *J* = 132.2 Hz)	71

A crystal of **3i** suitable for X-ray crystallography was obtained by slow evaporation of a concentrated solution of **3i** in $CHCl_3$. The structure is shown in Figure 4.1, and selected geometrical data are given in Table 4.2 along with data for the *o*-anisyl analogue **3j**, previously reported by Best *et al*. [15]

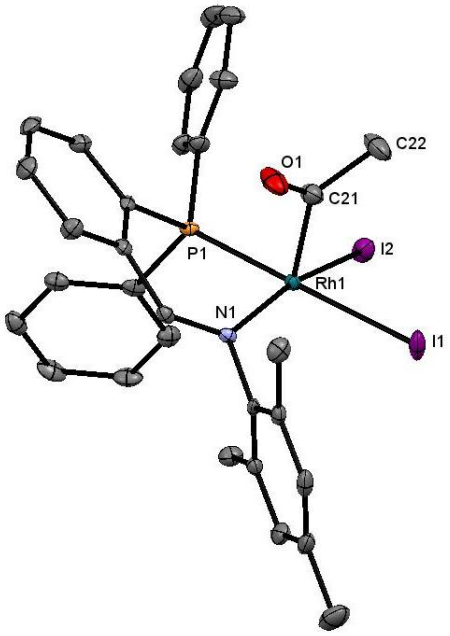

Figure 4.1: X-ray crystal structure for [Rh(PN-Mes)(COMe)I_2] (3i) with thermal ellipsoids shown at 50% probability level. Hydrogen atoms omitted for clarity

Table 4.2: Selected bond lengths (Å) and angles (deg) for 3i and 3j

Bond Length/ Angle	3i	3j
Rh(1)-I(1)	2.6979(3)	2.750(1)
Rh(1)-I(2)	2.6462(3)	2.657(1)
Rh(1)-P(1)	2.2572(8)	2.256(3)
Rh(1)-N(1)	2.097(3)	2.106(8)
Rh(1)-C(21)	1.991(3)	2.00(1)
N(1)-Rh(1)-P(1)	89.01(7)	86.9(2)
I(1)-Rh(1)-I(2)	89.18(2)	91.05(3)
C(21)-Rh(1)-I(1)	89.5(1)	87.6(3)
C(21)-Rh(1)-I(2)	102.9(1)	100.6(3)
C(21)-Rh(1)-P(1)	90.5(1)	89.8(3)
C(21)-Rh(1)-N(1)	94.1(1)	96.0(4)

Complex **3i** has a square-based pyramidal geometry, as observed in analogous Rh(chelate)(COMe)I_2 crystal structures.[2,3,16,22] The Rh(1)-I(1) bond trans to phosphorus is longer than Rh(1)-I(2) trans to nitrogen by roughly 0.05 Å due to the greater trans influence of the phosphine donor, as was the case for **3j**. The chelate bite angle is slightly larger than that for **3j**, probably due to the slight distortion caused by the coordinating *o*-anisyl group in **3j.**

4.1.2 Reaction of Rh(III) iminophosphine complexes 3g-j with [Bu_4N][OAc]

The reactions of [Bu_4N][OAc] with **3g-j** were monitored *in situ* by IR and NMR spectroscopy, under N_2 or CO. The reaction of **3g** and [Bu_4N][OAc] will be discussed in detail as a representative example.

A series of IR spectra obtained over 24 hours after the addition of [Bu_4N][OAc] to **3g** in CH_2Cl_2 under CO are shown in Figure 4.2. The acetyl ν(CO) band shifts to 1685 cm^{-1} after addition of acetate. This shift is consistent with acetate replacing an iodide ligand to give [Rh(PN-$^{i}Pr_2$Ph)(COMe)(OAc)I] (**4g**), analogous to the reactions of **3a-d** with acetate in Chapter 3. Absorptions for the coordinated acetate ν(CO_2) should occur in the region 1300-1700 cm^{-1}. However, due to bands from CH_2Cl_2 in this region, these cannot be discerned. As the band for intermediate **4g** decays, the growth of ν(CO) bands at 1825, 1756 and 1996 cm^{-1}, is indicative of reductive elimination of acetic anhydride and formation of [Rh(PN-$^{i}Pr_2$Ph)(CO)I] (**1g**) respectively. A weak band at 2059 cm^{-1} is likely due to formation of $[Rh(CO)_2I_2]^-$, for which the other carbonyl band at 1988 cm^{-1} is obscured by the intense absorption of **1g**. Similar observations were made for each of the reactant complexes, **3g-j**. The acetyl ν(CO) frequencies for complexes **4g-j** are given in Table 4.3.

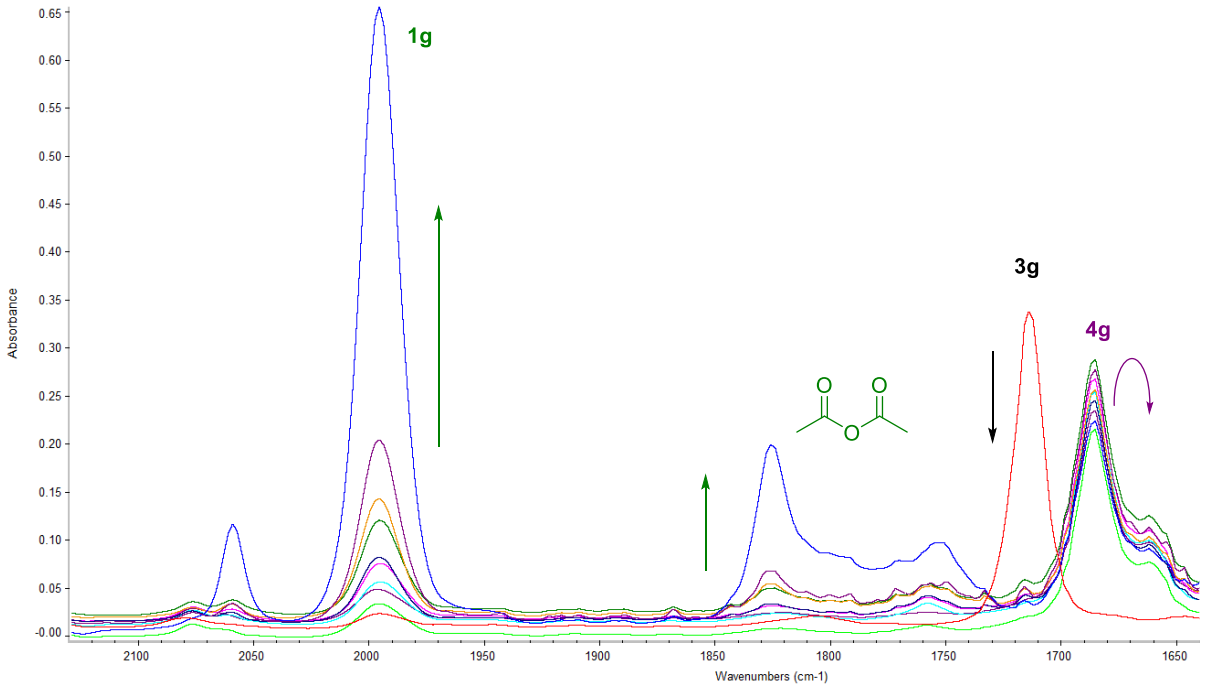

Figure 4.2: A series of IR spectra obtained after the addition of $[Bu_4N][OAc]$ to 3g in CH_2Cl_2 over 22 hours, CO atmosphere

Since the $\nu(CO_2)$ absorptions of coordinated acetate ligands are obscured by solvent bands when monitored *in situ*, a solid sample containing **4g** was obtained. The reaction of **3g** and $[Bu_4N][OAc]$ in CH_2Cl_2 was monitored by IR spectroscopy until complete formation of **4g** was observed. Solvent was then removed and an ATR IR spectrum of the resulting solid obtained. This showed absorptions for $\nu(CO_2)$ at 1563 and 1434 cm^{-1}, indicative of a chelate coordinated acetate.[23] However, it cannot be discerned from the IR data whether acetate is coordinated trans to N or P.

Figure 4.3 shows $^{31}P\{^1H\}$ NMR spectra of starting material (red) and 5 minutes after (blue) addition of one equivalent of $[Bu_4N][OAc]$ to **3g** in $CDCl_3$. After 5 minutes **3g** has completely reacted and a new doublet has grown around 48.35 ppm assigned as **4g**. This species then decays as formation of acetic anhydride is observed in the ^1H NMR spectrum. Under N_2 no

discernible Rh(I) product was observed, whereas under CO formation of a doublet at 39.98 ppm indicated formation of **1g**. The ^{31}P NMR data obtained for **4g-j** are given in Table 4.3.

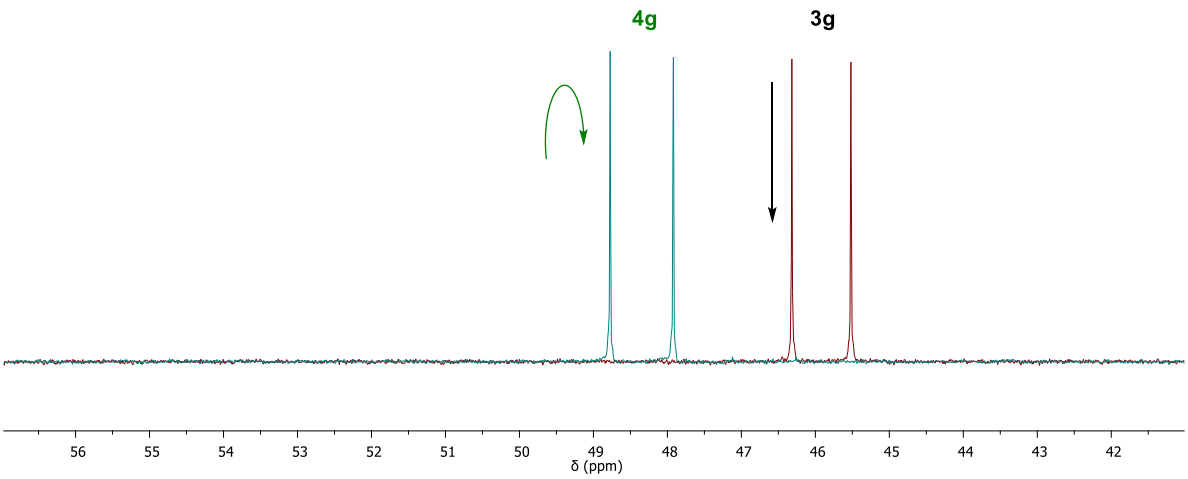

Figure 4.3: ^{31}P {^{1}H} NMR spectra obtained before (red) and after the addition (blue) of [Bu$_4$N][OAc] to 3g in CDCl$_3$ under N$_2$.

A ^{1}H NMR spectrum 5 minutes after addition of [Bu$_4$N][OAc] to **3g** shows complete depletion of **3g** and growth of a peak around 3.08 ppm assigned as COC*H*$_3$ for **4g.** As this peak decayed, formation of a peak at 2.25 ppm indicated formation of acetic anhydride. Complete reductive elimination to form acetic anhydride took ~3 days. However, complexes **4g-j** could not be isolated. The ^{1}H NMR data for COC*H*$_3$ for **4g-j** are reported in Table 4.3.

Table 4.3: Selected spectroscopic data for complexes 4g-j observed as intermediates in reactions of 3g-j with [Bu$_4$N][OAc]

[Rh(P-L)(COMe)(OAc)I]	ν(CO) cm^{-1} (CH_2Cl_2)	δ ^{1}H COC*H*$_3$ ($CDCl_3$)	δ ^{31}P ($CDCl_3$)	($J_{P\text{-}Rh}$) /Hz
PN-iPr$_2$Ph (**4g**)	1685	3.08	48.35	138
PN-Me$_2$Ph (**4h**)	1685	3.10	48.29	138
PN-Mes (**4i**)	1685	3.18	48.30	138
PN-oAnis (**4j**)	1700	3.03	46.06	142

Scheme 4.5 shows several possible isomeric structures for the coordination of acetate in complex **4g**, and by analogy, **4h-j**. Since the ATR-IR spectroscopic data indicate chelate carboxylate coordination , monodentate coordination was not considered. Isomer **$4g_1$** arising from substitution of iodide trans to P was expected to be the most likely due to the longer Rh-I bond length trans to P observed in the crystal structures of **3i** and **3j**.

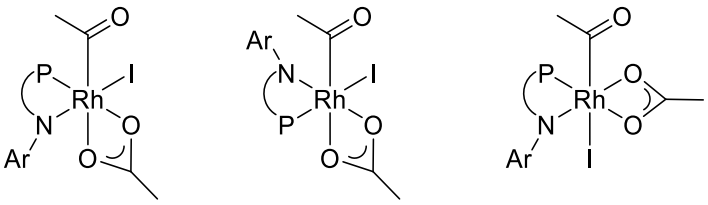

$4g_1$ **$4g_2$** **$4g_3$**

Scheme 4.5: Structural isomers proposed for 4g with PN ligand simplified for clarity, where Ar= 2,6 $^{i}Pr_2Ph$

DFT calculations (*Gaussian09,* B3LYP, 6-311G, SDD on Rh) were used to determine energies for these isomers, to elucidate the most likely coordination mode of acetate. Table 4.4 shows the computed relative energies for the isomers of each complex. As predicted, the isomer with acetate trans to phosphorus is the lowest in energy by 4-10 kJ mol^{-1}, relative to that with acetate trans to N.

Table 4.4: Calculated ΔG between isomers of 4g-j, relative to the isomer with acetate trans to P.

Isomer	ΔG/ kJ mol^{-1}	Isomer	ΔG/ kJ mol^{-1}	Isomer	ΔG/ kJ mol^{-1}	Isomer	ΔG/ kJ mol^{-1}
$4g_1$	0	**$4h_1$**	0	**$4i_1$**	0	**$4j_1$**	0
$4g_2$	8.39	**$4h_2$**	8.82	**$4i_2$**	10.51	**$4j_2$**	4.74
$4g_3$	52.7	**$4h_3$**	52.7	**$4i_3$**	52.5	**$4j_3$**	35.82

The proposed scheme for reaction of $[Bu_4N][OAc]$ with **3g-j** is shown in Scheme 4.6. Initial substitution of an iodide ligand trans to phosphorus gives an acetate coordinated intermediate

4g-j. This intermediate slowly eliminates acetic anhydride to give **1g-j** and some $[Rh(CO)_2I_2]^-$ under a CO atmosphere.

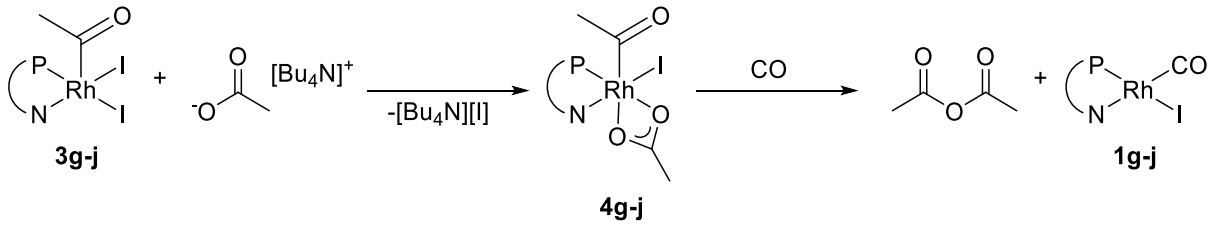

Scheme 4.6: Reaction scheme for addition of $[Bu_4N][OAc]$ to 3g-j forming a carboxylate coordinated intermediate 4g-j which eliminates acetic anhydride, PN ligand is simplified for clarity.

4.1.3 Reaction of Rh(III) iminophosphine complexes 3g-j with $[Bu_4N][OBz]$

The reactions of complexes **3g-j** with $[Bu_4N][OBz]$ were monitored by IR, ^1H and ^{31}P NMR spectroscopy. The reaction of **3g** will again be used as a representative example.

An IR spectrum taken 5 minutes after addition of $[Bu_4N][OBz]$ to **3g** in CH_2Cl_2 under CO, showed formation of a band at 1686 cm^{-1} assigned to $[Rh(PN\text{-}^iPr_2Ph)(COMe)(OBz)I]$ **5g**. The acetyl v(CO) frequencies for **5g-j** are listed in Table 4.5. As **5g** decays, formation of bands at 1810, 1734 and 1996 cm^{-1} corresponds to formation of AcOBz and **1g** respectively. Over 48 hours formation of several bands between 1825-1725 cm^{-1} indicates scrambling of anhydrides to give Ac_2O and Bz_2O, as was observed in chapter 3 for the reactions of **3a-d** with benzoate. Under N_2 no Rh(I) product is observed by IR spectroscopy, but formation of anhydrides and scrambling still occurs.

Figure 4.4 shows a $^{31}P\{^1H\}$ NMR spectrum before (blue) and 5 minutes after addition (red) of Bu_4NOBz to a solution of **3g** in $CDCl_3$. A new doublet in the ^{31}P NMR spectrum at 48.35 ppm and a singlet in the ^1H NMR spectrum at 3.30 ppm are assigned to **5g**. As this intermediate

decays formation of peaks at 2.41 and 2.25 ppm in the ^{1}H NMR spectrum indicate formation of AcOBz and Ac_2O respectively. Under N_2 no Rh(I) product was observed by NMR spectroscopy. Selected NMR data for intermediates **5g-j** are displayed in Table 4.5.

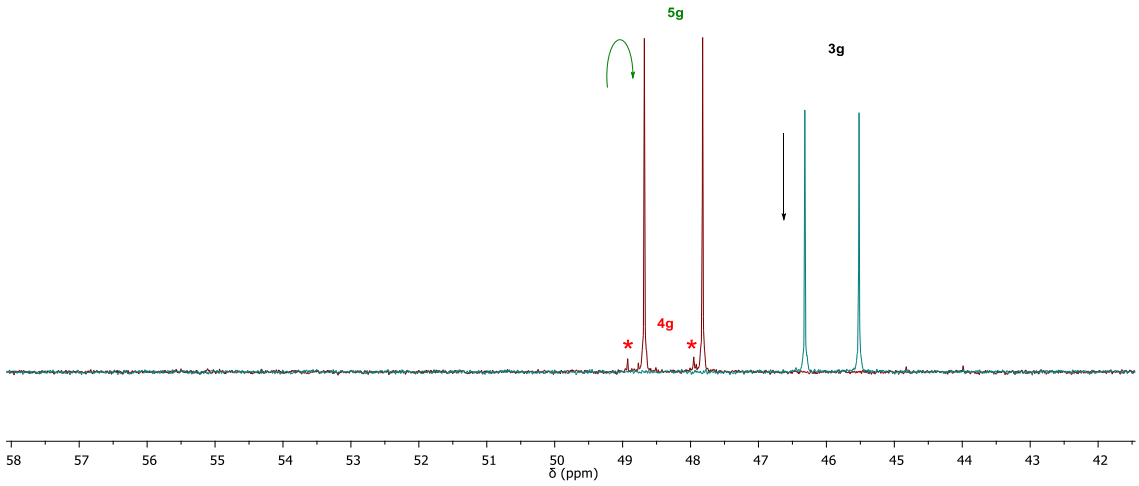

Figure 4.4: ^{31}P {^{1}H} NMR spectra obtained before (blue) and after the addition (red) of [Bu_4N][OBz] to 3g in $CDCl_3$ under N_2.

Traces of **4g** were observed in the ^{31}P and ^{1}H NMR spectra after addition of benzoate to **3g**. This is analogous to the traces of **4a-d** observed upon addition of benzoate to **3a-d** in Chapter 3. Oxidative addition of Ac_2O, formed by AcOBz scrambling in solution, is proposed to explain this presence of intermediates **4g-j**, as for analogous examples discussed in Chapter 3.

Table 4.5: Selected spectroscopic data for complexes 5g-j observed as intermediates in reactions of 3g-j with [Bu_4N][OBz].

[Rh(P-L)(COMe)(OBz)I]	ν(CO) cm^{-1} (CH_2Cl_2)	δ ^{1}H $COCH_3$ ($CDCl_3$)	δ ^{31}P ($CDCl_3$)	($J_{P\text{-}Rh}$) /Hz
PN-$^{i}Pr_2$Ph (**5g**)	1686	3.30	48.25	138.9
PN-Me_2Ph (**5h**)	1686	3.21	48.38	138.7
PN-Mes (**5i**)	1688	3.26	48.36	139.0
PN-oAnis (**5j**)	1697	3.14	45.74	142.5

DFT calculations to determine the most likely structural isomer of **5g** and **5i** were undertaken. Scheme 4.7 shows the structures investigated. ΔG values for the different structural isomers relative to the lowest energy isomer are given in Table 4.6.

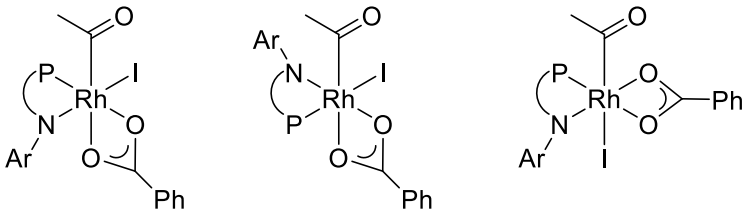

$5g_1$ **$5g_2$** **$5g_3$**

Scheme 4.7: Structural isomers proposed for 5i with PN ligand simplified for clarity, where Ar= 2,4,6 methyl

Table 4.6: ΔG calculated for isomers of 5g and 5i, compared with $5g_1$ and $5i_1$ the lowest energy isomer for each complex

Isomer	ΔG/ kJ mol^{-1}	Isomer	ΔG/ kJ mol^{-1}
$5g_1$	0	**$5i_1$**	0
$5g_2$	10.2	**$5i_2$**	14.4
$5g_3$	54.3	**$5i_3$**	53.6

The reactions of complexes **3g-j** with [Bu_4N][OBz] proceed by substitution of iodide by benzoate forming intermediate **5g-j**. Elimination of AcOBz then occurs over 2 days, as shown in Scheme 4.8. As in Chapter 3, AcOBz was found to scramble to form a mixture of AcOBz, Ac_2O and Bz_2O. The presence of traces of **4g-j** in ^{31}P and ^{1}H NMR spectra is proposed to be due to oxidative addition of acetic anhydride to the Rh(I) product formed upon elimination of anhydride. Under CO, formation of **1g-j** was observed after elimination of anhydride.

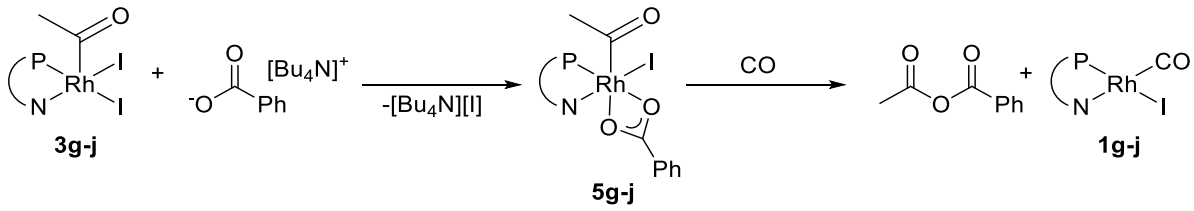

Scheme 4.8: Reaction scheme for addition of [Bu_4N][OBz] to 3g-j forming a carboxylate coordinated intermediate 5g-j which eliminates mixed anhydride AcOBz, PN ligand simplified for clarity.

4.1.4 Reaction of Rh(III) iminophosphine complexes 3g-i with [Ag][TFA]

The reactions of complexes **3g-i** with [Ag][TFA] were monitored *in situ* by IR, ^{1}H and ^{31}P NMR spectroscopy. An IR spectrum obtained 5 minutes after addition of silver trifluoroacetate to **3g** showed complete depletion of the reactant complex and formation of a band at 1706 cm^{-1}, assigned as [Rh(PN-$^{i}Pr_2$Ph)(COMe)(TFA)I] (**6g**). Acetyl ν(CO) bands for complexes **6g-i** are given in Table 4.7.

^{31}P NMR spectroscopy showed immediate formation of a new doublet at 49.31 ppm assigned as intermediate **6g**. ^{1}H NMR spectroscopy also indicated a shift of the acetyl peak to 3.25 ppm. Selected spectroscopic data for **6g-i** are given in Table 4.7. No elimination of anhydride was observed over 2 days for these species, allowing isolation as solids. The reaction scheme for synthesis of complexes **6g-i** is shown in Scheme 4.9. Double substitution of iodide to make [Rh(PN)(COMe)$(TFA)_2$] was not observed upon addition of one equivalent of AgTFA, indicating a significant difference in lability of the two iodide ligands, consistent with the unequal Rh-I bond lengths in **3i**.

Table 4.7: Selected IR, ^{31}P and ^{1}H NMR spectral data for isolated complexes 6g-i

[Rh(P-L)(COMe)(TFA)I]	ν(CO) cm^{-1} (CH_2Cl_2)	δ ^{1}H $COCH_3$ (CD_3CN)	δ ^{31}P (CD_3CN)	($J_{P\text{-}Rh}$) /Hz
PN-$^{i}Pr_2$Ph (6g)	1706	3.25	49.31	145.5
PN-Me_2Ph (6h)	1708	3.28	49.34	145.0
PN-Mes (6i)	1707	3.27	49.31	145.2

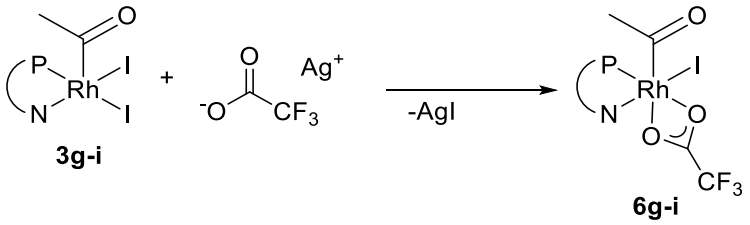

Scheme 4.9: Reaction of complexes 3g-j with silver trifluoroacetate to form carboxylate coordinated complexes 6g-i

A crystal of **6g** suitable for X-ray crystallography was obtained by slow evaporation of diethyl ether into a concentrated solution of **6g** in CH_2Cl_2. The structure is shown in Figure 4.5 and selected bond lengths and angles are given in Table 4.8. There is some disorder with 10 % iodide occupancy modelled in the vicinity of the acetyl ligand, although only one species is observed in the ^{31}P NMR spectrum. The trifluoroacetate coordinates in a bidentate manner, occupying the site trans to P which had the longer Rh-I bond in **3g**. The TFA bite angle of 56.7^{o} is typical of bidentate carboxylates.[24–26] The bite angle for the iminophosphine ligand is similar to that observed for **3i**. The use of the TFA ligand allowed for isolation of complexes **6g-j** that were more stable than the analogous complexes with acetate and benzoate, this is likely due to TFA being less electron donating.

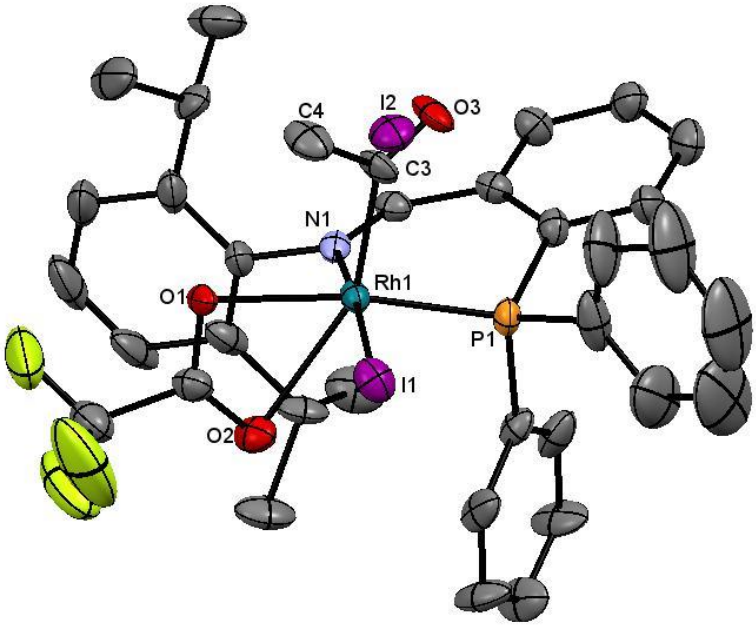

Figure 4.5: X-ray crystal structure for [Rh(PN-^{i}Pr$_2$Ph)(COMe)(TFA)I].CH_2Cl_2 (6g) with thermal ellipsoids shown at 50% probability level. Hydrogen atoms and CH_2Cl_2 omitted for clarity.

Table 4.8: Selected bond lengths (Å) and angles (deg) for 6g

Bond Length		Angles	
Rh(1)-I(1)	2.631(1)	O(1)-Rh(1)-O(2)	56.7(2)
Rh(1)-I(2)	2.609(8)	N(1)-Rh(1)-P(1)	89.3(2)
Rh(1)-P(1)	2.219(2)	P(1)-Rh(1)-O(1)	170.7(2)
Rh(1)-N(1)	2.069(7)	C(3)-Rh(1)-1(1)	95.8(4)
Rh(1)-C(3)	1.98(1)	C(3)-Rh(1)-N(1)	91.1(4)
Rh(1)-O(1)	2.189(6)	C(3)-Rh(1)-P(1)	91.4(4)
Rh(1)-O(2)	2.469(7)	C(3)-Rh(1)-O(2)	154.6(4)

4.2 Reaction of Rh(III)(dppmX) acetyl complexes with carboxylates (X = S, Se)

4.2.1 Synthesis of complexes 3k-l

The method according to Lobana [27] was used to synthesise dppmS (**k**), as shown in Scheme 4.10. An analogous procedure as described by Bond[28] was used to synthesise dppmSe (**l**), Scheme 4.11. Both ligands were isolated as off-white solids and characterised by ^{31}P and ^{1}H NMR spectroscopy and mass spectrometry.

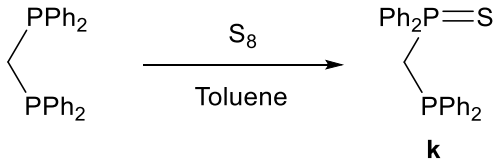

k

Scheme 4.10: Synthesis of dppmS ligand

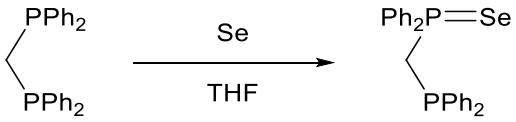

l

Scheme 4.11: Synthesis of dppmSe ligand

Complexes **3k-l** were synthesised using the same method as for complexes **3g-j**. Two equivalents of **k** or **l** were added to $[Rh(COMe)(NCMe)(CO)I_2]_2$ in toluene yielding **3k-l** as orange powders. Selected spectroscopic data for these complexes are given in Table 4.9.

Table 4.9: Selected spectroscopic data for complexes 3k-l

[Rh(dppmX)(COMe)I_2]	ν(CO) /cm^{-1} (CH_2Cl_2)	δ ^{1}H COCH_3 ($CDCl_3$)	δ ^{31}P ($J_{P\text{-}Rh}$, $J_{P\text{-}P}$)($CDCl_3$)
dppmS (3k)	1701	3.34s	57.93 (dd, *J* = 4, 47 Hz), 54.64 (dd, *J* = 137, 47Hz)
dppmSe (3l)	1698	3.32s	58.88 (dd, *J* = 143, 56 Hz), 37.61 (dd, *J* = 4, 56 Hz)

Satellites due to ^{31}P-^{77}Se coupling would be expected in the ^{31}P NMR spectrum of **3l**. However, due to low solubility of the complex in $CDCl_3$ and relatively low abundance of ^{77}Se (7.63 %) these could not be discerned from the baseline.

4.2.2 Reaction of complexes 3k-l with carboxylates

X-ray crystal structures of complexes **3k** and **3l** have been reported previously by Gonsalvi,[16] and Rose[21] respectively. As for complexes **3g-j** the two Rh-I bond lengths differ, due to the stronger trans effect of phosphorus relative to S/Se. It was therefore predicted that the longer rhodium-iodide bond, trans to phosphorus, would be preferentially substituted.

IR, ^{31}P and ^{1}H NMR spectroscopy was used to monitor the reactions of **3k-l** with [Bu_4N][OAc], [Bu_4N][OBz] and [Ag][TFA]. After addition of one equivalent of carboxylate, IR spectroscopy indicated a shift in the acetyl ν(CO) to lower frequency, consistent with formation of [Rh(dppmX)(COMe)(O_2CR)I]. ^{31}P NMR spectroscopy showed rapid formation of two new dd signals and the ^{1}H NMR spectra showed a shift of the acetyl peak from δ 3.3 ppm to around δ 3.1 ppm, consistent with carboxylate replacing an iodide ligand. Selected NMR data for these complexes are given in Table 4.10. These complexes did not eliminate anhydride over 2-3 days and as such could be isolated and characterised. ATR IR spectra showed ν(CO_2) bands at 1551 and 1436 cm^{-1} with a separation of 115 cm^{-1}, indicative of chelate carboxylate coordination. Selected IR data for these complexes are given in Table 4.10.

Table 4.10: Selected spectroscopic data for complexes 4-6k and 4-6l isolated from the reaction of 3k-l with carboxylates.

Complex	ν(CO) cm^{-1} (CH_2Cl_2)	δ ^1H ($CDCl_3$)	δ ^{31}P ($CDCl_3$)
[Rh(dppmS)(COMe)(OAc)I] (**4k**)	1690, 1668, 1551, 1434	2.26s (OAc), 3.04s ($COCH_3$)	50.40 (dd, *J* = 31.9, 1.8 Hz), 43.9 (dd, *J* = 139.8, 31.9 Hz)
[Rh(dppmS)(COMe)(OBz)I] (**5k**)	1692, 1673, 1552, 1436	3.07s ($COCH_3$)	50.15 (dd, *J* = 31.8, 1.3 Hz), 43.42 (dd, *J* = 140.6, 31.7 Hz)
[Rh(dppmS)(COMe)(TFA)I] (**6k**)	1686, 1663, 1574, 1435	3.10s ($COCH_3$)	49.70 (dd, *J* = 28.5, 1.8 Hz), 44.89 (dd, *J* = 146.8, 28.5 Hz)
[Rh(dppmSe)(COMe)(OAc)I] (**4l**)	1689, 1666, 1552, 1435	2.22s (OAc), 3.02s ($COCH_3$)	44.93 (dd, *J* = 141.9, 36.6 Hz), 29.71 (dd, *J* = 36.6, 1.7 Hz).
[Rh(dppmSe)(COMe)(OBz)I] (**5l**)	1693, 1667, 1551, 1434	3.18s ($COCH_3$)	45.0 (dd, *J* = 142.1, 36.7 Hz), 29.61 (d, *J* = 36.7 Hz).
[Rh(dppmSe)(COMe)(TFA)I] (**6l**)	1699, 1660, 1437, 1196	3.08s ($COCH_3$)	45.38 (dd, *J* = 148.7, 33.0 Hz), 28.85 (dd, *J* = 33.0, 4.0 Hz)

4.2.3 Crystal structures of rhodium carboxylate complexes

Crystals of **4k, 4l, 5k** and **6k** suitable for X-ray crystallography were obtained by slow evaporation of diethyl ether into concentrated solutions of **4k, 4l, 5k** and **6k** in CH_2Cl_2. The structures are shown in Figure 4.6-4.9, with selected bond lengths and angles shown in Table 4.11, along with data for the diiodo precursors **3k** and **3l**.

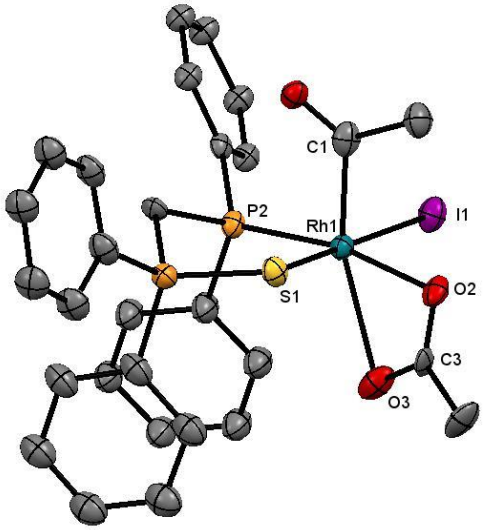

Figure 4.6: X-ray crystal structure for [Rh(dppmS)(COMe)(OAc)I] (4k) with thermal ellipsoids shown at 50% probability level. Hydrogen atoms omitted for clarity.

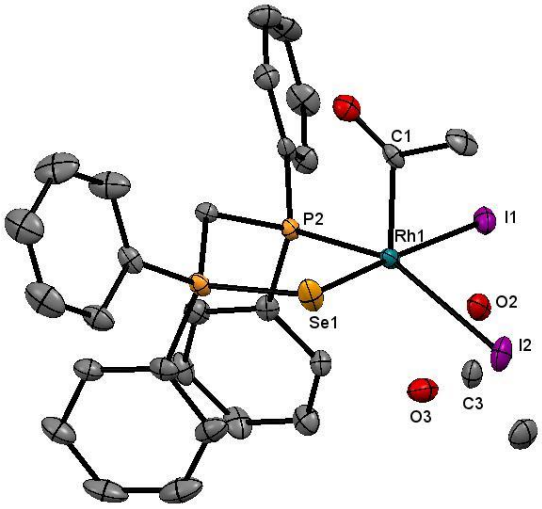

Figure 4.7: X-ray crystal structure for [Rh(dppmSe)(COMe)(OAc)I] (4l) with thermal ellipsoids shown at 50% probability level. Hydrogen atoms omitted for clarity.

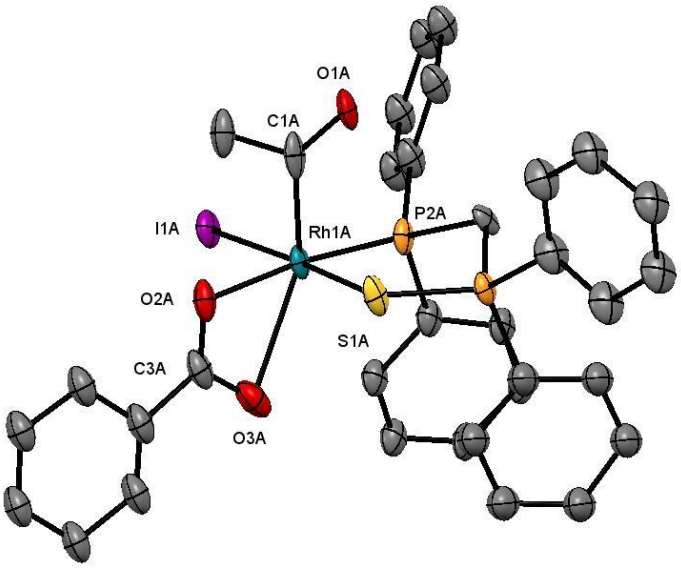

Figure 4.8: X-ray crystal structure for [Rh(dppmS)(COMe)(OBz)I].CH_2Cl_2 (5k) with thermal ellipsoids shown at 50% probability level. Hydrogen atoms and CH_2Cl_2 omitted for clarity.

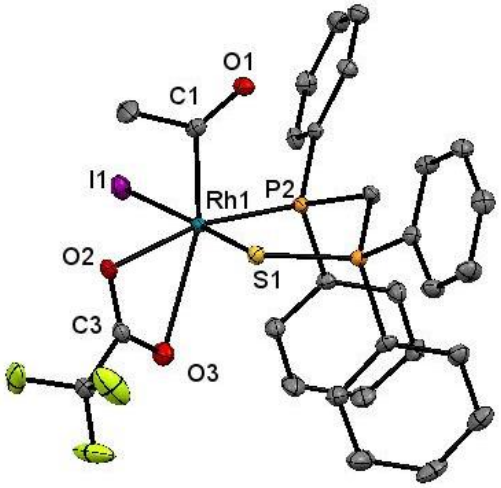

Figure 4. 9: X-ray crystal structure for [Rh(dppmS)(COMe)(TFA)I] (6k) with thermal ellipsoids shown at 50% probability level. Hydrogen atoms omitted for clarity.

Table 4.11: Selected bond lengths (Å) and angles (deg) for complexes 3k,[16] 3l,[21] 4k, 4l, 5k and 6k

Bond/Angle	3k	3l	4k	4l	5k	6k
Rh(1)-C(1)	1.951(6)	1.943 (19)	1.971(14)	1.958(6)	1.97(3)	1.957(3)
Rh(1)-S(1)/Se(1)	2.357(2)	2.452 (2)	2.355(4)	2.4673(9)	2.373(4)	2.3593(7)
Rh(1)-P(2)	2.256(2)	2.259 (5)	2.259(3)	2.247(2)	2.255(5)	2.2412(6)
Rh(1)-I(1)	2.6497(19)	2.648 (2)	2.6455(15)	2.6392(8)	2.6435(18)	2.6569(3)
Rh(1)-I(2)	2.7024(19)	2.710 (2)		2.753(9)		
Rh(1)-O(2)			2.147(8)	2.144(7)	2.130(12)	2.1842(17)
Rh(1)-O(3)			2.450(9)	2.407(7)	2.523(2)	2.543(2)
P(2)-Rh(1)- S(1)/Se(1)	90.47(9)	91.88 (13)	92.82(12)	93.34(5)	92.54(18)	92.79(2)
O(2)-Rh(1)-O(3)			57.1(3)	57.7(2)	55.7(5)	55.65(7)
C(1)-Rh(1)- S(1)/Se(1)	93.6(2)	95.3(6)	87.3(4)	88.3(2)	89.0(6)	86.87(8)
C(1)-Rh(1)-I(1)	92.2(2)	91.9 (6)	89.6(4)	91.1(2)	91.7(6)	90.54(8)
C(1)-Rh(1)-I(2)	104.8(2)	103.5 (6)		115.0(2)		
C(1)-Rh(1)-P(1)	92.8(2)	91.9 (6)	90.4(4)	91.4(2)	91.9(6)	91.55(8)
C(1)-Rh(1)-O(2)			99.5(5)	98.3(2)	96.6(7)	100.06(9)

Each of the structures shows a distorted octahedral geometry, due to the small bite angle of the bidentate carboxylate ligand. The carboxylate bite angle is similar (55.65-57.7°) in all of these crystal structures and is typical for a chelate coordinated carboxylate.[24,25,29] The carboxylate is found trans to P, as predicted based on the Rh-I distances in the precursors. Carboxylates coordinate with Rh-O(3) trans to acetyl ~0.3 Å longer than Rh-O(2) trans to P, due to the strong trans influence of acetyl. For [Rh(dppmS)(COMe)(O_2CR)I] complexes (**4k, 5k** and **6k**) there is an increase in the bite angle of the dppmS ligand (92.54-92.82°) relative to that observed for **3k** (90.47°). A similar increase in the bite angle of dppmSe in **4l** relative to **3l** was observed. This smaller bite angle in **3k** and **3l** is likely due to steric repulsion from the iodide group which is replaced by carboxylate. The structure obtained for **4l** was modelled with 10% occupancy of iodide trans to phosphorus, where acetate is coordinated. However, the bond lengths and angles for coordinated acetate can still be discerned.

4.2.4 DFT calculations for carboxylate coordinated complexes

Five possible isomers were considered for **4k** as shown in Scheme 4.12. DFT modelling (*Gaussian09,* B3LYP, 6-311G, SDD on Rh) was used to determine relative energies for these structures, reported in Table 4.12. Analogous structures were also considered for **5k**.

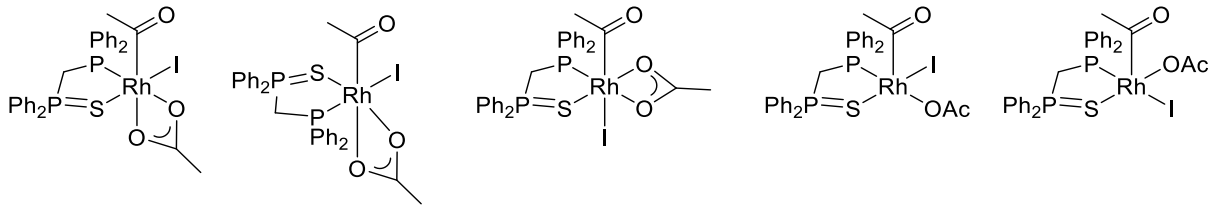

$4k_1$ **$4k_2$** **$4k_3$** **$4k_4$** **$4k_5$**

Scheme 4.12: Isomers of 4k modelled by DFT to determine lowest energy conformer

It was found that isomers **$4k_1$** and **$5k_1$** with carboxylate trans to P are the lowest in energy, consistent with the X-ray crystal structures. Isomers with monodentate carboxylates are ~20 kJ mol^{-1} higher in energy.

Table 4.12: ΔG calculated for isomers of 4k and 5k, relative to the lowest energy isomer for each complex.

Isomer	ΔG/ kJ mol^{-1}	Isomer	ΔG/ kJ mol^{-1}
$4k_1$	0	**$5k_1$**	0
$4k_2$	6.71	**$5k_2$**	11.89
$4k_3$	56.63	**$5k_3$**	59.34
$4k_4$	21.65	**$5k_4$**	24.78
$4k_5$	23.97	**$5k_5$**	20.79

Table 4.13: Calculated ν(CO) frequencies for 3k and $5k_1$ and $5k_2$.

Isomer	Acetyl ν(CO)	ν_{asym}(CO)	ν_{sym}(CO)
3k	1737	-	-
$4k_1$	1729	1592	1411
$4k_4$	1740	1660	1317

The calculated IR frequencies for **4k$_1$** show a decrease in acetyl ν(CO) wavenumber relative to **3k** and acetate ν(CO_2) frequencies that are similar to those observed experimentally. In contrast for **4k$_4$**, which has acetate coordinated monodentate, a slight increase in acetyl ν(CO) and greater separation of ν(CO_2) frequencies are predicted, which does not concur with the experimental data. [23]

4.2.5 Reactions of Rh acetyl carboxylate complexes with CO

It was found that upon bubbling CO through a solution of **4k** or **4l** in CH_2Cl_2 for 3 hours, ν(CO) bands at 1825, 1756 cm^{-1} formed indicating reductive elimination of Ac_2O as well as a band around 1987 cm^{-1} for **1k** or **1l**. When CO gas was bubbled through a solution of **5k** or **5l** in CH_2Cl_2, formation of bands at 1810, 1734 cm^{-1} indicated elimination of mixed anhydride AcOBz. After 2-3 hours formation of ν(CO) at 1825, 1756 and 1789, 1725 cm^{-1} were indicative of anhydride scrambling. Concurrent with elimination of anhydride under CO, bands at ~1987 cm^{-1} indicated formation of the corresponding Rh(I) carbonyl species **1k** and **1l** respectively as shown in Scheme 4.13. A similar reaction was observed with complexes **6k** and **6l,** however elimination was slower from these complexes.

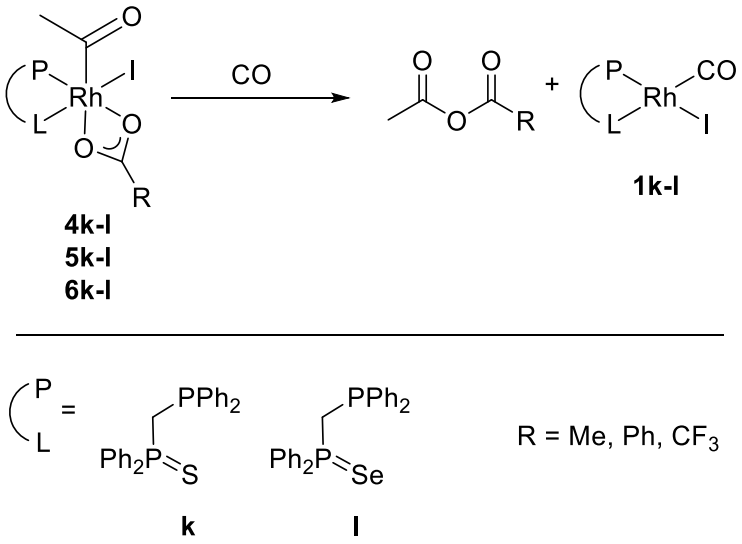

Scheme 4.13: Reactions of 4k,l, 5k,l and 6k,l with CO

4.2.6 DFT investigation of thermodynamics of anhydride elimination

Calculations were also carried out to investigate the thermodynamics of anhydride elimination according to the reaction shown in Scheme 4.14. The calculated ΔG and ΔH values are given in Table 4.14.

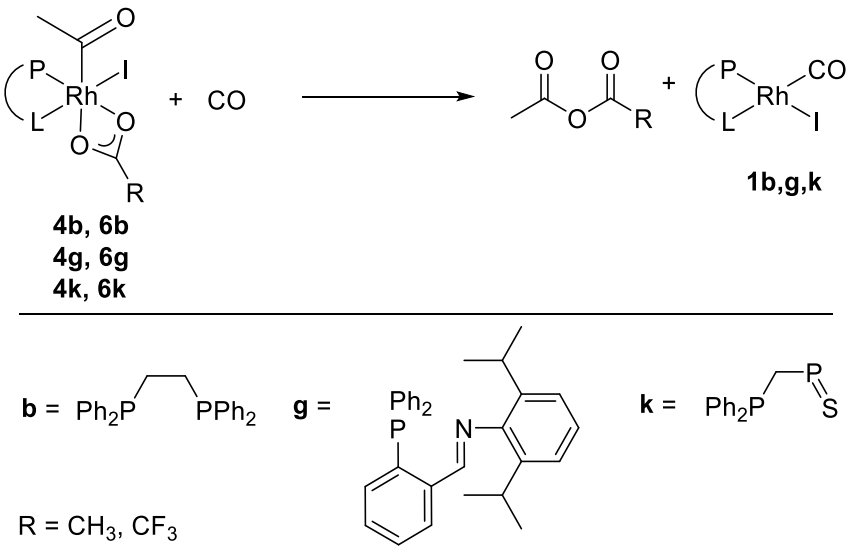

Scheme 4.14: Intermediates and products formed upon addition of OAc/TFA$^-$ to 3b,g,k for which relative energies were calculated and compared

Table 4.14 Reaction energies calculated for elimination of anhydride according to Scheme 4.12

Complex	Ligand (P-L)	Carboxylate (O_2CR)	ΔG/ kJ mol^{-1}	ΔH / kJ mol^{-1}
4b	Dppe	OAc	-69.84	-49.82
6b	Dppe	TFA	-35.55	-12.74
4g	PN-^{i}Pr$_2$Ph	OAc	-102.97	-82.00
6g	PN-^{i}Pr$_2$Ph	TFA	-54.60	-32.83
4k	dppmS	OAc	-75.88	-62.72
6k	dppmS	TFA	-42.59	-25.64

In all cases the reactions are calculated to be thermodynamically favoured, agreeing with the experimentally observed anhydride elimination and formation of [Rh(P-L)(CO)I] in the presence of CO. The elimination of trifluoroacetic anhydride from **6b,g,k** is less energetically favourable than elimination of acetic anhydride from **4b,g,k**. This may partially explain why complexes with trifluoroacetate coordinated were easier to isolate. The reaction of **4g** to give **1g** and acetic anhydride was thermodynamically favoured over elimination of anhydride from **4b**. However, experimentally elimination of anhydride occurred faster from **4b**, this may be due to a lower activation energy for elimination from anhydride from **4b**.

4.3 Summary

The reactions of [Rh(PN-Ar)(COMe)I_2] complexes with carboxylates were found to proceed with substitution of iodide by the carboxylate to form [Rh(PN-Ar)(COMe)(O_2CR)I]. The carboxylate coordination was determined to be bidentate by solid state IR spectroscopy. DFT calculations indicated a geometry with carboxylate coordinated trans to phosphorus, as was predicted based on Rh-I bond lengths in the crystal structure of [Rh(PN-Mes)(COMe)I_2]. Carboxylate complexes [Rh(PN-Ar)(COMe)(O_2CR)I] with acetate and benzoate were found to eliminate an anhydride over 2-3 days. In the presence of CO, [Rh(PN-Ar)(CO)I] was formed, whereas under N_2 no Rh(I) species were identified.

The mono-substituted complexes formed upon addition of [Ag][TFA] to [Rh(PN-Ar)(COMe)I_2] were stable, and several of these were isolated and characterised by ^{31}P, ^{1}H NMR and IR spectroscopy, mass spectrometry and in one case X-ray crystallography. This confirmed that the carboxylate substitutes an iodide ligand trans to phosphorus.

Addition of carboxylates to [Rh(dppmX)(COMe)I_2] (X = S, Se) yielded complexes of the formula [Rh(dppmX)(COMe)(O_2CR)I], which were stable and could be isolated. These complexes were characterised by ^{31}P, ^{1}H NMR and IR spectroscopy, mass spectrometry, elemental analysis and in some cases X-ray crystallography, and were found to have chelate coordinated carboxylates trans to phosphorus. The carboxylate complexes are analogous to those observed as intermediates in Chapter 3.

DFT calculations for the reactions of [Rh(P-L)(COMe)(O_2CR)I] with CO to give [Rh(P-L)(CO)I] and anhydride showed the reactions to be thermodynamically favourable in all cases. Elimination of trifluoroacetic anhydride from [Rh(P-L)(COMe)(TFA)I] is calculated to be less favourable than that of acetic anhydride from [Rh(P-L)(COMe)(OAc)I], consistent with the observed greater stability of the TFA coordinated species.

4.4 References

(1) Moloy, K. G.; Wegman, R. W. *Organometallics* **1989**, *8*, 2883–2892.

(2) Moloy, K. G.; Petersen, J. L. *Organometallics* **1995**, *14*, 2931–2936.

(3) Lamb, G.; Clarke, M.; Slawin, A. M. Z.; Williams, B.; Key, L.; Roukoss, C.; Fiddy, S.; de Mallmann, A.; Rendón, N.; Basset, J.-M.; Kuntz, E.; Copéret, C. *Dalton Trans.* **2007**, 5582–5589.

(4) Williams, G. L.; Parks, C. M.; Smith, C. R.; Adams, H.; Haynes, A.; Meijer, A. J. H. M.; Sunley, G. J.; Gaemers, S. *Organometallics* **2011**, *30*, 6166–6179.

(5) Bader, A.; Lindner, E. *Coord. Chem. Rev.* **1991**, *108*, 27–110.

(6) Wegman, R. W.; Abatjoglou, A. G.; Harrison, A. M. *J. Chem. Soc, Chem. Commun.* **1987**, 1891.

(7) Gonsalvi, L.; Adams, H.; Sunley, G. J.; Ditzel, E.; Haynes, A. *J. Am. Chem. Soc.* **1999**, *121*, 11233–11234.

(8) Gonsalvi, L.; Gaunt, J. A.; Adams, H.; Castro, A.; Sunley, G. J.; Haynes, A. *Organometallics* **2003**, *22*, 1047–1054.

(9) Wilson, J. M. Ligand effects on key steps in methanol carbonylation, PhD Thesis, University of Sheffield, 2006.

(10) Eiji Shirakawa; Hiroto Yoshida; Takuya Kurahashi; Yoshiaki Nakao, and; Hiyama, T., *J. Am. Chem. Soc.* **1998**, *120*, 2975-2976.

(11) Yoshida, H.; Honda, Y.; Hiyama, T.; Shirakawa, E. *Chem. Commun.* **2001**, 1880–1881.

(12) van den Beuken, E. K.; Feringa, B. L.; van den Beuken, E. K.; Smeets, W. J. J.; Spek, A. L. *J. Chem. Soc., Chem. Commun.* **1998**, 223–224.

(13) Koprowski, M.; Sebastián, R. M.; Maraval, V.; Zablocka, M.; Cadierno, V.; Donnadieu, B.; Igau, A.; Caminade, A. M.; Majoral, J. P. *Organometallics* **2002**, *21*, 4680–4687.

(14) Doherty, S.; Knight, J. G.; Scanlan, T. H.; Elsegood, M. R. .; Clegg, W. *J. Organomet.*

Chem. **2002**, *650*, 231–248.

(15) Best, J.; Wilson, J. M.; Adams, H.; Gonsalvi, L.; Peruzzini, M.; Haynes, A. *Organometallics* **2007**, *26*, 1960–1965.

(16) Gonsalvi, L.; Adams, H.; Sunley, G. J.; Ditzel, E.; Haynes, A. *J. Am. Chem. Soc.* **2002**, *124*, 13597–13612.

(17) Baker, M. J.; Giles, M. F.; Orpen, A. G.; Taylora, M. J.; Watta, R. J. *J. Chem. Soc. Chem. Commun.* **1995**, *1*, 197–198.

(18) Dutta, D. K.; Woollins, J. D.; Slawin, A. M. Z.; Konwar, D.; Sharma, M.; Bhattacharyya, P.; Aucott, S. M. *J. Organomet. Chem.* **2006**, *691*, 1229–1234.

(19) Lassauque, N.; Davin, T.; Nguyen, D. H.; Adcock, R. J.; Coppel, Y.; Le Berre, C.; Serp, P.; Maron, L.; Kalck, P. *Inorg. Chem.* **2012**, *51*, 4–6.

(20) Nguyen, D. H.; Lassauque, N.; Vendier, L.; Mallet-Ladeira, S.; Le Berre, C.; Serp, P.; Kalck, P. *Eur. J. Inorg. Chem.* **2014**, *2014*, 326–336.

(21) Rose, R. Reactivity of P-Se Chelate Complexes of Rhodium, MChem Thesis, University of Sheffield, 2009.

(22) Bailey, A.; Mann, E.; Manuel, P. **1992**, *200*, 111–118.

(23) Deacon, G.; Phillips, R. *Coord. Chem. Rev.* **1980**, *33*, 227–250.

(24) Chin, C. S.; Lee, H.; Lee, M. K.; Noh, S.; Eum, M.-S.; Hong, S. *J. Organomet. Chem.* **2005**, *690*, 1306–1313.

(25) Matas, L.; Muniente, J.; Ros, J.; Alvarez-Larena, Á.; F. Piniella, J. *Inorg. Chem. Commun.* **1999**, *2*, 364–367.

(26) Klein, H.-F.; Haller, S.; Sun, H.; Li, X.; Jung, T.; Rohr, C.; Florke, U.; Haupt, H.-J. *Zeitschrift für Naturforsch. B* **2014**, *53*, 587–598.

(27) Lobana, T.; Sharma, P. *Ind. J. Chem.* **1987**, *26*, 784–785.

(28) Bond, A. M.; Colton, R.; Panagiotidou, P. *Organometallics* **1988**, *7*, 1774–1782.

(29) Kovach, J.; Brennessel, W. W.; Jones, W. D. *J. Organomet. Chem.* **2015**, *793*, 192–199.

Chapter 5

Investigation into the reactions of Rh(III) acetyl complexes with nitrogen nucleophiles

5.0 Introduction

Chapter 3 and 4 discussed the reactions of a variety of Rh(III) acetyl complexes with carboxylate nucleophiles. Reactions of metal acyl complexes with other nucleophiles, such as alcohols and amines, are important steps for product formation in a range of catalytic carbonylation processes.

A significant example is the Pd catalysed methoxycarbonylation of ethene to methyl propanoate (C_2H_4 + CO + MeOH → $EtCO_2Me$).[1] Methyl propanoate is produced in over 120,000 tonnes per annum[2] and is primarily used in the production of paints, varnishes and methyl methacrylate. Two competing mechanisms, shown in Scheme 5.1, can occur depending on catalytic conditions. All of the palladium species in both cycles have been separately synthesised and studied spectroscopically.[3–6] The "hydride cycle" (left) is thought to be dominant under normal operating conditions and involves reaction of a Pd-acyl complex with methanol to form methyl propanoate. Closely related catalyst systems can also result in co-polymerisation of CO and ethene to give polyketones, via alternating insertion of CO and C_2H_4. By changing the spectator ligands, formation of either methyl propanoate or polyketones can be favoured.[7,8]

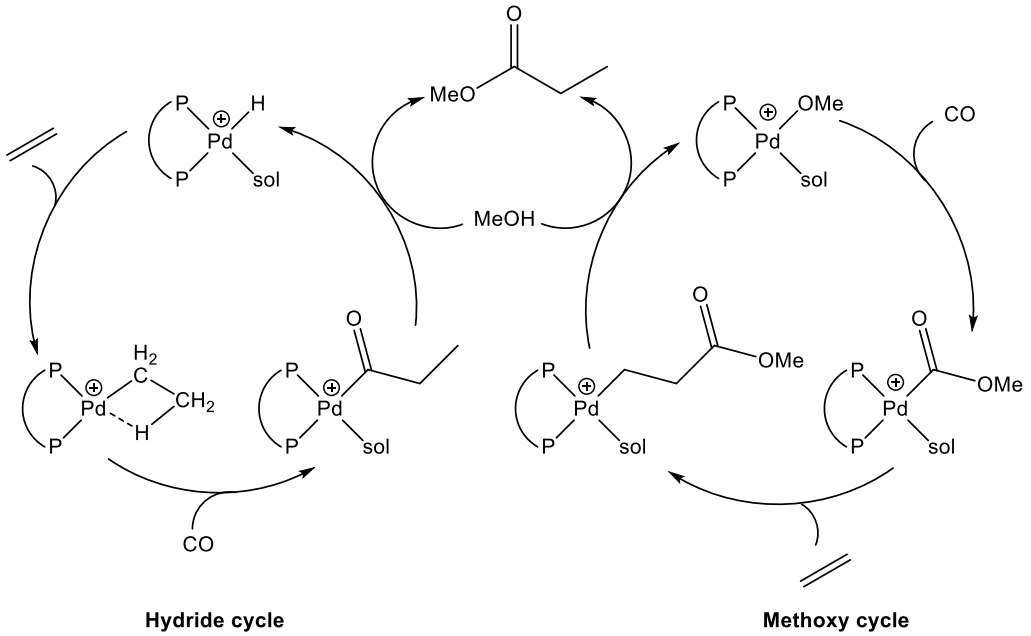

Scheme 5.1: Competing catalytic cycles for Pd-catalysed methoxycarbonylation of ethene.

A related catalytic process, which makes a C-N bond, is Pd catalysed aminocarbonylation of aryl halides to give amides (RX +CO + R'$_2$NH -> RCONR'$_2$ + HX), was first noted by Heck.[9] A wide range of such aminocarbonylations are known and recent work by Buchwald and co-workers[10] has employed the use of additives to allow for milder catalytic conditions. A study by Lin et al indicated a mechanism where amine coordinates to a Pd-acyl species and then undergoes migration before elimination of amide, as shown in Scheme 5.2.[11]

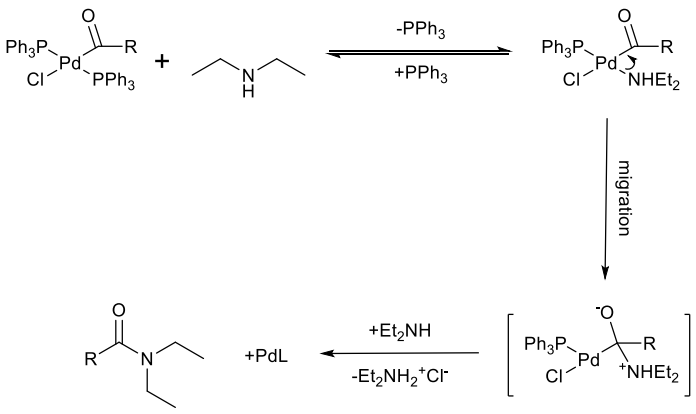

Scheme 5.2: Proposed formation of amides from reaction of Pd-acyl and amines

Much previous work focuses on using Pd as a catalyst for this type of reaction. However, the many Rh acyl complexes that are known provide a useful opportunity to further investigate reactivity of metal acyl complexes with nucleophiles such as amines. In this chapter the reactions of [Rh(P-P)(COMe)I_2] (**3a-e**) with amines are reported. Kinetic investigations under pseudo-first-order conditions of the reactions of [Rh(P-P)(COMe)I_2] (**3a-d**) with diethylamine were carried out to determine second order rate constants. Activation parameters were obtained for these reactions via variable temperature kinetic measurements.

5.1 Reactions of Rh(III) acetyl complexes with nucleophiles

The synthesis of Rh acetyl complexes **3a-e,k** has been discussed in previous chapters, using variations of known literature syntheses.[12–14] The reactivity of these complexes with amines was initially investigated to identify systems suitable for kinetic investigation.

It has previously been found that $[Rh(COMe)(CO)_2I_3]^-$ reacts rapidly with amines such as Et_2NH and Bu_2NH. These reactions were too fast to be conveniently monitored spectroscopically but reaction with the less basic secondary amine, N-methyl aniline (PhNHMe) to give the corresponding acetamide was slower and more easily monitored by IR spectroscopy.[15] Kinetic studies gave evidence for parallel first and second order pathways, with direct nucleophilic attack competing with unassisted reductive elimination, Scheme 5.3.

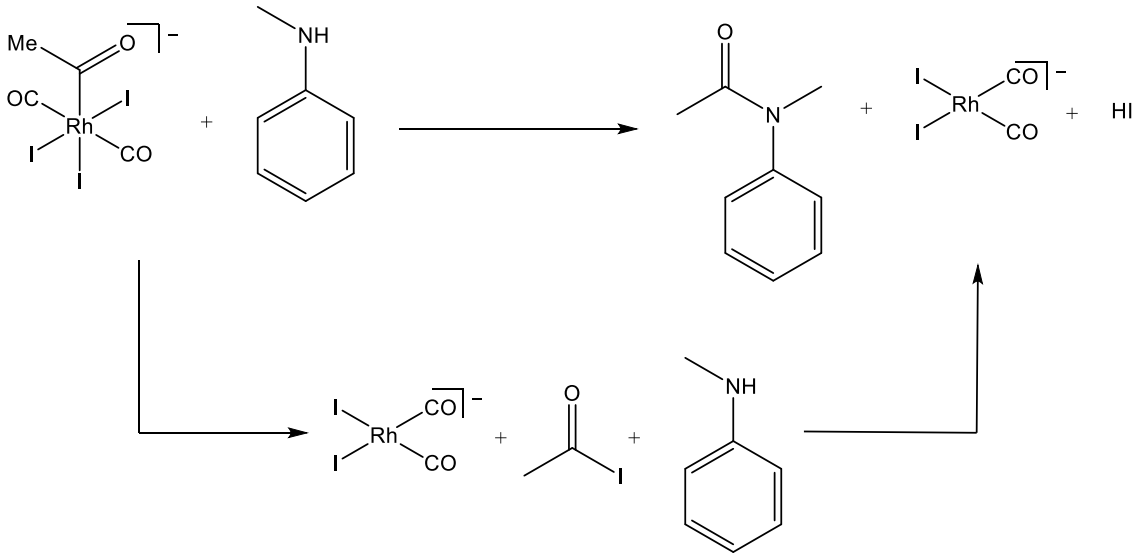

Scheme 5.3: Reaction of $[Rh(COMe)(CO)_2I_3]^-$ and N-methyl aniline

To probe whether our previously studied diphosphine complexes also reacted with N-methyl aniline, an excess of N-methyl aniline was added to a solution of **3b** in $CHCl_3$, under N_2. This mixture was heated to reflux for 24 hours and monitored periodically by IR spectroscopy. An absorption around 1660 cm^{-1} would be expected for an acetamide but after 24 hours no

change in the spectrum had occurred. Since N-methyl-N-phenyl acetamide has a high boiling point (256 ^{o}C), the solvent could be removed in vacuo and ^{31}P and ^{1}H NMR spectra of the residue indicated no reaction had occurred.

The lack of reactivity for these diphosphine complex (**3b**) with PhNHMe reflects the relative reactivity of $[Rh(COMe)(CO)_2I_3]^-$ and $[Rh(P\text{-}P)(COMe)I_2]$ with acetate. The diphosphine complexes react much slower, this may be due to steric hindrance and the more electron rich metal centre.

The reactivity of **3b** with a more nucleophilic amine was therefore tested. Ten molar equivalents of diethylamine were added to a solution of $[Rh(dppe)(COMe)I_2]$ **3b** in CH_2Cl_2 under CO, and the reaction monitored by IR spectroscopy.

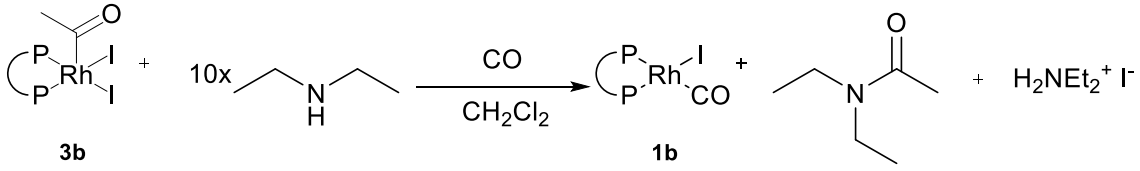

Scheme 5.4: Reaction of 3b with diethylamine under CO in CH_2Cl_2 (diphosphine ligand simplified for clarity).

Over 3 hours formation of bands at 1633 and 2010 cm^{-1} indicated formation of N,N-diethyl acetamide and [Rh(dppe)(CO)I] (**1b**) respectively, as shown in Scheme 5.4. The HI formed in this reaction is presumably scavenged by excess Et_2NH to give the ammonium salt As this reaction proceeded readily over 3 hours, the reactions of **3a-e,k** with diethylamine were considered for a kinetic investigation, described in section 5.2 below.

Another type of reaction known to occur for metal-acyl complexes is with imines. Lafrance et al.[16] found that imines of formula (*p*-tolyl)(R_2)C=NR_1 (where R^1 = H, ^{t}Bu R^2 = alkyl) could insert in metal-acyl bonds as shown in Scheme 5.5. A similar reaction was observed by Rania et al. [17]

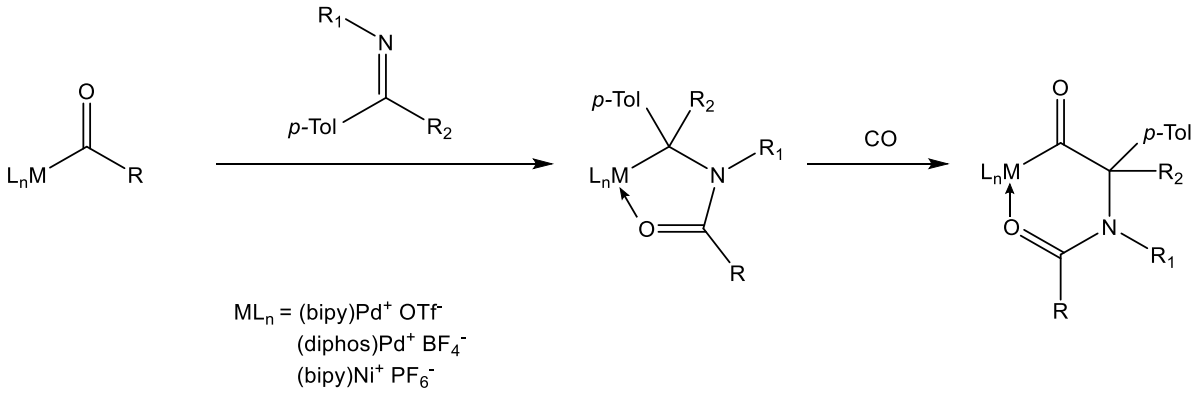

Scheme 5.5: Reaction of metal acyl complexes with imines observed by Lafrance et al.[16]

A similar imine insertion reaction is proposed to explain the formation of an N-acetylated iminophosphine ligand as described in Chapter 6 of this thesis. In an attempt to model this, the reaction of complex **3b** with a simple imine was attempted. An excess of N-(4-methylphenyl)methylene methanamide (Me-N=C(H)(p-tolyl)) was added to a solution of **3b** in $CHCl_3$, under N_2 and monitored by IR spectroscopy. However, after 2 days reflux, little change was observed in the IR spectrum and ^{31}P and ^{1}H NMR spectroscopy indicated no formation of new species.

5.2 Kinetic investigation of reactions of $HNEt_2$ with Rh(III) acetyl complexes

IR spectroscopy was used to monitor the reactions of **3a-d,k** with diethylamine. Kinetic experiments were carried out under pseudo first order conditions, using at least tenfold excess of diethylamine. Typical conditions used in these experiments are given in the experimental chapter of this thesis. Figure 5.1 shows a series of overlaid IR spectra obtained during a typical reaction of **3a** with $HNEt_2$ (0.064 M).

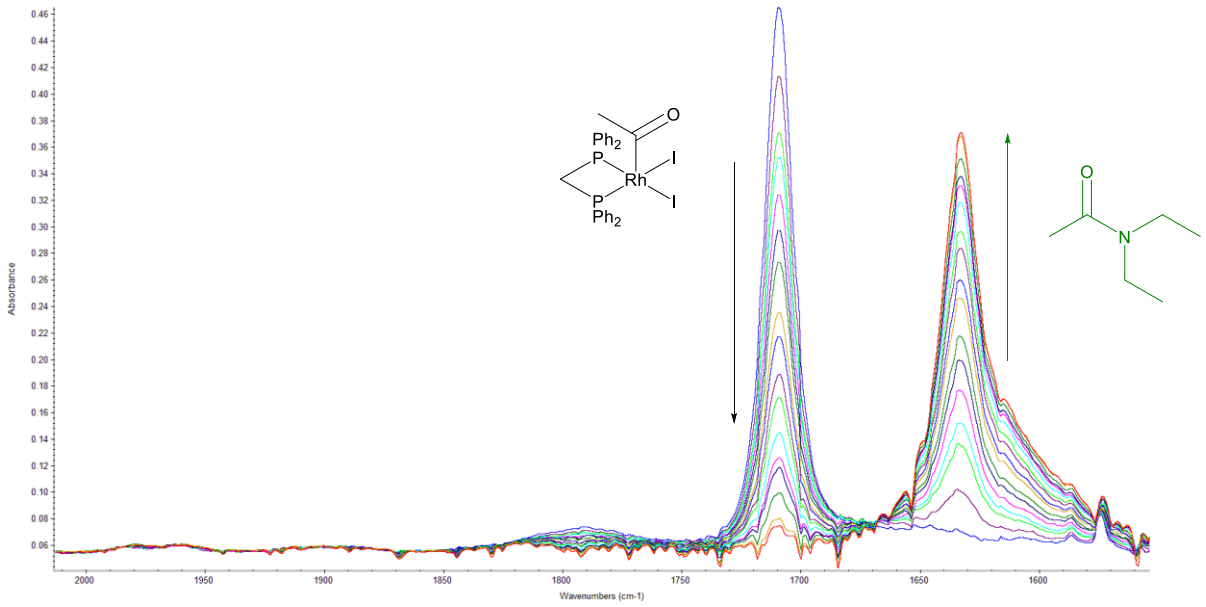

Figure 5.1: Series of IR spectra recorded during the reaction of 3a with diethylamine (0.064 M in CH_2Cl_2 at 23 °C)

Decay of the acetyl ν(CO) for **3a** at 1709 cm^{-1} was observed alongside growth of a band at 1633 cm^{-1}, corresponding to N,N-diethyl acetamide. The decay and growth of these absorbances were analysed to determine a pseudo first order rate constant (k_{obs}). Plots of absorbance vs. time were fitted to an exponential decay/growth curve indicating the reaction is first order with respect to the reactant Rh(III) complexes. Sample plots for the reaction of complex **3a**

with diethylamine (0.064 M), forming N,N-diethylacetamide, are shown in Figure 5.2 and Figure 5.3.

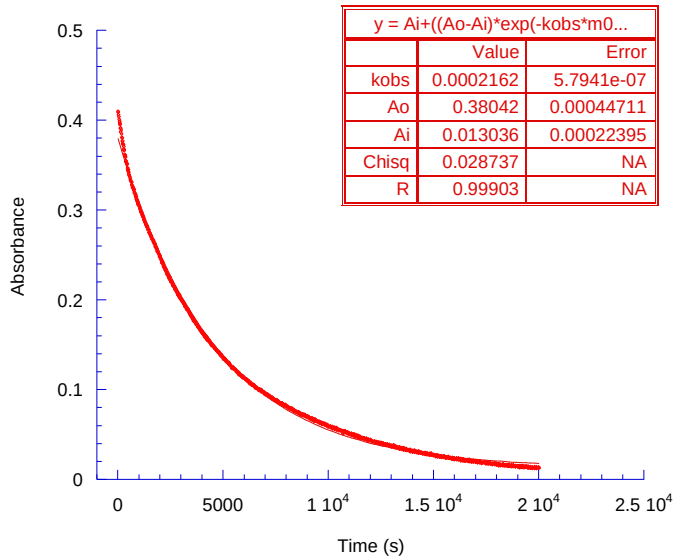

Figure 5.2: Plot of absorbance at 1709 cm^{-1} vs. time for the reaction of 3a with diethylamine (0.064 M in CH_2Cl_2 at 23 °C)

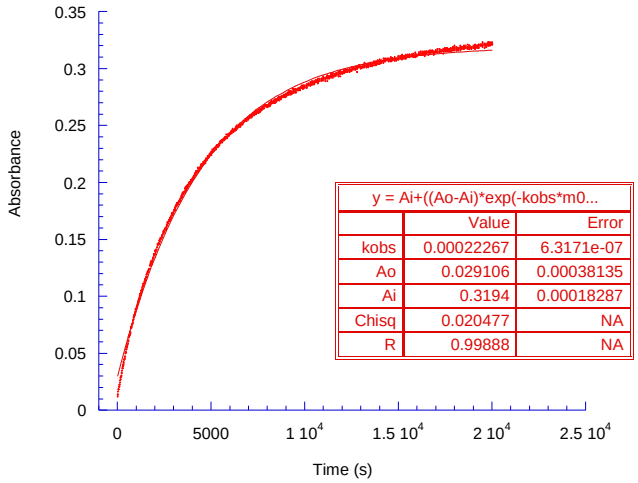

Figure 5.3: Plot of absorbance at 1633 cm^{-1} vs. time for the reaction of 3a with diethylamine (0.064 M in CH_2Cl_2 at 23 °C)

Plots of k_{obs} vs. [$HNEt_2$] were linear, indicating first order dependence on $HNEt_2$ and therefore second order behaviour overall. A sample plot of k_{obs} vs. [$HNEt_2$] for the reaction of complex **3a** in CH_2Cl_2 at 23 °C is shown in Figure 5.4. Second order rate constants (k_2) were determined from the gradients of these plots for complexes **3a-d** and are displayed in Table 5.1.

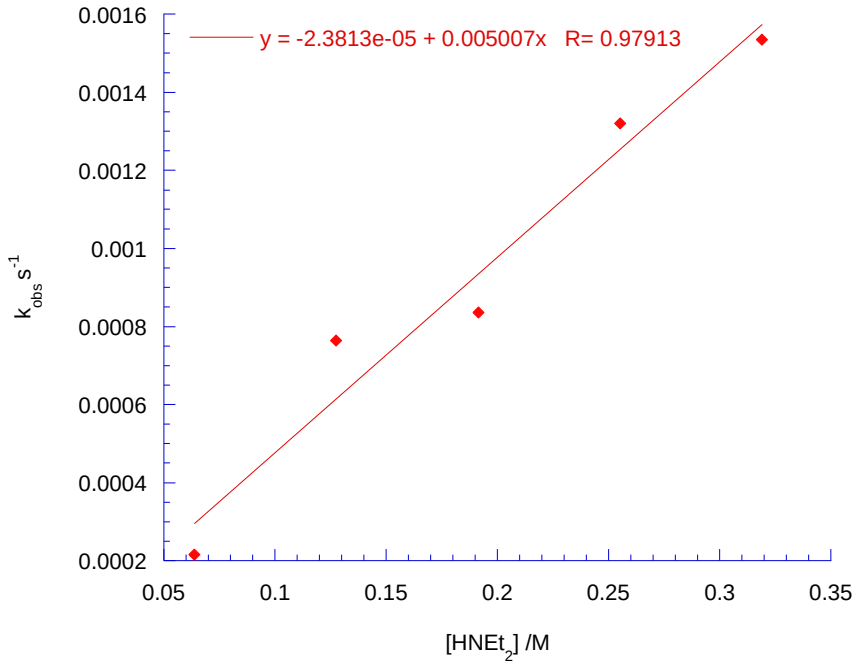

Figure 5.4: Plot of k_{obs} Vs [$HNEt_2$] for complex 3a to determine second order rate constant (k_2) at 23 °C in CH_2Cl_2

Table 5.1: Second order rate constants for reactions of 3a-d with $HNEt_2$, 23 °C, and ligand bite angles[13,14,18,19]

Complex	Ligand	v(CO)/ cm^{-1}	k_2 *10^3/ M^{-1} s^{-1}	k_{rel}	Ligand bite angle / °
3a	dppm	1709	4.96 (±0.52)	7.4	73.3
3b	dppe	1711	0.67 (±0.11)	1.0	84.7
3c	dppp	1701	1.31 (±0.29)	2.0	90.5
3d	dppb	1700	1.72 (±0.43)	2.6	99.1

The second order rate constants for these complexes are of similar magnitudes, with **3a** and **3d** being the fastest. There is no obvious correlation with the diphosphine bite angle. Complex **3k** with dppmS ligand was also found to react with diethylamine to produce an acetamide, however due to solubility issues reliable rate constants could not be obtained.

Rate constants were measured for the reactions of diethyl amine and complexes **3a-d** over a temperature range of 14-32 °C (data for these reactions are given in the appendix). From these data, Eyring plots, as shown in Figure 5.5, were used to determine activation parameters. Table 5.2 shows the determined activation parameters.

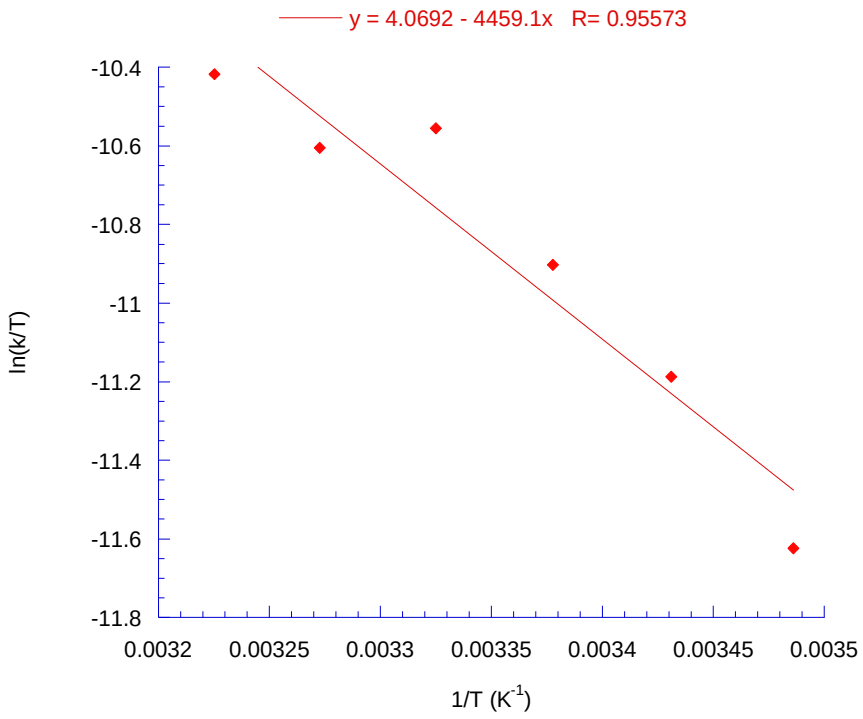

Figure 5.5: Eyring plot of 1/T Vs ln(k/T) for complex 3a at 0.191 M diethylamine in CH_2Cl_2

Table 5.2: Activation parameters for the reaction of $HNEt_2$ with 3a-d in CH_2Cl_2.

Complex	Ligand	$\Delta H^{\ddagger}$ /kJ mol^{-1}	$\Delta S^{\ddagger}$ /J K^{-1} mol^{-1}	$\Delta G^{\ddagger}_{298}$ /kJ mol^{-1}
3a	dppm	44.9 (±4.2)	-137 (±14)	85.8 (±8.2)
3b	dppe	50.0 (±15)	-130 (±50)	88.9 (±30)
3c	dppp	49.9 (±7.0)	-130 (±23)	88.5 (±14.0)
3d	dppb	37.1 (±5.7)	-164 (±19)	85.9 (±11.4)

The $\Delta H^{\ddagger}$ values are of a similar magnitude with **3a-c** all within uncertainty range of each other, though it is apparent that **3d** is lower in activation enthalpy.

These reactions show a large negative entropy of activation indicating an associative mechanism, with all $\Delta S^{\ddagger}$ values within the uncertainty range of each other. The second order rate and large negative entropy of activation are consistent with either direct attack by Et_2NH on acetyl or coordination of amine to Rh and subsequent elimination of acetamide, Scheme 5.6.

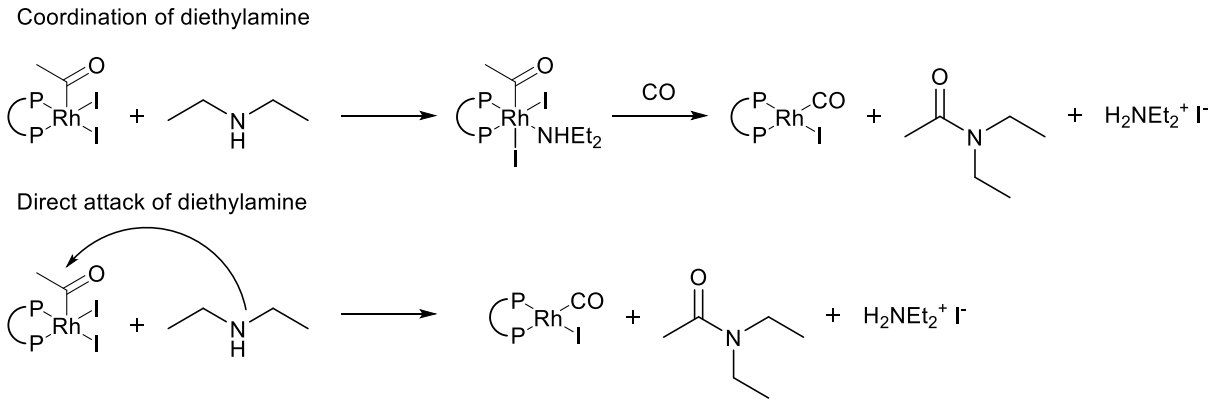

Scheme 5.6: Proposed mechanisms for acetamide formation

No reaction was observed between complex **3e** (with xantphos ligand) and diethyl amine. The lack of a reaction with **3e** implies a vacant site may be necessary for an amine to coordinate to rhodium before elimination of an acetamide. To test this an iodide ligand was abstracted from **3e** and replaced with acetonitrile to form the more labile [Rh(xantphos)(COMe)(NCMe)I][BF_4],

as in Chapter 3, and the reaction with diethylamine monitored spectroscopically. An excess of diethylamine was added to a solution of [Rh(xantphos)(COMe)(NCMe)I][BF_4] in CH_2Cl_2 and an IR spectrum taken. Immediate decay of the acetyl band at 1708 cm^{-1} and growth of a band at 1634 cm^{-1} indicates reaction of the rhodium acetyl and amine to form N,N-diethylacetamide. This further supports the mechanism of coordination of amine to a vacant site before reductive elimination of product, shown in Scheme 5.7.

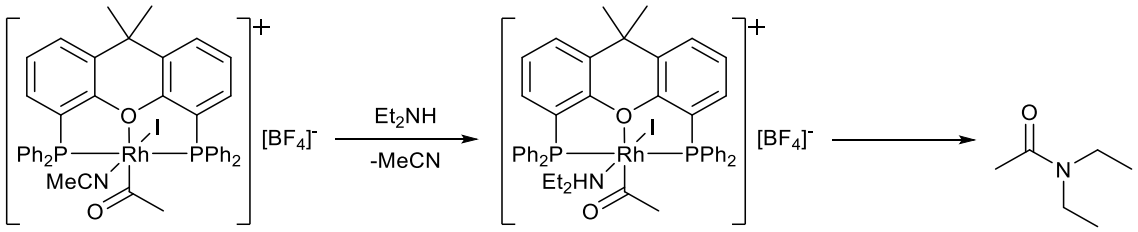

Scheme 5.7: Proposed mechanism of acetamide formation from the reaction of [Rh(xant)(COMe)(NCMe)I][BF_4] and diethylamine

5.3 Summary

The reactions of Rh(III) acetyl complexes with diethylamine to have been investigated. Under CO a Rh(I) carbonyl species was observed alongside formation of N,N-diethylacetamide. Under N_2 the acetamide was still observed but no Rh(I) species could be identified.

Second order rate constants and activation parameters were obtained for complexes [Rh(P-P)(COMe)I_2] (**3a-d**) with complexes containing dppm and dppb ligands achieving the highest rates. However, there is no obvious correlation between rate and diphosphine ligand bite angle.

Eyring plots gave activation parameters with large negative entropies of activation, which indicated that the reactions proceed by an associative mechanism. No reaction was observed between [Rh(xantphos)(COMe)I_2] (**3e**) and diethylamine but a rapid reaction was observed between [Rh(xantphos)(COMe)(NCMe)I][BF_4] and diethylamine, consistent with that a vacant coordination site being required. A mechanism where amine initially coordinates to Rh before reductive elimination of an acetamide is proposed.

5.4 References

(1) van Leeuwen, P. W. N. M.; Zuideveld, M. a; Swennenhuis, B. H. G.; Freixa, Z.; Kamer, P. C. J.; Goubitz, K.; Fraanje, J.; Lutz, M.; Spek, A. L. *J. Am. Chem. Soc.* **2003**, *125*, 5523–5539.

(2) Cornils, B.; Herrmann, W. A. (Wolfgang A. .; Beller, M.; Paciello, R. *Applied homogeneous catalysis with organometallic compounds : a comprehensive handbook in four volumes*; 1996.

(3) Eastham, G. R.; Tooze, R. P.; Heaton, B. T.; Iggo, J. A.; Whyman, R.; Zacchini, S. *Chem. Commun.* **2000**, 609–610.

(4) Clegg, W.; Eastham, G. R.; Elsegood, M. R. J.; Heaton, B. T.; Iggo, J. A.; Tooze, R. P.; Whyman, R.; Zacchini, S. *Organometallics* **2002**, *21*, 1832–1840.

(5) Wolowska, J.; Eastham, G. R.; Heaton, B. T.; Iggo, J. A.; Jacob, C.; Whyman, R. *Chem. Commun.* **2002**, 2784–2785.

(6) Liu, J.; Heaton, B. T.; Iggo, J. a; Whyman, R. *Angew. Chem. Int. Ed. Engl.* **2004**, *43*, 90–94.

(7) Zuidema, E.; Bo, C.; van Leeuwen, P. W. N. M. *J. Am. Chem. Soc.* **2007**, *129*, 3989–4000.

(8) Drent, E.; Budzelaar, P. H. M. *Chem. Rev.* **1996**, *96*, 663–682.

(9) Schoenberg, A.; Heck, R. F. *J. Org. Chem.* **1974**, *39*, 3327–3331.

(10) Martinelli, J. R.; Clark, T. P.; Watson, D. A.; Munday, R. H.; Buchwald, S. L. *Angew. Chemie* **2007**, *119*, 8612–8615.

(11) Lin, Y.-S.; Yamamoto, A. *Organometallics* **1998**, *17*, 3466–3478.

(12) Williams, G. L.; Parks, C. M.; Smith, C. R.; Adams, H.; Haynes, A.; Meijer, A. J. H. M.; Sunley, G. J.; Gaemers, S. *Organometallics* **2011**, *30*, 6166–6179.

(13) Gonsalvi, L.; Adams, H.; Sunley, G. J.; Ditzel, E.; Haynes, A. *J. Am. Chem. Soc.* **2002**, *124*, 13597–13612.

(14) Lamb, G.; Clarke, M.; Slawin, A. M. Z.; Williams, B.; Key, L.; Roukoss, C.; Fiddy, S.; de Mallmann, A.; Rendón, N.; Basset, J.-M.; Kuntz, E.; Copéret, C. *Dalton Trans.* **2007**, 5582–5589.

(15) Monti, D.; Haynes, A.; Bassetti, M.; Maitlis, P. M. *Unpubl. results* **2007**.

(16) Lafrance D.; Davis J. L.; Dhawan R., Arndtsen, B. A. *Organometallics,* **2001**, *20*, 1128-1136.

(17) Dghaym R. D.; Yaccato K. J.; Arndtsen B. A. *Organometallics,* **1998**, *17*, 4-6.

(18) Moloy, K. G.; Petersen, J. L. *Organometallics* **1995**, *14*, 2931–2936.

(19) Adams, H.; Bailey, N. A.; Mann, B. E.; Manuel, C. P. *Inorganica Chim. Acta* **1992**, *198–200*, 111–118.

Chapter 6

Investigation into the mechanism of Rh and Ir catalysed decarbonylative dehydration of long chain acids

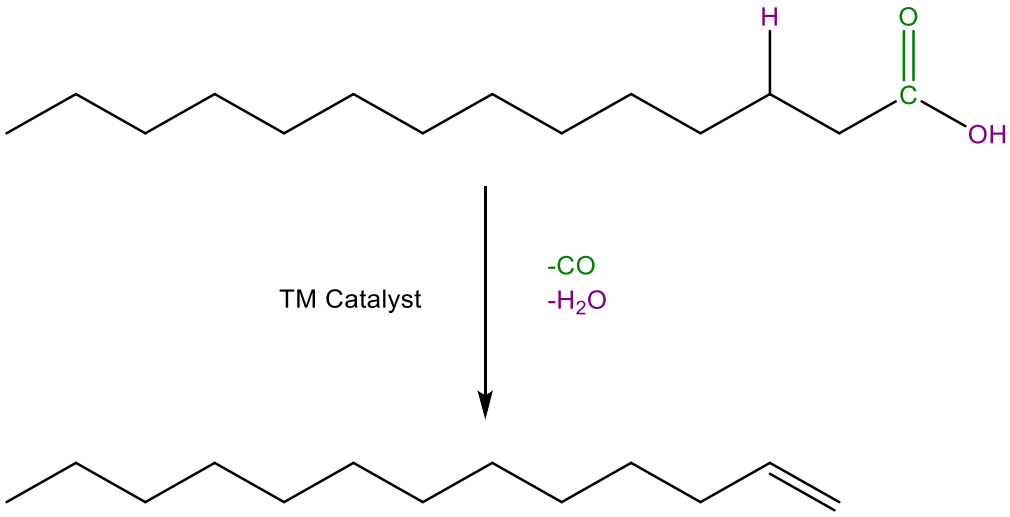

6.0 Introduction

6.0.1 Renewable sources of linear alpha olefins

Linear alpha olefins (LAOs) are key commodity chemicals and petrochemical intermediates used in a wide range of processes such as polyethylene production, synthesis of oxo alcohols (to give plasticisers and detergents) and in poly-alpha-olefin production for use as drilling fluids and lubricants.[1–3] Annual production exceeds 100,000 metric tons per year.[4] The global alpha olefins market was valued at 8.26 billion USD in 2016 and was forecast to continue growth.[5]

The main source of LAOs is fossil fuels, which undergo either fractional distillation, or cracking and then ethylene oligomerisation. However, the oligomerisation process only produces alkenes with an even number of carbons.[6–8] Another route is the Fischer-Tropsch process and subsequent dehydrogenation of the alkane product. This process is limited by the catalytic isomerisation of the kinetic products which lowers LAO yields.[9]

Due to the limited stocks of fossil fuels, and the potential to access a range of odd-carbon-numbered LAOs, alternative methods to produce LAOs from renewable feedstocks have been investigated. One major potential source is plant oils. Many plants contain fatty oils composed of glycerol and three equivalents of fatty acids as exemplified in Scheme 6.1. A range of fatty acids can be accessed from vegetable oils and animal fats.[10,11]

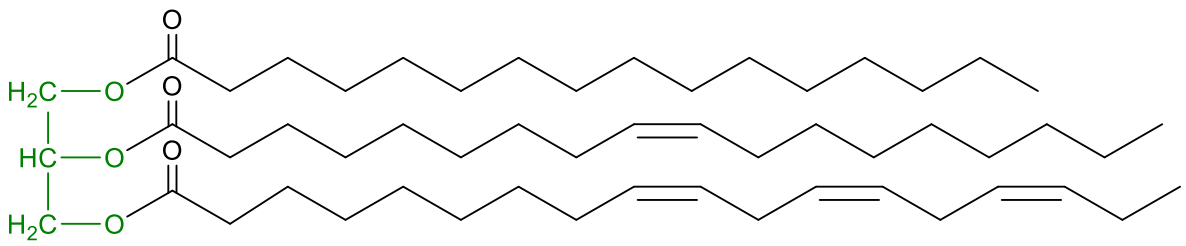

Scheme 6.1: Example of a triglyceride with glycerol (green) with three fatty acids attached.

One approach to LAOs from unsaturated oils is ethenolysis,[12] which will not be covered here. Another general method uses deoxygenation reactions, which remove oxygen from organic compounds, in the form of H_2O, CO or CO_2. Deoxygenation can be used to convert these oils and fats into in fuels and chemicals by processes such as decarbonylative dehydration and decarboxylation. These convert long chain acids into alkenes and alkanes respectively, as illustrated in Scheme 6.2 for palmitic acid.

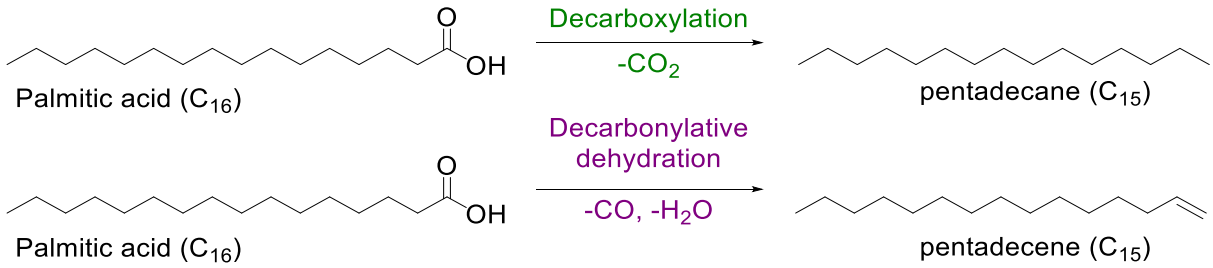

Scheme 6.2: Decarboxylation and decarbonylative dehydration of palmitic acid

LAOs formed by decarbonylative dehydration are appealing as they can be further functionalised, and they are also an important feedstock for the polymer industry. In recent years increased attention has been given to the development of catalysts that are effective for decarbonylative dehydration of long chain carboxylic acids and their derivatives, with high selectivity for terminal alkenes. [13–15]

6.0.2 Heterogeneous catalytic deoxygenation of fatty acids

Although heterogeneous catalysis is not the main focus of this chapter, some heterogeneous systems have been investigated for decarbonylative dehydration. Typically, dihydrogen is present in these reactions to inhibit catalyst deactivation, which can lead to hydrogenation of alkenes meaning greater selectivities for alkanes are typically achieved. Typically LAO

selectivity is low <30% and due to the mixture containing alkanes, olefins, ketones and other products, separation is difficult.[16–18]

High yields of alkanes with low catalyst loads have been achieved for stearic acid, shown in Scheme 6.3. The performance of different transition metals as heterogeneous catalysts has been investigated, including Ni, Ru, Pd, Pt, Ir, Os and Rh.[13,19–21]

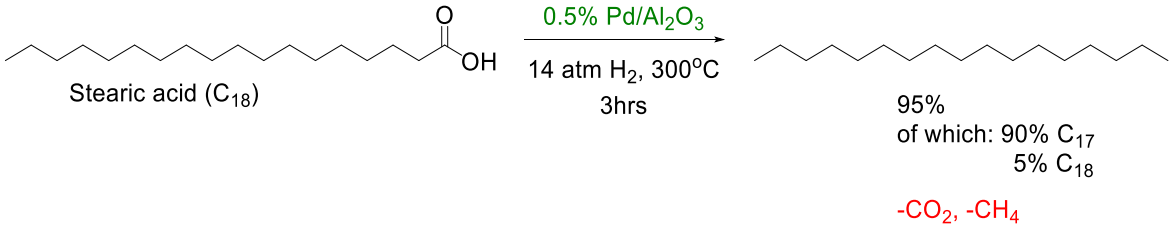

Scheme 6.3: Heterogeneous catalytic decarboxylation of stearic acid to alkane

6.0.3 Homogeneous catalysed deoxygenation of fatty acids

Various transition metal based organometallic complexes have been shown to catalyse the decarbonylative dehydration of fatty acids including examples containing Pd, Rh, Ir, Fe, Ru and Ni. Enzymatic catalysts have also been studied, but were found to be hindered by low catalyst stability and low volumetric productivity.[14,22]

6.0.4 Palladium catalysed decarbonylative dehydration

The first Pd catalysed decarbonylation of aliphatic acyl chlorides, to give olefins, CO and HCl was reported by Tsuji in 1968, Scheme 6.4.[23,24]

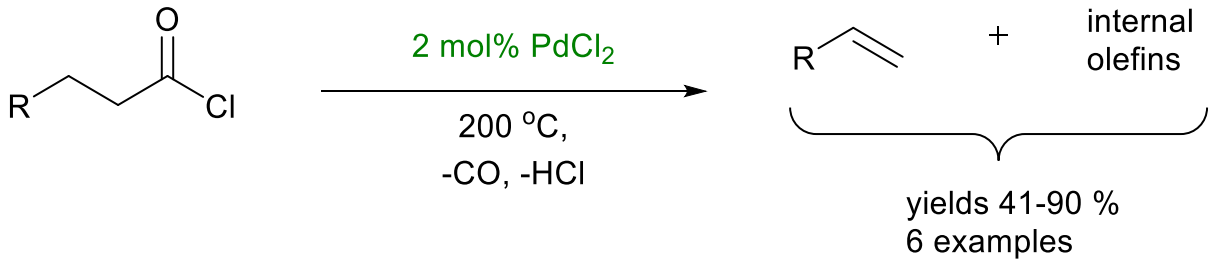

Scheme 6.4: Decarbonylation of aliphatic acyl chloride reported by Tsuji[23]

Decarbonylation of fatty acids was investigated around 10 years later by Foglia[25] using a $PdCl_2$ catalyst (10%) with a large excess of PPh_3 at 280 °C. This yielded a mixture of olefin isomers with low terminal alkene selectivity. It was observed that the reaction of the corresponding acid anhydride doubled the amount of product, and it was proposed that the catalytic mechanism proceeded *via* the anhydride.

Miller and co-workers[26] improved catalytic activity through the use of a mixed anhydride system with equimolar mixtures of acetic anhydride and carboxylic acid. This allowed the use of a much lower palladium loading, though still used a 50x excess of PPh_3 (Scheme 6.5).

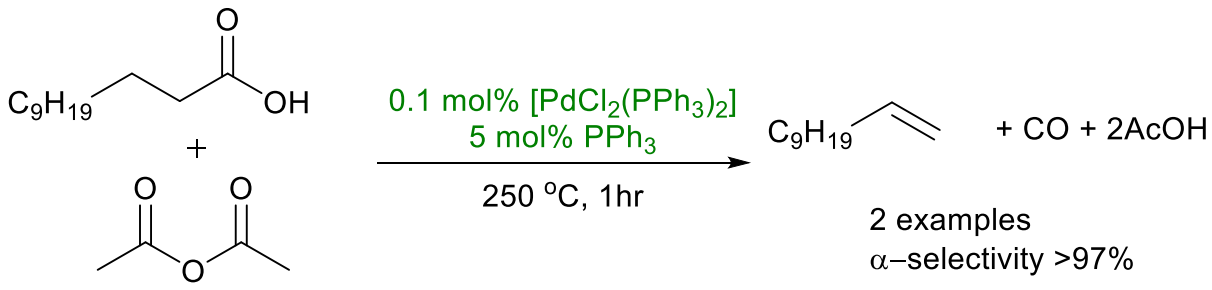

Scheme 6.5: Palladium catalysed decarbonylative dehydration of fatty acids to alkenes with anhydride additive[26]

Varying the phosphine ligand had little effect on selectivity for 1-alkenes. Turnover number was affected by varying the phosphine ligand in the order $PCy_3 > PPh_3 > P(o\text{-Tol})_3$.

Gooßen and co-workers[27] used pivalic anhydride (200 mol%) as an additive with $PdCl_2$ (3 mol%)/DPEphos (9 mol%) catalyst in N,N'-dimethylpropylene-urea (DMPU) to achieve decarbonylative dehydration of a range of carboxylic acids at low temperature (110 °C) with high terminal alkene selectivity.

These conditions were also used by Le Nôtre *et al*.[16] along with a triethylamine additive to give high yields and selectivities of LAOs from carboxylic acids. The NEt_3 was proposed to stabilise cationic intermediates formed in the catalytic reaction. When the solvent was changed from DPMU to MeCN a drastic change in alkene selectivity was observed from 99:1 1-alkene: 2-alkene in DPMU to 8:92 in MeCN. This was proposed to be due to formation of a $Pd(II)(MeCN)_2$ complex, which served as a tandem catalyst for decarbonylative dehydration and isomerisation.

Recently Grubbs, Stoltz and co-workers[28,29] used acidic additives and portion-wise addition of acetic anhydride to prevent alkene isomerisation. They also used a relatively low temperature (132 °C) and demonstrated tolerance for a wide range of functional groups, with amine and hydroxyl groups being tolerated in the presence of a protecting group. This approach also enabled the enantioselective synthesis of (-)-aspewentins A-C, Scheme 6.6.

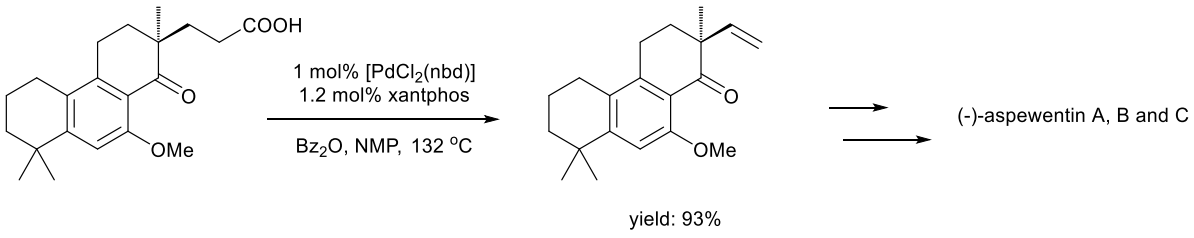

Scheme 6.6: Decarbonylative dehydration used in total synthesis of (-)-aspewentins A-C[28]

Miranda et al.[30] also showed the broad applicability of decarbonylative dehydration converting renewably sourced mono-alkyl succinates to alkyl acrylates (Scheme 6.7). These monomers have many uses industrially as building blocks for paints, coatings and in the textile industry. A

range of diphosphine ligands were investigated and DPEphos and xantphos found to be most active.

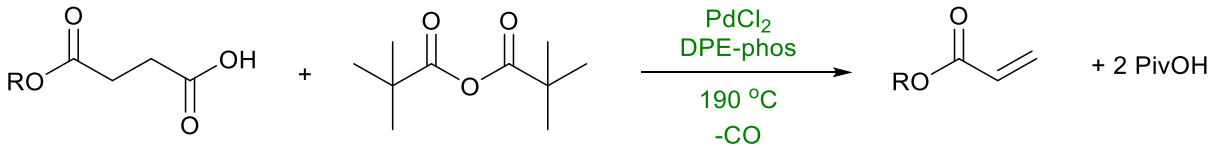

R	Acrylate	PivOR	PivOH
Me	64%	12%	49%
n-Butyl	45%	21%	60%
t-Butyl	18%	10%	90%

Scheme 6.7: Palladium catalysed decarbonylative dehydration of mono alkyl succinates.[30]

Minor amounts of alkyl pivalates (PivOR) detected in the reaction mixture were proposed to be due to cyclisation of alkyl succinates to form succinic anhydride and alcohol, and subsequent reaction of the alcohol with Piv_2O to give PivOH and the pivalic ester (Scheme 6.8). A control experiment in the absence of a metal catalyst showed this was not part of the catalytic cycle.

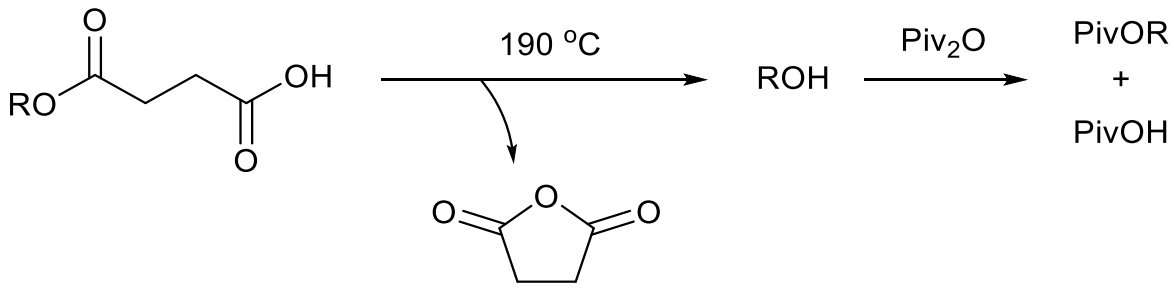

Scheme 6.8: Side reaction forming pivalic esters

The further development of decarbonylative dehydration catalysts has been slowed by the lack of mechanistic information. A molecular-level DFT investigation was conducted by Cramer and co-workers[31] and led to the development of a well-defined palladium-based catalyst precursor [Pd(DPEphos)(cinnamyl)Cl] for decarbonylative dehydration.[15] This allowed for the use of relatively low temperatures (110 °C) and gave high selectivities for a range of substrates.

6.0.5 Iron catalysed decarbonylative dehydration

As palladium, rhodium, iridium and other transition metals used for decarbonylative dehydration are expensive, iron was considered as an alternative catalyst by Maetani et al.[32] Scheme 6.9 shows the conditions used, giving alkenes in 79% yield with 81% terminal alkene selectivity.

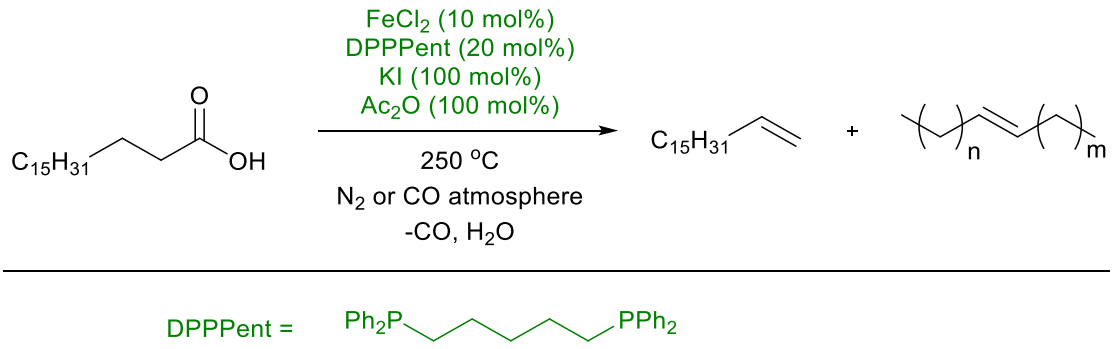

Scheme 6.9: Iron catalysed decarbonylative dehydration of stearic acid

The reaction conditions were optimised using DPPPent, a flexible chelating ligand, to give higher selectivity (97% terminal alkene) at lower temperature (240 °C) with CO atmosphere (20 bar) though the yield was lowered to 74%.

Conversions of long chain carboxylic acids to terminal alkenes are lower, and harsher conditions are required when using iron catalysts.

6.0.6 Iridium catalysed decarbonylative dehydration

Maetani et al also reported on the use of Vaska's complex ($[Ir(PPh_3)_2(CO)Cl]$) in decarbonylative dehydrations.[33] Selectivity was found to be dependent on conditions used, with internal alkenes as a major product in the absence of Ac_2O. Although internal alkenes are not as widely used as terminal alkenes they are still utilised in lubricants, surfactants and as paper sizing agents. Conditions using KI as an additive or KI and Ac_2O were investigated, shown in Scheme 6.10.

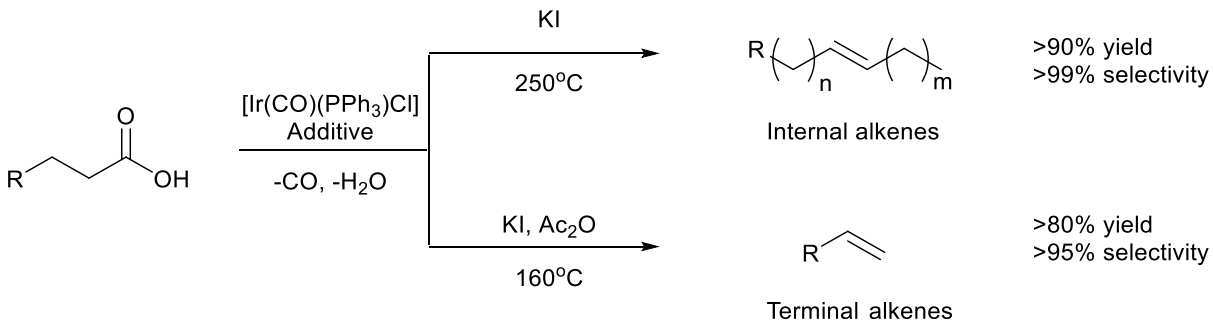

Scheme 6.10: Decarbonylative dehydration of long chain carboxylic acids using Vaska's complex as a catalyst

KI was suggested to act as a halide exchange reagent for reactions at 250°C. These catalysis conditions were tested with a range of fatty acids and gave yields >74% and generally good selectivity 99% for internal alkenes.

Hapiot and co-workers used the same conditions (160 °C, Ac_2O 200 mol%, KI 50 mol%) and $[Ir(COD)Cl]_2$ (2.5 mol%) with PPh_3 (15 mol%).[34] This system gave similar activity to Vaska's complex but had poorer terminal alkene selectivity (≤ 90%).

6.0.7 Rhodium catalysed decarbonylative dehydration

Decarbonylative dehydration using rhodium and palladium as catalysts were reported by Foglia and Barr, without any sacrificial anhydride.[25] A mixture of $RhCl_3$ (1 mol%) and PPh_3 (10 mol%) was used as shown in Scheme 6.11. This yielded heptadecenes in a 100 % yield. Yellow crystals inside the reaction vessel were found to be $[Rh(PPh_3)_2(CO)Cl]$.

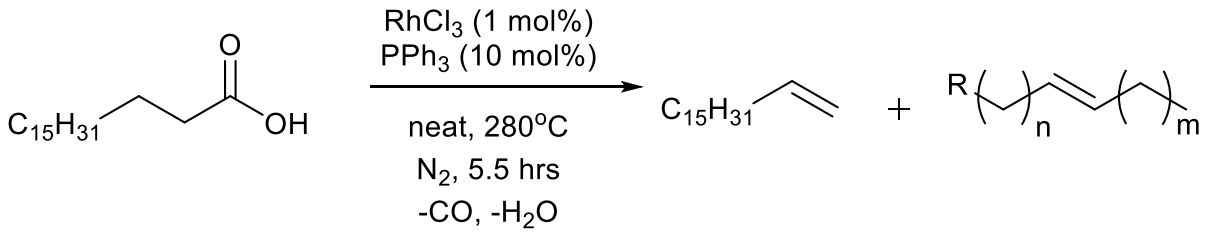

Scheme 6.11: Rhodium catalysed decarbonylative dehydration of stearic acid[25]

Miller et al.[26] investigated the use of [Rh(PMePh$_2$)$_2$(CO)Cl] (1 mol%) as a catalyst with either an equimolar amount of long chain anhydride or long chain carboxylic acid and acetic anhydride, Scheme 6.12. Both reagents gave olefin products, which were distilled from the reaction mixture ensuring a high degree of selectivity.

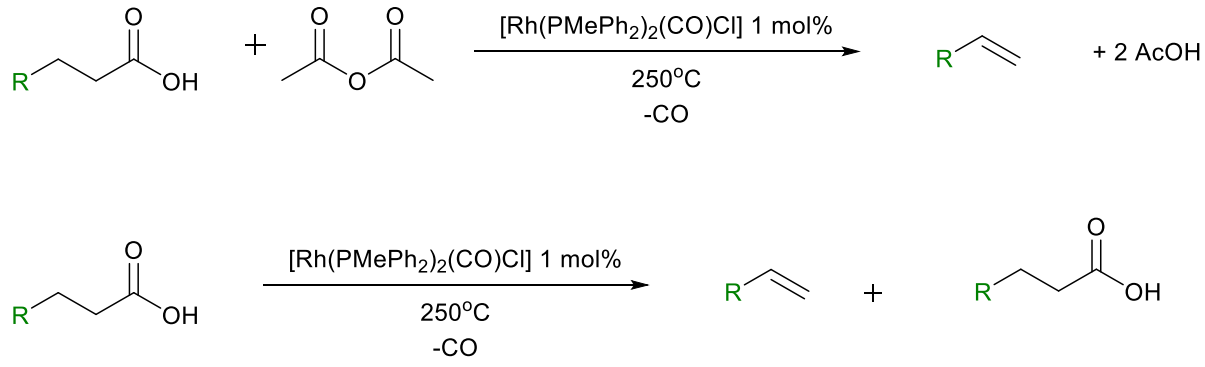

R = C_7H_{15} or C_9H_{19}

Scheme 6.12: Rhodium catalysed decarbonylative dehydration of long chain acids and anhydrides

CO evolution was observed at 180-190 ^{O}C indicating initiation of decarbonylative dehydration. Varying the phosphine ligand on [Rh(PR$_3$)$_2$(CO)Cl] had a large effect on turnover number with P(o-Tol)$_3$ > PMePh$_2$ > PPh$_3$ > PCy$_3$, these phosphines had little effect on product selectivity.

6.0.8 Mechanistic studies of decarbonylative dehydration

Few studies have been done to elucidate the mechanism of decarbonylative dehydration. Further understanding of the mechanistic steps is vital to tuning and improving catalysts for both turnover and selectivity.

Oxidative addition of anhydride was proposed by Miller et al.[26] and Foglia et al.[25] as the first organometallic step in decarbonylative dehydration. Typically, oxidative addition of C-O bonds has received little attention compared to that of carbon-halogen bonds, which are much more susceptible to oxidative addition to a metal centre. Deeming et al.[35] showed this through the

reaction of [Ir(PMePh$_2$)$_2$(CO)Cl] with methyl chloroformate, where a C-Cl bond is broken preferentially over a C-O bond (Scheme 6.13).

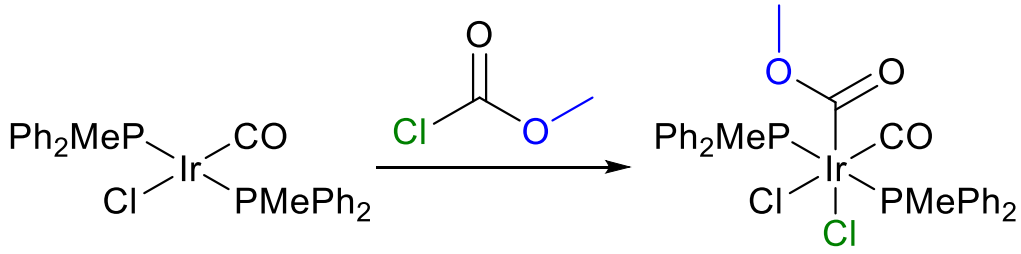

Scheme 6.13: Oxidative addition favouring C-Cl over C-O bond activation

However, as discussed in Chapters 1 and 3, examples of oxidative addition of anhydrides to transition metals are known. Miller et al.[36] investigated oxidative addition of propionic anhydride to [Rh(PR$_3$)$_2$(CO)Cl] and characterised a range of rhodium acyl carboxylate complexes, Scheme 6.14. Similar reactions are known for Ir(I)[37] and Ni(II)/Pt(II)[38].

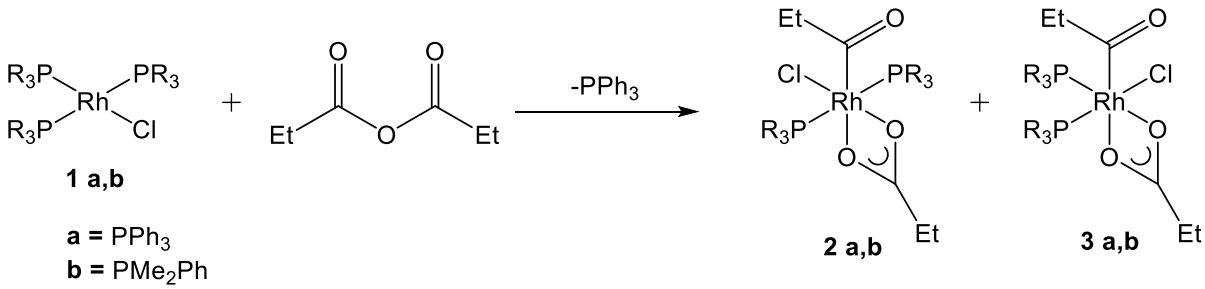

Scheme 6.14: Oxidative addition of propionic anhydride to form Rh(III) acyl carboxylate complexes

Eliasson et al.[39] recently reported a DFT investigation of the mechanisms of decarbonylative dehydration using [Rh(CO)(PPh$_3$)$_2$Cl] and [Pd(PPh$_3$)$_4$]. The generic reaction steps are shown in Scheme 6.15.

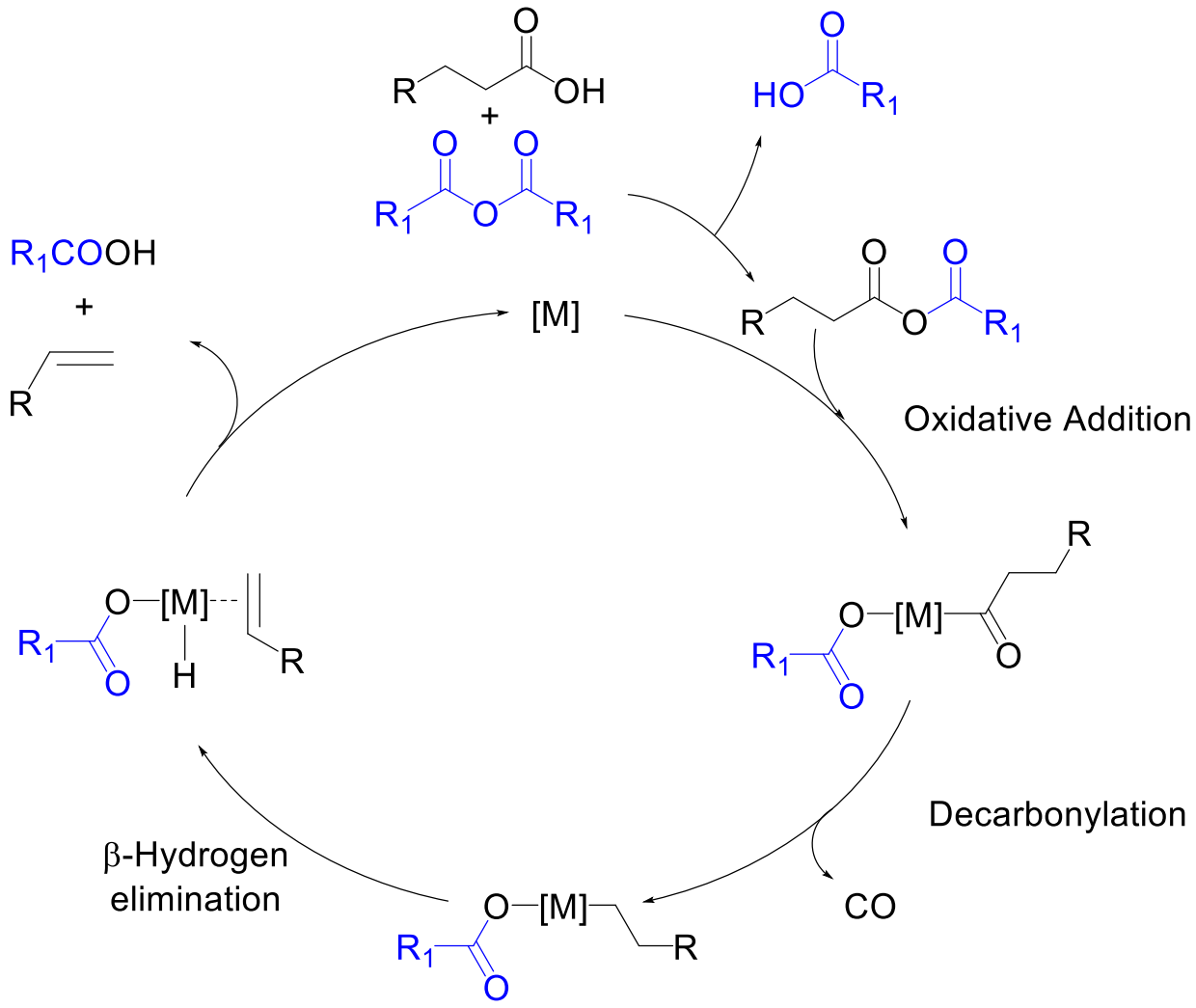

Scheme 6.15: Proposed mechanism for transition metal catalysed decarbonylative dehydration

The proposed mechanism first involves formation of a mixed anhydride before oxidative addition of the anhydride C-O bond which gives a metal acyl carboxylate species. In principle there are two possible C-O bonds in the anhydride that can be broken. Cleavage of the undesired C-O bond can be prevented through the use of symmetrical anhydrides,[29] or sterically demanding anhydrides,[27] although experiments have shown that the unwanted side reaction may be avoided without these strategies.[40] The metal acyl species then undergoes decarbonylation and subsequent β-hydride elimination to form the alkene product and a metal

hydride complex. Reductive elimination of a carboxylic acid and dissociation of the alkene regenerate the catalyst.

The calculations reported by Eliasson et al. [39] gave activation barriers consistent with Pd as the more active catalyst. For both metals β–hydrogen elimination was found to be rate determining. The rhodium cycle was found only to require one phosphine, in contrast to palladium which requires an excess of phosphine to regenerate the catalyst. The preference of rhodium for high coordination numbers relative to Pd was thought to hinder catalytic activity of rhodium species.

6.0.9 Previous work in the group

Previous work in the Haynes group by Cocker[41] used the same conditions described by Maetani et al, Scheme 6.16.[42]

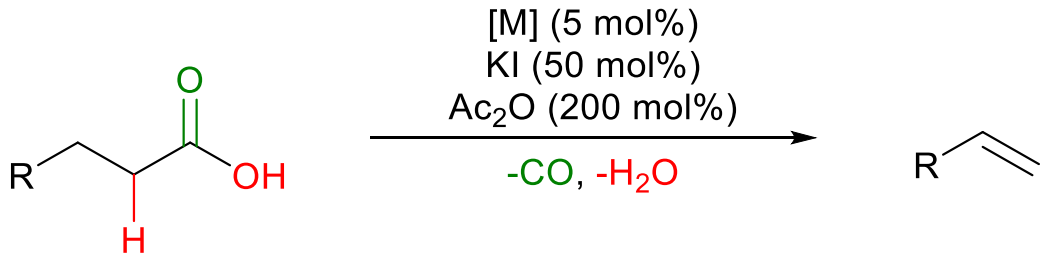

Scheme 6.16: General reaction for decarbonylative dehydration of long chain acids to alkenes

The effect of changing KI loading was tested, and yields reported by Cocker, Table 6.1

Table 6.1: Yield and selectivity of alkenes obtained with varying KI loading[41]

KI Additive (mol%)	Yield %	Terminal %	Internal %
50%	99	82	18
25%	81	85	15
5%	23	80	20

As KI loading decreases so does yield, indicating that potassium iodide may play a role in the mechanism for decarbonylative dehydration. Under these reaction conditions KI was proposed to react with mixed anhydrides formed in solution to give a long chain acyl iodide, which undergoes oxidative addition to the metal catalyst, as shown in Scheme 6.17. The resulting acyl species then undergoes decarbonylation forming an alkyl ligand. β-hydride elimination forms the alkene product and the catalyst is regenerated by reductive elimination of HI.

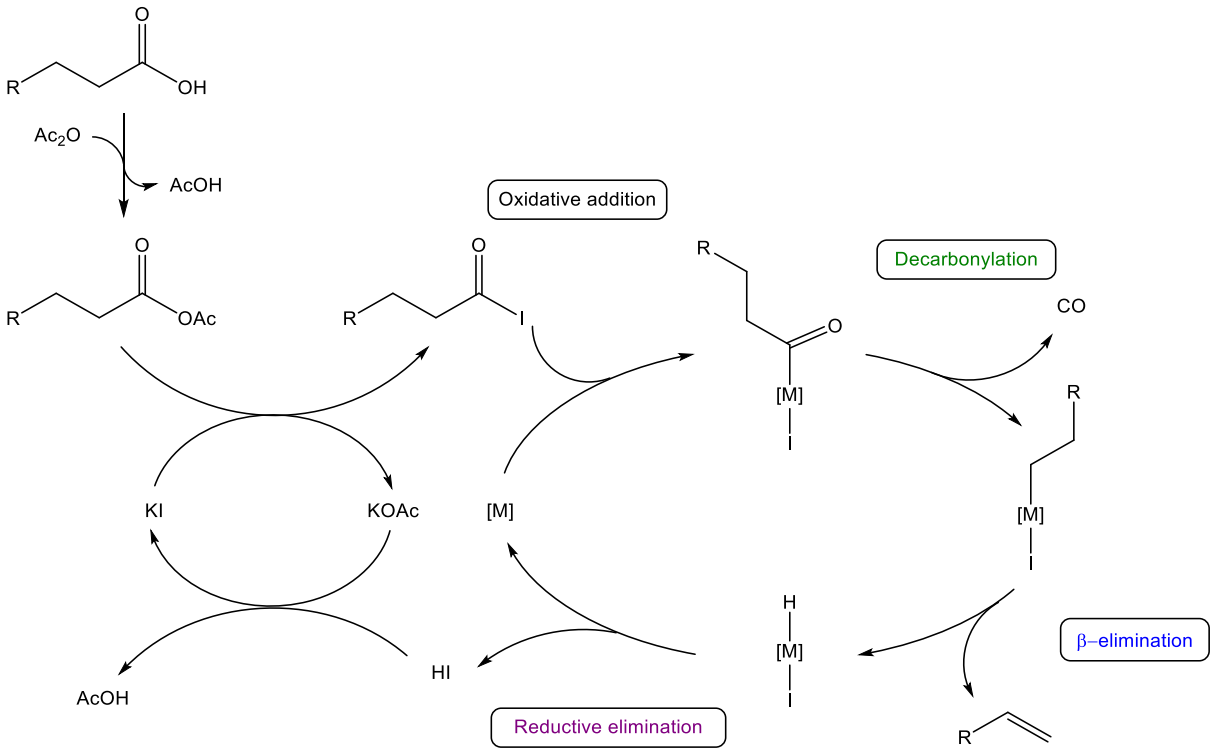

Scheme 6.17: Proposed mechanism for decarbonylative dehydration of long chain carboxylic acids

A range of Rh and Ir catalysts were tested. Variants of Vaska's complex [Ir(PR_3)(CO)Cl], with a series of phosphine ligands, all gave high yields. Selectivity for internal alkene was enhanced to 93% using PCy_3. Similarly complexes of formula [Rh(acac)(CO)(PR_3)] were tested and gave high alkene yields (>89%) but poor selectivity for terminal alkenes (52-70%). Some chelate complexes of formula [Rh(L-L)(CO)Cl] were also tested, with high yields being obtained for catalysts containing diphosphines (>85 %) and iminophosphines (72-85%).

When using Rh(I) iminophosphine complexes as catalysts, some were found to undergo an unexpected transformation to form a Rh(III) complex containing a phosphine acetamide ligand, shown in Scheme 6.18. These were found to still be catalytically active.

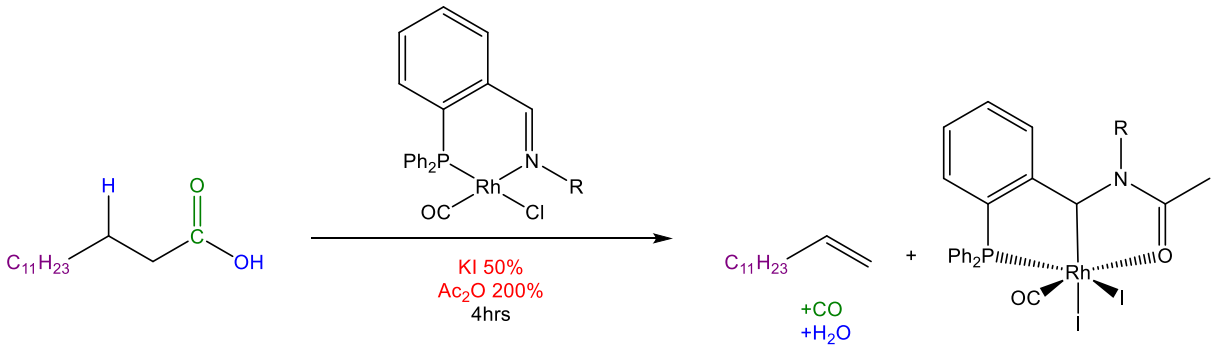

Scheme 6.18: Acylation of iminophosphine ligand in decarbonylative dehydration reactions to form PCO tridentate rhodium complex

Scheme 6.19 shows the suggested mechanism of acylation of the iminophosphine ligand involving formal insertion of the imine into the Rh-acetyl bond (or migration of acetyl into the imine nitrogen).

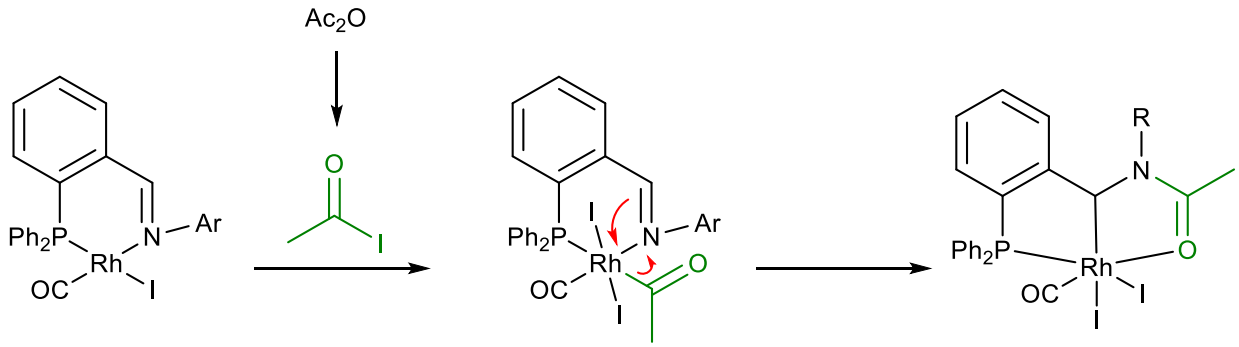

Scheme 6.19: Proposed mechanism for iminophosphine acetylation to form phosphine acetamide complex

Decarbonylative dehydration reactions using Rh phosphine acetamide complexes with d^6Ac_2O, conducted to probe if this acyl migration was reversible, were found to incorporate deuterium

into the C_{13} alkene products. This also occurred for reactions using Vaska's complex. Deuterium incorporation into the alkene product was explained by a proposed mechanism involving formation of a ketene and rhodium-deuteride species, shown in Scheme 6.20 and Scheme 6.21. Since the only source of deuterium in this reaction is d^6-Ac_2O, a C-D bond must be broken and transferred to rhodium forming a ketene as shown. A Rh-D complex can then react with a long chain ketene produced in situ to complete D-incorporation.

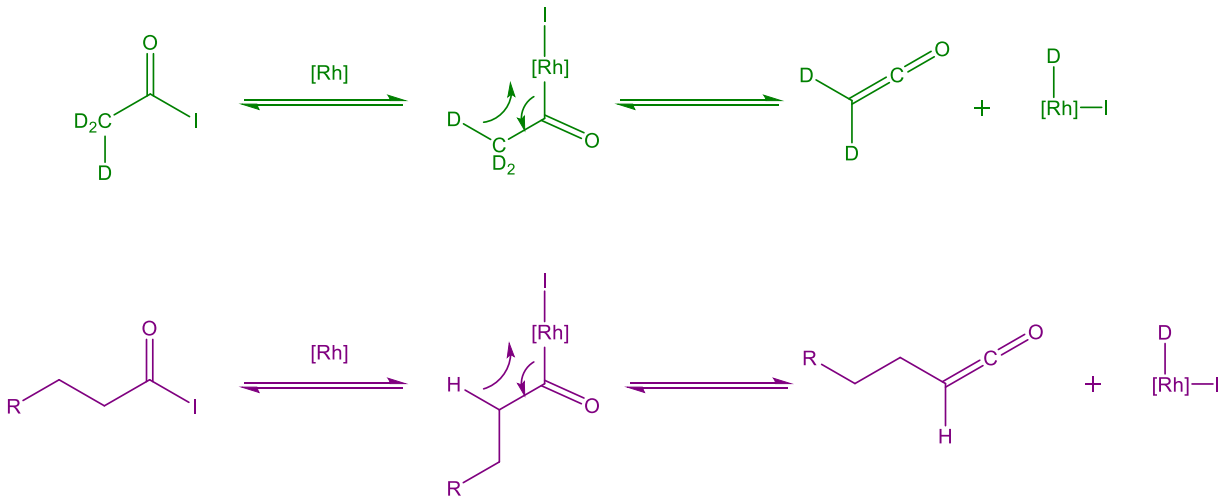

Scheme 6.20: Proposed mechanism for ketene formation in decarbonylative dehydration.

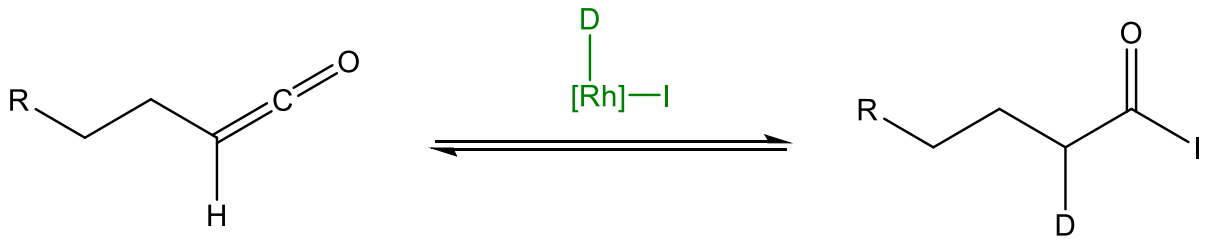

Scheme 6.21: Incorporation of deuterium into long chain ketene complex

Scheme 6.22 shows how this deuterated acyl iodide could subsequently undergo decarbonylation to produce a deuterated alkene.

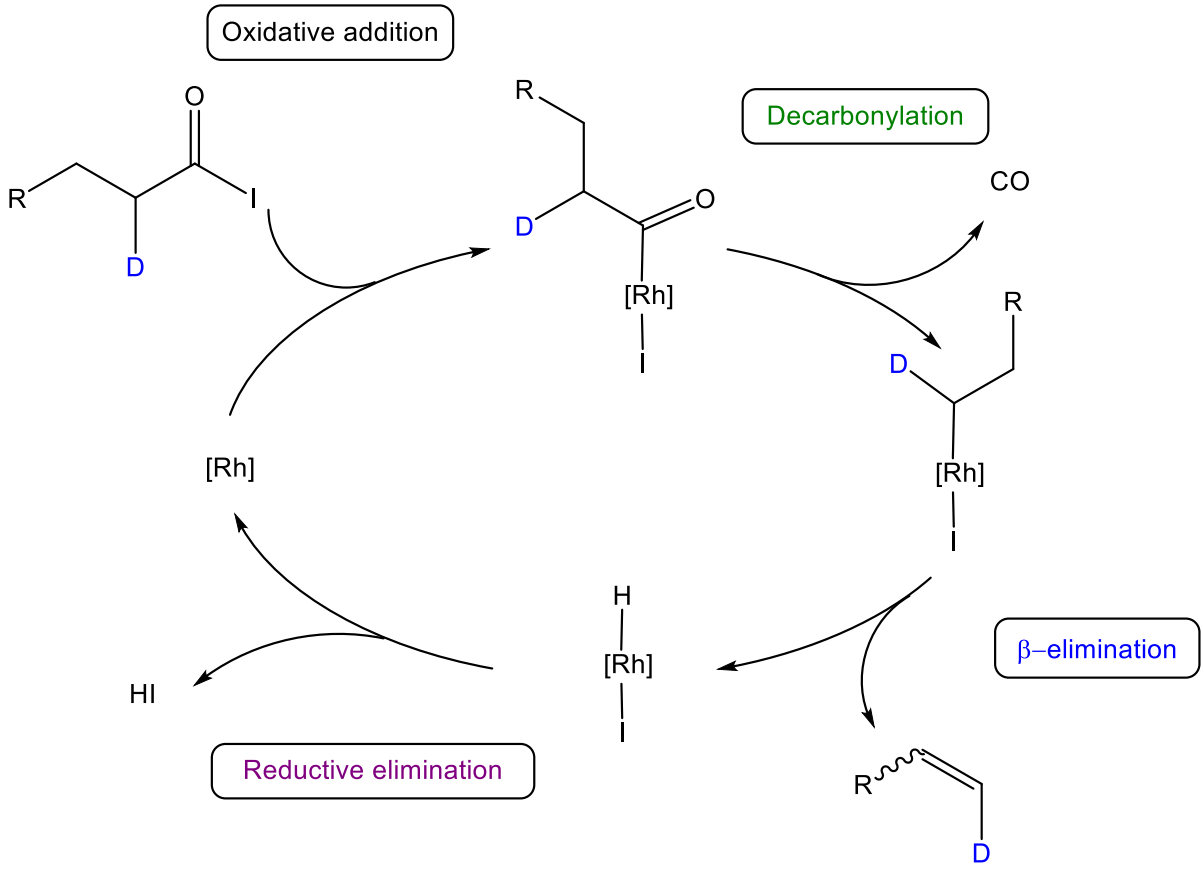

Scheme 6.22: Decarbonylative dehydration of D-containing acyl iodide to give deuterated alkene product.

This mechanism is similar to a reaction observed by Singh et al.[43] where d^3-acetyl chloride in the presence of a Ru(0) complex forms a Ru(II) deuteride complex and ketene as shown in Scheme 6.23.

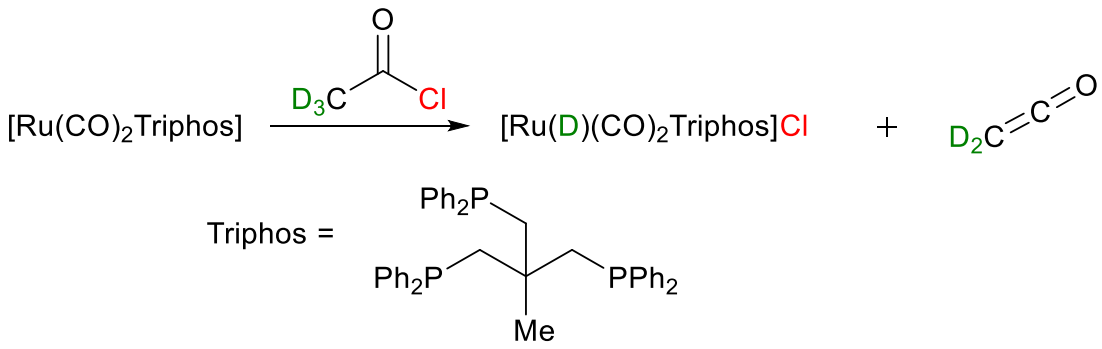

Scheme 6.23: Formation of a ruthenium deuteride species and ketene

A ketene intermediate has also been proposed for a heterogeneous decarbonylative dehydration process using MoS_2 and Ni-MoS_2 catalysts by Wagenhofer et al.[21]

This chapter will discuss an extended range of rhodium(I) catalysts in decarbonylative dehydration as well as investigating a range of Rh(III) complexes as catalysts. This is followed by an investigation into the acylation of rhodium iminophosphine ligands to form phosphine acetamide complexes previously observed by Cocker. A wider range of high yielding catalysts for decarbonylative dehydration have been tested as catalysts with d^6 Ac_2O additive, to determine if H/D scrambling is general. A series of studies with d^6 Ac_2O have also been conducted to further probe the mechanism of D-incorporation.

6.1 Results and discussion

6.1.1 General method of decarbonylative dehydration

The reactions were conducted using the standard method outlined in the Experimental section of this thesis based on conditions reported by Maetani et al.[42]

An NMR spectrum of the crude reaction mixture was obtained upon the completion of each experiment to analyse product formation and determine whether the added catalytic species remained intact. The alkene product was then isolated using column chromatography on silica, eluting with hexane to remove polar species and inorganic residues. The alkene products were isolated by removing hexane *in vacuo* and a yield obtained by mass.

To determine product selectivity for terminal (H_a and H_b) vs. internal (H_c) alkenes the integration intensities of the alkene peaks were compared and determined as a percentage. An example calculation is given in the Appendix for the spectrum shown in Figure 6.1.

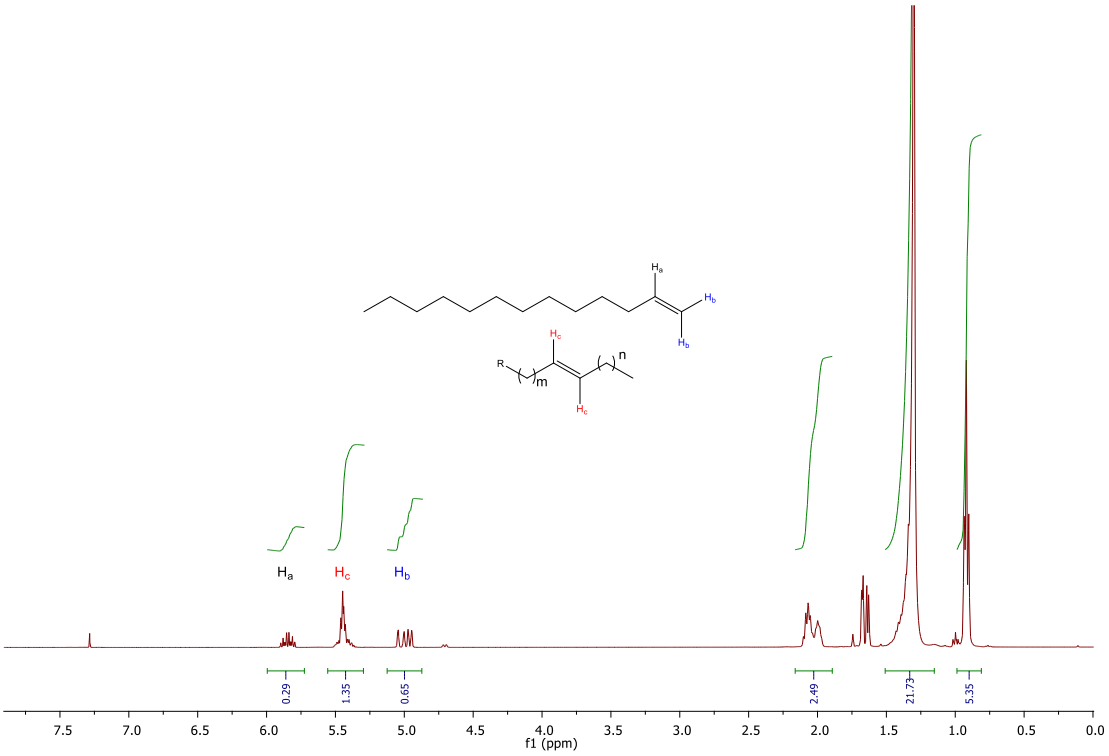

Figure 6.1: ^{1}H NMR spectrum of tridecene product formed from decarbonylative dehydration catalysed by [Rh(acac)(CO)(PPh_3)]

6.1.2 Decarbonylative dehydration using Rh(I) complexes

Cocker[41] investigated a wide variety of Rh and Ir complexes as catalysts for decarbonylative dehydration. This has been extended in the present study to include a range of rhodium diphosphine complexes, other Rh(I) and Ir(I) complexes, Rh(III) complexes and some Pd and Fe complexes. The general reaction scheme and conditions are shown in Scheme 6.24, yields and selectivity for these reactions are given in Table 6.2.

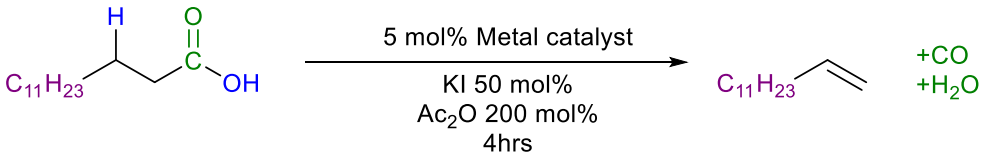

Scheme 6.24: Decarbonylative dehydration of myristic acid using Rh diphosphine complexes

Table 6.2: Yield and selectivity of $C_{13}H_{26}$ alkene products obtained using transition metal catalysts

	Reaction number	Complex	Yield %	Terminal %	Internal %
Rh(I) diphosphine complexes	**1**	$[Rh_2(dppm)_2(CO)_2Cl_2]$	41	90	10
	2	[Rh(dppe)(CO)Cl]	74	53	47
	3	[Rh(dppp)(CO)Cl]	71	57	43
	4	$[Rh_2(dppb)(CO)_2Cl_2]$	23	78	22
	5	[Rh(xantphos)(CO)Cl]	21	62	38
	6	[Rh(DPEphos)(CO)Cl]	46	73	27
Other Rh(I) complexes	**7**	$[Rh(CO)_2I_2][NBu_4]$	99	41	59
	8	$[Rh(CO)_2Cl]_2$	92	34	66
	9	$[Rh(CO)_2I]_2$	99+	33	67
	10	$[Cp^*Rh(CO)_2]$	81	59	41
	11	[Rh(dipiep)(CO)Cl]	90	54	46
	12	[Rh(dipimp)(CO)Cl]	95	60	40
	13	[Rh(dppmS)(CO)Cl]	15	60	40
Rh(III) complexes	**14**	$[Rh(CO)_2I_4][NBu_4]$	90	46	54
	15	$Cp^*Rh(COMe)(CO)I$	92	53	47
	16	$[Rh(PN\text{-}iPr_2Ph)(COMe)I_2]$	86	65	35
	17	$[Rh(xantphos)(COMe)I_2]$	14	39	61
	18	$[Cp^*RhCl_2]_2$	4	43	67
Ir(I) complexes	**19**	$[Ir(PPh_3)_2(CO)Cl]$	68	97	3
	20	$[Ir(CO)_2I_2][NBu_4]$	15	49	51
Pd(II) complexes	**21**	$Pd(nbd)Cl_2$ + xantphos **(50% KI)**	4	74	26
	22	$Pd(nbd)Cl_2$ + xantphos **(25% KI)**	42	49	51
	23	$Pd(nbd)Cl_2$ + xantphos **(0% KI)**	81	33	67
Fe(II) complexes	**24**	$FeCl_2$ + xantphos	0	-	-
	25	$FeCl_2$ + dppb	0	-	-

Most catalysts tested were successful, giving alkenes in a range of yields and selectivities. $[Cp^*RhCl_2]$ (reaction **18**) gave a yield of 4 % indicating the reaction may be stoichiometric under these conditions. The Fe systems, known to work at a higher temperature and pressure,[32] yielded no alkenes under our conditions.

The Rh(I) diphosphine complexes reactions **1-6** gave a range of yields (21-74 %) and generally poor selectivity for terminal alkenes. The $^{31}P\{^{1}H\}$ NMR spectra of the crude product mixtures from these reactions showed no J_{Rh-P} coupling, indicating that the phosphine ligands were no longer coordinated to rhodium.

Reactions **11** and **12** using rhodium pyridyl imine complexes, for which the iodide analogues have been previously studied by Haynes and co-workers as catalysts for methanol carbonylation,[44,45] gave high yields but poor selectivities. Most of the Rh(I) carbonyl catalysts gave high yields (>80%) but had higher selectivity for internal alkenes.

Grubbs and co-workers have used a variety of palladium catalysts with diphosphine ligands for the decarbonylative dehydration of long chain alkenes[29] under different catalytic conditions. The Pd catalysts are significantly lower yielding in the presence of KI and selectivity for terminal alkenes is higher at higher KI loading. At 50 % KI a yield of 4 % may mean that under these conditions the reaction was stoichiometric, not catalytic. When no KI was used the highest yield of 81 % was obtained, a selectivity of 67 % internal alkene was also observed. This indicates that the Pd catalysed system may follow a different mechanism as the Rh and Ir catalysts require KI additive to achieve high yields. The iron catalysts failed to produce any alkene product under these conditions.

Previous research has focused on Rh(I) d^8 complexes as catalysts for decarbonylative dehydration. However, Cocker found that the Rh(III) phosphine acetamide diiodide complexes formed by using [Rh(PN-Ar)(CO)Cl] complexes in decarbonylative dehydration were catalytically active.

A range of Rh(III) acetyl complexes of the type $[Rh(L\text{-}L)(COMe)I_2]$ (as discussed in chapter 3, 4 and 5) were tested as catalysts. These complexes are similar to the proposed Rh(III) acyl iodide intermediates for decarbonylative dehydration. The examples tested produced alkenes in yields ranging from 14-92 %, with only $[Rh(xantphos)(COMe)I_2]$ (reaction **17**) giving a yield

below 85 %, this is likely due to the lack of a vacant site. Selectivity for terminal alkenes ranged from 39-65 %. $[Rh(CO)_2I_4]^-$ (reaction **14**) an inactive form of the catalyst used in the Monsanto cycle, [46] was high yielding for decarbonylative dehydration.

$[Rh(PN\text{-}^iPr_2Ph)(COMe)I_2]$ (reaction **16**) also gave a high yield of alkenes (86 %) when used as a catalyst for decarbonylative dehydration. Similarly to $[Rh(PN\text{-}^iPr_2Ph)(CO)Cl]$, the product of this reaction was a rhodium phosphine acetamide diiodide complex indicating that acetyl migration occurred. This acetylation of the iminophosphine ligand was further probed.

6.1.3 Investigation of iminophosphine acylation

The complex $[Rh(PN\text{-}^iPr_2Ph)(COMe)I_2]$ may, in the presence of CO, undergo acetyl migration to form the phosphine acetamide ligand as shown in Scheme 6.19 above. To investigate if [Rh(PN-Ar)(COMe)I_2] can undergo ligand acylation an experiment with $[Rh(PN\text{-}^iPr_2Ph)(COMe)I_2]$ in $CHCl_3$ was conducted. A solution of $[Rh(PN\text{-}^iPr_2Ph)(COMe)I_2]$ was heated to reflux under a CO atmosphere and monitored by IR spectroscopy, Scheme 6.25 shows the species formed with corresponding ν(CO) absorptions. Growth of ν(CO) absorptions at 2080 cm^{-1} indicated formation of $[Rh(PN\text{-}^iPr_2Ph)(Me)(CO)I_2]$[47] and subsequent growth of a band at 2002 cm^{-1} indicated formation of $[Rh(PN\text{-}^iPr_2Ph)(CO)I]$ showing that this species has undergone decarbonylation and eliminated iodomethane. No acetyl migration to form the rhodium phosphine acetamide complex was observed spectroscopically, however the observed decarbonylation is indicative of the proposed mechanism for decarbonylative dehydration.

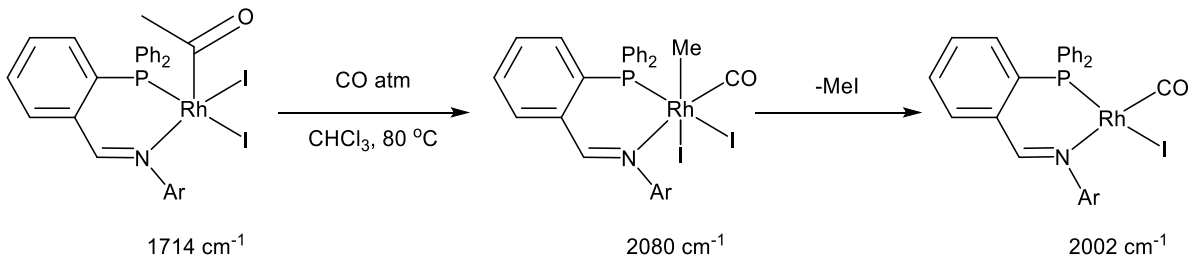

Scheme 6.25: Decarbonylation of $[Rh(PN\text{-}^iPr_2Ph)(COMe)I_2]$ in $CHCl_3$ under CO atmosphere

Reaction of [Rh(PN-Ar)(CO)I] with a longer chain acyl iodide to form [Rh(PN-Ar)(COR)I_2] was undertaken to see if the same decarbonylation occurred. Preparation of myristoyl iodide from carboxylic acids using diiodosilane and iodine was undertaken as outlined by Keinan *et al.*[48] Addition of this long chain acyl iodide to [Rh(PN-Mes)(CO)I] in $CHCl_3$ under argon was monitored by IR spectroscopy.

Figure 6.2 shows a series of spectra obtained after the addition of [Rh(PN-Mes)(CO)I] in $CHCl_3$ to freshly distilled myristoyl iodide. A range of new absorptions between 2100-1700 cm^{-1} were observed.

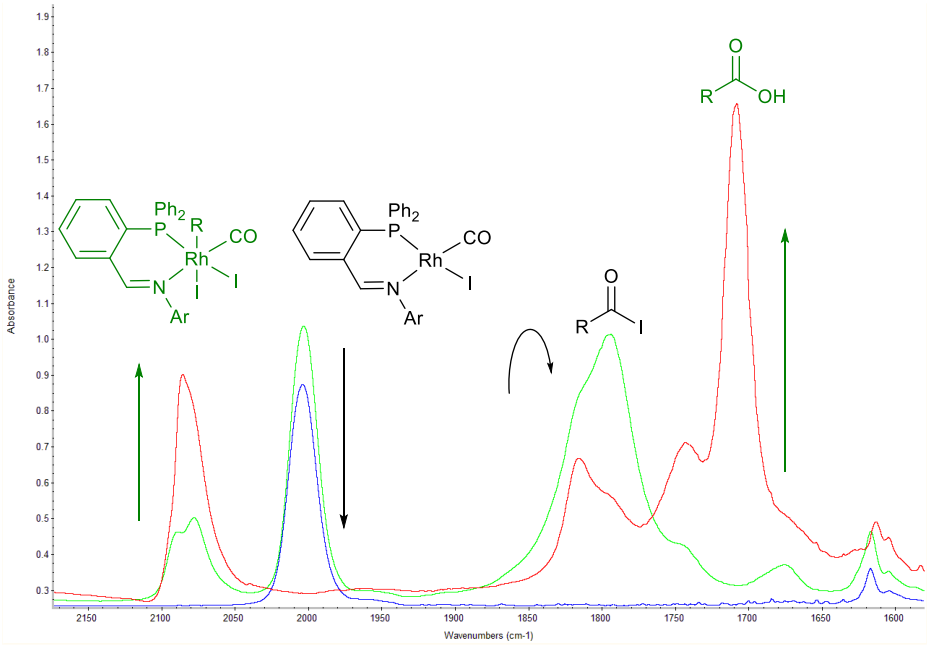

Figure 6.2: IR spectra obtained of [Rh(PN-Mes)(CO)I] in CH_2Cl_2 (blue), 5 minutes after addition of myristic iodide (green) and 4 hours after addition of myristoyl iodide (red)

Growth of bands at 1795 and 1814 cm^{-1} are assigned as myristoyl iodide (1795 cm^{-1}) and myristoyl chloride (1814 cm^{-1}).[49] The presence of myristoyl chloride is likely due to halogen exchange with the chlorinated solvent. After 4 hours growth of a band at 1709 cm^{-1} with a shoulder at 1741 cm^{-1} indicated formation of myristic acid, this is likely due to trace amounts of water reacting with the long chain acyl iodides.

Other ν(CO) bands at 2089 and 2078 cm^{-1} grow over time. Wilson found that [Rh(PN-R)(CO)(Me)I_2] bands appeared in this region meaning oxidative addition of myristic iodide and subsequent decarbonylation may have led to bands in this region.[49] No ν(CO) absorptions are present around 1560 cm^{-1} for the acetyl of the phosphine acetamide ligand as such it is unlikely that these bands correspond to acylation of the iminophosphine ligand. ^{31}P NMR spectroscopy of the resulting product had a doublet δ ~46 (d, J_{Rh-P} = 130 Hz) indicative of a [Rh(PN-Mes)(COR)I_2] complex.

The reaction of **[**Rh(PN-$^{i}Pr_2Ph$)(CO)I] with myristoyl iodide appears to proceed by oxidative addition to form [Rh(PN-$^{i}Pr_2Ph$)(COR)I_2] this can undergo decarbonylation to give [Rh(PN-$^{i}Pr_2Ph$)(CO)(R)I_2] or react with water to form myristic acid. The formed acyl iodide can also react with trace amounts of water to give myristic acid.

6.1.4 Investigation into non-metal mediated iminophosphine acetylation

As the reaction of [Rh(PN-$^{i}Pr_2Ph$)(COMe)I_2] under CO did not reveal any acetylation of the iminophosphine ligand it was proposed that the ligand may detach from the metal centre, undergo acetylation and re-coordinate to form the phosphine acetamide complex. To probe this mechanism a PN-Ar ligand was put under the conditions used for decarbonylative dehydration, as shown in Scheme 6.26. A ^{31}P NMR analysis of the crude products indicated several phosphorus containing species around δ ~30 indicative of an oxidised phosphine. This mixture of products was separated and a phosphinyl acetamide compound isolated. This compound is similar to the observed phosphine acetamide ligand, however the phosphorus is oxidised. Phosphinyl acetamides were obtained for the reactions of both PN-$^{i}Pr_2Ph$ and PN-Me_2Ph under these conditions.

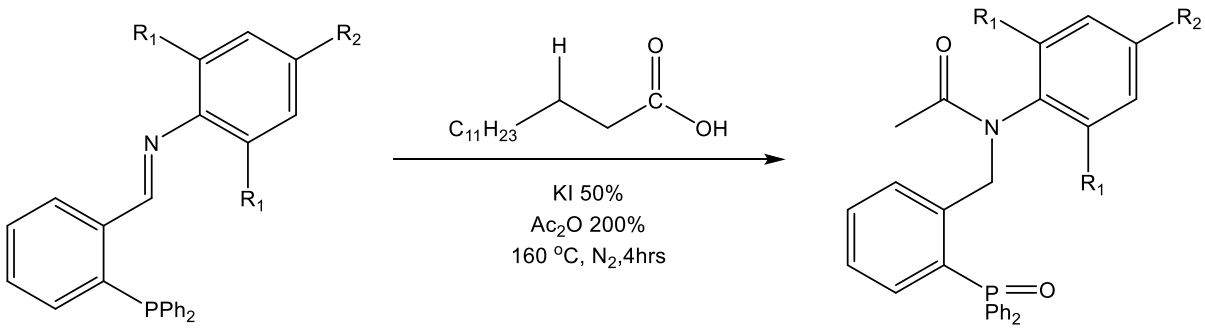

Scheme 6.26: Reaction conducted to probe the mechanism of ligand acylation for iminophosphine complexes

A crystal of N-[[2-(diphenylphosphinyl)phenyl]methyl]-N-(2,6 diisopropylbenzyl)-acetamide suitable for X-ray crystallography was obtained by slow evaporation of diethyl ether into a concentrated solution of phosphinyl acetamide in CH_2Cl_2. The structure is shown in Figure 6.3 and selected bond lengths and angles given in Table 6.3.

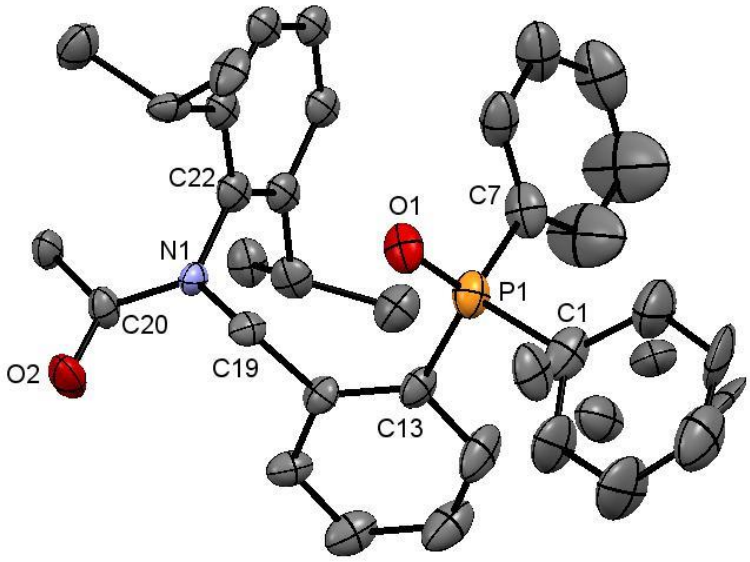

Figure 6.3: X-ray crystal structure for N-[[2-(diphenylphosphinyl)phenyl]methyl]-N-(2,6 diisopropylbenzyl)-acetamide with thermal ellipsoids shown at 50% probability level. Hydrogen atoms omitted for clarity.

Table 6.3: Select bond lengths (Å) and angles (deg) for N-[[2-(diphenylphosphinyl)phenyl]methyl]-N-(2,6 diisopropylbenzyl)-acetamide.

Bond		Angle	
P(1)-O(1)	1.490(6)	O(1)-P(1)-C(1)	111.1(4)
P(1)-C(1)	1.831(8)	O(1)-P(1)-C(7)	112.2(4)
P(1)-C(7)	1.82(1)	O(1)-P(1)-C(13)	114.0(4)
P(1)-C(13)	1.819(8)		
O(2)-C(20)	1.23(1)		
N(1)-C(19)	1.49(1)		
N(1)-C(20)	1.35(1)		
N(1)-C(22)	1.45(1)		

There is some disorder for one of the phenyl rings attached to phosphorus with 65:35 distribution at the disordered sites. The structure otherwise shows typical bond lengths and angles for P-Ph, P=O and amide bonds.

This phosphinyl acetamide is similar to the observed acylated ligand, however the presence of phosphorus oxide however indicates that a different mechanism may occur. A search of the literature revealed a paper by Kurtzweil et al which elaborated a possible mechanism for this formation of an acylated oxidised phosphine from an O-acetylhydroxylamine, which could potentially form in our reaction, shown in Scheme 6.27 [50]

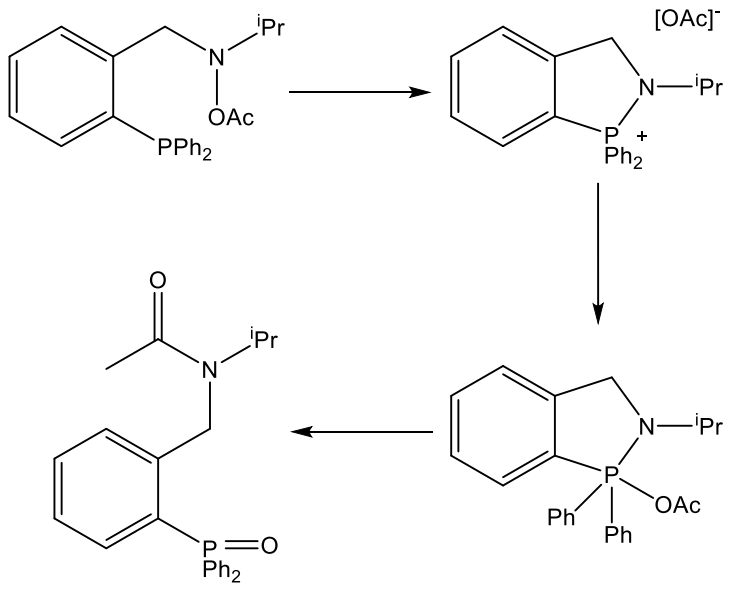

Scheme 6.27: Mechanism for formation of phosphinyl acetamide as discussed by Kurtzweil et al[50]

This shows that while the iminophosphine can be acetylated by dissociating from the metal, the species formed differs from the rhodium phosphine acetamide complex as it has an oxidised phosphine. This indicates that it is unlikely that acetylation of the iminophosphine ligand during decarbonylative dehydration occurs via dissociation of the phosphine from the metal.

6.2 Mechanism for D/H exchange

6.2.1 Deuterium incorporation into alkene product

Decarbonylative dehydration of myristic acid using rhodium phosphine acetamide complexes and deuterated acetic anhydride, shown in Scheme 6.28, resulted in deuterium incorporation in the C_{13} alkene product in both terminal and internal positions.[41] A range of high yielding decarbonylative dehydration catalysts were used to see if this deuterium incorporation was unique to phosphine acetamide containing complexes or more general for other complexes.

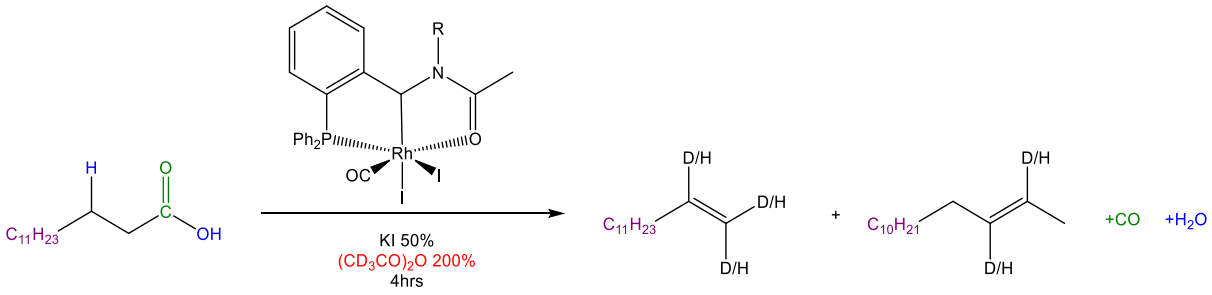

Scheme 6.28: Decarbonylative dehydration of myristic acid using d^6Ac_2O

To determine the extent of deuterium incorporation into the alkene products, one molar equivalent of methyl benzoate was added to the purified alkene product in experiments using either Ac_2O or d^6 Ac_2O. The integrations relative to the methyl peak at δ 3.95 ppm were used to determine deuterium incorporation, sample spectra are shown in Figure 6.4. For alkene products with no deuterium the sum of the signals at δ 5.45 and 4.95 ppm should be 2 relative to the 3 protons for methyl benzoate at 3.95 ppm. The difference between the obtained and expected peaks for the deuterated C_{13} product was then used to determine a percentage D-incorporation. Table 6.4 shows the calculated D-incorporation into the H_a, H_b and H_c positions.

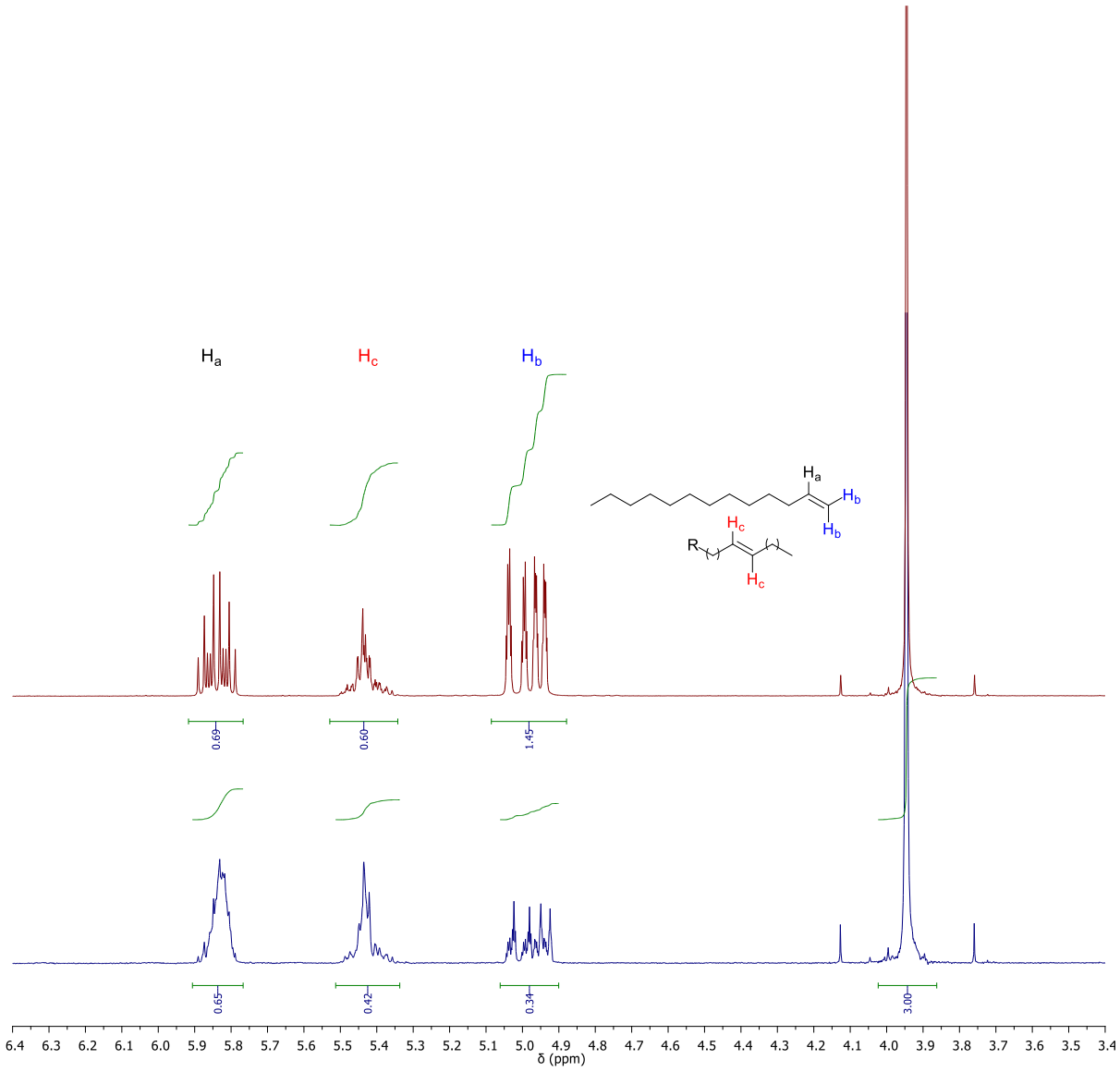

Figure 6.4: ^{1}H NMR spectra for decarbonylative dehydration products + methyl benzoate for [Rh(PN-iPr$_2$Ph)(CO)Cl] using Ac$_2$O (red) and d^6-Ac$_2$O (blue) integrated relative to methyl peak of methyl benzoate.

^{2}H NMR spectra were also obtained to confirm the presence of deuterium in C_{13} products. A sample spectrum is shown in Figure 6.5, and assigned according to comparison with data obtained by Lazzaroni *et al*.[51] for deuterated alkenes obtained as products from hydroformylation experiments using CO/D_2. Intense resonances at δ 1.4-1.6 are attributable to deuteration at C-1 of the internal alkene products and the intense resonance at δ 4.8-5.0

indicates deuterium incorporation at the C-1 position of the terminal 1-alkene product. Cocker *et al.* found no signals at δ 5.4 or 5.8, whereas we have found small signals present at these shifts indicating some D-incorporation in the C-2 position for both terminal and internal alkene products. This D-incorporation into C-1 and C-2 in terminal and internal alkenes was also apparent from the reduction in integrated intensity of these peaks in the ^{1}H NMR spectra.

Mass spectroscopy was also used to confirm D-incorporation into the C_{13} alkene prod for these experiments. The presence of peaks with mass of 181.2, 182.2, 183.2 and 184.2 indicates the presence of $C_{13}H_{25}^{+}$, $C_{13}H_{24}D^{+}$, $C_{13}H_{23}D_2^{+}$ and $C_{13}H_{22}D_3^{+}$.

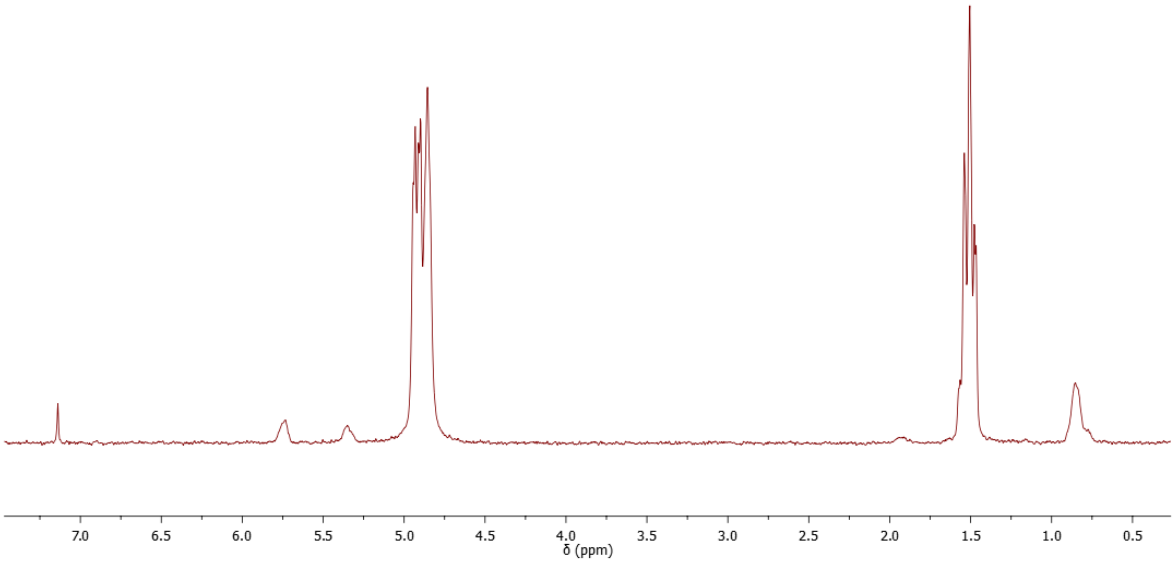

Figure 6.5: ^{2}H NMR spectrum of deuterated C_{13}- alkene product when using [Rh(acac)(PPh_3)(CO)] as a catalyst ($CDCl_3$, 298K)

Using ^{1}H NMR spectroscopy the amount of D-incorporation was measured for a series of high yielding decarbonylative dehydration catalysts as discussed above. The results are shown in Table 6.4. All the catalysts tested showed some D-incorporation. The greatest % of the D-incorporation occurred into the C-1 position for the terminal alkene product. Several catalysts showed no D-incorporation at the C-2 position for internal alkene product.

Table 6.4: Percentage decrease of C_{13} alkene peaks determined by integration relative to methyl benzoate additive

Complex	%D-H_a	%D-H_b	%D-H_c
[Rh(PN-Mes)(CO)Cl]	10	73	5
[Rh(PN-iPr_2Ph)(CO)Cl]	6	77	29
[Rh(PN-Et_2Ph)(CO)Cl]	3	77	6
[Rh(acac)(CO)(PPh_3)	19	56	0
[Rh(dipiep)(CO)Cl]	8	67	0
[Rh(dipimp)(CO)Cl]	9	61	4
[Ir(PPh_3)$_2$(CO)Cl]	9	76	0
[Ir(PCy_3)$_2$(CO)Cl]	2	55	33
Pd(nbd)Cl_2 + xantphos	0	32	0

6.2.2 Deuterium scrambling experiments

In order to further probe the D-incorporation mechanism, a series of experiments were conducted using a 1:1 mixture of Ac_2O and d^6-Ac_2O, 50 % molar equivalents KI and 5% molar equivalent of a rhodium catalyst and heated to 160 ^{o}C for 2 hours, as shown in Scheme 6.29.

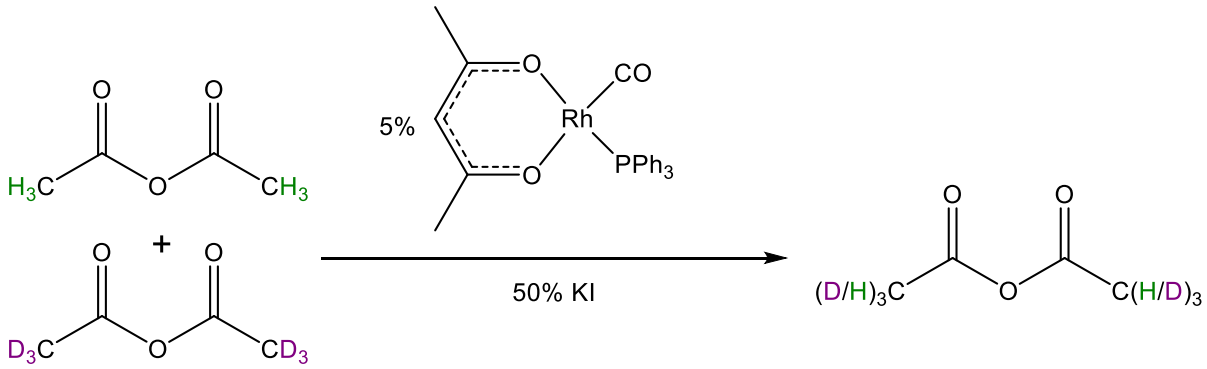

Scheme 6.29: Deuterium scrambling experiment using a 1:1 mixture of d^6-Ac_2O:Ac_2O, [Rh(acac)(PPh_3)(CO)] (5 %) and KI (50 %)

The products of this reaction were analysed by ^1H and ^{13}C NMR spectroscopy and mass spectrometry to determine if deuterium scrambling occurred. Figure 6.6 shows a ^1H NMR spectrum obtained from this reaction.

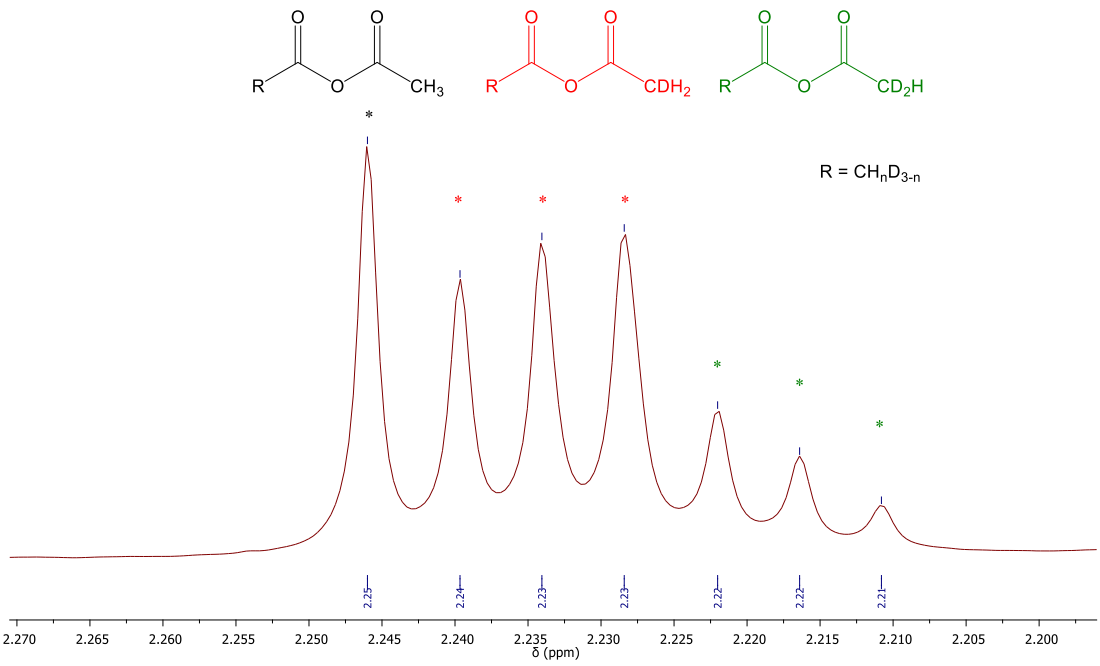

Figure 6.6: ^1H NMR spectrum for crude product obtained from 1:1 reaction of d^6Ac_2O:Ac_2O heated to 160 °C under N_2 for 2hrs with [Rh(acac)(PPh_3)(CO)] (5 %) and KI (50 %)

The presence of multiple signals between δ 2.20-2.26 is indicative of formation of a range of isotopologues. The singlet at δ 2.25 is consistent with CH_3OCOR indicating some non-deuterated starting material remains. The 1:1:1 triplet centred at δ 2.23 is assigned to the proton of CDH_2OCOR due to coupling to ^2H which has spin I=1. A partially obscured 1:2:3:2:1 pentet centred at δ 2.22 is due to the proton of CHD_2OCOR with coupling to two deuterium nuclei. These peaks shift upfield with increasing numbers of deuterium atoms due to isotopic shift, heavier isotopes causing a shift in ppm.

A $^{13}C\{^1H\}$ NMR spectrum was also obtained, as shown in Figure 6.7. It shows a singlet signal at δ 22.1 for $(CH_3CO)OR$, a 1:1:1 triplet (red) due to $(CDH_2CO)OR$ and a 1:2:3:2:1 pentet (green) indicative of $(CHD_2CO)OR$. Minor peaks corresponding to the $(CD_3CO)OR$ starting material are also present (purple).

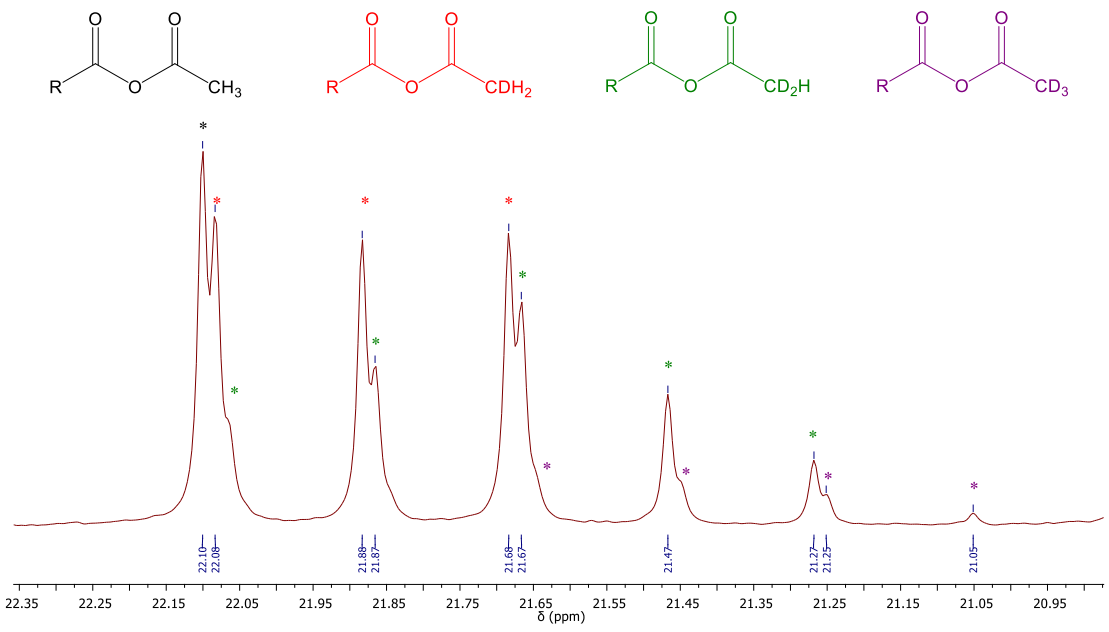

Figure 6.7: ^{13}C NMR spectra for crude product obtained from 1:1 reaction of d^6Ac_2O:Ac_2O heated to 160 °C under N_2 for 2hrs with [Rh(acac)(PPh_3)(CO)] (5 %) and KI (50 %)

To determine if this deuterium scrambling was mediated by the metal catalyst a control experiment was conducted in the absence of metal complex, as shown in Scheme 6.30, using Ac_2O, d^6-Ac_2O and KI (50 %) heated to 160 °C for 2 hours under N_2 atmosphere.

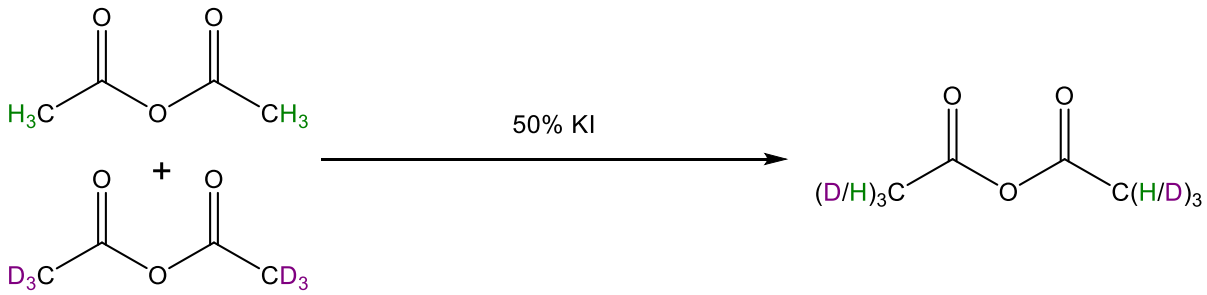

Scheme 6.30: Deuterium scrambling control experiment with 1:1 d^6Ac_2O:Ac_2O and KI (50 %)

Figure 6.8 shows a ^{1}H NMR spectrum of the crude reaction mixture from this experiment.

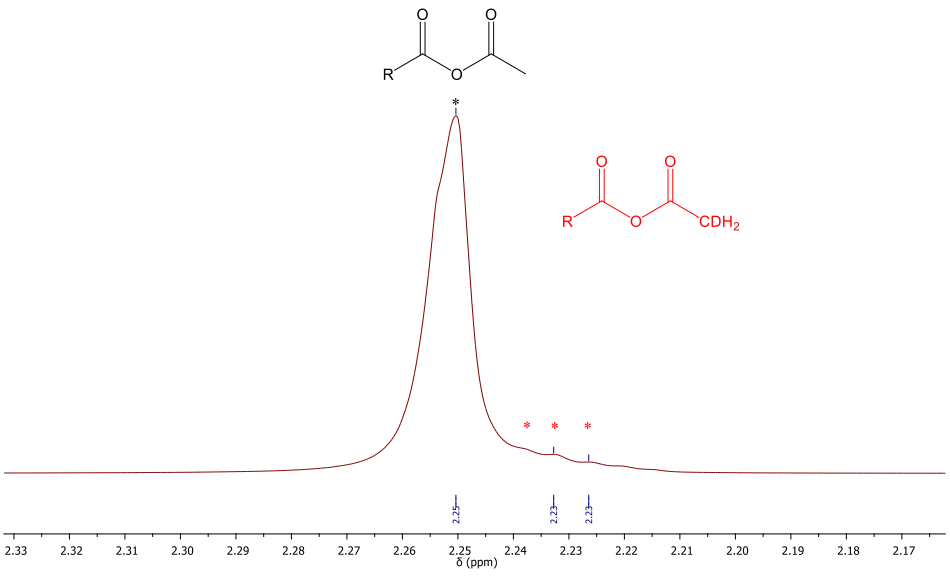

Figure 6.8: ^{1}H NMR spectrum for crude product obtained from 1:1 reaction of d^6Ac_2O:Ac_2O heated to 160 °C under N_2 for 2 hrs with and KI (50 %)

A major peak at δ 2.25 indicates starting material $(CH_3CO)OR$, the other starting material $(CD_3CO)OR$ cannot be seen in the ^{1}H NMR spectrum. Small signals between δ 2.22-2.24

indicate a small amount of $(CDH_2CO)OR$ with protons split into a 1:1:1 pattern indicating a small amount of deuterium scrambling occurs without a metal catalyst present. A ^{13}C {H} NMR spectrum of the crude reaction mixture is shown in Figure 6.9.

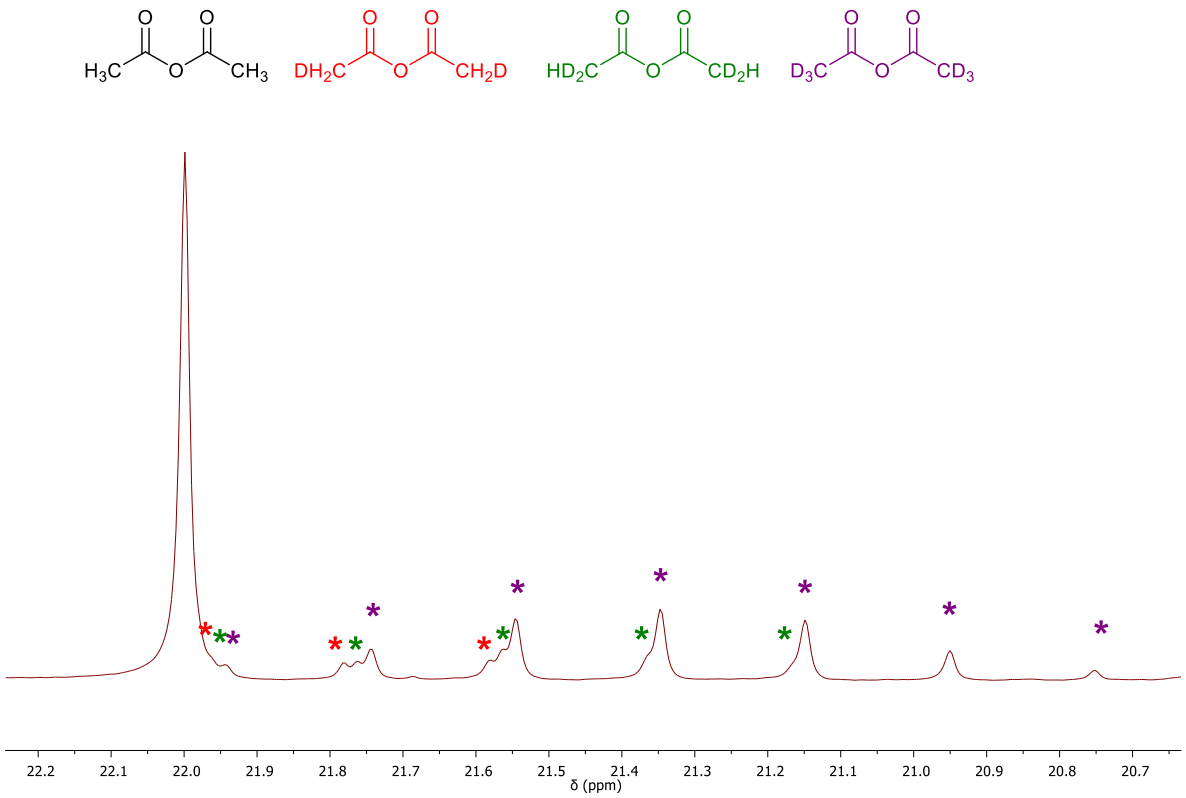

Figure 6.9: ^{13}C NMR spectrum of acetic anhydride $C(H/D)_3$ carbon showing partial exchange of deuterium

The major observable species are $(CH_3CO)OR$ at δ 22.0 and $(CD_3CO)OR$ as a 1:3:6:7:6:3:1 septet. A small triplet for CDH_2OR and a minor pentet with 1:2:3:2:1 indicate that some deuterium scrambling occurred without a metal catalyst present. GCMS of this product had major signals at 43.0 (CH_3CO^+) and 46.0 (CD_3CO^+) with minor peaks at 44.0 and 45.0 for (CDH_2CO^+) and (CD_2HCO^+) respectively. These results show that while a minor amount of

deuterium scrambling occurred the extent of scrambling is much less than that observed with a metal catalyst present.

6.2.3 Generating ketene intermediate *in situ*

Due to the proposed role of ketenes in the deuterium incorporation mechanism, generation of a ketene *in situ* was considered as a route to test this mechanism. Industrially, thermal elimination of H_2O from acetic acid is one route to generating ketenes, however this requires temperatures above 923 K.[52] There are several other routes to generating ketenes, such as dehalogenation of an acyl chloride with Hünig's base,[53,54] carbonylation of carbenes and by photochemical processes.[55] Another route to ketenes used in the synthesis of polymers is from derivatives of Meldrum's acid, which is known to decompose upon heating into acetone, carbon dioxide and a ketene.[56] Due to a lack of other necessary regents and by products of acetone and CO_2, Meldrum's acid derivatives were considered ideal to generate a ketene *in situ*. To test our proposed ketene intermediate a variant of Meldrum's acid was made with a propyl chain which should decompose when heated to give a ketene as shown in Scheme 6.31. When decarbonylated this ketene should form butene.

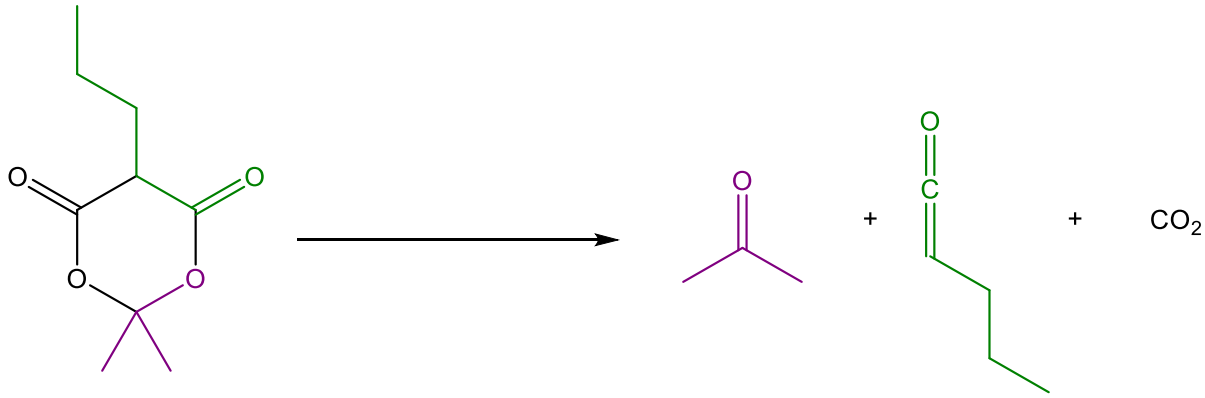

Scheme 6.31: Decomposition of propyl-Meldrum's acid to acetone, CO_2 and a ketene

The propyl derivative of Meldrum's acid was heated to 160 °C in a microwave tube and the resultant mixture analysed by ^{1}H NMR spectroscopy. A signal at δ 2.17 ppm indicated

formation of acetone, but minor peaks for starting material were present indicating complete decomposition had not occurred.

In a separate experiment one equivalent propyl-Meldrum's acid was added to a decarbonylative dehydration reaction as shown in Scheme 6.32. Upon reaching room temperature the microwave tube was further cooled to – 78 °C to allow for condensation of butene, if formed.

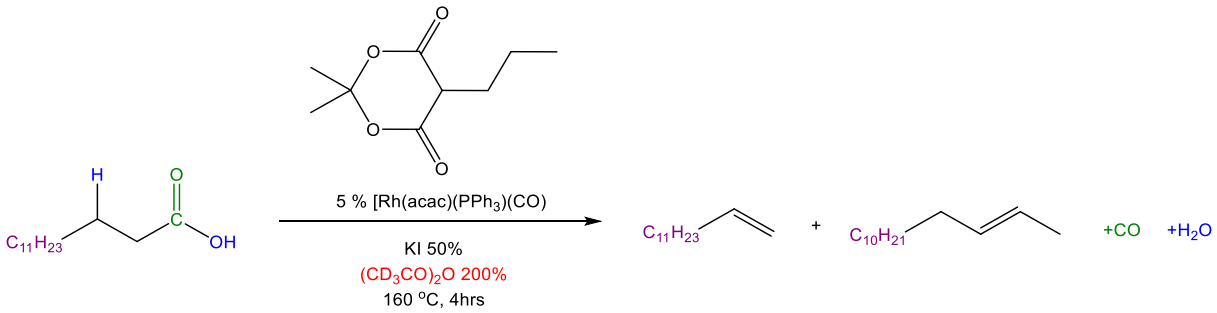

Scheme 6.32: Decarbonylative dehydration of myristic acid with propyl-Meldrum's acid additive

While at low temperature, $CDCl_3$ was added and an NMR spectrum of the crude reaction mixture taken. The major species observed in the ^1H NMR spectrum was propyl-Meldrum's acid indicating that decomposition had not occurred. No evidence for butene formation was observed.

6.3 Summary

A variety of catalysts were tested for decarbonylative dehydration of myristic acid to C_{13} alkenes. Most were found to be effective with some giving yields of 90+ % alkene products. Most catalysts gave poor selectivities for 1-tridecene.

The formation of phosphine acetamide complexes when using rhodium iminophosphine catalysts was probed. A reaction heating [Rh(PN-$^{i}Pr_2Ph$)(COMe)I_2] to reflux in $CHCl_3$ under CO atmosphere showed decarbonylation leading to formation of [Rh(PN-$^{i}Pr_2Ph$)(Me)(CO)I_2] and then [Rh(PN-$^{i}Pr_2Ph$)(CO)I], supporting the proposed reaction mechanism for decarbonylative dehydration. A reaction using PN-$^{i}Pr_2Ph$ under catalytic conditions was used to see if PCO chelate complex formation occurred via the ligand dissociating and being acylated, then reattaching. It was found that the nitrogen of the iminophosphine compound was acylated, however the phosphorus atom was oxidised indicating a different mechanism may have led to formation of this species.

Experiments using d^6 Ac_2O indicated deuterium is incorporated into the alkene product for a wide variety of catalysts. This D-incorporation was probed with some d^6 Ac_2O/ Ac_2O scrambling experiments, which found a significant amount of deuterium scrambling leading to formation of $(CDH_2CO)OR$ and $(CD_2HCO)OR$. These experiments support the previously proposed mechanism of ketene formation, leading to deuterium incorporation into the alkene product.

6.4 References

(1) Franke, R.; Selent, D.; Börner, A. *Chem. Rev.* **2012**, *112*, 5675–5732.

(2) Imokawa, G.; Tsutsumi, H.; Kurosaki, T.; Hayashi, M.; Kakuse, J. Detergent composition. US4139485A, February 22, 1977.

(3) Lengyel, S. P. Mixed ethoxylated alcohol/ethoxy sulfate surfactants and synthetic detergents incorporating the same. US4464292A, January 2, 1981.

(4) Chatterjee, A.; Hopen Eliasson, S. H.; Jensen, V. R. *Catal. Sci. Technol.* **2018**, *8*, 1487–1499.

(5) Alpha Olefins Market Size & Share | Global Industry Report, 2018-2025 https://www.grandviewresearch.com/industry-analysis/alpha-olefins-market (accessed Jul 12, 2018).

(6) Skupinska, J. *Chem. Rev* **1991**, *91*, 613–648.

(7) McGuinness, D. S. *Chem. Rev.* **2011**, *111*, 2321–2341.

(8) Agapie, T. *Coord. Chem. Rev.* **2011**, *255*, 861–880.

(9) Kumar, A.; Bhatti, T. M.; Goldman, A. S. *Chem. Rev.* **2017**, *117*, 12357–12384.

(10) Petrus, L.; Noordermeer, M. A. *Green Chem.* **2006**, *8*, 861.

(11) Miao, X.; Wu, Q. *Bioresour. Technol.* **2006**, *97*, 841–846.

(12) Bidange, J.; Fischmeister, C.; Bruneau, C. *Chem. - A Eur. J.* **2016**, *22*, 12226–12244.

(13) Santillan-Jimenez, E.; Crocker, M. *J. Chem. Technol. Biotechnol.* **2012**, *87*, 1041–1050.

(14) Kang, M.-K.; Nielsen, J. *J. Ind. Microbiol. Biotechnol.* **2017**, *44*, 613–622.

(15) Chatterjee, A.; Hopen Eliasson, S. H.; Törnroos, K. W.; Jensen, V. R. *ACS Catal.* **2016**, 7784–7789.

(16) Dawes, G. J. S.; Scott, E. L.; Le Nôtre, J.; Sanders, J. P. M.; Bitter, J. H. *Green Chem.* **2015**, *17*, 3231–3250.

(17) Lopez-Ruiz, J. A.; Pham, H. N.; Datye, A. K.; Davis, R. J. *Appl. Catal. A Gen.* **2015**, *504*, 295–307.

(18) Santillan-Jimenez, E.; Crocker, M. *J. Chem. Technol. Biotechnol.* **2012**, *87*, 1041–1050.

(19) Morgan, T.; Grubb, D.; Santillan-Jimenez, E.; Crocker, M. *Top. Catal.* **2010**, *53*, 820–829.

(20) Snåre M.; Kubičková I.; Mäki-Arvela P.; Eränen K.; Murzin, D. Y. *Ind. Eng. Chem. Res,* **2006**, *45*, 5708-5715.

(21) Wagenhofer, M. F.; Baráth, E.; Gutiérrez, O. Y.; Lercher, J. A. *ACS Catal.* **2017**, 1068–1076.

(22) Herman, N. A. *Curr. Opin. Chem. Biol.* **2016**, *35*, 22–28.

(23) Tsuji, J.; Ohno, K. *Synthesis (Stuttg).* **2002**, *1969*, 157–169.

(24) Tsuji, J.; Ohno, K. *J. Am. Chem. Soc.* **1968**, *90*, 94–98.

(25) Foglia, T. A.; Barr, P. A. *J. Am. Oil Chem. Soc.* **1976**, *53*, 737–741.

(26) Miller, J. A.; Nelson, J. A.; Byrne, M. P. *J. Org. Chem.* **1993**, *58*, 18–20.

(27) Gooßen, L. J.; Rodríguez, N. *Chem. Commun.* **2004**, 724–725.

(28) Liu, Y.; Virgil, S. C.; Grubbs, R. H.; Stoltz, B. M. *Angew. Chem. Int. Ed.* **2015**, *54*, 11800–11803.

(29) Liu, Y.; Kim, K. E.; Herbert, M. B.; Fedorov, A.; Grubbs, R. H.; Stoltz, B. M. *Adv. Synth. Catal.* **2014**, *356*, 130–136.

(30) Miranda, M. O.; Pietrangelo, A.; Hillmyer, M. A.; Tolman, W. B. *Green Chem.* **2012**, *14*, 490.

(31) Ortuño, M. A.; Dereli, B.; Cramer, C. J. *Inorg. Chem.* **2016**, *55*, 4124–4131.

(32) Maetani, S.; Fukuyama, T.; Suzuki, N.; Ishihara, D.; Ryu, I. *Chem. Commun.* **2012**, *48*, 2552.

(33) Maetani, S.; Fukuyama, T.; Suzuki, N.; Ishihara, D.; Ryu, I. *Organometallics* **2011**, *30*, 1389–1394.

(34) Ternel, J.; Lebarbé, T.; Monflier, E.; Hapiot, F. *ChemSusChem* **2015**, *8*, 1585–1592.

(35) Deeming, A. J.; Shaw, B. L. *J. Chem. Soc. A* **1969**, 443–446.

(36) Miller, J. A.; Nelson, J. A. *Organometallics* **1991**, *10*, 2958–2961.

(37) Blake, D.; Shields, S.; Wyman, L. *Inorg. Chem.* **1974**, *13*, 1595–1600.

(38) Sano, K.; Yamamoto, T.; Yamamoto, A. *Bull. Chem. Soc.* **1984**, *57*, 2741–2747.

(39) Eliasson, S.; Chatterjee, A.; Occhipinti, G.; Jensen, V. *Inorganics* **2017**, *5*, 87.

(40) Le Nôtre, J.; Scott, E. L.; Franssen, M. C. R.; Sanders, J. P. M. *Tetrahedron Lett.* **2010**, *51*, 3712–3715.

(41) Cocker, D. Synthesis and reactivity of Rh(I) and Ir(I) complexes and their application in catalytic decarbonylative dehydration reactions, PhD Thesis, University of Sheffield, 2015.

(42) Maetani, S.; Fukuyama, T.; Suzuki, N.; Ishihara, D.; Ryu, I. *Organometallics* **2011**, *30*, 1389–1394.

(43) Singh, S.; Baird, M. C. *J. Organomet. Chem.* **1988**, *338*, 255–260.

(44) Gonsalvi, L.; Adams, H.; Sunley, G. J.; Ditzel, E.; Haynes, A. *J. Am. Chem. Soc.* **2002**, *124*, 13597–13612.

(45) Gonsalvi, L.; Gaunt, J. A.; Adams, H.; Castro, A.; Sunley, G. J.; Haynes, A. *Organometallics* **2003**, *22*, 1047–1054.

(46) Haynes, A.; McNish, J.; Pearson, J. M. *J. Organomet. Chem.* **1998**, *551*, 339–347.

(47) Wilson, J. M. Ligand Effects On Key Steps In Methanol Carbonylation, University of Sheffield, 2006.

(48) Keinan, E.; Sahai ', M. *J . Org. Chem* **1990**, *55*, 3922–3926.

(49) Ramsey, J. A.; Ladd, J. A. *J. Chem. Soc. B Phys. Org.* **1968**, *0*, 118.

(50) Kurtzweil, M. L.; Beak, P. *J. Am. Chem. Soc.* **1996**, *118*, 3426–3434.

(51) Lazzaroni, R.; Uccello-Barretta, G.; Benetti, M. *Organometallics* **1989**, *8*, 2323–2327.

(52) Sebbar, N.; Appel, J.; Bockhorn, H. *Combust. Sci. Technol.* **2016**, *188*, 745–758.

(53) Ibrahim, A. A.; Nalla, D.; Van Raaphorst, M.; Kerrigan, N. J. *J. Am. Chem. Soc.* **2012**, *134*, 2942–2945.

(54) Chen, S.; Ibrahim, A. A.; Peraino, N. J.; Nalla, D.; Mondal, M.; Van Raaphorst, M.; Kerrigan, N. J. *J. Org. Chem.* **2016**, *81*, 7824–7837.

(55) Allen, A. D.; Tidwell, T. T. *European J. Org. Chem.* **2012**, *2012*, 1081–1096.

(56) Dumas, A. M.; Fillion, E. *Acc. Chem. Res.* **2010**, *43*, 440–454.

Chapter 7

Conclusions and future work

7.1 Conclusions

This project has investigated the reactions of a range of Rh(III) acetyl complexes with carboxylates and amines, as well as investigating the mechanism of decarbonylative dehydration of long chain acids to alkenes using transition metal catalysts.

Firstly, the reactions of Rh(III) acetyl complexes containing diphosphine ligands ([Rh(P-P)(COMe)I_2]) with acetate, benzoate and trifluoroacetate were investigated. The reactions with acetate and benzoate were found to proceed by replacement of an iodide ligand by carboxylate before reductive elimination of an anhydride. Many intermediates with carboxylate coordinated were observed, although these could not be isolated. ATR IR spectroscopy and DFT calculations indicated carboxylates coordinated in a bidentate manner. Under a CO atmosphere formation of Rh(I) carbonyl species was observed upon reductive elimination of anhydride. Anhydride elimination was found to be reversible.

The reaction of Rh(III) acetyl complexes with triethylammonium trifluoroacetate proceeded very slowly. Instead, silver trifluoroacetate was used to abstract an iodide ligand. The reaction of [Rh(P-P)(COMe)I_2] complexes with one equivalent of silver trifluoroacetate gave a mixture of complexes [Rh(P-P)(COMe)I_2], [Rh(P-P)(COMe)(TFA)I] and [Rh(P-P)(COMe)$(TFA)_2$] these eliminated anhydrides slowly, over the course of days.

The reactions of [Rh(P-L)(COMe)I_2] complexes containing unsymmetrical heterodifunctional ligands with carboxylates were investigated. The reactions proceeded by substitution of iodide by carboxylate and subsequent reductive elimination of anhydrides. Many intermediates with carboxylate coordinated were observed *in situ* and several species were isolated and characterised by X-ray crystallography. Isolated Rh carboxylate complexes were found to eliminate anhydride in the presence of CO, also forming [Rh(P-L)(CO)I]. DFT calculations comparing the relative energies of Rh carboxylate complexes and CO with the products from anhydride elimination indicated product formation was favourable in all cases.

Chapter 5 investigated the reactions of Rh(III) acetyl complexes containing diphosphine ligands ([Rh(P-P)(COMe)I_2]) with amines. No reaction occurred with N-methyl aniline, however a rapid reaction with diethylamine occurred and was monitored kinetically. The kinetics were conducted under pseudo-first order conditions and were first order with respect to diethylamine. Activation parameters were obtained from Eyring plots and a large negative entropy of activation indicated an associative mechanism. A lack of reaction of [Rh(xantphos)(COMe)I_2] with diethylamine contrasted with the rapid reaction of [Rh(xantphos)(COMe)(NCMe)I][BF_4] and diethylamine indicating a vacant site was required for reaction. The reaction was proposed to proceed via coordination of amine to rhodium before reductive elimination of an acetamide.

Decarbonylative dehydration of long chain carboxylic acids to alkenes was investigated. The scope of Rh(I) carbonyl catalysts was widened, with most catalysts giving good alkene yields but poor terminal alkene selectivity. Rhodium (III) complexes were investigated for decarbonylative dehydration and generally gave good alkene yields but poor terminal alkene selectivity. Palladium catalysts were more effective at lower KI loadings, indicating a different mechanism may occur for Pd catalysed decarbonylative dehydration.

Formation of phosphine acetamide complexes when using iminophosphine was probed and a mechanism where the ligand detached from the metal and was acylated *in situ* was rejected. The incorporation of deuterium into the alkene product was investigated and quantified for a range of catalysts. This was previously proposed to be due to a ketene generated *in situ*. Experiments with d^6 Ac_2O and Ac_2O showed intermolecular H/D scrambling, supporting metal mediated ketene formation. Derivatives of Meldrum's acid were used to attempt to generate a ketene *in situ*, however no product from ketene generation was observed.

7.2 Future work

7.2.1 Extension of reactions of metal acyl complexes with nucleophiles

Gonsalvi et al isolated some Rh (III) acetyl diimine and pyridyl imine complexes.[1] The reactions of these complexes with carboxylates to produce anhydride could be of interest. There are several known complexes in equilibrium between [Rh(L-L)(Me)(CO)I_2] and [Rh(L-L)(COMe)I_2],[1,2] Scheme 7.1, the reactions of these complexes with carboxylates may yield methyl acetate or push the equilibrium to the right and yield an anhydride

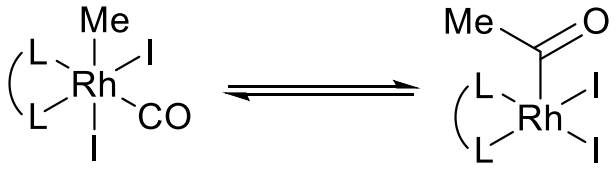

Scheme 7.1: Equilibria between [Rh(L-L)(Me)(CO)I_2] and [Rh(L-L)(COMe)I_2]

The reactions of carboxylates with other metal acyl complexes would also be of interest. There are many known ruthenium acyl and iridium acyl complexes.

7.2.2 DFT calculations for transition states

Lei et al[3] investigated transition states for anhydride reductive elimination and oxidative addition to rhodium, which involve similar intermediates to those observed in this thesis. DFT calculations for transition states of anhydride elimination may elucidate why some carboxylate coordinated intermediates could be isolated, whereas others readily eliminated anhydride.

7.2.3 Decarbonylative dehydration reactions

Some questions remain to be answered about this project. The mechanism of acetylation of the iminophosphine ligand is still uncertain. Heating [Rh(PN-R)(COMe)I_2] complexes under CO at higher temperatures than attempted may induce acetylation.

A range of phosphine acetamide compounds could be separately synthesised and coordinated to Rh(I) to probe the formation of Rh(III) phosphine acetamide complexes, Scheme 7.2.

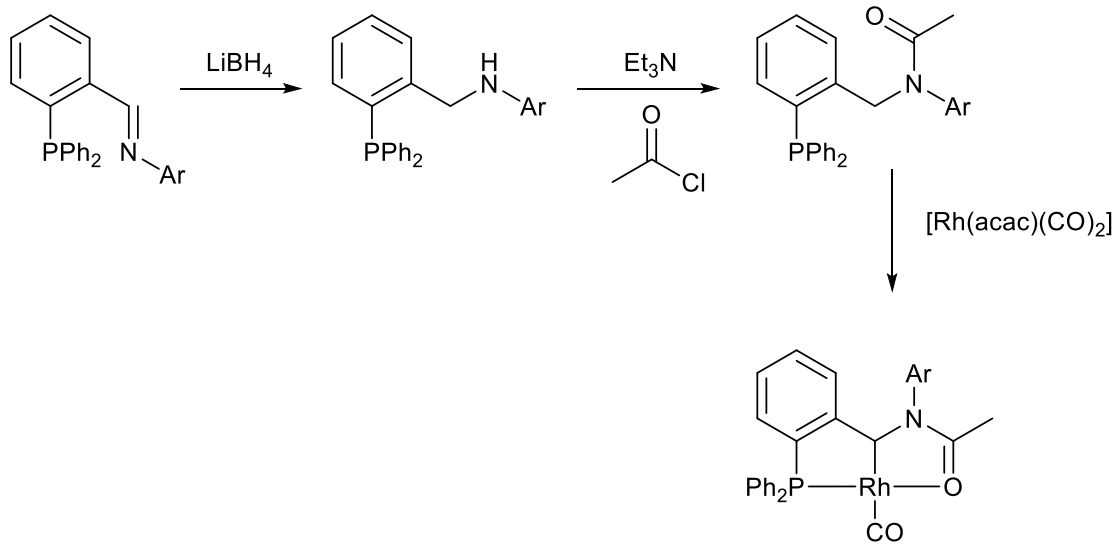

Scheme 7.2: Proposed synthesis of phosphine acetamide and formation of a Rh(I) complex

Generation of a ketene by derivatives of Meldrum's acid did not give an expected alkene product, this may be due to the low boiling points of the expected alkenes. Using different Meldrum's acid derivatives, such as those used in polymer ketene dimerization shown in Scheme 7.3,[4] the role of ketene in decarbonylative dehydration could be further probed.

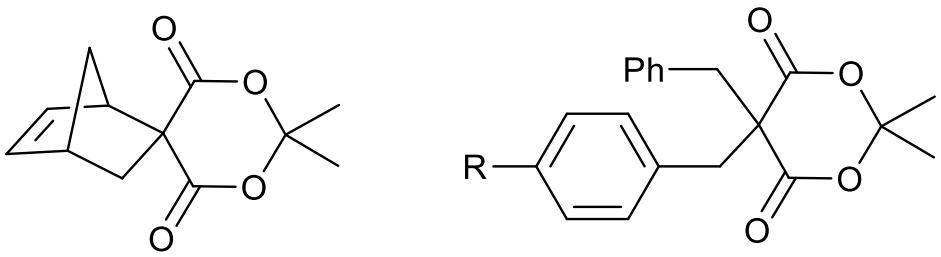

Scheme 7.3: Meldrum's acid derivatives used in polymer ketene dimerizations

7.3 References

(1) Gonsalvi, L.; Gaunt, J. A.; Adams, H.; Castro, A.; Sunley, G. J.; Haynes, A. *Organometallics* **2003**, *22*, 1047–1054.

(2) Best, J.; Wilson, J. M.; Adams, H.; Gonsalvi, L.; Peruzzini, M.; Haynes, A. *Organometallics* **2007**, *26*, 1960–1965.

(3) Lei, Z.-Q.; Pan, F.; Li, H.; Li, Y.; Zhang, X.-S.; Chen, K.; Wang, X.; Li, Y.-X.; Sun, J.; Shi, Z.-J. *J. Am. Chem. Soc.* **2015**, *137*, 15, 5012-5020.

(4) Allen, A. D.; Tidwell, T. T. *Eur. J. Org. Chem.* **2012**, *2012*, 1081–1096.

Appendix

Tables A.1-A.9 – Crystallographic data

Analysis of ABX splitting

ATR IR spectrum for 4b

ATR IR spectrum for 4g

Tables A.10-A.17 Kinetic data

Figure A.3-A.6 k_{obs} vs. [$HNEt_2$] to determine pseudo-first order rate constants

Figure A.7-A.10 Eyring plots

Determining alkene selectivity

Deuterium incorporation calculation

Table A.1: Crystal data and structure refinement for [Rh(dppe)(COMe)(TFA)$_2$]

Identification code	IAH744s_run2_0m
Empirical formula	$C_{32}H_{27}F_6O_5P_2Rh$
Formula weight	770.38
Temperature/K	100
Crystal system	triclinic
Space group	P-1
a/Å	10.3489(3)
b/Å	10.9172(3)
c/Å	13.8181(4)
α/°	91.523(2)
β/°	102.548(2)
γ/°	98.792(2)
Volume/Å^3	1503.09(8)
Z	2
ρ_{calc}g/cm^3	1.702
μ/mm^{-1}	0.754
F(000)	776.0
Crystal size/mm^3	0.2 × 0.08 × 0.05
Radiation	MoKα (λ = 0.71073)
2Θ range for data collection/°	3.026 to 55.542
Index ranges	-13 ≤ h ≤ 13, -14 ≤ k ≤ 14, -18 ≤ l ≤ 18
Reflections collected	47451
Independent reflections	7057 [R_{int} = 0.0716, R_{sigma} = 0.0529]
Data/restraints/parameters	7057/0/416
Goodness-of-fit on F^2	1.104
Final R indexes [I>=2σ (I)]	R_1 = 0.0586, wR_2 = 0.1555
Final R indexes [all data]	R_1 = 0.0809, wR_2 = 0.1699
Largest diff. peak/hole / e Å^{-3}	3.18/-1.17

Table A.2: Crystal data and structure refinement for [Rh_2(μ-dppm)$_2$(μ-CO)(μ-I)(CO)$_2$]I.3CH_2Cl_2

Identification code	IAH716_0m_A
Empirical formula	C56 H50 Cl6 I2 O3 P4 Rh2
Formula weight	1567.16
Temperature/K	97(2) K
Crystal system	Monoclinic
Space group	$P2_1/c$
a/Å	10.7928(10)
b/Å	26.406(3)
c/Å	22.524(2)
α/°	90
β/°	97.135(5)
γ/°	90
Volume/Å^3	6369.6(10)
Z	4
ρ_{calc}g/cm^3	1.634
μ/mm^{-1}	1.879
F(000)	3072
Crystal size/mm^3	0.430 x 0.340 x 0.290
Radiation	MoKα (λ = 0.71073)
2Θ range for data collection/°	1.791 to 27.590
Index ranges	-14<=h<=13, -34<=k<=34, -29<=l<=29
Reflections collected	79221
Independent reflections	14682 [R(int) = 0.0616]
Data/restraints/parameters	14682 / 21 / 680
Goodness-of-fit on F^2	1.05
Final R indexes [I>=2σ (I)]	R1 = 0.0404, wR2 = 0.0967
Final R indexes [all data]	R1 = 0.0492, wR2 = 0.1027
Largest diff. peak/hole / e Å^{-3}	1.623 and -1.316

Table A.3: Crystal data and structure refinement for [Rh(PN-Mes)(COMe)I_2] 3i

Identification code	iah732v_0m_try_a
Empirical formula	C32 H30 Cl5 I2 N O P Rh
Formula weight	1009.5
Temperature/K	99.96 K
Crystal system	Orthorhombic
Space group	Pbca
a/Å	17.6028(8)
b/Å	19.6866(9)
c/Å	20.5487(9)
α/°	90
β/°	90
γ/°	90
Volume/Å^3	7120.9(6) Å3
Z	8
ρ_{calc}g/cm^3	1.883
μ/mm^{-1}	21.587
F(000)	3904
Crystal size/mm^3	0.16 x 0.13 x 0.07 mm3
Radiation	MoKα (λ = 0.71073)
2Θ range for data collection/°	3.997 to 66.729°.
Index ranges	-19<=h<=20, -23<=k<=23, -24<=l<=24
Reflections collected	238943
Independent reflections	6306 [R(int) = 0.0890]
Data/restraints/parameters	6306 / 24 / 401
Goodness-of-fit on F^2	1.043
Final R indexes [I>=2σ (I)]	R1 = 0.0253, wR2 = 0.0557
Final R indexes [all data]	R1 = 0.0318, wR2 = 0.0580
Largest diff. peak/hole / e Å^{-3}	1.426 and -0.982

Table A.4: Crystal data and structure refinement for [Rh(PN-^{i}Pr$_2$Ph)(COMe)(TFA)I] 6g

Identification code	IAH738s
Empirical formula	$C_{34.79}H_{34.69}F_3I_{1.1}NO_{2.9}PRh$
Formula weight	844.12
Temperature/K	100
Crystal system	orthorhombic
Space group	Pbcn
a/Å	42.267(3)
b/Å	9.8416(7)
c/Å	18.1545(13)
α/°	90
β/°	90
γ/°	90
Volume/Å^3	7551.9(9)
Z	8
ρ_{calc}g/cm^3	1.485
μ/mm^{-1}	1.443
F(000)	3353.0
Crystal size/mm^3	0.306 × 0.22 × 0.05
Radiation	MoKα (λ = 0.71073)
2Θ range for data collection/°	3.854 to 55.16
Index ranges	-54 ≤ h ≤ 55, -12 ≤ k ≤ 12, -23 ≤ l ≤ 23
Reflections collected	77239
Independent reflections	8731 [R_{int} = 0.0748, R_{sigma} = 0.0439]
Data/restraints/parameters	8731/37/421
Goodness-of-fit on F^2	1.198
Final R indexes [I>=2σ (I)]	R_1 = 0.0896, wR_2 = 0.1858
Final R indexes [all data]	R_1 = 0.1043, wR_2 = 0.1916
Largest diff. peak/hole / e Å^{-3}	1.93/-1.75

Table A.5: Crystal data and structure refinement for [Rh(dppmS)(COMe)(OAc)I] 4k

Identification code	IAH744s_run2_0m
Empirical formula	$C_{32}H_{27}F_6O_5P_2Rh$
Formula weight	770.38
Temperature/K	100
Crystal system	triclinic
Space group	P-1
a/Å	10.3489(3)
b/Å	10.9172(3)
c/Å	13.8181(4)
α/°	91.523(2)
β/°	102.548(2)
γ/°	98.792(2)
Volume/Å^3	1503.09(8)
Z	2
ρ_{calc}g/cm^3	1.702
μ/mm^{-1}	0.754
F(000)	776.0
Crystal size/mm^3	0.2 × 0.08 × 0.05
Radiation	MoKα (λ = 0.71073)
2Θ range for data collection/°	3.026 to 55.542
Index ranges	-13 ≤ h ≤ 13, -14 ≤ k ≤ 14, -18 ≤ l ≤ 18
Reflections collected	47451
Independent reflections	7057 [R_{int} = 0.0716, R_{sigma} = 0.0529]
Data/restraints/parameters	7057/0/416
Goodness-of-fit on F^2	1.104
Final R indexes [I>=2σ (I)]	R_1 = 0.0586, wR_2 = 0.1555
Final R indexes [all data]	R_1 = 0.0809, wR_2 = 0.1699
Largest diff. peak/hole / e Å^{-3}	3.18/-1.17

Table A.6: Crystal data and structure refinement for [Rh(dppmSe)(COMe)(OAc)I] 4l

Identification code	IAH745k_0m
Empirical formula	$C_{28.79}H_{27.68}I_{1.11}O_{2.79}P_2RhSe$
Formula weight	802.27
Temperature/K	100
Crystal system	monoclinic
Space group	$P2_1/c$
a/Å	16.298(3)
b/Å	12.140(3)
c/Å	16.588(3)
α/°	90
β/°	116.944(3)
γ/°	90
Volume/Å^3	2926.0(10)
Z	4
ρ_{calc}g/cm^3	1.821
μ/mm^{-1}	3.131
F(000)	1561.0
Crystal size/mm^3	0.25 × 0.1 × 0.05
Radiation	MoKα (λ = 0.71073)
2Θ range for data collection/°	4.34 to 55.08
Index ranges	-21 ≤ h ≤ 20, -15 ≤ k ≤ 15, -16 ≤ l ≤ 21
Reflections collected	39763
Independent reflections	6736 [R_{int} = 0.0889, R_{sigma} = 0.0678]
Data/restraints/parameters	6736/0/346
Goodness-of-fit on F^2	1.029
Final R indexes [I>=2σ (I)]	R_1 = 0.0513, wR_2 = 0.1000
Final R indexes [all data]	R_1 = 0.0897, wR_2 = 0.1158
Largest diff. peak/hole / e Å^{-3}	5.37/-2.96

Table A.7: Crystal data and structure refinement for [Rh(dppmS)(COMe)(OBz)I] 5k

Identification code	iah698_0m
Empirical formula	C69 H62 Cl2 I2 O6 P4 Rh2 S2
Formula weight	1705.7
Temperature/K	150(2) K
Crystal system	Triclinic
Space group	P -1
a/Å	12.215(4)
b/Å	16.516(5)
c/Å	17.366(6)
α/°	88.868(11)
β/°	75.947(12)
γ/°	89.936(10)
Volume/Å^3	3397.9(19)
Z	2
ρ_{calc}g/cm^3	1.667
μ/mm^{-1}	1.679
F(000)	1692
Crystal size/mm^3	0.430 x 0.210 x 0.120
Radiation	MoKα (λ = 0.71073)
2Θ range for data collection/°	1.209 to 27.906°.
Index ranges	-15<=h<=15, -21<=k<=21, -22<=l<=22
Reflections collected	44553
Independent reflections	15650 [R(int) = 0.2792]
Data/restraints/parameters	15650 / 512 / 786
Goodness-of-fit on F^2	1.099
Final R indexes [I>=2σ (I)]	R1 = 0.1456, wR2 = 0.3477
Final R indexes [all data]	R1 = 0.2846, wR2 = 0.4393
Largest diff. peak/hole / e Å^{-3}	6.918 and -4.586

Table A.8: Crystal data and structure refinement for [Rh(dppmS)(COMe)(TFA)I] 6k

Identification code	IAH717s_0m
Empirical formula	C29 H25 F3 I O3 P2 Rh S
Formula weight	802.3
Temperature/K	100(2) K
Crystal system	Triclinic
Space group	P-1
a/Å	9.6775(2)
b/Å	12.8428(3)
c/Å	13.1921(3)
α/°	82.1895(10)
β/°	71.4668(10)
γ/°	70.5436(10)
Volume/Å^3	1464.97(6)
Z	2
ρ_{calc}g/cm^3	1.819
μ/mm^{-1}	1.867
F(000)	788
Crystal size/mm^3	0.180 x 0.150 x 0.080
Radiation	MoKα (λ = 0.71073)
2Θ range for data collection/°	1.629 to 27.701°.
Index ranges	-12<=h<=12, -16<=k<=16, -17<=l<=17
Reflections collected	48341
Independent reflections	6844 [R(int) = 0.0345]
Data/restraints/parameters	6844 / 7 / 362
Goodness-of-fit on F^2	1.065
Final R indexes [I>=2σ (I)]	R1 = 0.0255, wR2 = 0.0580
Final R indexes [all data]	R1 = 0.0300, wR2 = 0.0606
Largest diff. peak/hole / e Å^{-3}	1.490 and -1.089

Table A. 9: Crystal data and structure refinement for N-[[2-(diphenylphosphinyl)phenyl]methyl]-N-(2,6 diisopropylbenzyl)-acetamide

Identification code	iah742k_0m
Empirical formula	$C_{33}H_{36}NO_2P$
Formula weight	509.60
Temperature/K	100
Crystal system	monoclinic
Space group	C2/c
a/Å	12.817(3)
b/Å	11.494(3)
c/Å	37.778(8)
α/°	90
β/°	91.378(17)
γ/°	90
Volume/Å^3	5564(2)
Z	8
ρ_{calc}g/cm^3	1.217
μ/mm^{-1}	0.129
F(000)	2176.0
Crystal size/mm^3	0.2 × 0.13 × 0.084
Radiation	MoKα (λ = 0.71073)
2Θ range for data collection/°	2.156 to 38.088
Index ranges	$-11 \leq h \leq 9$, $-10 \leq k \leq 10$, $-34 \leq l \leq 34$
Reflections collected	7971
Independent reflections	2234 [R_{int} = 0.1485, R_{sigma} = 0.1399]
Data/restraints/parameters	2234/333/346
Goodness-of-fit on F^2	1.028
Final R indexes [I>=2σ (I)]	R_1 = 0.0643, wR_2 = 0.1197
Final R indexes [all data]	R_1 = 0.1470, wR_2 = 0.1561
Largest diff. peak/hole / e Å^{-3}	0.24/-0.22

Solution of ABX splitting for 4c [Rh(dppp)(COMe)(OAc)I]

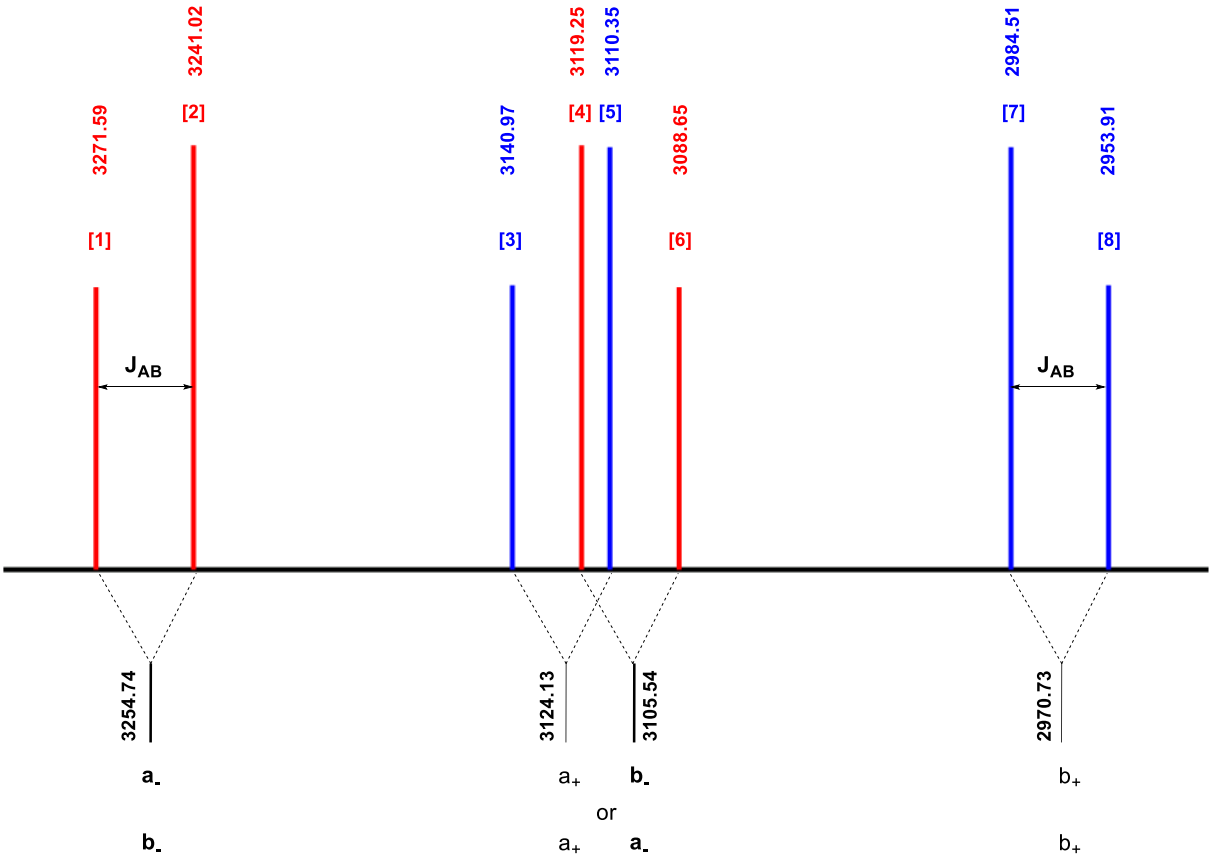

1. AB part of an ABX spin system consists of up to 8 peaks
2. The AB part can be broken down into two AB quartets, marked in red and blue
3. Analysis gives $|J_{AB}|$, J_{AX}, J_{BX} and δ_{AB}
4. Here J_{AB} can be calculated by $\mathbf{J_{AB}}$ = [1]-[2] = [4]-[6] = [3]-[5] = [7]-[8] = 30.6 Hz
5. Calculate the four chemical shifts ν_{a+}, ν_{b+} and ν_{a-}, ν_{b-}

$$c_- = ([2]+[4])/2 = 3180.14$$
$$\Delta\nu_{ab-} = \delta_- = \sqrt{([1]-[6])([2]-[4])} = 149.25$$
$$c_- \pm \frac{\delta_-}{2} = 3180.14 \pm 74.6 = 3254.74, 3105.54$$

$$c_+ = ([5]+[7])/2 = 3047.43$$
$$\Delta\nu_{ab+} = \delta_- = \sqrt{([3]-[8])([5]-[7])} = 153.43$$
$$c_+ \pm \frac{\delta_-}{2} = 3047.43 \pm 76.7 = 3124.13, 2970.73$$

6. Determine the two solutions

$$J_{AX} = a_- - a_+ = 3254.74 - 3105.54 = 149.2$$
$$or\ 3105.54 - 3124.13 = -18.59$$
$$J_{BX} = b_- - b_+ = 3105.54 - 2970.73 = 134.81$$
$$or\ 3254.74 - 2970.73 = 284.01$$

7. This gives two solutions 1: J_{AX} = 149.2 and J_{BX} = 134.8 or 2: J_{AX} =-18.6 or J_{BX} =284.0 as solution 2 gives a negative coupling constant it is rejected and solution 1 gives the coupling constants for J_{AX} and J_{BX}

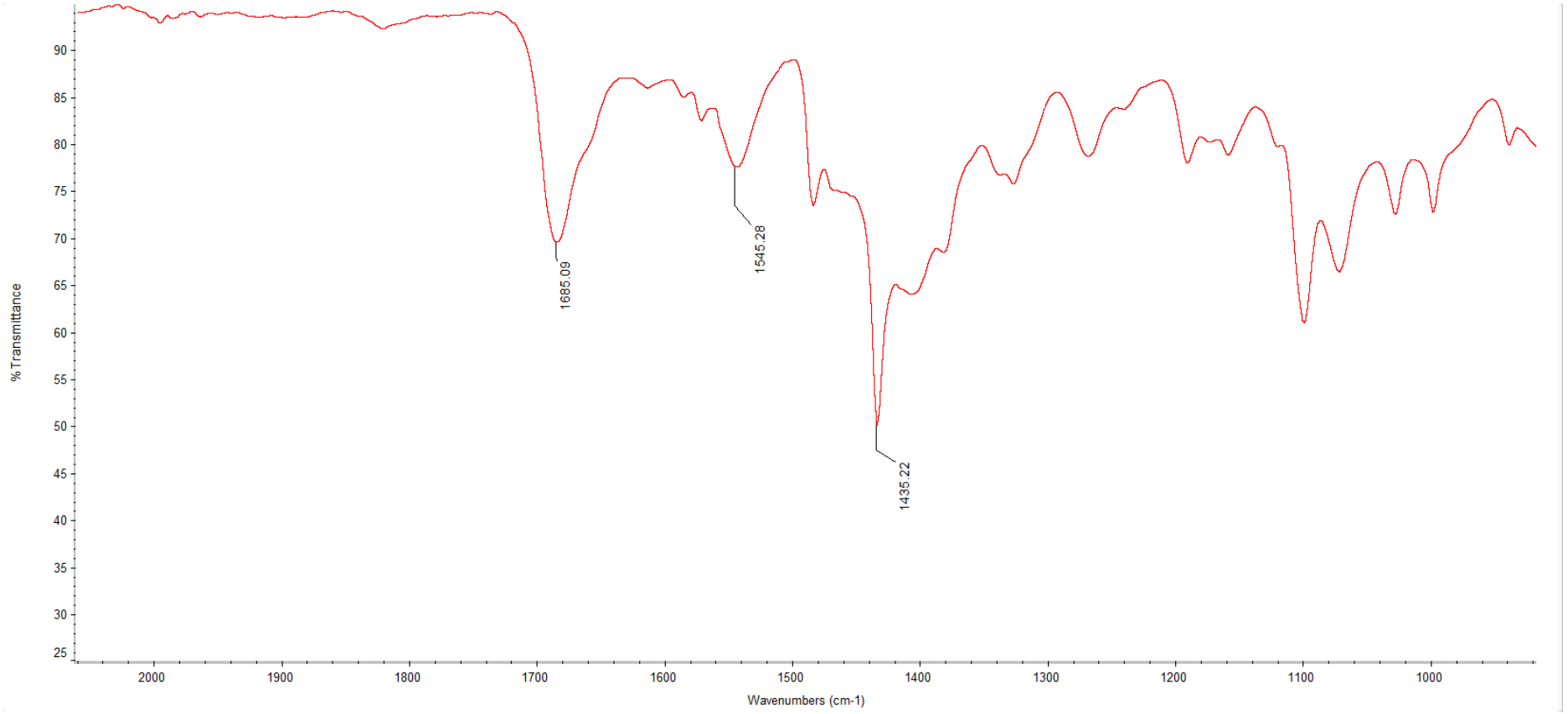

Figure A.1: ATR-IR spectrum of 4b [Rh(dppe)(COMe)(OAc)I]

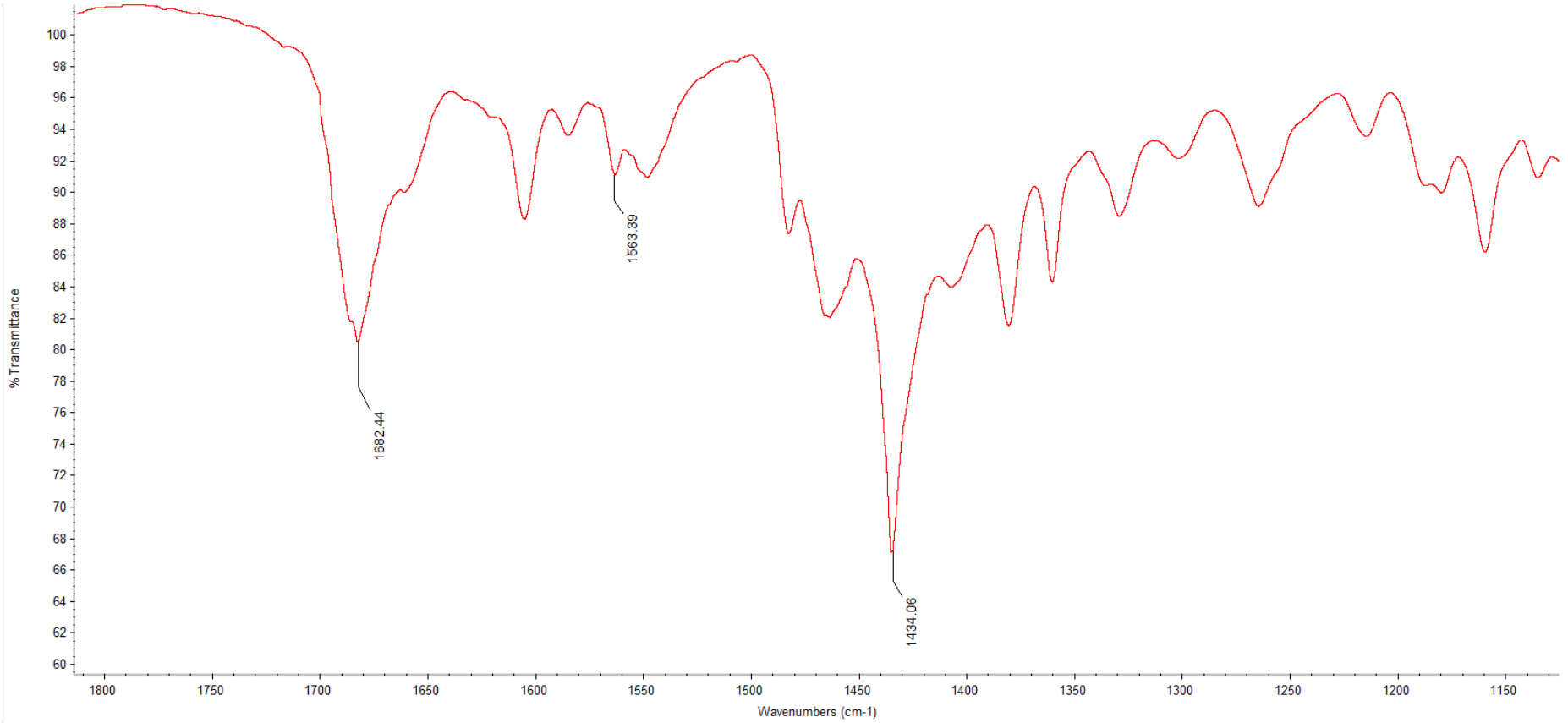

Figure A.2: ATR-IR spectrum of 4g [Rh(PN-$^{i}Pr_2Ph$)(COMe)(OAc)I]

Table A.10: Values of k_{obs} for reaction of **3a** with $HNEt_2$ at 23 °C

$[HNEt_2]$/M	k_{obs} / s^{-1}
0.064	0.0002227
0.128	0.0007624
0.191	0.0008765
0.255	0.0012917
0.319	0.0015375

Table A.11: Values of k_{obs} for reaction of **3b** with $HNEt_2$ at 23 °C

$[HNEt_2]$/M	k_{obs} / s^{-1}
0.064	0.0000835
0.128	0.0001545
0.191	0.0001594
0.255	0.0001937
0.319	0.0002774

Table A.12: Values of k_{obs} for reaction of **3c** with $HNEt_2$ at 23 °C

$[HNEt_2]$/M	k_{obs} / s^{-1}
0.064	0.0000814
0.128	0.0001117
0.191	0.0001886
0.255	0.0003893
0.319	0.0003587

Table A.13: Values of k_{obs} for reaction of **3d** with $HNEt_2$ at 23 °C

$[HNEt_2]$/M	k_{obs} / s^{-1}
0.064	0.0002312
0.128	0.0005299
0.191	0.0005719
0.255	0.0006804
0.319	0.0007047

Table A.14: k_{obs} observed at varying temperature for reaction of **3a** and [0.19M] diethylamine (**Figure A.7**)

T (K)	k_{obs}
308.9	0.00388
305.1	0.00343
300.8	0.00250
296.3	0.00133
287.1	0.00092

Table A.15: k_{obs} observed at varying temperature for reaction of **3b** and [0.19M] diethylamine (**Figure A.8**)

T (K)	k_{obs}
309.6	0.00405
305.1	0.00283
300.7	0.00179
296.3	0.00083
287.1	0.00092

Table A.16: k_{obs} observed at varying temperature for reaction of **3c** and [0.19M] diethylamine (**Figure A.9**)

T (K)	k_{obs}
304.7	0.00848
299.9	0.00735
296.1	0.00438
291.6	0.00393
287.0	0.00264

Table A.17: k_{obs} observed at varying temperature for reaction of **3d** and [0.19M] diethylamine (**Figure A.10**)

T (K)	k_{obs}
305.5	0.00758
300.8	0.00784
296.1	0.00545
291.5	0.00403
286.9	0.00257

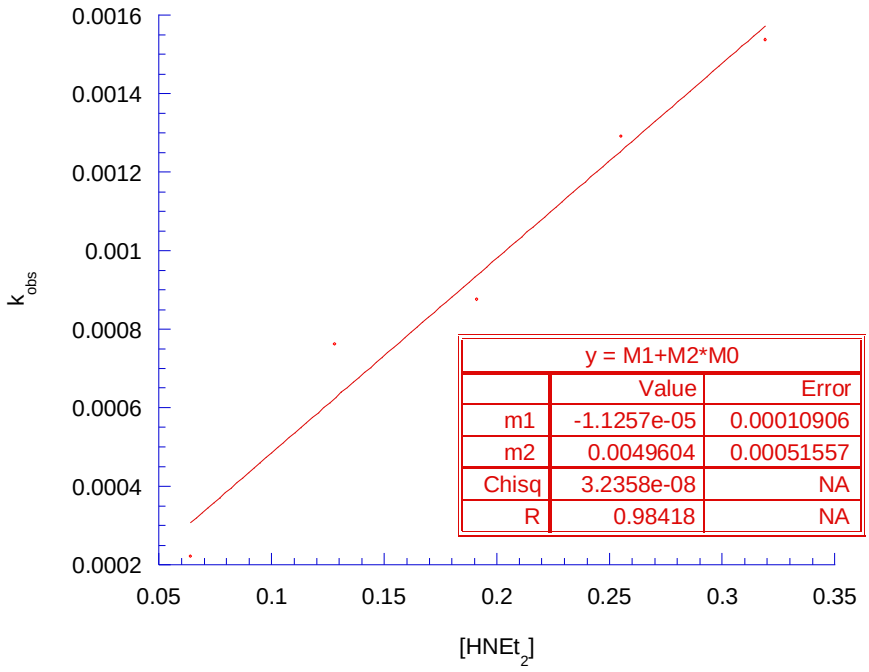

Figure A.3: Plot of k_{obs} vs. concentration of diethylamine for reactions of **3a** with diethylamine in CH_2Cl_2 at 23 °C

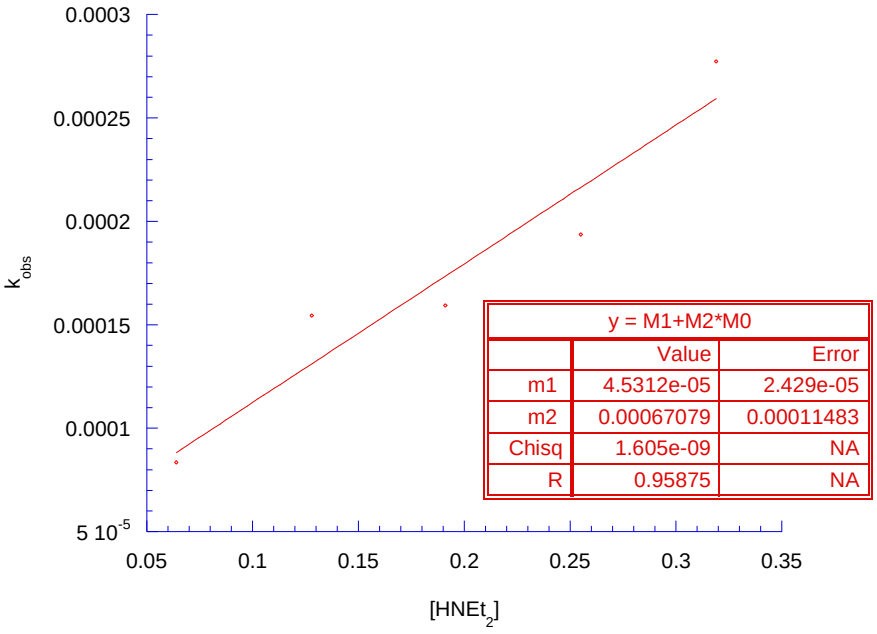

Figure A.4: Plot of k_{obs} vs. concentration of diethylamine for reactions of **3b** with diethylamine in CH_2Cl_2 at 23 °C

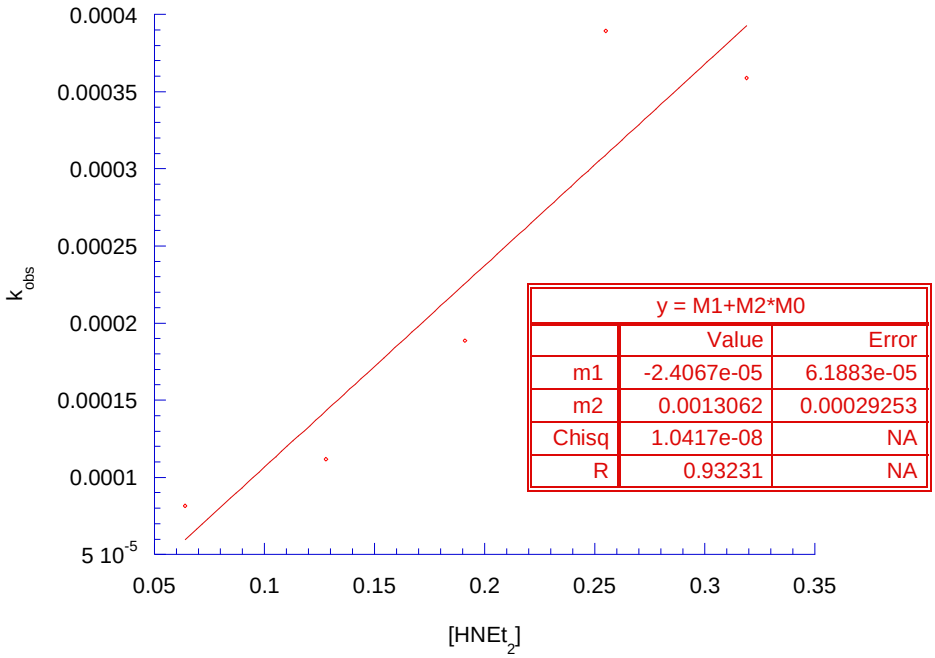

Figure A.5: Plot of k_{obs} vs. concentration of diethylamine for reactions of **3c** with diethylamine in CH_2Cl_2 at 23 °C

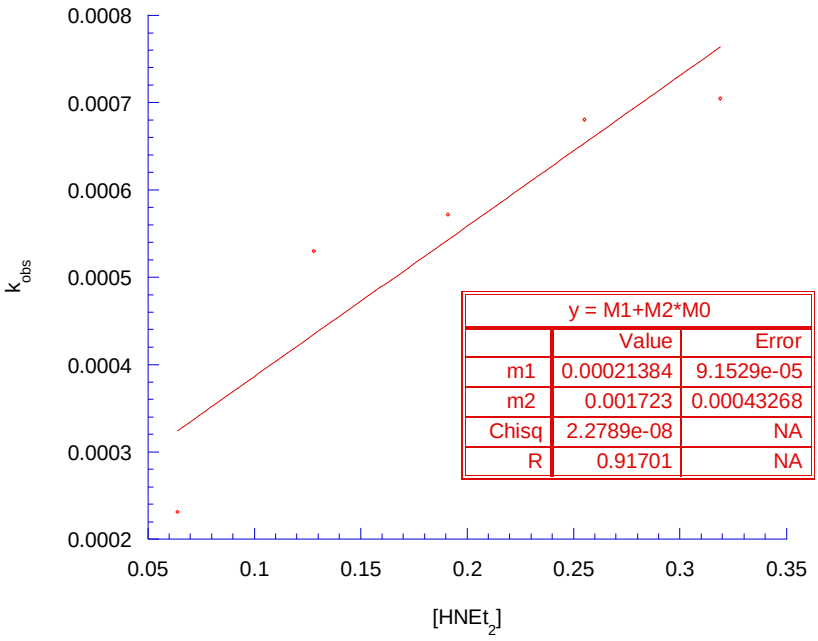

Figure A.6: Plot of k_{obs} vs. concentration of diethylamine for reactions of **3d** with diethylamine in CH_2Cl_2 at 23 °C

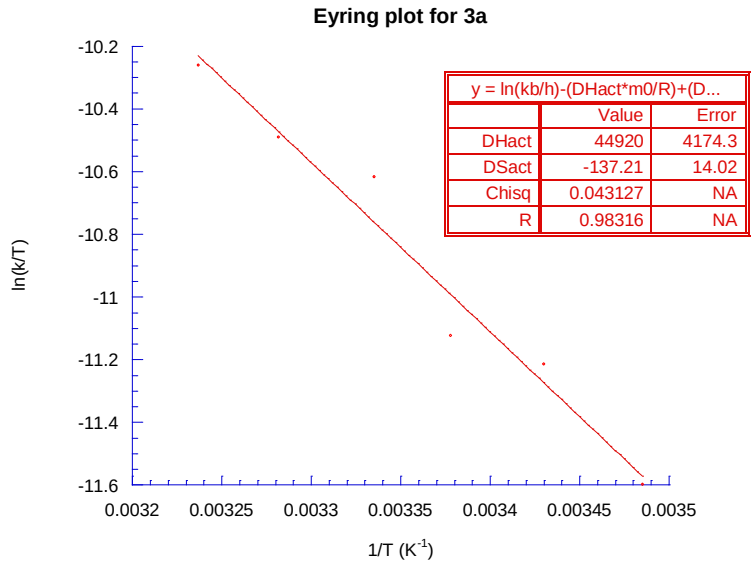

Figure A.7: Eyring plot for reaction of **3a** with $HNEt_2$ in CH_2Cl_2

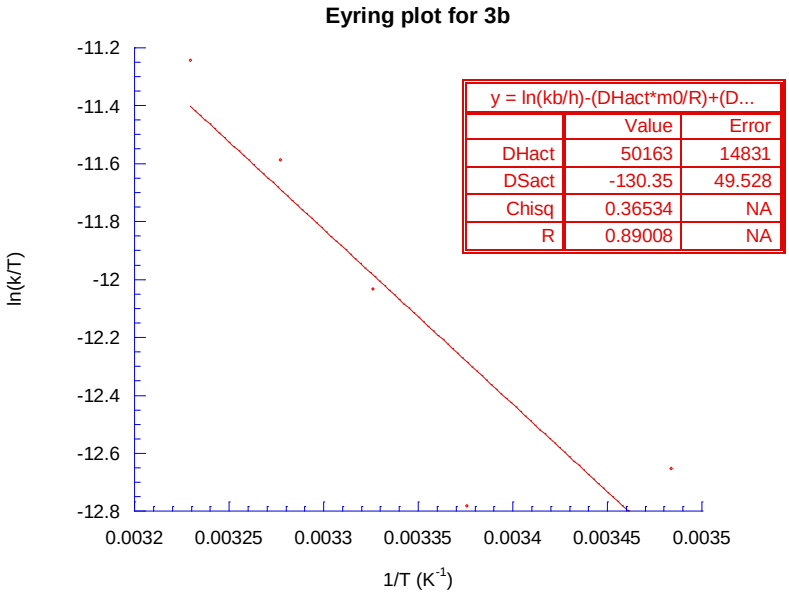

Figure A.8: Eyring plot for reaction of **3b** with $HNEt_2$ in CH_2Cl_2

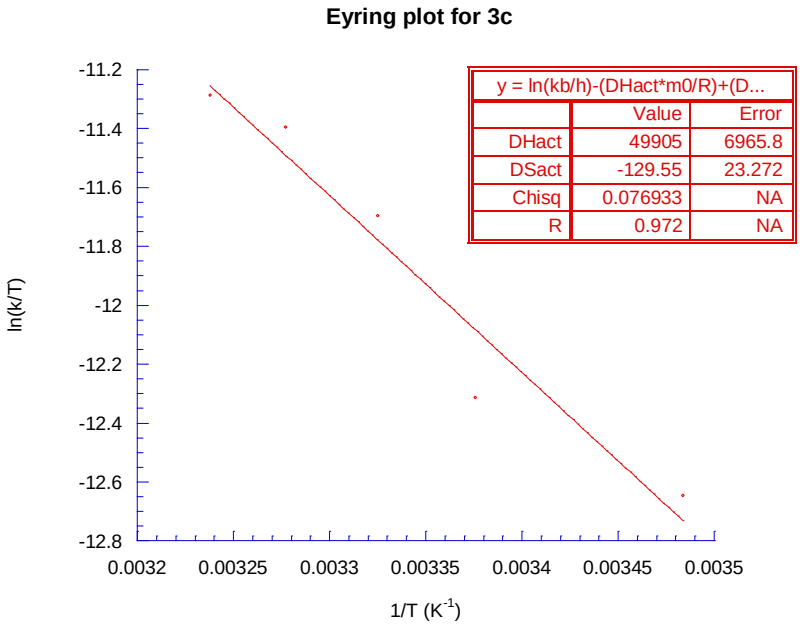

Figure A.9: Eyring plot for reaction of **3c** with $HNEt_2$ in CH_2Cl_2

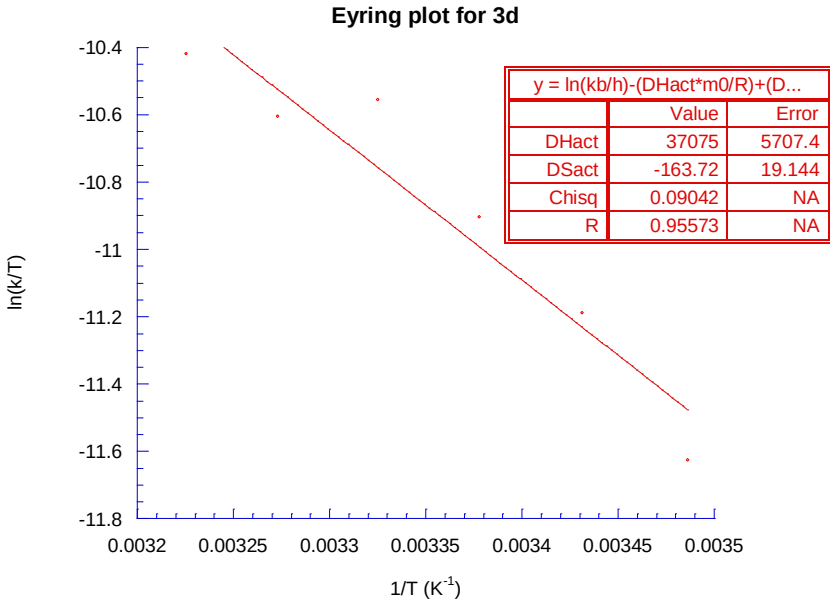

Figure A.10: Eyring plot for reaction of **3d** with $HNEt_2$ in CH_2Cl_2

Selectivity Calculation

Integration of 1-alkene peak: 2.0

Integration of internal alkene peak: 1.48

Both signals correspond to two olefinic hydrogens, as such can be compared to determine a percentage

Thus (2.0/3.48)*100 = 57% terminal alkenes

100%-57% = 43% internal alkenes

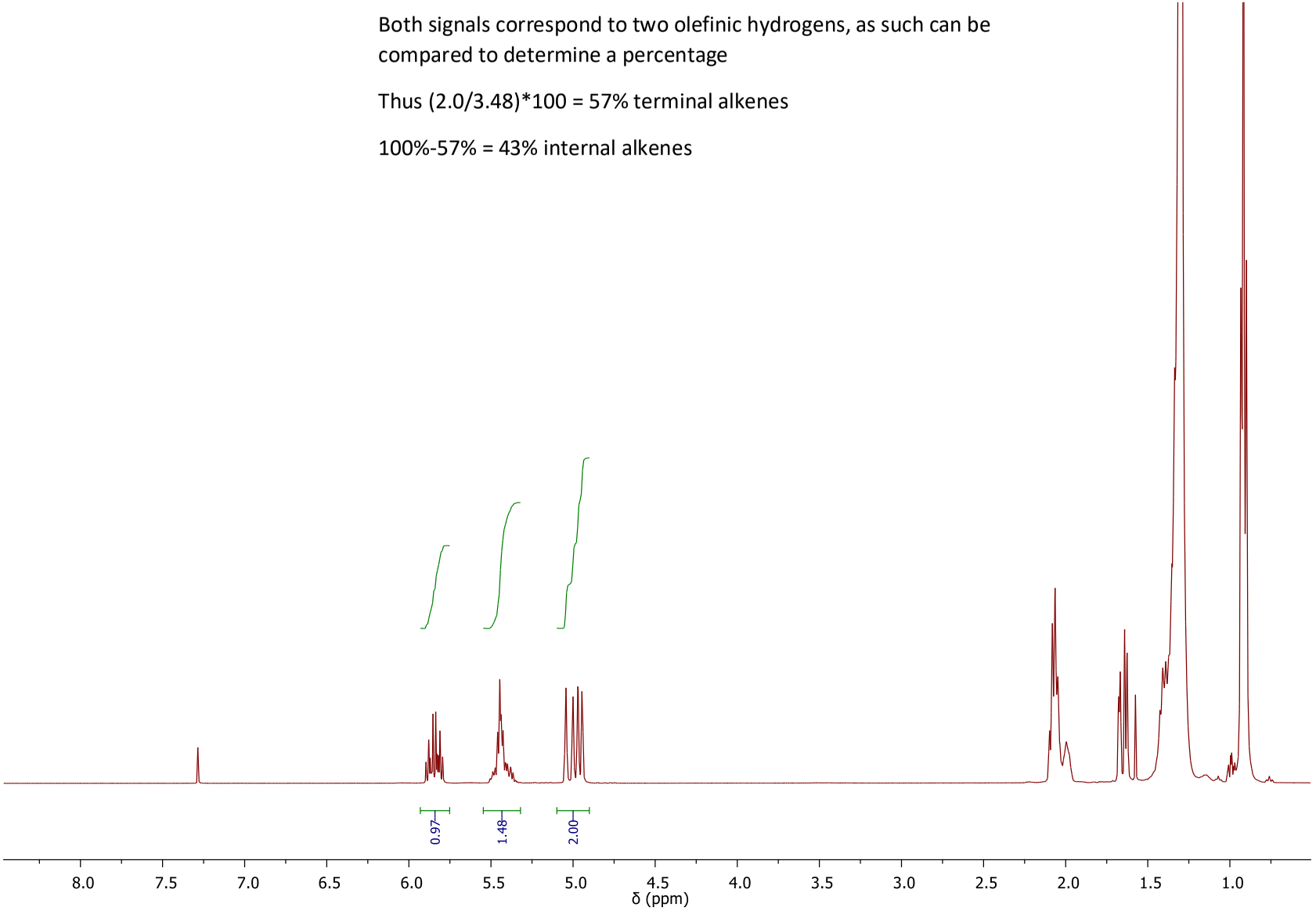

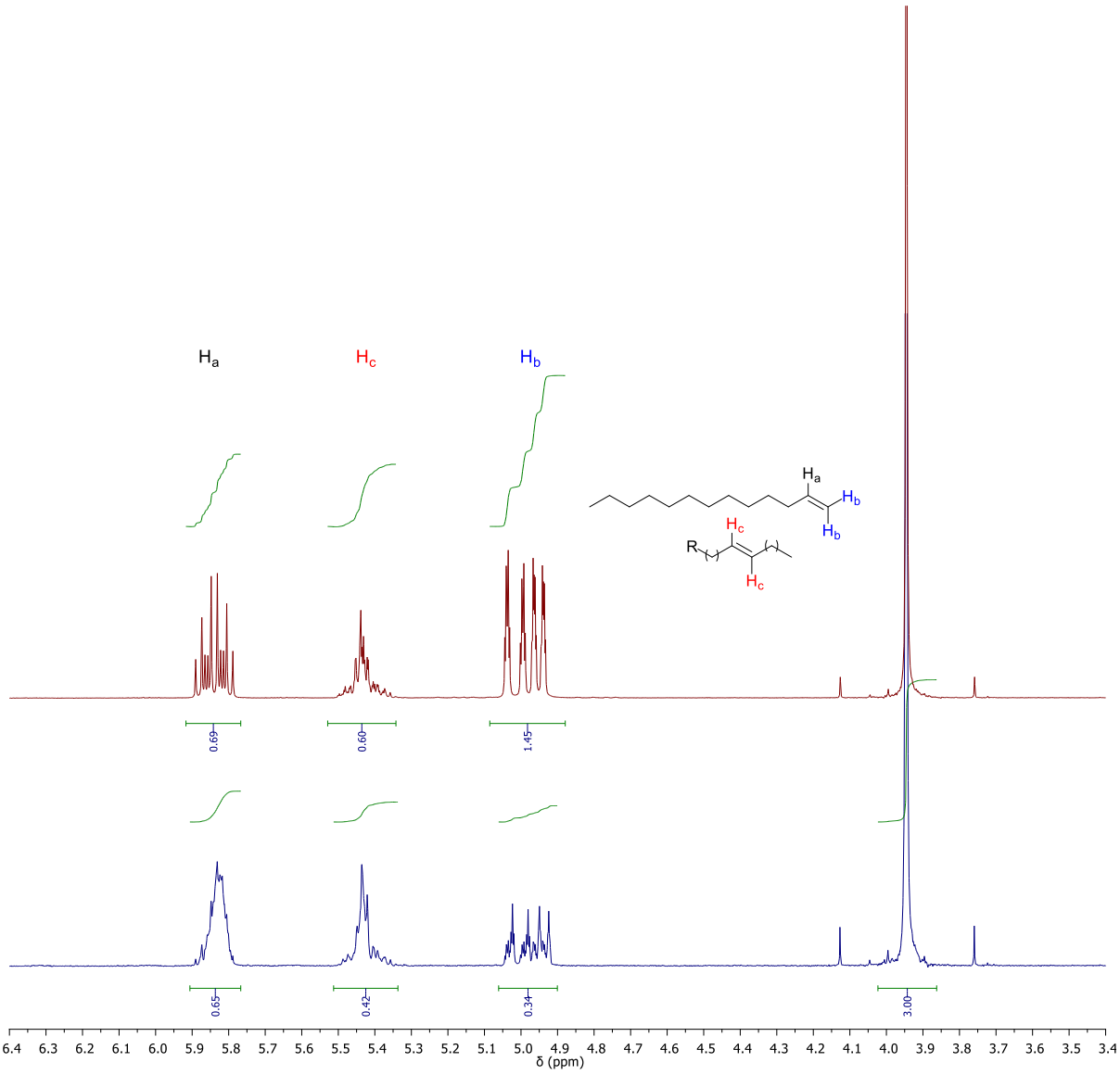

Deuterium incorporation calculation

Integration of H_b peak relative to methyl benzoate additive: 1.45

Integration of H_b peak from d^6 Ac_2O experiment relative to methyl benzoate additive: 0.34

Decrease in integration intensity is due to deuterium incorporation and can be determined as a percentage.

Thus (0.34/1.45)*100 = 23% hydrogen atoms in H_b position.

100%-23% = 77% deuterium incorporation into H_b

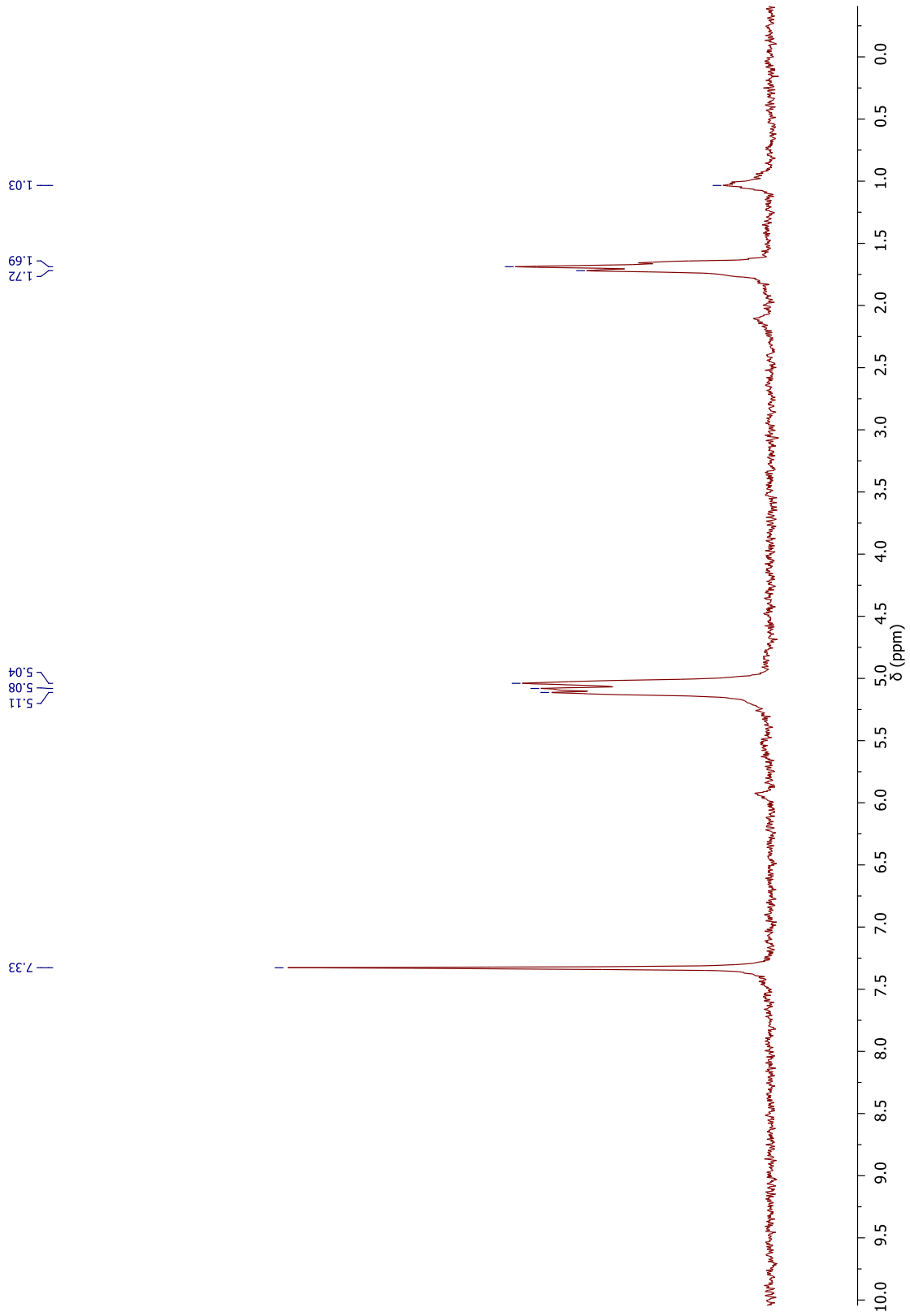

Figure A.11: ^{2}H NMR spectrum ($CHCl_3$) of deuterated C_{13} chain length alkenes obtained after catalysis using [Rh(acac)(PPh_3)(CO)]